

AD 607419

✓RADC-TDR-64-184, Vol 1A  
✓FINAL REPORT



# HARDENED ANTENNA STUDIES (U)

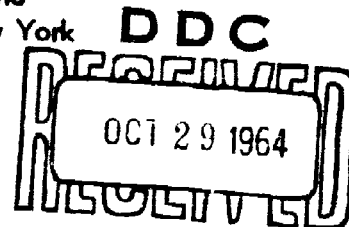
Electrical Investigation of Hardened HF Antennas

COPY	1	OF	3
HARD COPY	\$ 7.00		
MICROFICHE	\$ 1.75		

TECHNICAL DOCUMENTARY REPORT NO. RADC-TDR-64-184, Vol 1A

September 1964

Communications Techniques Branch  
Rome Air Development Center  
Research and Technology Division  
Air Force Systems Command  
Griffiss Air Force Base, New York



Project No. 4519, Task No. 451906 DDC-IRA D

(Prepared under Contract No. ✓AF30(602)-2932 by Sylvania  
Electronic Systems East, Waltham, Mass., A Division of  
Sylvania Electric Products Inc.)

# ARCHIVE COPY

**CLEARINGHOUSE FOR FEDERAL SCIENTIFIC AND TECHNICAL INFORMATION CFSTI  
DOCUMENT MANAGEMENT BRANCH 410.11**

**LIMITATIONS IN REPRODUCTION QUALITY**

**ACCESSION #**

*ADL607419*

- ☒ 1. WE REGRET THAT LEGIBILITY OF THIS DOCUMENT IS IN PART UNSATISFACTORY. REPRODUCTION HAS BEEN MADE FROM BEST AVAILABLE COPY.
- ☐ 2. A PORTION OF THE ORIGINAL DOCUMENT CONTAINS FINE DETAIL WHICH MAY MAKE READING OF PHOTOCOPY DIFFICULT.
- ☐ 3. THE ORIGINAL DOCUMENT CONTAINS COLOR, BUT DISTRIBUTION COPIES ARE AVAILABLE IN BLACK-AND-WHITE REPRODUCTION ONLY.
- ☐ 4. THE INITIAL DISTRIBUTION COPIES CONTAIN COLOR WHICH WILL BE SHOWN IN BLACK-AND-WHITE WHEN IT IS NECESSARY TO REPRINT.
- ☐ 5. LIMITED SUPPLY ON HAND: WHEN EXHAUSTED, DOCUMENT WILL BE AVAILABLE IN MICROFICHE ONLY.
- ☐ 6. LIMITED SUPPLY ON HAND: WHEN EXHAUSTED DOCUMENT WILL NOT BE AVAILABLE.
- ☐ 7. DOCUMENT IS AVAILABLE IN MICROFICHE ONLY.
- ☐ 8. DOCUMENT AVAILABLE ON LOAN FROM CFSTI (TT DOCUMENTS ONLY).
- ☐ 9.

**TSL-107-10 64**

**PROCESSOR:** *CA*

## FOREWORD

The work described in this report (Vol. I and II) was supported by the Communications Division of the AF Systems Command, Rome Air Development Center, Griffiss Air Force Base, under Contract AF30(602)-2932.

The following people at Sylvania Electronic Systems have contributed significantly to the work reported here.

a) Electrical Investigation

Mr. E. Tahan - Applied Research Laboratory

Dr. R. Wundt - Applied Research Laboratory

Mr. D. Meyers - Applied Research Laboratory

b) Survivability Analyses

Mr. H. Zeltzer - SES East - Hardened Antenna Staff

Mr. J. Snitkoff - SES East - Hardened Antenna Staff

Mr. E. Stefaniak - SES East - Hardened Antenna Staff

Key Words: Antennas, Antenna Configurations, Communication Systems

#### ABSTRACT

This report discusses the results of a twelve month engineering investigation of Hardened HF and UHF Antennas, sponsored by the Communications Division of Rome Air Development Center, Air Force Systems Command. This engineering study has resulted in the generation of efficient antenna techniques consistent with the capabilities to withstand the effects of nuclear weapons. The HF antenna techniques considered in this study are useful throughout the 2-30 mc frequency band; the UHF antennas operate in the 225-400 mc region. The program was divided into two phases. Phase I was a theoretical study of antenna techniques which were investigated with regard to feasibility, configuration required, bandwidth possibilities, efficiency, radiation patterns, hardness ratings, debris effects, and economic analysis. Phase II involved the fabrication and test of electrical models of the most promising designs. This phase resulted in design data, cost and hardness estimates for antennas for the HF and UHF bands.

#### PUBLICATION REVIEW

This report has been reviewed and is approved. For further technical information on this project, contact Donald J. Waters, EMC1W-1.

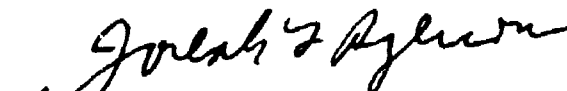
Approved:



DONALD J. WATERS

Chief, Antenna & Special Tech Unit  
Wideband Transmission Section  
Communications Division

Approved:



T.B. SWANSON  
Colonel, USAF

Chief, Communications Division

FOR THE COMMANDER:



IRVING GABELMAN  
Chief, Advanced Studies Group



**HARDENED ANTENNA STUDIES  
RADC-TDR-64-184**

**GENERAL CONTENTS**

**VOLUME IA. ELECTRICAL INVESTIGATION OF HARDENED HF ANTENNAS**

- 1 INTRODUCTION
- 2 ANNULAR SLOT ANTENNA
- 3 LOG SPIRAL ANTENNA
- 4 LINEAR SLOT ANTENNA
- 5 WIRE SLOT ANTENNA
- 6 BURIED WIRE ANTENNA
- 7 SUMMARY OF ADDITIONAL HF ANTENNA CHARACTERISTICS

**VOLUME IB. ELECTRICAL INVESTIGATION OF HARDENED HF ANTENNAS  
(Continued)**

- 8 CONCLUSIONS

APPENDIX A. CHARACTERISTICS OF DEBRIS FOR HARDENED ANTENNA STUDY,  
ESSAD TAHAN, RESEARCH NOTE NUMBER 412, 31 JULY 1963

APPENDIX B. DESIGN DATA FOR HF ANTENNA SITE AND HF SCALE MODEL  
ANTENNAS, PROPOSAL CONTRACT NO. AF30(602)-2932  
10 MARCH 1964

APPENDIX C. INSTRUCTION MANUAL FOR SCALE MODEL LOG SPIRAL LINEAR  
SLOT AND WIRE SLOT ANTENNAS, PROPOSAL CONTRACT NO.  
AF30(602)-2932, 10 MARCH 1964

APPENDIX D. LOG PERIODIC DIPOLE (LPD) AND MONOPOLE ARRAY

APPENDIX E. SURFACE WAVE ANTENNAS

APPENDIX F. DEBRIS MEASUREMENTS AT WALTHAM, MASS.

**VOLUME II. ENVIRONMENTAL ANALYSIS OF HARDENED HF ANTENNAS**

- 1 ENVIRONMENTAL ANALYSIS OF ASPHALTIC CONCRETE EMBEDDED  
HIGH FREQUENCY ANTENNAS
- 2 ENVIRONMENTAL ANALYSIS OF EXPOSED HARDENED ANTENNAS

**VOLUME III. A STUDY OF HARDENED UHF ANTENNAS**

- 1 SYNOPSIS
- 2 CYLINDRICAL ARRAY
- 3  $TM_{01}$  MODE CIRCULAR APERTURE
- 4 THE SHUNT FED COAXIAL ANTENNA

**VOLUME IV. A STUDY OF HARDENED UHF ANTENNAS (Continued)**

- 5 SURFACE WAVE ANTENNAS IN GENERAL
- 6 RECOMMENDATIONS FOR CONTINUED STUDY
- 7 BIBLIOGRAPHY

## TABLE OF CONTENTS VOL. I

<u>Section</u>	<u>Page</u>
1 INTRODUCTION	1
1.1 Summary	1
2 ANNULAR SLOT	15
2.1 Theoretical Considerations	15
2.1.1 Introduction	15
2.1.2 Radiation Characteristics (Radiation Pattern and Directivity, K Foster)	15
2.1.3 Admittance of the Annular Slot Antenna	25
2.1.4 Efficiency of the Annular Slot Antenna	39
2.1.4.1 General Efficiency Considerations	40
2.1.4.2 Results of Computations of Efficiency	51
2.1.4.3 Effects of Debris on the Annular Slot Antenna	55
2.2 Experimental Investigation and Computations for the HF Annular Slot Antenna Located in Warrensburg, Missouri	63
2.2.1 Introduction	63
2.2.2 Annular Slot Computations	63
2.2.3 Discussion of Predicted Results	65
2.2.4 Warrensburg Antenna Site	77
2.2.5 Measured Terminal Input Impedance and Field Intensity	83
2.2.6 Debris Characteristics at Antenna Site	96
2.2.6.1 Debris Measurement Technique	96
2.2.6.2 Summary of Debris Parameter Measurements	96
2.2.6.3 Calculation of Debris Parameters and Summary of Debris Constants	100
2.2.6.4 Conductivity Measurements by the 97 CPS Probe Technique	105
2.2.7 Evaluation of Impedance Measurements of Annular Slot Antenna	108

# TABLE OF CONTENTS VOL. I - continued

<u>Section</u>	<u>Page</u>
2.2.8 Measured Properties of Asphaltic Concrete	120
2.2.8.1 Q Factor	120
2.2.8.2 Dielectric Constant	120
2.2.9 Analysis of Data and Conclusions	124
2.2.9.1 Notches in Efficiency	124
2.2.9.2 High Efficiency	124
2.2.9.3 Performance of Antenna Under a Debris Cover	125
2.3 Design Procedure for the Annular Slot Antenna	129
3 LOG SPIRAL ANTENNA	137
3.1 Introduction	137
3.2 Design Procedure	137
3.3 Radiation Pattern	141
3.4 Input Impedance	141
3.5 Experimental Investigation of the Log Spiral Antenna	142
3.6 Summation of Experimental Results	157
3.6.1 Input Impedance	157
3.6.2 Radiation Pattern	160
4 LINEAR SLOT	163
4.1 Linear Slot Antenna Backed by a Rectangular Cavity	163
4.2 Design of Antenna	166
4.3 Efficiency Considerations	169
4.4 Summary	170
4.5 Experimental Investigations	175
4.5.1 Scale Model	175
4.5.2 Input Impedance Considerations	178
4.5.3 Field Intensity Measurements	178

# TABLE OF CONTENTS VOL. I - continued

<u>Section</u>		<u>Page</u>
5	WIRE SLOT ANTENNA	187
5.1	Introduction	187
5.2	Analysis of the WSA	187
5.3	Radiation Pattern and Radiation Resistance	191
5.4	Discussion of Measured Field Intensity (WSA)	197
5.5	Evaluation of WSA Performance	200
5.6	Wire Slot Experimental Investigation	204
5.6.1	Scale Model	204
5.6.2	Input Impedance Measurements	204
5.6.3	Field Intensity Measurements	209
6	BURIED WIRE ANTENNA	215
6.1	Introduction	215
6.2	Buried Horizontal Wire Antennas with Standing Wave Current Distribution	216
6.2.1	Impedance Properties of the Buried Dipole Antenna	216
6.2.2	Radiation Characteristics and Efficiency of Single Element	221
6.2.3	Buried Dipole Efficiency	227
6.2.4	Buried Dipole Array	233
6.2.5	Omnidirectional Patterns	237
6.2.6	Feed Arrangements of Buried Dipole Arrays	242
6.2.7	Summary, Buried Dipole Antennas	243
6.3	Buried Traveling-Wave Antenna	245
6.3.1	Characteristics of Basic Current Element	246
6.3.2	Half-Wave Dipole, Center Fed, with Standing Wave Current Distribution	250
6.3.3	The Single Horizontal Insulated Buried Straight Wire, Center Fed, with Traveling Wave Current Distribution	255

# TABLE OF CONTENTS VOL. I - continued

<u>Section</u>		<u>Page</u>
	6.3.4 Zig-Zag Antenna	264
	6.3.5 Rhombic Antennas	277
	6.3.6 Square Antenna	278
	6.3.7 Circle Antenna	288
	6.3.8 Field Pattern of Circular Antenna with Finite Attenuation	303
7	SUMMARY OF ADDITIONAL HF ANTENNA CHARACTERISTICS	307
	7.1 Letter Rack Flush Slot Array	307
	7.2 Log Periodic Structure	311
	7.3 Other Configurations	314
8	CONCLUSIONS	315
	8.1 Discussion	315
	8.2 Summary of Antenna Characteristics	317
	8.2.1 Annular Slot	317
	8.2.2 Log Spiral	322
	8.2.3 Linear Slot	327
	8.2.4 Wire Slot Antenna	331
	8.2.5 Buried Wire Antennas	338
	8.2.6 Letter-Rack Flush-Slot Array	353
	8.2.7 Log Periodic Structures	357
	8.3 Tabulation of Antenna Hardness and Cost	360
	8.4 Design Data	361
	8.5 Debris Condition's Under Which Antennas Were Investigated	362

## Appendix

- A CHARACTERISTICS OF DEBRIS FOR HARDENED ANTENNA STUDY,  
Essad Tahan, Research Note Number 412, 31 July 1963.
- B DESIGN DATA FOR HF ANTENNA SITE AND HF SCALE MODEL  
ANTENNAS, Proposal Contract No. AF30(602)-2932  
10 March 1964.

TABLE OF CONTENTS VOL. I - continued

Appendix

- C INSTRUCTION MANUAL FOR SCALE MODEL LOG SPIRAL LINEAR  
SLOT AND WIRE SLOT ANTENNAS, Proposal Contract No.  
AF30(802)-2832, 10 March 1964.
- D LOG PERIODIC DIPOLE (LPD) AND MONOPOLE ARRAY
- E SURFACE WAVE ANTENNAS
- F DEBRIS MEASUREMENTS AT WALTHAM, MASS.



## LIST OF ILLUSTRATIONS

### SECTION 1

<u>Figure</u>		<u>Page</u>
1-1	Sylvania Antenna Site	9
1-2	Layout of Sylvania Antenna Site	10
1-3	Sylvania HF Antenna Site and Field Intensity Monitoring Stations	11

### SECTION 2

2-1	Basic Configuration of HF Annular Slot	16
2-2	Radiation Conductance and Directivity "K" Versus $\kappa\rho$	20
2-3	Normalized Radiation Pattern for Annular Slot (Constant Field Intensity Along Ground)	22
2-4	Radiation Patterns of Annular Slot in Vertical Plane (Constant Radiated Power)	24
2-5	Directivity and Main Lobe Elevation Angle	26
2-6	Total Susceptance of 40' Annular Slot Versus Frequency With and Without Debris	31
2-7	Total Conductance of 40' Annular Slot Versus Frequency With and Without Debris	33
2-8	Radiation Conductance of 40' Annular Slot Versus Frequency With and Without Debris	34
2-9	Total Conductance-Susceptance Ratio Versus $b/\lambda$ for 40' Annular Slot	36
2-10	Equivalent Antenna Circuit Including Dielectric and Ground Losses	37
2-11	Efficiency of 40' Annular Slot With and Without Debris (Semilog Plot)	52
2-12	Efficiency of 40' Annular Slot With and Without Debris (Rectangular Plot)	53



# LIST OF ILLUSTRATIONS - continued

<u>Figure</u>		<u>Page</u>
2-13	Efficiency of 40' Annular Slot Versus Frequency with Backup Cavity Depth as a Varying Parameter	56
2-14	Slot Geometry Used for Analysis of Debris Effects	58
2-15	Configuration for a Hardened Annular Slot Antenna	64
2-16	Computed Inside Conductance of Warrensburg Antenna Versus Frequency	66
2-17	Computed Inside Susceptance of Warrensburg Antenna Versus Frequency	67
2-18	Computed Outside Conductance of Warrensburg Antenna	69
2-19	Computed Outside Susceptance of Warrensburg Antenna	70
2-20	Computed Radiation Conductance of Warrensburg Antenna	72
2-21	Theoretical Efficiency Versus Frequency	73
2-22	Annular Slot Antenna Efficiency Versus Asphalt Blanket Thickness	75
2-23	Configuration of the Warrensburg Antenna	78
2-24	Experimental Set-up at Warrensburg	79
2-25	Expanded View of Access Hole Showing Electrical Connection to the Antenna	80
2-26	Profile of Annular Slot Looking in NW Direction	81
2-27	View of Antenna from Test Shed Looking in SE Direction	82
2-28	Conditions Under Which Antenna was Tested	85
2-29	Terminal Impedance of Antenna, 1.16-13 Mc, No Debris	86
2-30	Terminal Impedance of Antenna, 11.2-25 Mc, No Debris	87
2-31	Terminal Impedance of Antenna, 2-17.2 Mc, Half Cover 1'	88
2-32	Terminal Impedance of Antenna, 13-29.96 Mc, Half Cover 1'	89

# LIST OF ILLUSTRATIONS - continued

<u>Figure</u>		<u>Page</u>
2-33	Terminal Impedance of Antenna, 0.44-24.1 Mc, Full Cover 1'	90
2-34	Terminal Impedance of Antenna, 0.44-24.1 Mc, Full Cover 2'	91
2-35	Theoretical and Measured Field Intensity Along the Ground - No Debris	92
2-36	Measured Field Intensity Along the Ground Half Cover Debris 1'	93
2-37	Measured Field Intensity Along the Ground Full Cover Debris 1'	94
2-38	Measured Field Intensity Along the Ground Full Cover Debris 2'	95
2-39	Technique for Measuring Debris Parameters	97
2-40	Plot of $X_{\text{debris}}$ Versus Frequency for Debris Cover	98
2-41	Plot of $R_{\text{debris}}$ Versus Frequency for Debris Cover	99
2-42	Equivalent Circuit for Debris Measuring Circuit	101
2-43	Debris Conductivity at Warrensburg Versus Frequency	104
2-44	Debris Conductivity Measurements by Four Electrode Method	106
2-45	Radial Transmission Line Model for Annular Slot Antenna	109
2-46	Equivalent for Computing Antenna Input Impedance for Radial Line Model	115
2-47	Input Impedance Versus Frequency for Radial Line - 1.16 to 13 Mc	116
2-48	Input Impedance Versus Frequency for Radial Line - 11.2 to 25.3 Mc	117
2-49	Asphaltic Q Versus Frequency	121

# LIST OF ILLUSTRATIONS - continued

## SECTION 3

<u>Figure</u>		<u>Page</u>
3-1	Radiation Pattern of Log Spirals	138
3-2	Parameter for Equiangular Spiral	139
3-3	Log Spiral Antenna	142
3-4	Log Spiral Antenna Feed Arrangement	143
3-5	Photo of Scale Model of HF Spiral	144
3-6	Cross-section Log Spiral Antenna and Back-up Cavity	145
3-7	Input Impedance of 10' Diameter Log Spiral No Debris	147
3-8	Input Impedance of 10' Diameter Log Spiral Half Cover of Debris	148
3-9	Input Impedance of 10' Diameter Log Spiral Full Cover of Debris	149
3-10	VSWR Versus Frequency for Log Spiral With and Without Debris	150
3-11	Elevation Pattern ( $E_v$ , $E_{vd}$ ) for Log Spiral With and Without Debris at station 6	151
3-12	$E_v$ , $E_{vd}$ , $E_4$ , $E_{4d}$ Versus $\theta_e$ for Log Spiral at Station 6	152
3-13	Elevation Pattern for Log Spiral and $\geq 4$ Monopole With and Without Debris	154
3-14	Measured Field Intensity Versus Elevation Angle for Log Spiral at Station 5 With and Without Debris	155
3-15	Measured Field Intensity Versus Elevation Angle for Log Spiral at Station 1 With and Without Debris	156
3-16	Azimuthal Plots of Log Spiral (With and Without Debris) and the Reference $\geq 4$ Monopole	158
3-17	Log Spiral Antenna $E_v$ Versus Frequency Station 1	162

# LIST OF ILLUSTRATIONS - continued

## SECTION 4

<u>Figure</u>		<u>Page</u>
4-1	Cavity Backed Linear Slot Antenna in Air	164
4-2	Configuration of Linear Slot Centrally Located- (10-20 Mc)	171
4-3	Configuration of Linear Slot at End of Cavity (10-20 Mc)	173
4-4	Radiation Pattern of Linear Slot	176
4-5	Photo of Linear Slot Scale Model Antenna	177
4-6	Linear Slot Input Impedance Versus Frequency (No Debris)	182
4-7	Linear Slot Input Impedance Versus Frequency (With 18" Half Cover Debris)	183
4-8	Linear Slot Input Impedance Versus Frequency (With 18" Full Cover Debris)	184
4-9	Linear Slot and Reference Monopole Azimuthal Patterns ( $\theta_e = 18^\circ$ )	185
4-10	Field Intensity Versus Frequency for Linear Slot Model at Station 1	186

## SECTION 5

5-1	Wire Slot Antenna	188
5-2	Photo of Scale Model Wire Slot Antenna	198
5-3	Smith Plot of Input Impedance vs Frequency	206
5-4	Smith Plot of Input Impedance vs Frequency	207
5-5	Smith Plot of Input Impedance vs Frequency	208

# LIST OF ILLUSTRATIONS - continued

<u>Figure</u>		<u>Page</u>
5-6	Field Patterns in Azimuth for Wire Slot at 76 and 90 Mc and Monopole at 90 Mc	210
5-7	Field Intensity vs Frequency - Monopole and Wire Slot with and without Debris	212
SECTION 6		
6-1	Radiation Pattern for a Single Buried Horizontal Dipole	222
6-2	Radiation Pattern of a Short Vertical Monopole Over Perfect Ground	224
6-3	Buried Horizontal Dipoles - Rectangular Array	234
6-4	Buried Horizontal Dipoles - Z-type Array	236
6-5	Feed Arrangements for Omnidirectional Pattern	238
6-6	Buried Horizontal Dipoles - Circular Array	239
6-7	Radiation Pattern for Circular Array	240
6-8	Orientation of Basic Current Element	247
6-9	Single and Folded Dipole	251
6-10	Straight Wire - Center Feed	256
6-11	Straight Wire - Azimuthal Pattern $ E_{\epsilon} $	259
6-12	Straight Wire - Elevation Pattern $E_{\epsilon}$	260
6-13	Straight Wire: Center Feed - End Feed Azimuthal Pattern $ E_{\epsilon} $	262
6-14	Straight Wire: Center Feed - End Feed Elevation Pattern $ E_{\epsilon} $	263
6-15	Zig-Zag Antenna - Orientation	265
6-16	Zig-Zag Antenna - Azimuthal Pattern $ E_{\epsilon} $	273

## LIST OF ILLUSTRATIONS - continued

<u>Figure</u>		<u>Page</u>
6-17	Zig-Zag Antenna - Elevation Pattern $ E_{\epsilon} $	274
6-18	Zig-Zag Antenna - Efficiency	276
6-19	Square Antenna - Orientation	279
6-20	Square Antenna - Azimuthal Patterns $ E_{\epsilon} $	285
6-21	Square Antenna - Elevation Patterns, $ E_{\epsilon} $ , $ E_{\psi} $	286
6-22	Circle Antenna - Orientation	289
6-23	Circle Antenna - Azimuthal Pattern $ E_{\epsilon} $	295
6-24	Circle Antenna - Elevation Pattern $ E_{\epsilon} $	296

### SECTION 7

7-1	Configuration for Letter Rack Flush Slot Array	308
7-2	Design Data for Letter Rack Flush Slot Array	309
7-3	Log Periodic Monopole Array (12-30 Mc)	312
7-4	Log Periodic Monopole Array (25-30 Mc)	313

### SECTION 8

8-1	Configuration of the Annular Slot Antenna	318
8-2	Radiation Patterns of an Annular Slot in Vertical Plane	319
8-3	Configuration of Log Spiral Slot with Back-up Cavity	323
8-4	Radiation Patterns of a Log Spiral Slot in Vert'cal Plane	324
8-5	Configuration of Linear Slot at End of Cavity	328
8-6	Configuration of Linear Slot Centrally Located	329
8-7	Radiation Pattern of Linear Slot	330

# LIST OF ILLUSTRATIONS - continued

<u>Figure</u>		<u>Page</u>
8-8	Configuration of a Flush Wire Slot Antenna	332
8-9	Configuration of a Low Profile Wire Slot Antenna	333
8-10	Radiation Pattern of a Single Wire Slot	335
8-11	Cost Versus Overpressure for a Wire Slot in Air	337
8-12	Buried Horizontal Dipole - Rectangular Array	339
8-13	Buried Horizontal Dipole - Z-Type	340
8-14	A Rectangular Omnidirectional Array	341
8-15	A Circular Omnidirectional Array	343
8-16	Radiation Pattern for Directional Array	345
8-17	Radiation Pattern for Circular Array	346
8-18	Buried Traveling Wave Antenna - Zig-Zag Array	348
8-19	Buried Traveling Wave Antenna - Square Array with 1, 2, and 3 Turns	350
8-20	Configuration for Letter Rack Flush Slot Array	354
8-21	Parameters of a Letter Rack Flush Slot Array	355
8-22	Log Periodic Monopole Array (12-30 Mc)	358
8-23	Log Periodic Monopole Array (25-30 Mc)	359

## EVALUATION

This contract was awarded to Sylvania to investigate HF and UHF antenna designs capable of withstanding the effects of repeated nuclear attacks. The program provided analysis, electrical test of models, design data and cost estimates of several very attractive antennas. These antennas represent the latest in the field of hardened antennas and provide better performance, electrical and physical, and lower cost with greater confidence than any previous systems.

The information obtained during the contract is part of a continuing effort in the area of survivable communications. Upon completion of this program the focal point for hardened antennas was established at RADC. These results will be used as the technological base for continued efforts in antenna survivability and in providing consulting services to the various using commands and system offices.





## **SECTION 1**

### **INTRODUCTION**

This program was a 12 month engineering investigation of HF antennas designed to withstand the effects of a nuclear weapon. The results are presented in two volumes entitled:

#### **HARDENED HF ANTENNA STUDY**

**Volume I - Electrical Investigation of Hardened HF Antennas**

**Volume II - Survivability Analyses of Hardened HF Antennas**

Volume I contains the results of an electrical investigation of 12 HF antenna techniques considered in this study together with the results of an experimental investigation of the four most promising types, the Annular Slot, Linear Slot, Wire Slot, and Log Spiral Antennas.

A detailed theoretical analysis of the behavior of the Annular Slot antenna with and without a debris cover is presented together with the results of an experimental program on a HF Annular Slot located in Warrensburg, Missouri. Scale models were used in the experimental evaluation program of the other three antennas.

Volume II contains a detailed analysis of the nuclear weapon threat together with mechanical analysis of the various HF antenna configurations as to failure modes, cost estimates for each of the hardened antennas considered, design data, and specifications for the most promising antenna types designed to withstand particular overpressure levels.

Hardness ratings for the antennas have been classified as A, B, C, D in Volume I and are discussed in Volume II. Lowest Hardness rating is class A, maximum hardness is class D.

#### **1.1 SUMMARY**

The Hardened HF Antenna Study was conducted at Sylvania's Applied Research Laboratory located in Waltham, Massachusetts. The electrical study

program was divided into two phases. Phase I was concerned with a theoretical study of the suitable antenna techniques in HF region and Phase II involved an experimental program to demonstrate some of the electrical characteristics predicted in Phase I.

The HF band encompasses a frequency range of 2 to 30 Mc and antennas optimized for operation in this band are inherently large structures. Additional constraints placed upon the antennas in this study were their capability for hardening and ability to operate with reasonable efficiencies under the effects of a debris cover. Techniques used at UHF and higher frequencies such as debris pits around or integral with the antenna and ground plane could not be utilized at HF because these features seriously degraded the hardness of the antenna, and sharply increased the cost. Thus it became apparent during phase I of this study that antenna techniques capable of exhibiting reasonable radiation efficiencies when radiating through a debris layer were to be investigated. This property coupled with the ability to design such structures to carry a maximum hardness rating at a reasonable cost was our basic approach in this investigation.

During Phase I, 12 different types of antenna techniques were studied for application in the HF region. Our approach has been to study each technique with regard to feasibility, configuration required, broad bandwidth possibilities, efficiency, radiation pattern and directivity, polarization (preferably vertical), hardness rating and the degrading effects of debris on the antenna electrical performance. The 12 antenna techniques fall into the following three general categories:

- (a) Antennas in air
- (b) Antennas flush with the ground or of low profile  
embedded in asphaltic concrete
- (c) Antennas buried in the ground

Under category (a), the following four types were considered:

- (1) Wire slot
- (2) Log-Periodic vertical monopoles (LPM type)
- (3) Spherical antenna
- (4) Prolate-spheroidal antennas

The wire slot antenna represents an attractive, simple, and relatively inexpensive HF technique especially in the 10 - 30 Mc region. This antenna falls into categories (a) and (b). It represents a directional type antenna having a directivity of approximately 5.3 db (compared to an isotropic antenna above perfect ground) and can be used down to 2 Mc at moderate costs. Three configurations of the wire slot antenna are feasible -- a four-foot high wire slot above ground in air (hardness class A,B,C), one embedded in asphaltic concrete above ground (hardness class D) and another located in a trough below ground (Hardness class D).

The results of our initial studies indicate that the log periodic vertical structure represents an expensive antenna of low hardness rating. The cost of such an antenna is high because of the size of reinforced concrete foundation required for this case. Electrically, the log periodic structures possess desirable broad band characteristics, however the cost to performance ratio is high for the vertical monopole array.

Spherical antennas with a narrow slot between the two hemispheres and the prolate spheroidal design were considered because of the broad band characteristics at HF frequencies. The evaluation of these antennas from the hardness point of view indicated the need for extremely large and costly foundations for a hardness ratings class A; thus, they are not recommended for the HF region.

The antennas that fall into category (b) are as follows:

1. Annular Slot
2. Linear Slot
3. Log Spiral
4. Wire Slot

5. Letter Rack Flush-Slot Array
6. Direct Driven Resonant Radiator (Hula Hoop)
7. Surface Wave Types
8. Helical Antennas

All of these antennas with the exception of the surface wave types can be classified as very hard antennas capable of withstanding overpressures in hardness classification D. The surface wave type antennas carry a C hardness rating.

Annular and linear slot antennas represent attractive medium cost techniques for HF communication, possess high efficiency (25% to 65%), desirable radiation patterns and directivity. The effects of debris on the efficiency of an annular slot has been experimentally determined on a full scale HF antenna and the results indicate a degradation in operating efficiency of -3 to -7 db in the frequency range of 3.5 to 13.5 Mc. This degradation is for a one foot full cover of debris on a 60 foot diameter antenna optimized for operation in the 3-5 to 13.5 Mc range and located in Warrensburg, Missouri.

The log spiral antenna was found to be a desirable HF technique and may be in the form of a spiral with conductive arms or spiral slots backed up with a cavity. The efficiency of properly designed spirals neglecting dielectric losses is approximately 50% with cavity backing. It appears at this point that a four-arm spiral operating in the second higher order mode displays a desirable omnidirectional radiation pattern for this frequency band. The spiral technique is attractive from the broad band characteristics of such devices, constant input impedance, efficiency, hardness rating, and moderate cost.

Investigation of the wire slot antenna indicated operation at maximum efficiency when such structures are built above the ground and periodically supported with dielectric rods. Antennas supported in this manner carry a hardness rating of A,B at the low end of the HF band, and higher ratings C in the 20-30 Mc region. Embedding this structure in asphaltic concrete increases the hardness rating to D with a sacrifice in operating efficiency

due to asphaltic losses and burial depth. Calculations indicate efficiencies of 8 to 25% are realizable from 8 to 30 Mc for a four foot high wire slot embedded in asphaltic concrete.

Utilization of the log periodic principle in the design of a so-called letter rack flush slot array in the ground was also investigated. The letter rack flush slot array, when embedded in asphaltic concrete, was found to be a moderately good, medium-cost, antenna for the HF region. A fine-slot array shows promise as one with broad bandwidth possibilities ( $\sim 2:1$ ), high efficiency, and desirable radiation patterns and directivity.

Consideration was also given to an open-pit type letter rack antenna with a debris pit at its base. A cursory investigation indicated that such a design required a rather elaborate concrete foundation and carried a very low hardness rating (category A), thus the results derived from this investigation show that such an open pit structure is not practical in the HF region.

The Directly Driven Resonant Radiator (DDRR) or Hula Hoop antenna is in essence a top loaded monopole, in the form of an inverted L antenna, where the L is bent into a loop. This antenna requires only a short height (4 feet at 2 Mc) and yields good efficiency if mounted above ground in air over an excellent ground screen; however, its bandwidth is very small (about 1/3%). In order to harden this antenna to ratings of class C or D it must be embedded in asphaltic concrete. This reduces the efficiency by a factor of approximately 50 so that the resulting efficiency of the hardened antenna is extremely low. Comparing the Hula Hoop antenna with a top loaded monopole of the top hat type with the monopole in the center, one finds that the top hat antenna has a greater capacity for the same cylindrical volume and therefore results in a more efficient use of a given volume. Therefore the top loaded monopole is preferred to the Hula Hoop as a hardened antenna in the 2-6 Mc region.

Surface wave type antennas in the HF region were not found suitable because of their large size, and relatively high cost to overall performance ratio. Hardness rating of such structures is class C.

Helical antennas were also considered as to their application in the HF region. Two modes of operation were considered -- the normal mode and the axial mode. In the normal mode of operation, the radiation pattern of a helix is similar to that of a short monopole and top loading techniques would have to be used to increase the effective height and efficiency of the antenna. In effect, top loading reduces this antenna to a top loaded monopole. Also, the helix operating in this mode is a very narrow band antenna.

Operation of the helix in the axial mode (the usual mode of operation) results in a radiation pattern along the helical axis with directivities of the order of 10 db. The physical dimensions of such a structure are very large at HF frequencies. Thus from above, the helix does not seem to offer an advantage over other competitive types in the HF region and was eliminated from further study.

Antennas buried in the ground represent the third main classification of HF antennas. The configurations available in this category are subdivided into two groups as follows:

- I. Buried Horizontal Dipole Arrays with Standing Wave Current Distribution
  - 1) Buried Horizontal Dipole Linear Array, Directional Type
  - 2) Buried Horizontal Dipole Crossed Linear Array, Omnidirectional Type
  - 3) Buried Horizontal Dipole Circular Array, Omnidirectional Type
- II. Buried Horizontal Wire Antennas with Traveling Wave Current Distribution
  - 1) Linear Antennas, Directional Type
  - 2) Horizontal Loop Antennas, Omnidirectional Type

These insulated wire antennas, when buried to a depth of 4 feet, represent a relatively low-cost structure with a high hardness rating (class D). Reducing the depth of burial results in a more efficient but lower hardness antenna. Another advantage of such antennas is that debris degradation is

less than with antennas of category (b) which are embedded in asphaltic concrete, because the former are designed to work in a medium having characteristics similar to those of debris. Standing Wave (Type I) are recommended for use in the 2-6 Mc region for narrow band operation; above 6 Mc, the lower operating efficiency together with debris degradation make it inferior compared to the annular or linear slot, the log spiral or wire slot.

Broad band operation can be achieved from buried horizontal wire antennas (Type II) operating in the traveling wave mode. The buried Zig-Zag antenna and particularly the buried rhombic antenna provide radiation patterns of comparatively high directivity but lower efficiency than the corresponding buried wire antennas of Type I which are only useable over a narrow band. Buried Type II wire antennas display constant input impedance characteristics over a wide frequency band and exhibit radiation patterns that change slightly with frequency. Omnidirectional patterns are obtained with horizontal square or circular configuration using a number of turns. These antennas also have constant input impedance characteristics which are slightly affected by changes in soil conductivity; in addition, they have an efficiency in the order of 0.5 to 1 percent, require only one feed cable, and are lower in cost than Type I antennas.

The buried horizontal square or circular configuration is suggested for application in the 2-4 Mc region as a low-cost, wide band antenna covering a 2:1 frequency range. Computed performance of this buried antenna appears to be down approximately 3 db from the Warrensburg Annular Slot antenna (~ 60' dia) at 2 Mc (without debris) and comparable for the case of a uniform half cover over the Warrensburg antenna.

The results of the theoretical studies conducted in Phase I indicated four antenna techniques warranting experimental investigation. They are as follows:

1. Annular Slot
2. Linear Slot
3. Wire Slot
4. Log Spiral



Phase 2 was concerned with an experimental evaluation of these four antenna techniques with and without a debris cover.

The experimental evaluation of the annular slot antenna was conducted at Warrensburg, Missouri on a full-scale antenna embedded in asphaltic concrete and having a diameter of approximately 60 feet. This antenna was built by Sylvania Electronic Systems - East during investigations for the Minuteman Antenna Program and provided an opportunity to correlate theoretical predictions with actual performance in the HF range.

Evaluation of the linear slot, wire slot, and log spiral antennas was performed at the Sylvania Antenna Site in Waltham, Massachusetts shown in Figure 1-1. Scale models of these antennas together with a reference( $\lambda/4$ ) monopole were built and laid out as shown in Figure 1-2. The antenna site occupied an area measuring 39 x 32 feet. Drainage for the site was provided by a 12-inch gravel base. An asphalt pad, six inches thick, was placed on the gravel to provide a good ground base for all the model antennas. This type of base results in minimum degradation of the antenna back-up cavities because of nonuniform ground effects and results in optimum efficiencies.

A fine mesh (copper wire insect screening) was laid down over the asphalt pad and provided the base for the back-up cavity used with each model antenna. This also served as the ground plane for the reference ( $\lambda/4$ ) monopole.

The sidewalls of the back-up cavities for each antenna were fabricated from plywood and the screening stapled to it was soldered to the base screen. A cavity depth of 18 inches was used for all antennas. Loam fill was placed on top of the asphalt pad to a depth of 18 inches. All feed coaxial cables to the antennas are approximately 100' in length and are passed through an underground pipe system to a test shed located approximately 30' from the antenna site. A 40' diameter air-inflatable radome was used at Sylvania to cover the entire antenna site and protect the antennas from the effects of weather, thus reducing the down time in running antenna tests. Figure 1-3 shows a layout of the antenna site together with location of field intensity monitoring stations and coordinator used in the experimental program.



Figure 1-1. Sylvania Antenna Site.

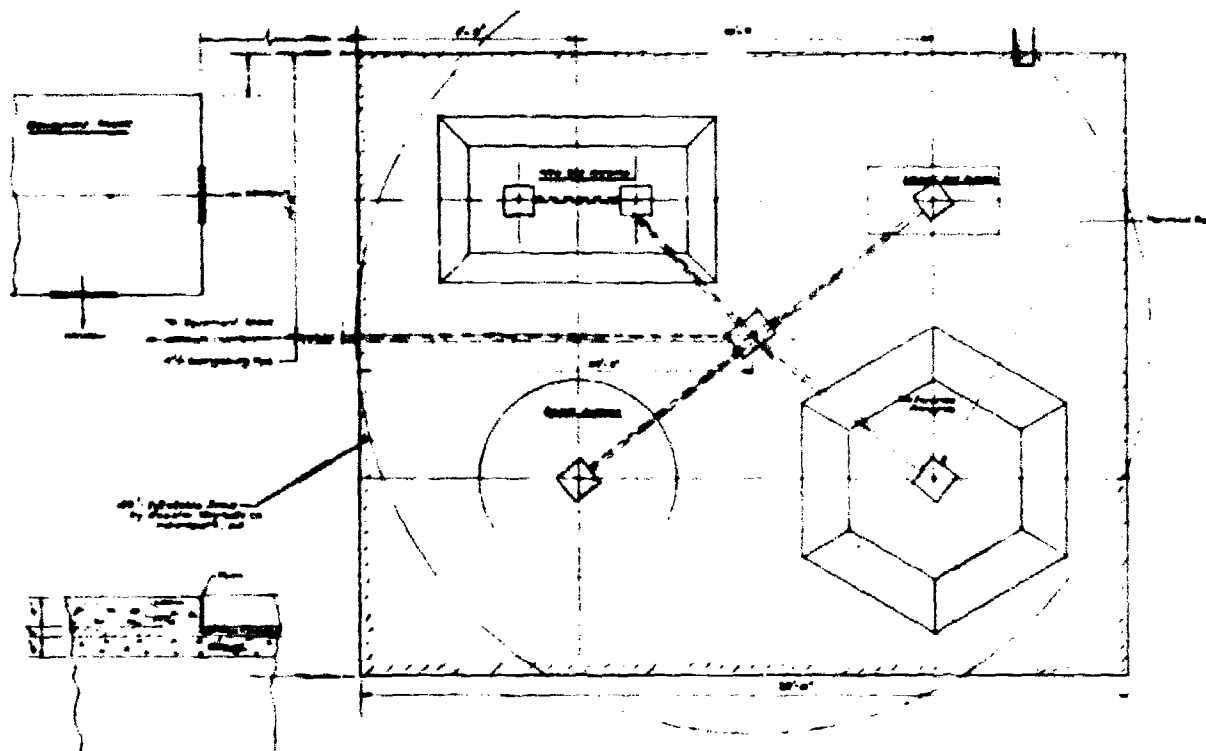


Figure 1-2. Layout of Sylvania Antenna Site.

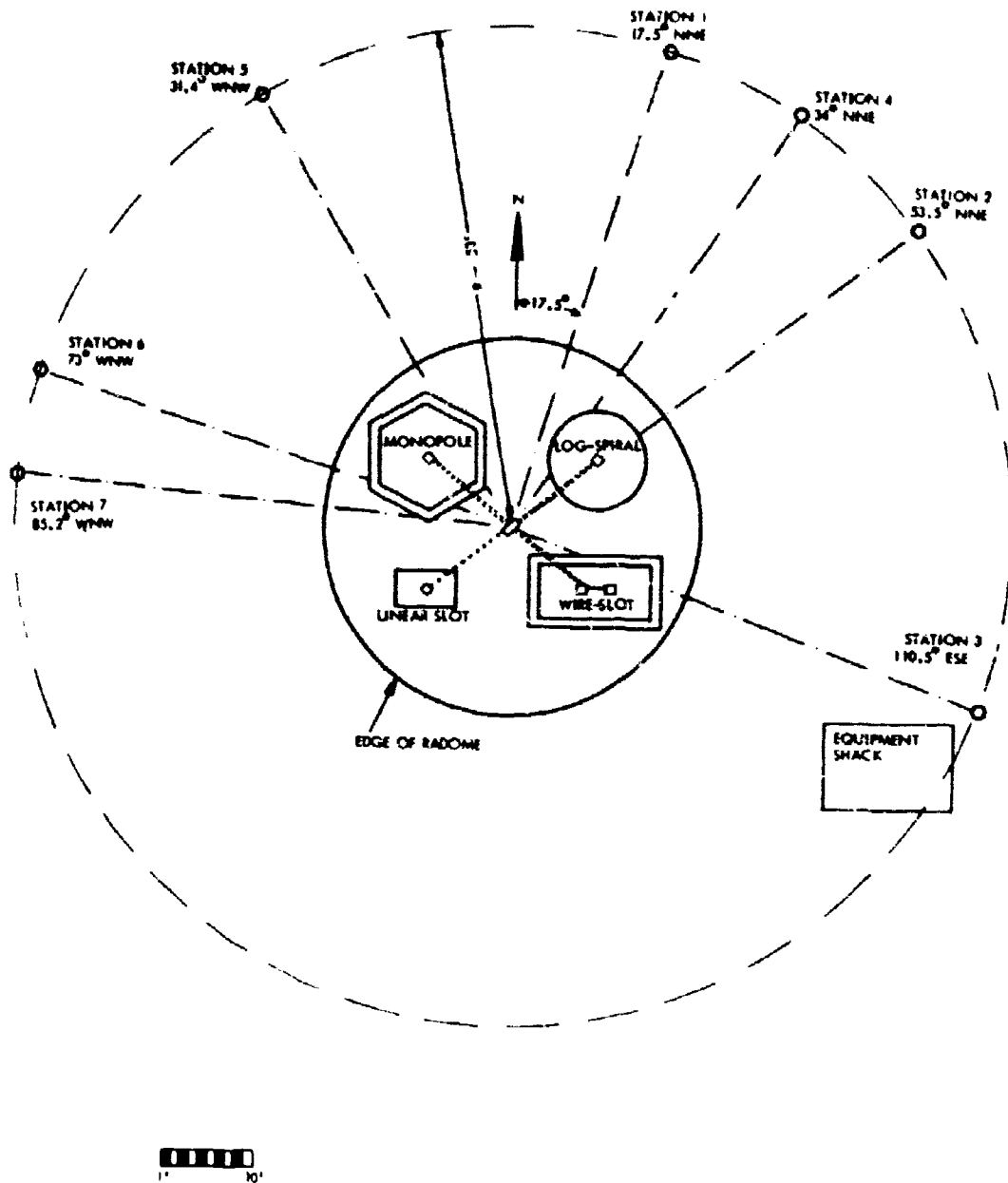


Figure 1-3. Sylvania HF Antenna Site and Field Intensity Monitoring Stations.

The design frequency for each of the antennas is as follows:

Log Spiral	- Frequency range 60 - 240 Mc
Linear Slot	- Design center frequency is 90 Mc
Wire Slot	- Frequency range 76-90 Mc

A reference  $\lambda/4$  monopole adjustable in height, was used throughout this program for field intensity comparison with the above mentioned antennas. Additional detail drawings and specifications for the antenna site are given in Appendix B

The mechanical engineering investigations as presented in Volume II on the HF antenna study program were concerned with an analysis of the various HF antenna configurations as to their ability to survive all of the effects of a nuclear weapon such as overpressure and dynamic pressure, thermal radiation, nuclear radiation, ground shock and debris. It involved the specification of antenna geometry for particular overpressure levels, cost estimates, and included an evaluation of the mechanical failure modes for each of the basic antenna classification categories; i.e.

- 1) Antennas of low profile embedded in asphaltic concrete, such as the Annular Slot, Log Spiral, Wire Slot, etc. D Hardness Rating.
  - a) Wedge Action - Sections of antenna being blown off from slope of structure.
  - b) Shear Bending - Shear between the loaded and unloaded portions of the antenna.
  - c) Rebound or Bouncing Effect - Antenna bouncing out of ground due to tensile waves induced in asphalt.
  - d) Sliding - Structure moving along ground.
  - e) Crack - Natural and others due to environmental conditions.
  - f) Heating and Nuclear Effects.

- 7) Antennas flush with the ground such as the linear slot and letter rack slot-array. D Hardness rating.
- a) Shear Bending.
  - b) Rebound or Bouncing Effect.
  - c) Cracks.
  - d) Heating and Nuclear Effects.
- 3) Surface Wave Types - C Hardness rating. Failure modes are the same as (a) through (f) under paragraph (1), above.
- 4) Log Periodic Monopoles in Air - A,B, C Hardness rating.
- a) Failure is in combination flexure and shear as a cantilever beam.
- 5) Buried Horizontal Wire Antennas - D Hardness rating for a 4 foot burial.
- a) Failure of individual dipoles or elements and feed transmission lines in tension.
  - b) Failure of transmission line and junctions due to ground shock.
  - c) Probably no temperature or nuclear effects.
- 6) Antennas flush with the ground - open-pit structure having a hardness rating of class A

Letter-Rack Slot-Array - Technique No. 1.

- a) Wires will break under wind and thermal heat loads or a combination of both. This limits rating to class A.
- b) Uneven ground upheaval.
- c) Concrete foundation carries rating of class A.

Letter-Rack Slot-Array - Technique No. 2.

- a) Cantilever action of concrete walls which separate the individual cavities of the array under reflected and dynamic pressure limit rating to class A.



## SECTION 2

### ANNULAR SLOT

#### 2.1 THEORETICAL CONSIDERATIONS

##### 2.1.1 Introduction

Figure 2-1 shows a cross-section of an annular slot antenna. It consists of a disk and a cylindrical back-up cavity. From the hardening viewpoint this type of antenna is attractive, since it is flush with the ground and can withstand enormous overpressures if the cavity is filled with a suitable dielectric material which has low losses and good compressive strength. It has been found that asphalt concrete, if properly treated and prepared, is well suited for this purpose and is economical so that it can be used in large quantities. We consider first the radiation characteristics.

##### 2.1.2 Radiation Characteristics

Radiation characteristics of the annular slot have been considered by several authors.<sup>1,2,3</sup> The effects of a back-up cavity have been examined by J. Galejs and T. W. Thompson.<sup>4</sup> For dimensions of the annular slot antenna, which are very small compared to the wavelength, the antenna can be treated as a top loaded very short monopole which has a large top hat capacity.<sup>5,6</sup>

The radiation pattern of the annular slot (also called Circular Diffraction Antenna) has been calculated by Pistolokors.<sup>1</sup> The electric field intensity  $E$  in the far field over perfectly conducting ground, at distance  $D$  is

$$E = \frac{k\rho_o V_g}{D} J_1(k\rho_o \sin \theta) = \frac{x J_1(x \sin \theta)}{D} V_g = F(x, \theta) \frac{V_g}{D} \left[ \frac{V}{m} \right] \quad (2.1)$$

$$\rho_o = \frac{a + b}{2} \text{ average slot radius } m$$

$$k = \frac{2\pi}{\lambda} ; x = k\rho_o = \frac{2\pi\rho_o}{\lambda} ; \left( \frac{\pi}{2} - \theta \right) = \text{elevation angle}$$



4-1-0546

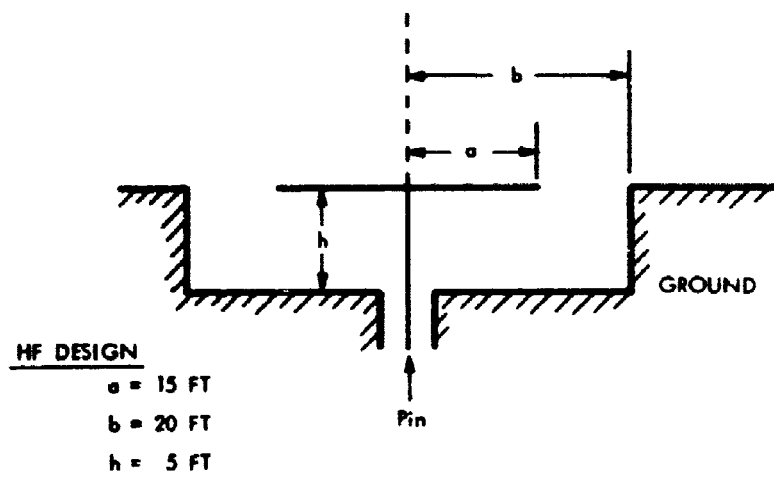


Figure 2-1. Basic Configuration of HF Annular Slot.

$J_1(x)$  = Bessel Function, first order

$V_g$  = Voltage across the slot.

$F(x, \theta) = x J_1(x \sin \theta)$  is the field pattern function. (2.2)

Normalizing this with respect to the field on the ground ( $\theta = 90^\circ$ ) yields the normalized pattern function.

$$F_n(x, \theta) = \frac{J_1(x \sin \theta)}{J_1(x)} = \frac{F(x, \theta)}{F(x, \frac{\pi}{2})} \quad (2.3)$$

The relation between the field intensity  $E$  and radiated power  $P_R$  is given by the basic equations

$$\frac{g P_R}{4\pi D^2} = \frac{E^2}{120\pi} \quad \text{and} \quad V_g^2 G_R = P_R$$

Thus

$$ED = \sqrt{30 g P_R} = \sqrt{30 g G_R} V_g \quad (2.4)$$

$G_R$  is the radiation conductance referred to the slot voltage  $V_g$ , and  $g$  is the directivity of the antenna compared to an isotropic radiator.

The relation between the directivity  $g$ , the pattern function  $F$ , and the radiation conductance  $G_R$  is obtained by combining Equations (2.1) and (2.4):

$$g = \frac{F^2(x, \theta)}{30 G_R} = \frac{x^2 J_1^2(x \sin \theta)}{30 G_R} \quad (2.5)$$

The directivity  $g$  is a function of the angle  $\theta$ . Along the ground ( $\theta = 90^\circ$ ) the directivity is

$$g_o = \frac{x^2 J_1^2(x)}{30 G_R}$$

It is convenient to compare the field intensity of an annular slot, as given by (2.4) with the field intensity obtained from a short vertical monopole over perfect ground. The vertical monopole has a sinusoidal field pattern with the maximum field intensity on the ground, and a directivity of 3. The field intensity is therefore  $(ED)_{VM} = \sqrt{3.30 P_R}$ . The ratio of the field intensity of the annular slot and that of the vertical monopole in the same direction ( $\theta$ ) defines the K-factor;

$$K = \frac{(ED)_{AS}}{(ED)_{VM}} = \frac{\sqrt{30g P_R}}{\sqrt{90 P_R}} = \sqrt{\frac{g}{3}}; g = 3K^2 \quad (2.6)$$

Thus

$$K = \frac{xJ_1(x \sin\theta)}{\sqrt{90 G_R}} = \frac{F(x, \theta)}{\sqrt{90 G_R}}$$

and the field intensity of the annular slot is

$$(ED)_{AS} = K \cdot (ED)_{VM} = \sqrt{90 P_R} \cdot K \quad (2.7)$$

$$= \sqrt{\frac{P_R}{G_R}} xJ_1(x \sin\theta) = \sqrt{\frac{P_R}{G_R}} F(x, \theta)$$

The radiation conductance  $G_R$  of a narrow annular slot in a conducting plane (perfect ground) has been calculated by Pistolnikors without limitation of the size of the slot diameter:

$$G_R = \frac{\pi x}{80} \left\{ J^2_{3/2}(x) + \frac{7}{2} J^2_{7/2}(x) + \dots \right\} \quad (2.8)$$

$$= \frac{x^4}{360} \left\{ \frac{9\pi}{2x^3} J^2_{3/2}(x) + \frac{63\pi}{16x^3} J^2_{7/2}(x) + \dots \right\}$$

$$= \frac{x^4}{360} \left\{ 1 - \frac{x^2}{5} + \frac{x^4}{56} \dots \right\} = \frac{x^4}{360} C_g.$$

Plots of  $G_R$  and  $K_0$  as a function of  $x$  are shown in Figure 2-2.

For electrically small antennas ( $x = k\rho_0 \ll 1$ ) the basic equations (2.2) (2.8) assume a very simple form:

$$F(x, \theta) \cong \frac{x^2}{2} \sin \theta \quad (2.2a)$$

$$F_n(\theta) \cong \sin \theta \quad (2.3a)$$

$$G_R \cong \frac{x^4}{360} \quad (2.8a)$$

$$g \cong \frac{360}{x^4} \frac{x^2 x^2 \sin^2 \theta}{4.30} = 3 \sin^2 \theta \quad (2.5a)$$

The directivity and the K-factor on the ground ( $\theta = 90^\circ$ ) are

$$g_0 \cong 3 ; K = 1$$

and the field intensity on the ground is

$$(ED)_0 = \sqrt{30 g_0 P_R} = \sqrt{90 P_R} \quad (2.4a)$$

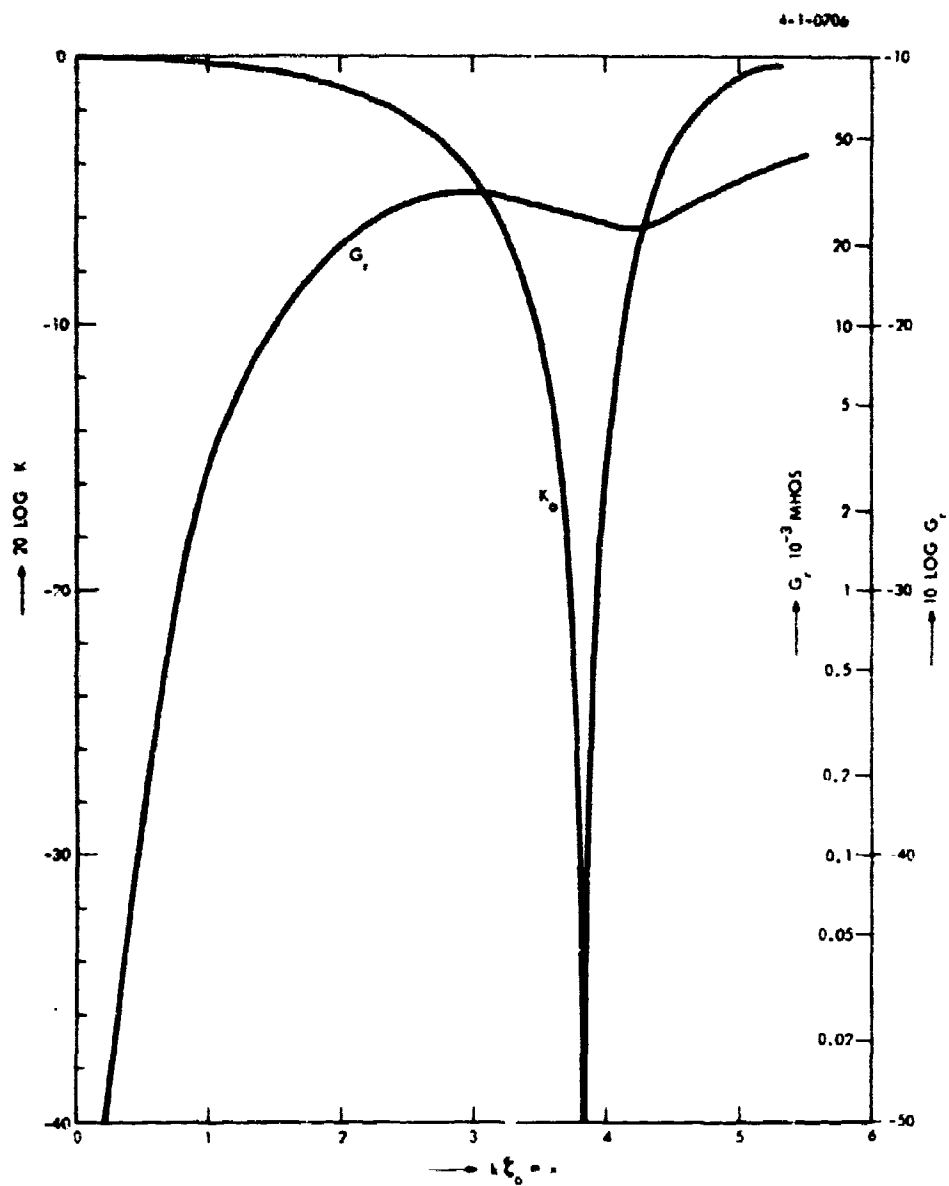


Figure 2-2. Radiation Conductance and Directivity "K" Versus  $k\rho$ .

It is evident from these relations that the annular slot of small electrical size has the same characteristics as a short vertical monopole: The elevation pattern (Figure 2.3) is sinusoidal, the directivity  $g_0=3$ , therefore  $K=1$ , which means that both antennas yield the same field intensity when energized with the same power.

As the relative size of the annular slot antenna is increased radiation pattern, directivity, and radiation conductance change. The pattern function and directivity are functions of  $x$  and the angle  $\theta$ .  $x = \frac{2\pi b}{\lambda} = \frac{\omega}{c} \rho_0$  is proportional to frequency for constant antenna dimensions.

The normalized radiation pattern  $F_n$ , referenced to the ground field intensity is given by (2.3). This is the pattern for constant slot voltage  $V_g$ . The variation of  $F_n$  with  $x$  for a given antenna size; i.e., the variation of pattern shape with frequency for a fixed medium slot radius  $\rho_0$  is shown in Figure 2-3. The dimensions of the antenna are suitable for operation up to a frequency of 30 Mc.

Cavity radius	$b = 20$ ft	6 m
Hat radius	$a = 15$ ft	4.57 m
Slot width	$b-a =$ ft	1.525 m
Medium slot radius $\rho_0 =$	$\frac{a+b}{2} = 17.5$ ft	5.29 m

It is seen that the pattern is sinusoidal as long as  $b \ll \lambda$  ( $x \ll 1$ ). As i.e., the frequency is increased the pattern broadens until  $x = 1.84$  where the Bessel function  $J_1(x \sin \theta)$  has a maximum. Up to this point the maximum of the pattern is on the ground. As the frequency is further increased the main lobe lifts off the ground and increases in size. The radiated power increases also as is evident from the increased area covered by the pattern. The lobe maximum is at an angle  $\theta_m$  determined by the first maximum of  $J_1(x \sin \theta_m)$  which occurs at  $x \sin \theta_m = 1.84$ . Thus  $\sin \theta_m = 1.84/x$ .

4-1-0749

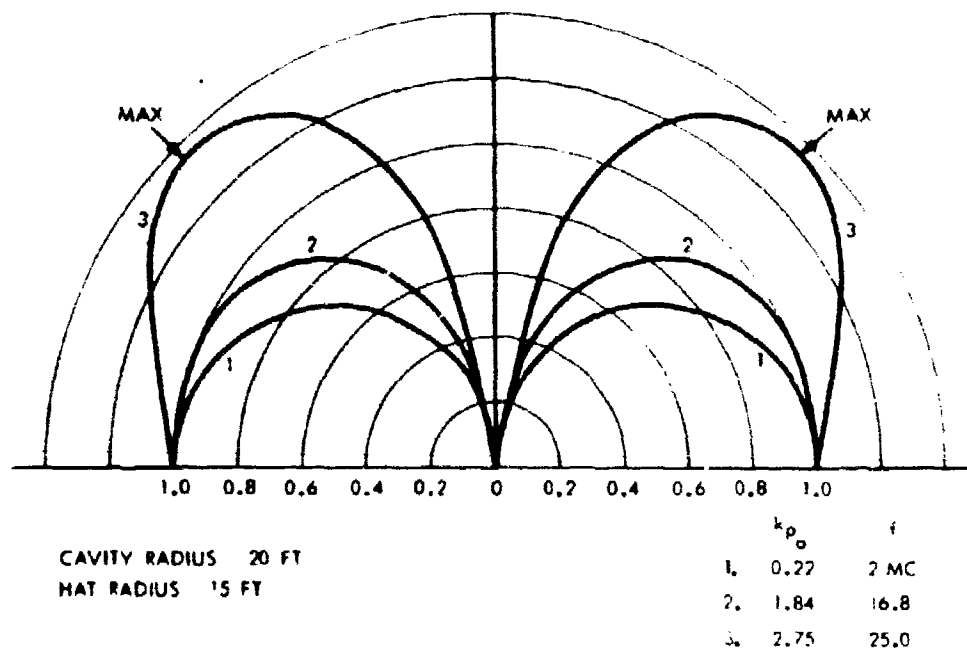


Figure 2-3. Normalized Radiation Pattern for Annular Slot  
(Constant Field Intensity Along Ground).

The radiation pattern for constant radiated power is given by (2.7). The field intensity at constant distance in the far field is proportional to  $K$ . The variation of the field intensity on the ground ( $\theta = 90^\circ$ ) is represented by  $K_o = \frac{x J_1(x)}{\sqrt{90 G_R}}$  and is plotted on Figure 2-2 as a function of  $x$ .

Figure 2-4 shows radiation patterns at various frequencies for the same antenna ( $b = 20$  feet) as used for Figure 2-3. As the frequency is increased the ground field intensity is reduced and a lobe develops whose elevation increases as the frequency is increased. The reduction of the ground field intensity is due to the fact that the radiation is more and more concentrated at higher elevation angles and therefore, with the same total radiated power, the radiation at the lower angles is reduced. This is in contrast to the case of constant slot voltage  $V_g$  where constant ground field intensity is maintained at the expense of increased radiated power. When the frequency is increased to the point where  $x = 3.83$  or  $\rho_o/\lambda = 0.61$ , the Bessel function  $J_1$  passes through zero and the ground field is zero,  $K_o = 0$  (Figure 2-2). All the energy goes into higher elevation angles, the maximum of the lobe appearing at an angle given by  $\sin \theta_m = 1.84/x$ . At still higher frequencies ( $x > 3.83$ ) a second lobe develops on the ground, giving rise to a ground field intensity that is almost as large as it is at low frequencies ( $x < 1$ ). This is apparent from Figure 2-2 which shows  $K_o \approx 1$  at  $x = 5.4$ .

The directivity  $g$  of the annular slot is given by (2.5). It is a function of  $x$  and the angle  $\theta$ . Of particular interest is the directivity ( $g_o$ ) in the direction  $\theta = 90^\circ$  (along the ground), and the directivity  $g_m$  in the direction of the first lobe maximum. From (2.5) we obtain

$$g_o = \frac{[x J_1(x)]^2}{30 G_R} = 3 K_o^2$$

$$g_m = \frac{[x J_1(x \sin \theta_m)]^2}{30 G_R} = \frac{F^2(x, \theta_m)}{30 G_R}$$



4-1-0545

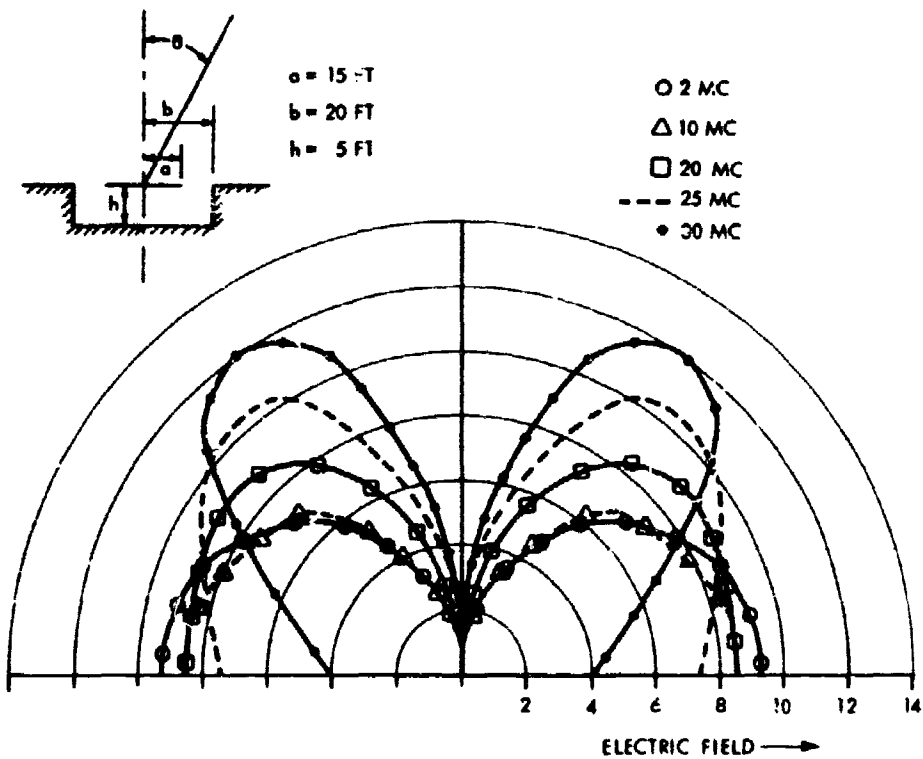


Figure 2-4. Radiation Patterns of Annular Slot in Vertical Plane  
(Constant Radiated Power).

These directivities together with the elevation angle  $\epsilon_m = 90^\circ - \theta_m^\circ$  of the first lobe maximum are plotted versus  $x = k\rho_0$  on Figure 2-5. For  $x \leq 1.84$  the lobe maximum is on the ground ( $\epsilon_m = 0^\circ$ ) and  $g_o = g_m$ . The directivity  $g_o = 3$  for  $x < 0.5$ , and decreases (because of pattern broadening) until  $g_o = g_m = 2.42$  at  $x = 1.84$ . With increase of  $x$  beyond 1.84 ( $x > 1.84$ ), the main lobe lifts off the ground, and  $g_o$  (which is proportional to the radiated power density along the ground) decreases to zero at  $x = 3.8$ , since  $J_1(3.8) = 0$ . At this point the pattern has a null on the ground. For  $x > 3.8$  the ground directivity  $g_o$  increases again up to value of 2.8, which is close to the value at low frequencies. In this same range  $x > 1.84$   $g_m$ , after a very slight dip, increases rapidly past the point  $x = 3.8$  where the ground field has its null ( $g_o = 0$ ), until a maximum is reached. This occurs at  $x = 4.4$  where  $g_m = 8.9$  and the lobe elevation angle  $\epsilon_m = 65^\circ$ . In the range  $1.84 \leq x \leq 3$  the lobe elevation angle increases rapidly from  $0^\circ$  up to  $52^\circ$ . For  $x > 3$  the increase of  $\epsilon_m$  is somewhat slower.

### 2.1.3 Admittance of the Annular Slot Antenna

To establish the efficiency and bandwidth of the annular slot antenna, as well as the tuning and matching circuits, one must know the terminal admittance of the antenna. Since the radiation or far field of the antenna is due almost entirely to the fringing of the electric field maintained across the gap between the disk and adjacent highly conducting ground it was possible to derive the radiation characteristics by considering the circular diffraction of an annular slot in a perfectly conducting screen. To obtain the admittance one must consider the environment of the annular slot. Below the top disk at a distance  $h$  is a highly conducting ground screen. This together with the surrounding earth forms a cylindrical cavity. Thus the antenna may be considered as a cavity backed annular slot with an electric field across the slot producing the radiation. An analysis of the performance of a cavity backed annular slot antenna - without a lossy layer of debris over it - has been given by Galejs and Thompson.<sup>4</sup> Their results have been expanded by Galejs and Row (ARL Research Report No. 359) to cover the question of debris effects on the performance of the annular slot antenna.

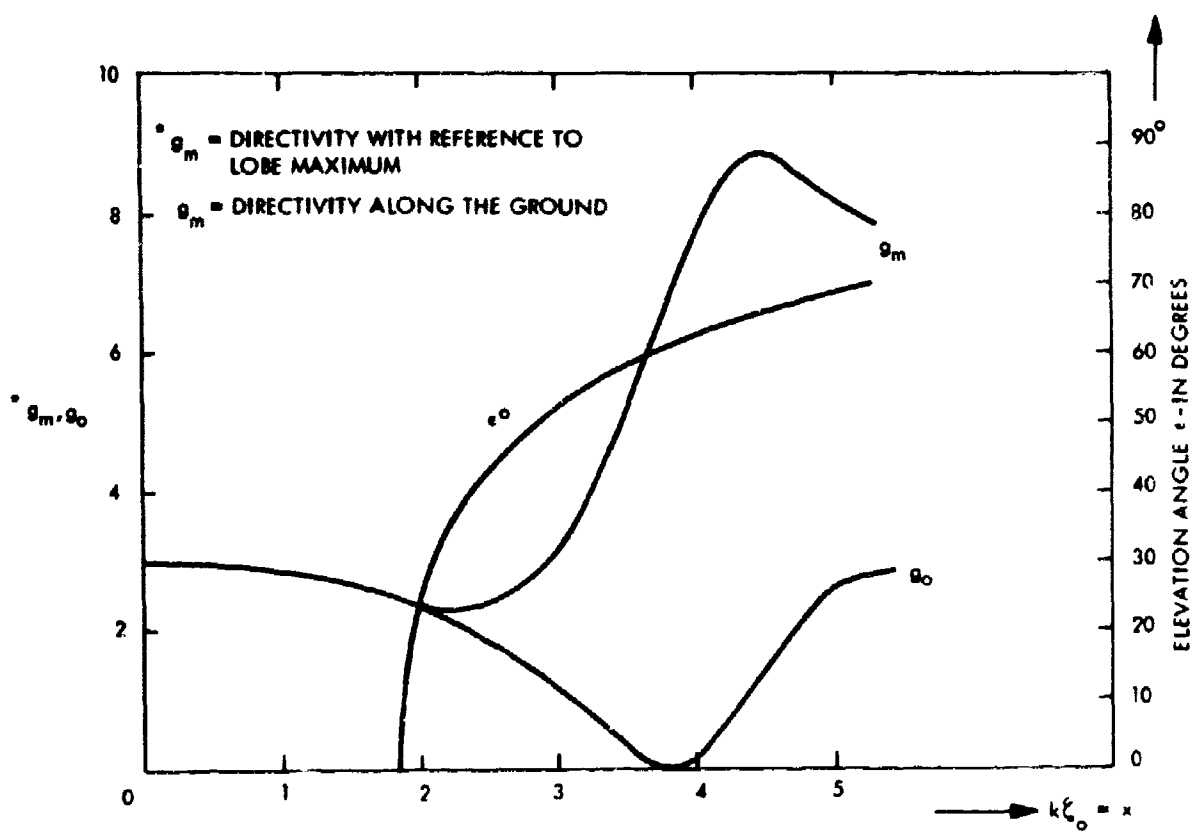


Figure 2-5. Directivity and Main Lobe Elevation Angle.

The analysis of the cavity backed annular slot antenna without debris cover yields the admittance across the slot. The edge of the disk and the edge of the cavity are considered as terminals. The actual feed points of the antenna are at the center of the disk and the ground plane forming the bottom of the cavity. To obtain the terminal admittance at this point the slot admittance must be transformed to the center feed point, which can be accomplished by using radial transmission line analysis. (See Section 2.2.7)

The admittance  $Y_0$  across the slot is composed of two parts:

$$Y_T = Y^+ + Y^-$$

$Y^+$  is the admittance reflected to the slot plane by the outside space,

$Y^-$  is the admittance reflected by the cavity.

Using a zero order approximation of the field distribution across the slot ( $E_0(\rho) = a_0/\rho$ ) one finds:

$$Y^+ = \frac{(k\rho_0)^4}{360} \left[ 1 - \frac{(k\rho_0)^2}{5} + \frac{(k\rho_0)^4}{56} + \dots \right] \quad (2.9)$$

$$+ j \frac{k\rho_0}{60\pi} \left[ \ln \frac{8\rho_0}{\rho_2 - \rho_1} - \frac{1}{2} + \frac{2}{3} (k\rho_0)^2 + \dots \right] = G_R + jB_S$$

where  $\rho_0 = (a + b)/2$ . This is in agreement with the principal mode admittance seen by a coaxial line that radiates into a half space, as calculated by Levine and Papas.<sup>2</sup>

The real part of  $x^+$  is the radiation conductance  $G_R$  which is in agreement with (2.8). The imaginary part of  $x^+$  is a capacitive susceptance ( $B_S$ ) representing the slot fringe capacity due to the outside field. Both  $G_R$  and  $B_S$  are independent of the dielectric constant of the medium inside the cavity.

The admittance reflected by the cavity is

$$Y^- = -4\pi j\omega\epsilon_1 \left( \frac{\rho_0}{b-a} \right)^2 \sum_{q=1}^{\infty} \frac{\coth \left[ \sqrt{\lambda_q^2 - k_1^2} h \right]}{\sqrt{\lambda_q^2 - k_1^2}} \quad (2.10)$$

$$\left[ \frac{J_0(\lambda_q a) - J_0(\lambda_q b)}{\lambda_q b J_1(\lambda_q b)} \right] = G^- + j B^-$$

where the height  $h$  of the cavity is taken negative :  $h < 0$ .  $\lambda_q$  is defined by  $J_0(\lambda_q b) = 0$ .  $k_1$  is the complex wave number:

$$k_1 = \omega \sqrt{\mu_0 \epsilon_1} \sqrt{1 - \frac{\sigma_1}{\omega \epsilon_1}} ; \quad \epsilon_1 = \epsilon_0 \epsilon_{1r}$$

$\epsilon_{1r}$  is the dielectric constant of the cavity fill material  $\epsilon_{1r}$  and  $\sigma_1$  are the dielectric constant and conductivity respectively of the cavity fill material. Its loss tangent is  $\tan \delta_1 = \frac{\sigma_1}{\omega \epsilon_1}$  and this determines the magnitude of  $G^- = 0$ . It is apparent that, while  $Y^+$  is dependent on  $k_1$ ,  $Y^-$  is dependent on  $k_1$ . This means that  $Y^+$  is not affected by the dielectric in the cavity, but  $Y^-$  is affected because the velocity of propagation inside the cavity is reduced by  $\sqrt{\epsilon_{1r}}$ .

The total admittance is then

$$Y_T = (G_R + G^-) + j (B_S + B^-) = G_R + j B_T \quad (2.11)$$

with

$$G_T = G_R + G^- \text{ and } B_T = B_S + B^-$$

Considering the susceptance  $B^-$ , one finds that it is capacitive for small values of  $b/\lambda$ . Then all the cavity modes are below cutoff and the cavity reflects a capacitive susceptance. Since  $B_s$  is also capacitive, representing the slot capacity due to the outside field, the total susceptance  $B_T$  is capacitive for small values of  $b/\lambda$ . As the frequency is increased one of the cavity modes will propagate. Now cutoff occurs when  $\lambda_q^2 = k_1^2 = (2\pi/\lambda)^2 \epsilon_{1r}$ , and where the  $\lambda_q$  are determined by the roots of  $J_0(\lambda_q b)$ . In the case of a low-loss cavity-fill material  $k_1^2 \cong (\frac{2\pi}{\lambda})^2 \epsilon_{1r}$ . Thus with the first three roots of  $J_0(\lambda_q b)$  the following relations are obtained:

$$\lambda_{q1} b = 2.403 = bk_1$$

$$\lambda_{q2} b = 5.52 = bk_1 \quad (2.12)$$

$$\lambda_{q3} b = 8.65 = bk_1$$

This results in  $b/\lambda$  values as tabulated, both for air in the cavity and asphalt ( $\epsilon_{1r} = 2.8$  and  $\epsilon_{1r} = 3.65$ ).

$bk_1$	$b/\lambda$ for air $\epsilon_{1r} = 1$	$b/\lambda$ for asphalt $\epsilon_{1r} = 2.8$	$b/\lambda$ for asphalt $\epsilon_{1r} = 3.65$
2.40	0.384	0.23	0.20
5.52	0.878	0.525	0.45
8.65	1.385	0.822	0.72

Thus, the first propagating mode starts when  $b/\lambda > 0.23$  or  $b/\lambda > 0.20$  if the cavity is filled with asphalt which has a dielectric constant,  $\epsilon_{1r} = 2.8$  or  $\epsilon_{1r} = 3.65$ , respectively.

For the case  $b/\lambda \ll 1$  the antenna acts like a radiating capacitor. The total capacity is that of the disk against the cylindrical cavity, including the fringe field. The capacity  $C_T$  is approximately equal to the capacity of two parallel plates at a distance  $h$ , one of the plates being very large, representing the ground plane.

$$C_T = \frac{\epsilon_1 \pi a^2}{h} \left[ 1 + \frac{2h}{\pi a} \left( \ln \frac{4\pi a}{h} + 1 \right) \right] \quad (2.13)$$

The computation of the admittance of the annular slot antenna can be accomplished with a digital computer after the dimensions of the antenna have been chosen. The cavity diameter  $2b$  is determined by the desired radiation pattern at the upper end of the frequency band in which the antenna shall operate, in our case 30 Mc. The size of  $b$  determines the medium cavity radius  $\rho_0 = \frac{a+b}{2}$  and thereby  $x = \frac{\omega \rho_0}{c} = \frac{2\pi}{\lambda} \rho_0$  where  $\lambda$  is the wavelength in air. It should be noted that the radiation characteristics are not affected by the dielectric in the cavity, whereas the admittance depends on the characteristics of the cavity fill material. Therefore the relations describing the radiation characteristics as presented before can be used without change.

The limits in the choice of  $x$ ; i.e., of  $\rho_0$  are determined as follows: If  $x$  is made large, lobing of the radiation pattern occurs and the energy is radiated at high elevation angles. Thus with a choice of  $x = 3.84$  one would obtain a lobe elevation angle of  $60^\circ$  and there would be no radiation along the ground. On the other hand, the efficiency drops as  $b$  is made smaller, since the radiation conductance  $G_R$  is proportional to  $x^4$  and therefore drops very rapidly as  $x$  and therefore  $b$  is decreased, as shown in Figure 2-2. This then determines the lower end of the useful frequency band of the antenna.

The computation of the admittance was carried out for the antenna dimensions shown in Figure 2-1. The radiation patterns of this antenna are shown on Figure 2-4. The results of the computation are shown on Figures 2-6, 2-7, 2-8, and 2-9 together with curves describing the effects of debris covering the antenna\*. Figure 2-6 shows  $\text{Im} \{Y_0\} = B_S + B^- = B_T$  versus frequency (curve marked 0 debris). The total susceptance  $B_T$  is composed of two parts.  $B_S$  is the susceptance of the fringe capacity  $C_S$  between the edge of the disk and

---

\* Effects of debris will be discussed in a following section

4-1-0750

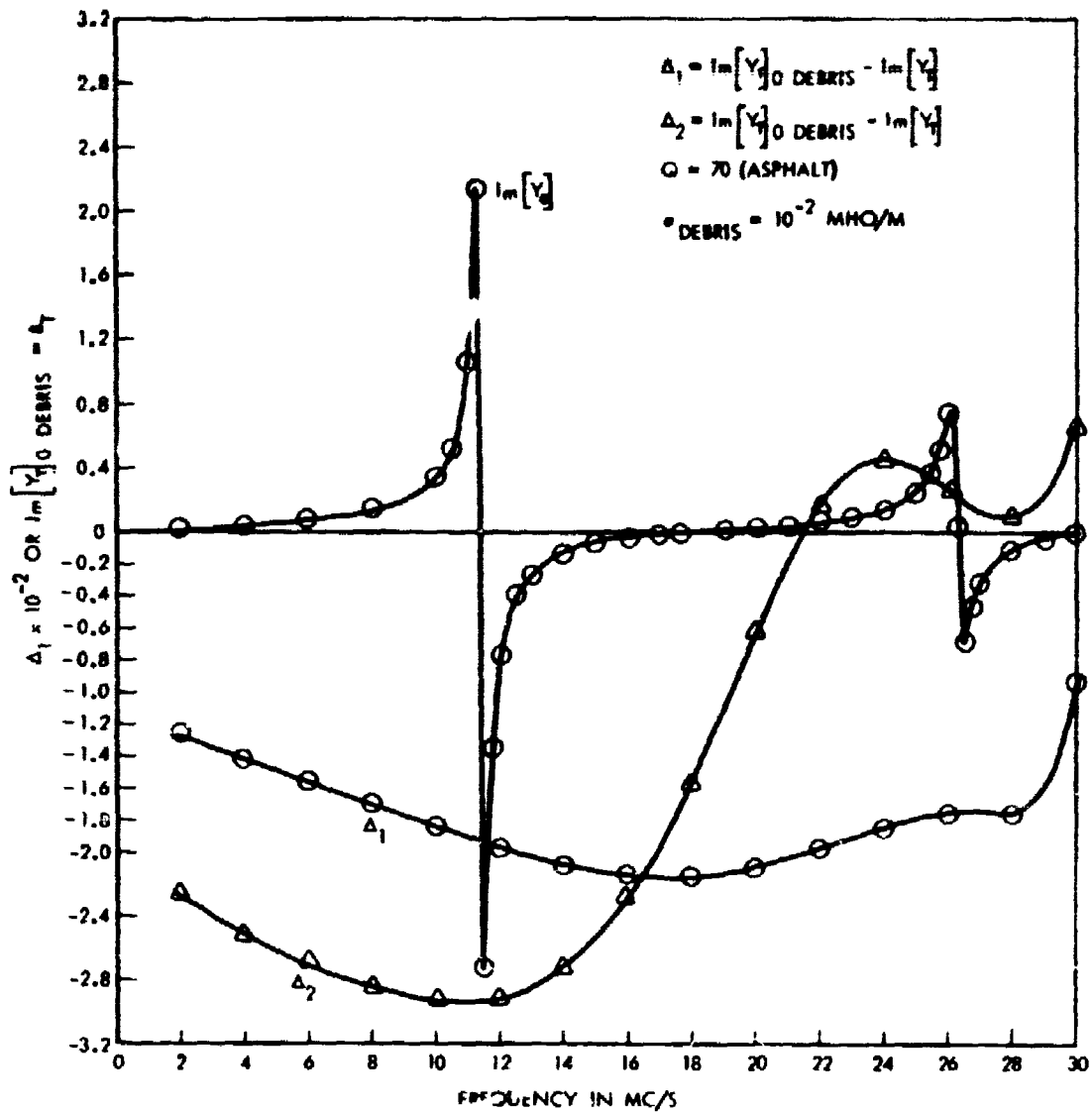


Figure 2-6. Total Susceptance of 40° Annular Slot Versus Frequency With and Without Debris.



the cavity. Its value changes slightly with frequency, and varies from approximately  $300 \mu\mu F$  at 3 Mc to  $25^0 \mu\mu F$  at the upper end of the band.  $B^-$  is capacitive until the first cutoff frequency is reached. This is the case for  $b/\lambda = 0.23$ ,  $f_c = 11.5$  Mc, for a cavity fill material with  $\epsilon_{1r} = 2.8$ . At this point  $B^-$  becomes very large and changes sign. As the frequency is increased above  $f_c$ ,  $B^-$  represents an inductive susceptance which decreases with frequency goes through zero, and becomes capacitive again until the second cutoff frequency is reached at the point where  $b/\lambda = 0.525$ ;  $f_{c2} = 26.2$  Mc. At this point  $B^-$  has a positive maximum again, but not as pronounced as at the first cutoff frequency, changes sign and becomes inductive, thus repeating a similar variation as occurred at the first cutoff frequency.  $B_T$  is the parallel combination of the slot susceptance  $B_S$  and the cavity susceptance  $B^-$ . Its variation is shown on Figure 2-6. The cutoff frequencies are easily recognizable at those points where  $B_T$  abruptly changes sign. This is similar to the series resonance of a series L - C circuit. In between the two cutoff frequencies, a parallel resonance condition is reached at about 18 Mc. This is the case when  $B^- = -B_S$ ; i.e., when there is parallel resonance between the capacitance  $B_S$  of the slot and the inductance of the cavity.

The real part of the admittance  $Y_T$  or total conductance is shown in Figure 2-7:  $\text{Re } Y_T = G_T = G_R + G^-$ . The total conductance is composed of two parts.  $G_R$  is the radiation conductance, which is the same as in the air case ( $\epsilon_{1r} = 1$ ), Equations (2.8) and (2.9). The variation of  $G_R$  with frequency is shown in Figure 2-8.  $G_R$  is extremely small at low frequencies and increases very rapidly with the forth power of the frequency. At  $x \approx 3$  a maximum is reached with  $G_R \approx 0.03$  mho, at a frequency  $f = 26.9$  Mc. The cavity conductance  $G^-$  has been computed using a loss tangent of the cavity dielectric  $\text{tg } \delta_1 = \frac{1}{70}$  Figure 2-7.  $G^-$  has two pronounced maxima of 4 mho and 1.5 mho at the cutoff frequencies: 11.5 Mc and 26.2 Mc. These are rather high values and, since the cavity susceptance is almost zero at these points, this has a shunting effect. The slot is shunted by a comparatively low resistance, so that a power loss is experienced at these frequencies. Between the two cutoff frequencies the conductance  $G^-$  is low, reaching a

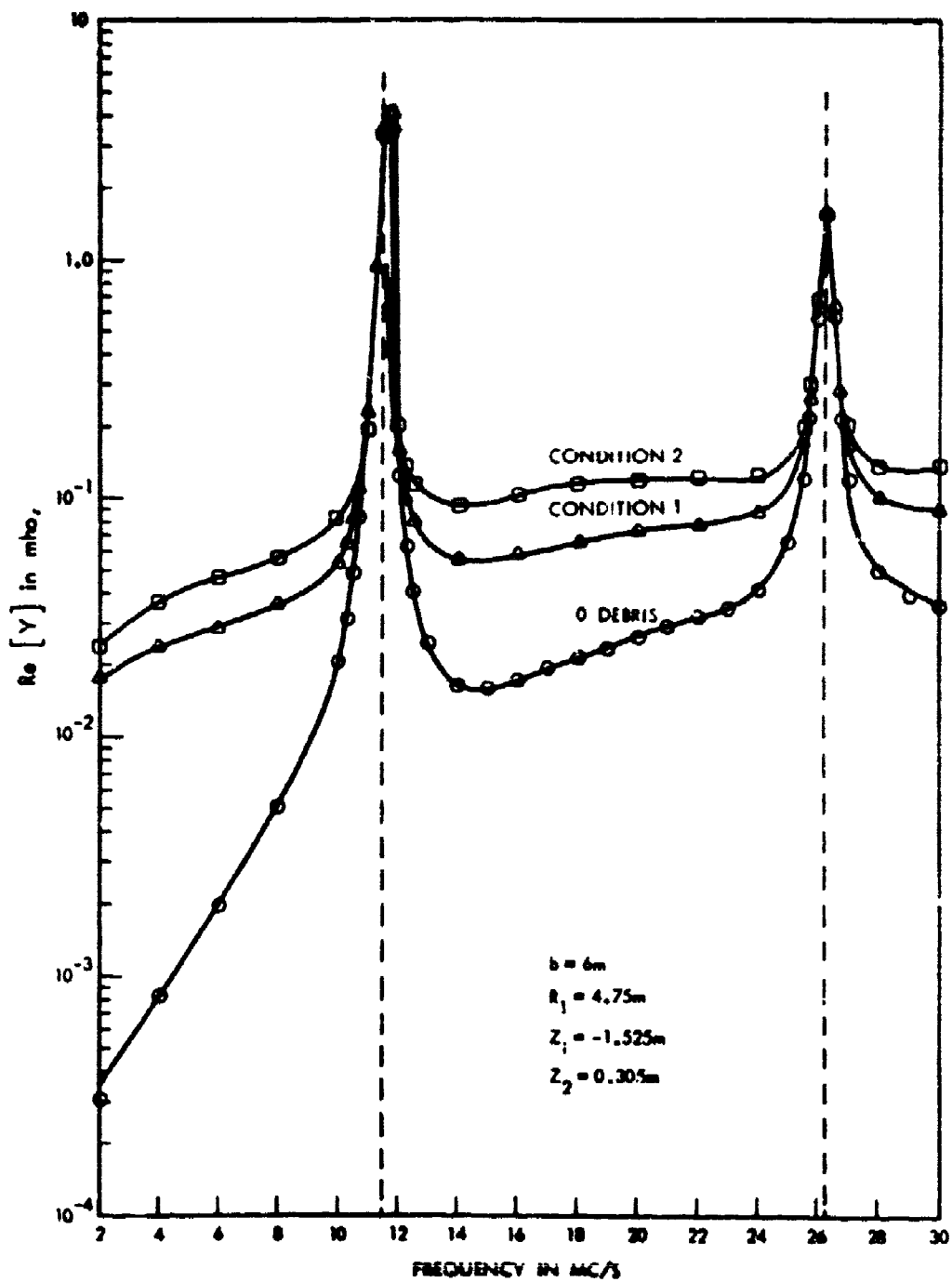


Figure 2-7. Total Conductance of 40° Annular Slot Versus Frequency With and Without Debris.

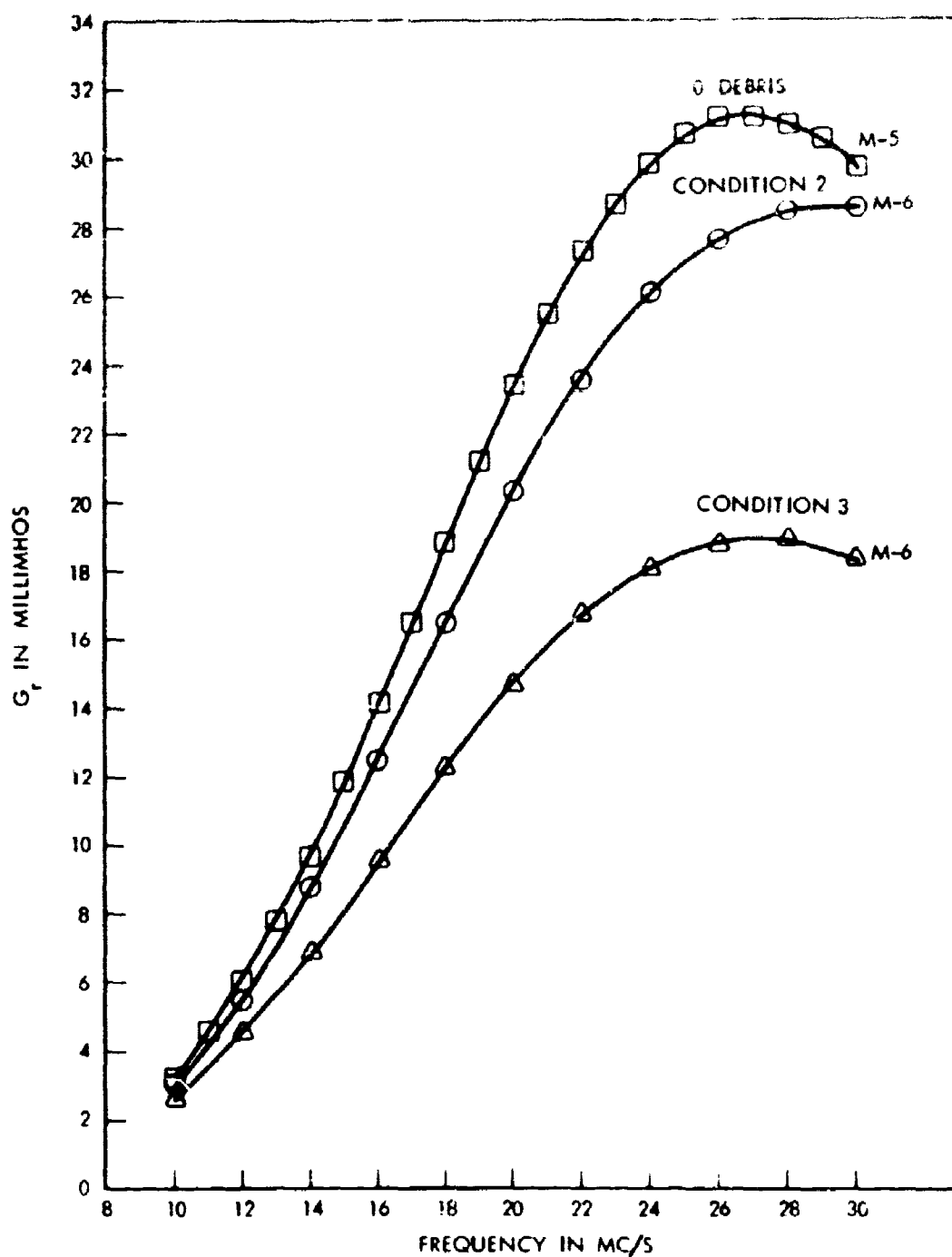


Figure 2-8. Radiation Conductance of 40° Annular Slot Versus Frequency With and Without Debris.

minimum at about 15 Mc. Figure 2-9 shows the conductance/susceptance ratio of this antenna as a function of  $b/\lambda(\text{asph})$ . There are three points where the  $G_T/B_T$  ratio has extrema. These are

$b/\lambda(\text{asph})$	0.39	0.58	0.88	
$\lambda(\text{asph})$	15.4	10.3	6.83	m
$\lambda_{\text{air}} = 2.8 \lambda(\text{asph})$	26.0	17.3	11.4	m
f	11.5	17.4	26.2	Mc

The first and third extremum are at the cutoff frequencies of the cavity. Here  $G^-$  representing losses in the cavity is comparatively large.  $G_R = G^- + G_T$  is therefore also comparatively large. At these points the efficiency of the antenna is low, as will be shown in the following section.

The point in between at  $f = 17.4$  Mc is of a different nature, as far as  $G^-$  is concerned.  $G^-$  is very small at this frequency and  $G_R$  is considerably larger than  $G^-$  so that  $G_T = G^- + G_R$  is again comparatively large. But in this case the efficiency is high because  $G_R \gg G^-$  and  $G_R \sim G_T$ . As will be shown in the following section, parallel resonance occurs at the middle frequency (18.4 Mc) and this is the condition for high efficiency. At the cutoff frequencies there is a series resonance condition which yields very low efficiency. In all three cases the total susceptance  $B_T = 0$  and changes sign, but at the cutoff frequencies the losses ( $G^-$ ) are high, whereas at the parallel resonance frequency the losses are small.

Knowing the variation of the admittance with frequency as described by the  $B_T$  and  $G_T$  curves one can define an equivalent circuit which has the same resonance points and similar behaviour over the frequency range of interest. (Figure 2-10) and is useful in describing the general behaviour of the admittance variation. The circuit consists of a susceptance  $B_S$  representing the slot capacity. Parallel with  $B_S$  are series circuits of  $L, C$  and small  $R$ , one for each cutoff frequency. At the cutoff frequency  $\omega_1 L_1 = \frac{1}{\omega_1 C_1}$  for the

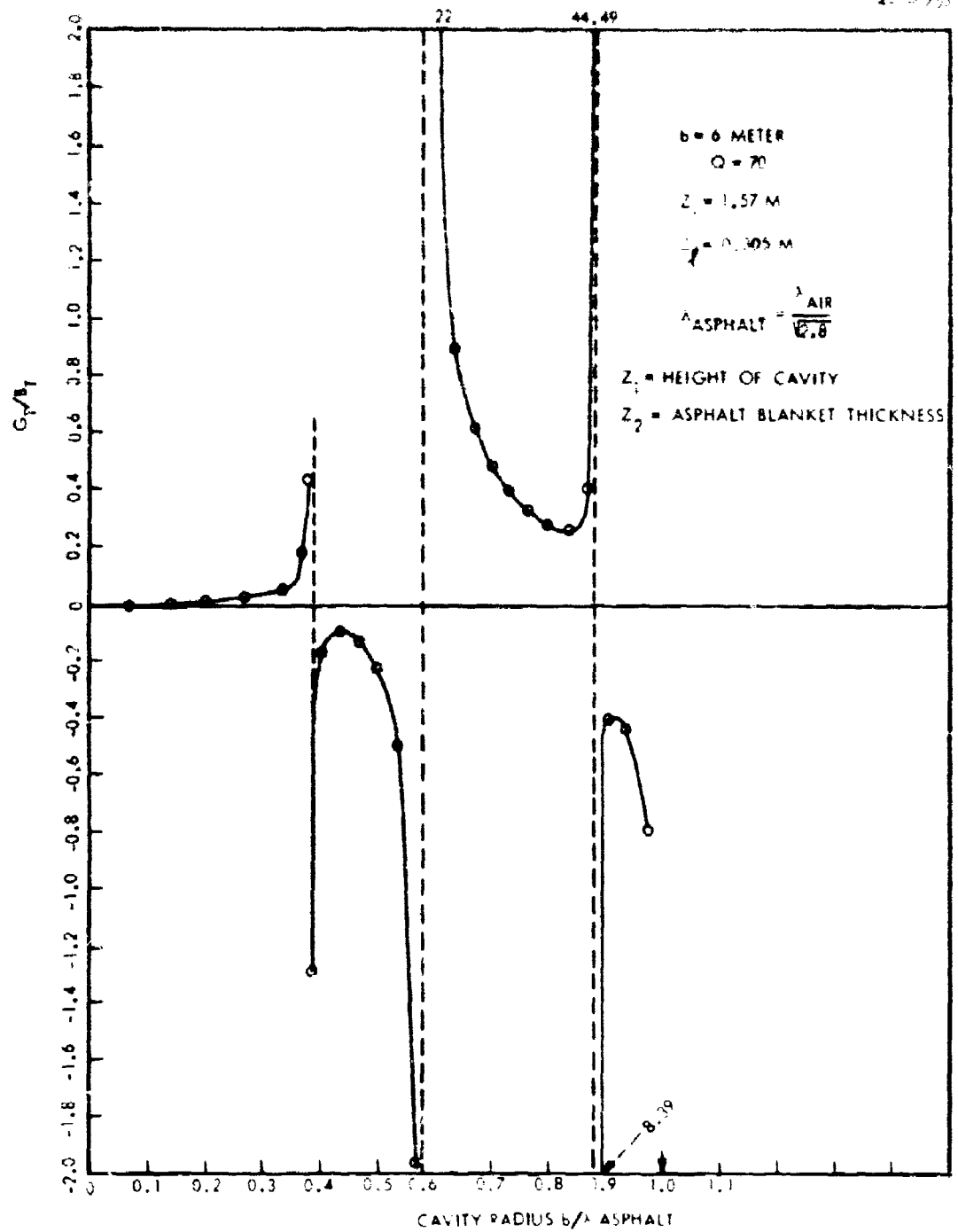
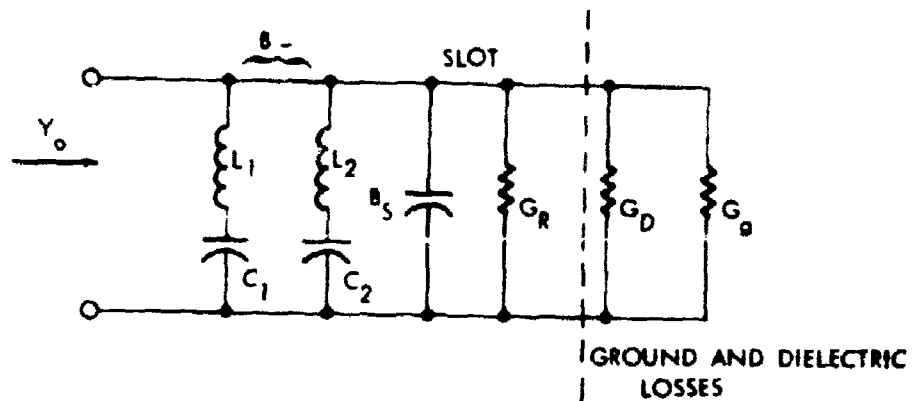


Figure 2-9, Total Conductance-Susceptance Ratio Versus  $b/\lambda$  for 40° Annular Slot.

4-1-0765



$G_R$  = RADIATION CONDUCTANCE

$B_s$  = SLOT SUSCEPTANCE

$B^-$  = CAVITY SUSCEPTANCE

$G_D$  = DIELECTRIC LOSS CONDUCTANCE

$G_g$  = GROUND LOSS CONDUCTANCE

$Y_o$  = INPUT ADMITTANCE

Figure 2-10. Equivalent Antenna Circuit Including Dielectric and Ground Losses.

first cutoff frequency  $f_1$ , and  $\omega_2 L_2 = \frac{1}{\omega_2 C_2}$  for the second cutoff frequency  $f_2$ , etc. Figure 2-10 shows two series circuits for the two cutoff frequencies occurring in the frequency range 2-30 Mc. In addition there are the conductances,  $G_R$  representing the radiation losses,  $G^-$  representing cavity losses, and  $G_g$  representing ground losses. The parallel resonances are obtained when the susceptance  $B_s$  of the slot capacity is equal in magnitude to the inductive susceptance of the series circuits; i.e., every time when  $B^- = -B_s$ . The slot capacity is then in resonance with the resulting inductance of one of the series circuits. As mentioned before these are important conditions since they yield high efficiency.

The parameters of the equivalent circuit can be obtained from the computed conductance as a function of frequency. For this purpose we consider the admittance of a series resonance circuit near resonance.

$$Y_1 = \frac{1}{R + j(\omega L - \frac{1}{\omega C})} \cong G_o \frac{1 - j 2\delta Q}{[1 + (2\delta Q)^2]} = G - j B$$

with

$$G_o = \frac{1}{R}; Z_o = \sqrt{\frac{L}{C}}; Q = \frac{\omega_o L}{R} = Z_o G_o; \omega_o = \frac{1}{\sqrt{LC}}$$

$$\delta = \frac{\omega - \omega_o}{\omega_o} = \frac{\Delta\omega}{\omega_o}$$

The conductance of this series circuit has a frequency dependence near its resonance frequency which is quite similar to the computed conductance curve of the annular slot antenna near the cutoff frequencies. The conductance  $G$  has a sharp peak of magnitude  $G_o$  at the resonance frequency  $f_o$ , which is thereby determined. The bandwidth  $\Delta\omega$  is determined from those frequencies where  $G$  has dropped to one half of the peak value. From  $\omega_o$ ,  $G_o$ , and  $\delta = \frac{\Delta\omega}{\omega_o}$  one obtains

$$Q = \frac{1}{2\delta} ; Z_0 = \frac{Q}{G_0} = \frac{1}{2\delta G_0}$$

and finally

$$C = \frac{1}{\omega_0 Z_0} ; L = \frac{Z_0}{\omega_0} ; \frac{1}{G_0} = R = \frac{Z_0}{Q} = Z_0 2\delta$$

If, on the other hand, one does not have the conductance of the antenna as a function of frequency one can estimate the static capacity of the antenna and thereby get  $C$ . Then the losses in the antenna cavity can be estimated from the  $Q$  of the cavity filler material. The cutoff frequency is equal to the resonance frequency, thus yielding  $\omega_0$ . From these  $L$ ,  $R$  and  $Z_0$  can be calculated.

This technique describes only the behavior of the admittance close to the first cutoff frequency. It can be refined by assuming several series circuits, each resonating at the consecutive cutoff frequencies as mentioned before. The determination of the various components of the equivalent circuit becomes then rather cumbersome.

A simpler representation of the behavior of the admittance frequency function using transmission line analogy is given in the following section in connection with efficiency considerations.

#### 2.1.4 Efficiency of the Annular Slot Antenna

The efficiency of an antenna is determined by the ratio of the radiated power to the total input power of the antenna. The total input power is composed of two parts: the radiated power and the power caused by the losses in the antenna. There are two kinds of losses in the antenna proper (not considering the tuning circuit); i.e., losses in the dielectric filling the cavity, and ground losses in the surrounding ground including copper losses. The dielectric losses are  $V_g^2 G^-$ , the ground losses are  $V_g^2 G_g$ . The radiated power is  $V_g^2 G_R$ , hence the efficiency



$$\eta = \frac{V_g^2 G_R}{V_g^2 (G_R + G^- + G_g)} = \frac{G_R}{G_R + G_L} = \frac{1}{1 + G_L/G_R}$$

where  $G_L = G^- + G_g$  represents the sum of all losses in the antenna. In the case of debris covering the antenna the ground losses are increased, resulting in an increase of  $G_g$ . The total susceptance of the antenna is  $B_T = B_S + B^-$ .

#### 2.1.4.1 General Efficiency Considerations

To obtain a first estimate of the losses which determine the efficiency of the antenna we make use of some basic energy relations. In circuits as well as in transmission lines the effect of losses can be estimated by considering the ratio of the average stored electromagnetic power and the average dissipated power which is the Q-factor of the system. In a component with the admittance  $Y = G + jB$  the average stored power is  $V^2 B$  and the average dissipated power is  $V^2 G$ , so that  $Q = B/G$ . If there are a number of components in parallel connection one has the total conductance

$$G_T = G_1 + G_2 + \dots G_n$$

The average stored total power in a circuit of parallel components with the same voltage applied to each of them can be expressed by  $W_p = V^2 B_c$ .  $B_c$  is a capacitive susceptance which contains the same stored power as the whole system. In a resonant parallel system of L, C and G,  $B_c = Y_o = \sqrt{\frac{C}{L}}$  whereas at very low frequencies  $B_c = \frac{1}{\omega L}$  and at very high frequencies  $B_c = \omega C$ .

Relating the conductance of each component to the average total stored power in the circuit one obtains the Q of each component as  $Q_n = \frac{B_c}{G_n}$  and the following expression for the total  $Q_T$ , which is defined as

$$Q_T = \frac{B_c}{G_T} :$$

$$\frac{B_c}{Q_T} = \frac{B_c}{Q_1} + \frac{B_c}{Q_2} + \dots \frac{B_c}{Q_n}$$

or

$$\frac{1}{Q_T} = \frac{1}{Q_1} + \frac{1}{Q_2} + \dots + \frac{1}{Q_n}$$

With the aid of the Q-factors the losses in the circuit can be evaluated, since the Q-factors are characteristics of the components and materials and can be readily estimated.

In an antenna the active power divides into two parts: radiated power and dissipated power. The ratio of radiated power and stored power defines the radiation power factor  $p$  of the antenna, which plays an important role in efficiency considerations:

$$p = G_R/B_c = \frac{1}{Q_R}$$

The radiation power factor is the reciprocal of the radiation  $Q_R$ .

With respect to efficiency the antenna is characterized by the following data:

The effective susceptance designating the stored power	$B_c$
The radiation power factor	$p = G_R/B_c$
The loss-Q of the antenna	$Q_L = B_c/G_L$
The total-Q of the antenna	$Q_T = B_c/G_T$

With

$$\frac{1}{Q_T} = \frac{1}{Q_R} + \frac{1}{Q_L} = p + \frac{1}{Q_L}$$

and

$$p Q_L = G_R/G_L$$

The efficiency can be expressed as

$$\eta = \frac{G_R}{G_T} = p Q_T = \frac{p Q_L}{1 + p Q_L} = \frac{1}{1 + G_L/G_R}$$

$Q_T$  is related to the bandwidth  $\Delta\omega$  of the antenna considered as a circuit loading the generator:

$$\frac{1}{Q_T} = \frac{\Delta\omega}{\omega}$$

Hence

$$\frac{\eta}{Q_T} = \eta \left( \frac{\Delta\omega}{\omega} \right) = p = \frac{G_R}{B_c}$$

The efficiency bandwidth product is equal to the radiation power factor which, therefore, is a measure of performance of the antenna. Electrically small antennas have a small radiation power factor because the radiation conductance is small, and have a  $Q_L$  which is much smaller than  $1/p$  so that the efficiency  $\eta \approx p Q_L$ , and the efficiency bandwidth product are small. The only way to increase the efficiency of the small antenna is to make  $Q_L$  as large as possible; i.e., decreasing the losses, thereby reducing the bandwidth.

Electrically large antennas, however, have a large radiation power factor because the radiation conductance is large. The loss  $Q_L$  can be small or large depending on the resonance conditions. Parallel resonance conditions are favorable since  $Q_L$  is then relatively large, resulting in  $p Q_L \gg 1$ . In this case the efficiency

$$\eta = 1 - \frac{1}{p Q_L} = 1 - G_L/G_R$$

can be quite high, depending on  $Q_L$ .

The antenna losses are conveniently determined from  $Q_c$  of the antenna. The controlling factor are the dielectric losses in the material with which the antenna is filled. Considering only the dielectric losses one obtains

$$Q_c = \omega C_1 / G_1 = 1 / \tan \delta$$

where  $\tan \delta$  is the loss tangent of the dielectric. Measurements of the loss tangent of asphaltic material in the frequency range 0.5 to 30 Mc show that  $Q_c$  values ranging from 50 to 100 and higher can be obtained. To these dielectric losses ground and copper losses can be added thus reducing  $Q_c$ . Our measurements indicate that  $Q_c$  values of 25 to 40 and up to 70, including all losses, for frequencies up to 18 Mc are realizable. Both the upper and lower limits of  $Q_c$  have been used in the computations.

The preceding results of computations of the prototype annular slot antenna show that the admittance of the antenna across the slot is similar in behavior to that of an open ended transmission line with low losses. A brief analysis of a resonant transmission line using the basic energy relations outlined above will be useful in explaining the behavior of the efficiency and admittance dependance of the antenna.

To bring out the basic characteristics of the antenna in the simplest form, we consider a uniform transmission line open at both ends whose length is an integer multiple of quarter waves ( $n \lambda/4$ ) and therefore displays series resonance phenomena for odd multiples of  $\lambda/4$ , and parallel resonance phenomena for even multiples of  $\lambda/4$ . One open end represents the slot of the antenna. The voltage and current distribution on the line are practically sinusoidal since the losses in the line are assumed low. The voltage maximum  $V$  appears  $\lambda/4$  removed from the slot and the current maximum appears at the slot if the line length is an odd multiple of  $\lambda/4$ , and the conductance at the slot is high. The role of  $V$  and  $I$  are reversed if the line length is an even multiple of  $\lambda/4$  and the conductance at the slot is low. In both cases of resonance the average stored power on the line is

$$\frac{C_1}{2} v^2 n \frac{\lambda}{4} \omega = v^2 \frac{n\pi}{4Z_0} = v^2 B_c$$

$B_c$  is the susceptance representing the average stored power in the line.

$B_c = \frac{n\pi}{4} Y_0$  is proportional to the characteristic admittance  $Y_0$  of the line and proportional to its length.

The average dissipated power on the line, considering both dielectric and resistive losses, is

$$\begin{aligned} W &= \frac{v^2}{2} \left\{ G_1 n \frac{\lambda}{4} + \frac{R_1}{Z_0} n \frac{\lambda}{4} \right\} \\ &= v^2 \left\{ G_1 + \frac{R_1}{Z_0} \right\} \frac{n\pi}{4\beta} \\ &= v^2 \left\{ \frac{G_1}{\omega C_1} + \frac{R_1}{\omega L_1} \right\} \frac{n\pi}{4Z_0} = v^2 B_c \left\{ \frac{G_1}{\omega C_1} + \frac{R_1}{\omega L_1} \right\} \end{aligned}$$

Thus the line  $-Q$  is given by

$$\frac{1}{Q_c} = \frac{W}{v^2 B_c} = \frac{G_1}{\omega C_1} + \frac{R_1}{\omega L_1}$$

$Q_c$  can be estimated from the  $Q$  factor representing the losses in the dielectric material of the line, for instance asphaltic concrete, and from the  $Q$  factor representing ohmic losses.

From the radiation conductance and the average stored power the radiation power factor is determined as:

$$P = \frac{G_R}{B_c} = \frac{G_R Z_0^4}{n\pi}$$

Finally the conductance at the end of the line, representing the slot, is needed for the calculation of the efficiency. Conditions are different for the series resonant quarter-wave line, and the parallel resonant half-wave line. In the first case ( $n = 1, 3, 5 \dots$ ) the current is maximum at the slot end, and the power dissipated in the slot conductance is equal to the total dissipated power in the line:  $I^2/G_{1/4} = W$ . This yields the slot conductance  $G_L$  for the  $\lambda/4$  - case

$$\left. \begin{aligned} G_L = G_{1/4} &= \frac{V^2}{Z_o^2 W} = \frac{Q_c}{Z_o^2 B_c} = \frac{4Q_c}{n\pi Z_o} \\ \text{and} \\ Q_L = \frac{B_c}{G_L} &= \frac{(n\pi Z_o)^2}{4Q_c} = \left(\frac{n\pi}{4}\right)^2 \frac{1}{Q_c} \end{aligned} \right\} n = 1, 3, 5 \dots$$

The frequency dependence of the conductance  $G_{1/4}$  near resonance points is characterized by a high peak of magnitude  $4Q_c/n\pi Z_o$  as shown above and a bandwidth  $\Delta\omega/\omega_o = \frac{1}{Q_c}$ , where  $\Delta\omega$  is the difference of the frequencies at which the conductance  $G_L$  has dropped to one half of the peak value. Thus

$$\frac{\Delta\omega}{\omega_o} = \frac{1}{Q_c}$$

The bandwidth of the  $G_L$  curve is determined by the  $Q_c$  of the line.

Having found a simple expression for  $G_L$  and the radiation power factor  $\rho$ , the efficiency at the  $\lambda/4$  points is readily obtained as

$$\eta = \frac{\rho Q_L}{1 + \rho Q_L} = \frac{1}{1 + \frac{1}{\rho Q_L}} = \frac{1}{1 + \frac{Q_c}{G_R Z_o} \frac{4}{n\pi}}$$

with

$$p = \frac{G_R Z_o^4}{n\pi} \quad \text{and} \quad pQ_L = \frac{G_R Z_o}{Q_c} \frac{n\pi}{4}$$

In most cases  $pQ_L \ll 1$  so that

$$\eta \approx \frac{G_R Z_o}{Q_c} \frac{n\pi}{4} \ll 1$$

Hence the efficiency is small at the quarter wave resonance points, depending largely on  $1/Q_c$ . Summarizing the essential points for the  $\lambda/4$  - case, we find that:

- a) the maximum of  $G_L = \frac{4Q_c}{n\pi Z_o}$  is proportional to  $Q_c$
- b)  $Q_L$  is inversely proportional to the line -  $Q_c$  hence low
- c) the  $Q_c$  of the line, not  $Q_L$  determines the bandwidth of the  $G_L$  curve:  
 $Q_c = \omega_o / \Delta\omega$
- d) the efficiency is small, proportional to  $G_R Z_o / Q_c$ .  $G_L$  and the efficiency can be estimated from a knowledge of  $Q_c$  and the characteristic impedance  $Z_o$ .

In the half-wave resonance points ( $n = 2, 4, 6 \dots$ ) conditions are inverse to those at the quarter-wave resonance points. The voltage is maximum at the slot end. Thus  $V^2 G_{1/2} = W$ . This yields the slot conductance for the  $\lambda/2$  case

$$G_L = G_{1/2} = \frac{W}{V^2} = \frac{B_c}{Q_c} = \frac{n\pi}{4Q_c Z_o}$$

and

$$Q_L = B_c / G_L = Q_c$$

The frequency dependance of the conductance  $G_{1/2}$  around the resonance points is characterized by a very small variation with frequency, and a small magnitude of  $G_{1/2}$ . The bandwidth is broad. The relation between the minima of  $G_{1/2}$  at the  $\lambda/2$ - points and the maximum of the first  $\lambda/4$  point ( $n = 1$ ) is

$$G_{1/2} = \frac{n}{Z_o^2 G_{1/4}} = \frac{n Y_o^2}{G_{1/4}} \quad n = 2, 4, 6 \dots$$

$G_{1/2}$  and  $G_{1/4}$  are inverse to each other.

The efficiency at the  $\lambda/2$  - points is

$$\eta = \frac{\rho Q_L}{1 + \rho Q_L} = \frac{1}{1 + \frac{1}{G_R Z_o Q_c} \cdot \frac{n\pi}{4}}$$

with

$$\rho = \frac{G_R Z_o^4}{n\pi} \quad \text{and} \quad \rho Q_L = G_R Z_o Q_c \frac{4}{n\pi}$$

If  $Q_c$  is sufficiently large, then  $\rho Q_L \gg 1$  and

$$\eta \approx 1 - \frac{n\pi}{4} \frac{1}{G_R Z_o Q_c}$$

can assume values greater than 0.8, thus yielding efficiencies of 80 percent and more.

Following are the essential results for the  $\lambda/2$  - case.

- a) The slot conductance  $G_L$  is not constant, but varies strongly with frequency, assuming low values at the  $\lambda/2$  - resonances, and high values at the  $\lambda/4$  - resonances. The minimum value of  $G_L = \frac{n\pi}{4Q_c Z_o}$  is inversely proportional to  $Q_c$ .



- b)  $Q_L = Q_c$ .  $Q_L$  is determined directly by the line -  $Q_c$ ,
- c) The efficiency for sufficiently high line  $Q_c$  is high and can be estimated from a knowledge of  $Q_c$  and  $Z_o$ .

Having outlined the behavior of the antenna at the resonance point there remains to outline the frequency dependence of the antenna in the region below the first quarter-wave resonance. The antenna behaves similar to a short open-ended transmission line with a comparatively high  $Q_c$ . The conductance at the slot end

$$G_L = \frac{2Y_o Q_c \beta l}{4Q_c^2 \text{ctg}^2(\beta l) + (\beta l)^2} = \frac{Y_o (\beta l)^3}{2Q_c}$$

where the second expression is an approximation for  $\beta l \ll 1$ ; i.e., for small line length  $l$  compared to the wavelength. For this case the radiation conductance is approximately

$$G_R = \frac{(kl)^4}{360} \text{ according to equation (2.8), and the efficiency}$$

$$\eta = \frac{1}{1 + G_L/G_R} = \frac{Q_c (kl)}{180 Y_o \left(\frac{\beta}{k}\right)^3 + Q_c kl}$$

$$\approx \frac{Q_c Z_o (\beta l)}{180 (\beta/k)^4} \text{ for } kl = \frac{2\pi l}{\lambda_o} \ll 1.$$

with

$$\beta/k = \lambda_o/\lambda_c$$

$\lambda_o$  = wavelength in air

$\lambda_c$  = wavelength on transmission line.

For an electrically small antenna ( $\beta l \ll 1$ ) the radiation conductance  $G_R$  is very small so that a small loss conductivity and hence a large  $Q_c$  are required to get the best possible efficiency. The efficiency is proportional to  $Q_c$  and increases linearly with  $\beta l$ ; i.e., with frequency for constant length.

As the frequency increases and the quarter wave resonance is approached  $G_L = \frac{2Q_c}{Z\beta l}$  becomes large and the efficiency drops to a minimum at the quarter wave point. At a frequency below the quarter wave resonance a maximum of efficiency is reached at a point where the rapid increase of  $G_R$  is outweighed by the increase of the loss conductance  $G_L$ . A comparison of the results of the preceding transmission line model with the computations of the admittance and efficiency of the annular slot antenna yields the following table, which summarizes the basic facts.

Two kinds of resonance phenomena ( $Q_c \gg 1$ )

Series or  $\lambda/4$  Resonance  
at cutoff frequencies

Parallel or  $\lambda/2$  Resonance  
in between cutoff frequencies

Slot Susceptance

$$B_T = 0$$

Large negative slope  $dB_T/d\omega$   
proportional to  $Q_c$

$$B_T = 0$$

Small positive slope  $dB_T/d\omega$   
proportional to  $1/Z_o$

Loss Conductance

$$G_L = \frac{4Q_c}{n\pi Z_o}$$

High sharp maximum  
proportional to  $Q_c$

$$G_L = \frac{n\pi}{4 Z_o Q_c}$$

Low flat minimum  
Proportional to  $1/Q_c$

Bandwidth of G vs  $\omega$  curve

$$\frac{\Delta\omega}{\omega_o} = \frac{1}{Q_c} = \left(\frac{4}{n\pi}\right)^2 Q_L$$

Narrow

Wide

Loss  $Q_L$

$$Q_L = \left(\frac{n\pi}{4}\right)^2 \frac{1}{Q_c} \text{ Low}$$

High losses

$$Q_L = Q_c \text{ High}$$

Low losses

Radiation Power Factor

$$P = \frac{4}{n\pi} G_R Z_o$$

$$PQ_L = \frac{n\pi}{4} \frac{G_R Z_o}{Q_c} \ll 1$$

$$= \frac{P}{Q_c} \left(\frac{n\pi}{4}\right)^2$$

$$PQ_L = G_R/G_L$$

$$PQ_L = \frac{4}{n\pi} G_R Z_o Q_c \gg 1$$

$$= PQ_c$$

$$\text{Efficiency } \eta = \frac{1}{1 + (\rho Q_L)^{-1}}$$

$$\eta_{\min} = \rho Q_L = \frac{n\pi}{4} \frac{G_R Z_o}{Q_c} \ll 1$$

Deep and sharp minimum

The bandwidth of the  $\eta$  vs frequency  
curve, where  $\eta_1 = 2\eta_o$ , is

$$\frac{\Delta\omega}{\omega_o} = \frac{1}{Q_c}$$

$$\eta_{\max} \approx 1 - \frac{1}{\rho Q_c} \text{ close to } 1$$

Flat maximum

In both cases: With a knowledge of the loss  $Q_c$  and the characteristic impedance  $Z_o$  the quantities  $G_L$ ,  $Q_L$ ,  $\frac{\Delta\omega}{\omega_o}$  and  $\eta$  can be estimated.

The cavity acts similarly to a radial transmission line consisting of the disk and the ground plane (bottom of cavity). The line length is approximately equal to the average slot radius  $\rho_o = (a + b)/2$ . The characteristic impedance varies with radius. The resonance phenomena, as described in above table, are therefore shifted in frequency, but they are in principle the same as those of the uniform transmission line.

#### 2.1.4.2 Results of Computations of Efficiency

The efficiency of the annular slot (Figure 2-1) has been computed and is plotted in Figure 2-11 by using  $\eta = G_R/G_T$ . The main source of losses is the dielectric material which fills the cavity. These losses are taken into consideration by using a complex wave number

$$k_1 = \omega \sqrt{\mu_o \epsilon_1} \sqrt{1 - \frac{\sigma_1}{\omega \epsilon_1}}$$

where  $\frac{\sigma_1}{\omega \epsilon_1}$  is the loss tangent of the dielectric, and the reciprocal of this is the Q factor:  $Q_D = \frac{\omega \epsilon_1}{\sigma_1}$  as value of  $70 = Q_D$  was chosen. This actually includes all the losses in the antenna. Considering the curve marked "0" debris in Figure 2-11, and 2-12 the following results are obtained:

At the cutoff frequencies the efficiency drops to very low values, causing deep notches in the efficiency curve.

At the same frequencies the  $B_T$  curve (Figure 2-6) passes with a high slope through zero and the  $G_T = G_L$  curve (Figure 2-7) has a high, sharp peak. Thus all typical series resonance phenomena are exhibited. The bandwidth of the  $G_T$  and  $\eta$  curves  $\frac{\Delta\omega}{\omega_o} = \frac{1}{70}$ , according to the assumed  $Q_c$ . From  $G_o = 4.3 \text{ mho}$  and  $1.6 \text{ mho}$  at the first and second cutoff frequency an estimate of the characteristic impedance  $Z_o = 21\Omega$  and  $19\Omega$  respectively is obtained,

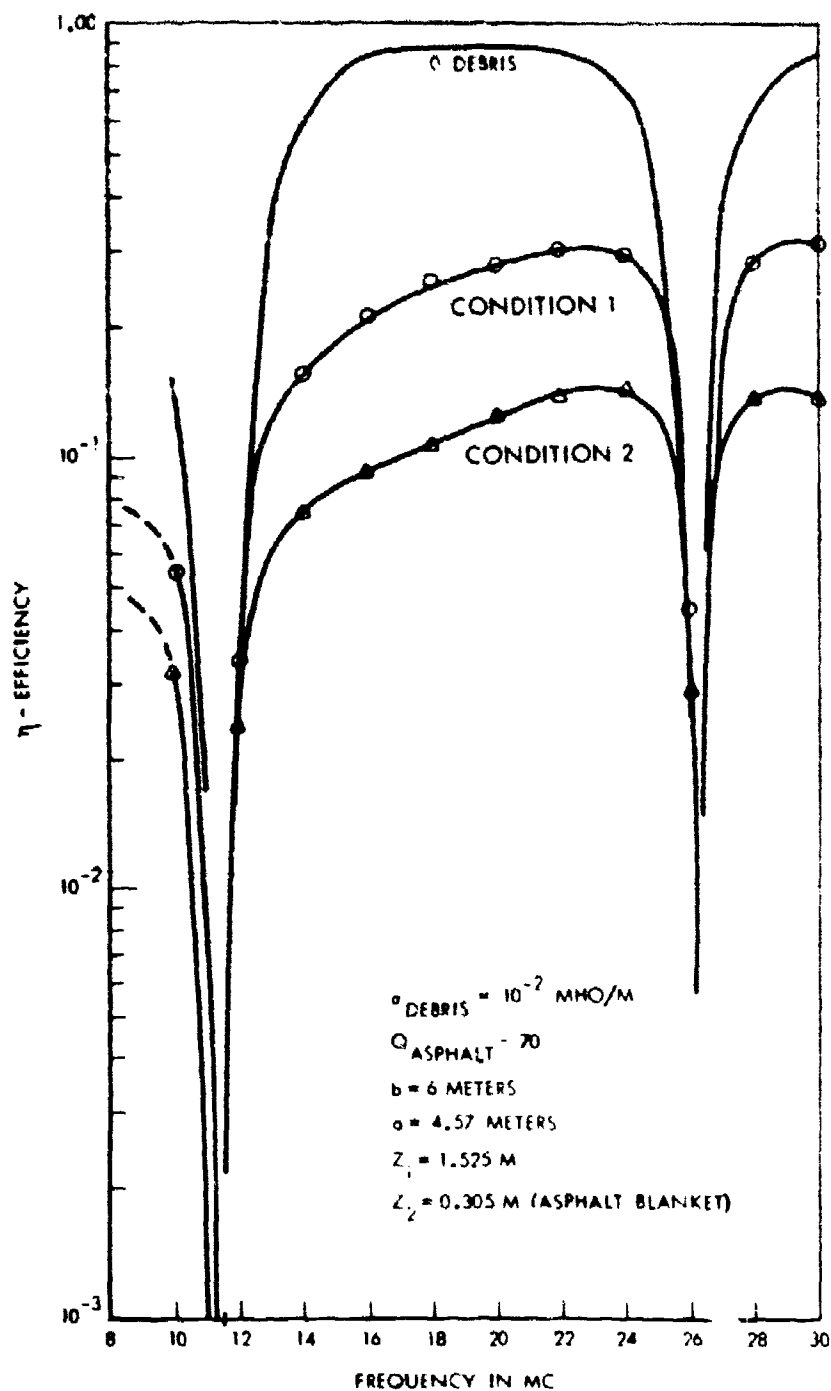


Figure 2-11. Efficiency of 40° Annular Slot With and Without Debris (Semilog Plot).

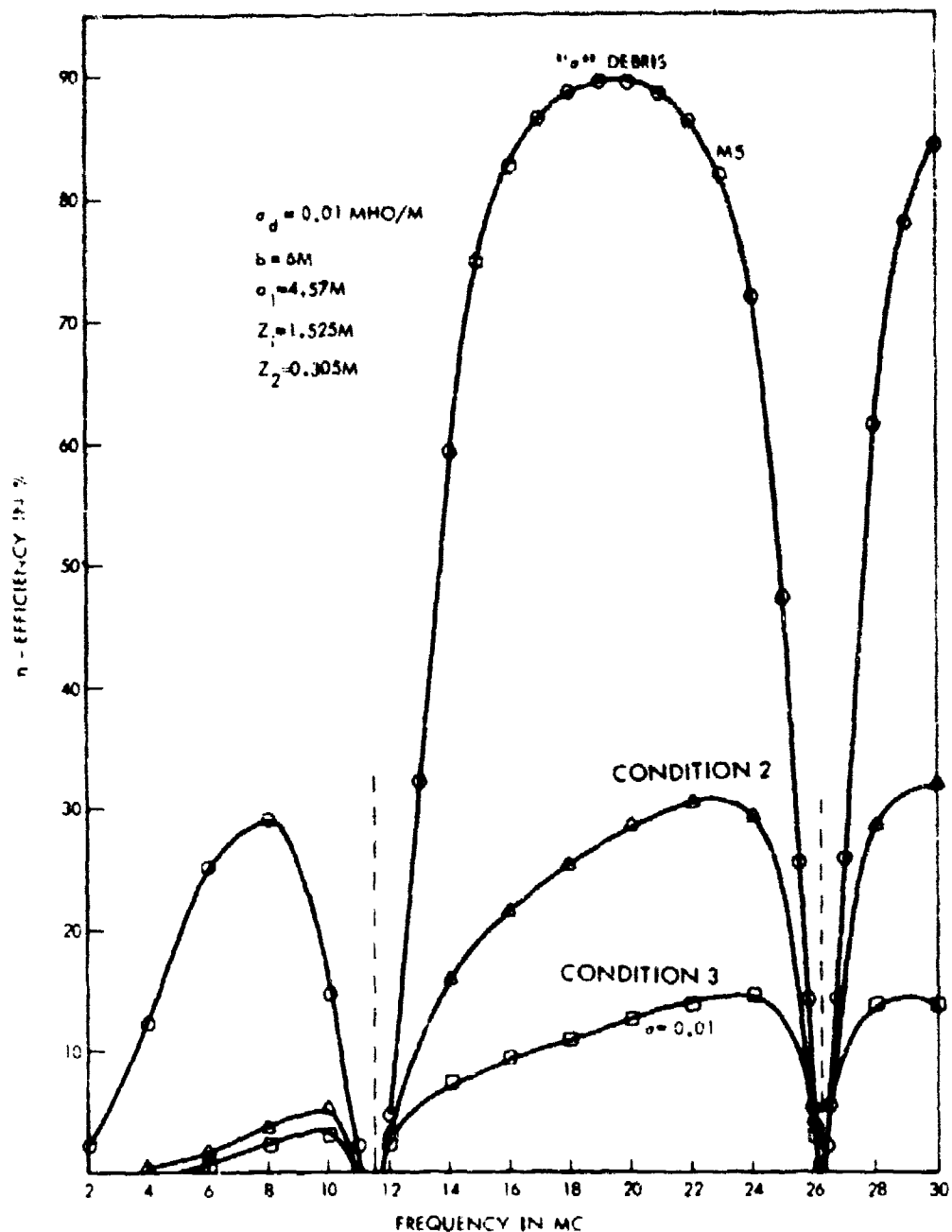


Figure 2-12. Efficiency of 40° Annular Slot With and Without Debris (Rectangular Plot).

using the relation  $G_L = 4Q_C / (\pi^2 Z_0)$ . The radiation power factor is comparatively high for all frequencies beyond the first cutoff frequency, but  $pQ_L \sim p/Q_C$  is low because of the high  $Q_C$ , so that the efficiency is very low. The high loss conductances at the cutoff frequencies have a shunting effect on the slot and thus cause these efficiency notches.

At  $f = 18.5$  Mc we find the typical phenomena of parallel resonance:  $B_T = 0$ , and the  $B_T$  curve has a small slope at this frequency, the loss conductance  $G_L$  and therefore the losses are very low, down by a factor of  $2/Z_0^2 \sim 1/200$  from its value at the first cutoff frequency, and also smaller than  $G_R$ . The efficiency is therefore high, reaches about 88 percent and exhibits a flat maximum. Using the linear transmission line formula similar results are obtained by using  $Q_C = 35$  and  $Z_0 = 20$ , and  $G_R = 20$  millimho as obtained from Figure 2-8. This gives  $p = 0.255$ ,  $pQ_C = 8.9$  and  $\eta = \eta = (1 - \frac{1}{8.9}) 100 = 89$  percent.

It can be seen from Figure 2-11 and 2-12 that the optimum operating frequency band of the annular slot antenna is between the first and second cutoff frequency. This particular antenna with a cavity radius of 20 feet is capable of covering a frequency band of 2:1, extending from 12.8 to 25.8 Mc with an efficiency higher than 25 percent.

Below the first cutoff frequency there is a maximum of efficiency which, however, is much lower than the main efficiency maximum, because at this low frequency  $x = k\rho_0$  is small and therefore the radiation conductance  $G_R$  is small. This maximum is at 8 Mc and reaches a value of 29 percent. The explanation of the maximum is, that at low frequencies  $G_R$  increases with the fourth power of the frequency, but  $G_L$  increases only with the third power, as outlined earlier. As the cutoff frequency is approached the increase of  $G_R$  slows down, but  $G_L$  increases fast and reaches a high value at the cutoff frequency. The maximum of  $\eta = \frac{G_R}{G_R + G_L}$  lies there where the rate of increase of  $G_R$  and  $G_L$  are the same.

At very low frequencies the efficiency is very low, amounting only to a few percent and less.

Above the second cutoff frequency another efficiency maximum is reached which is however lower than the main maximum because losses increase at the higher frequencies.

It is evident from these observations that the optimum frequency range of operation of the annular slot antenna is between the first and second cutoff frequency.

The effect of varying the cavity depth  $h$  is shown of Figure 2-13. This shows efficiency curves for two cavity depths:  $Z_1 = 2.5$  ft and  $Z_1 = 10$  ft this is  $1/2$  and 2 times the cavity depth which was used in Figure 2-11. The cutoff frequencies remain unchanged. The effect of increasing the cavity depth from 2.5 ft to 10 ft is to slightly broaden the efficiency curve. The difference in efficiency near the maximum is small, amounting only to a few percent. However at frequencies closer to the cutoff frequencies the efficiency of the deeper cavity can be 2 or 3 times greater. It is to be expected, of course, that the deeper cavity gives higher efficiencies, but the gain in efficiency is at the expense of volume; i.e., cost. The 10 foot cavity has 4 times the volume than the 2.5 foot cavity and therefore would cost about 4 times as much since the whole cavity has to be filled with dielectric material. In view of these facts a cavity depth of 5 feet, as has been chosen for the computations appears to be a practical compromise.

#### 2.1.4.3 Effects of Debris on The Annular Slot Antenna

In the preceeding section the performance of the annular slot antenna under normal conditions has been described; i.e., with no layer of lossy dielectric above the top hat.

An analysis of the performance of this cavity-backed annular slot antenna - without a lossy layer over it - had been worked out by Galejs and Thompson<sup>4</sup> and could be used to compute the admittance appearing across the slot due to the asphalt filled cavity. This analysis has been extended by



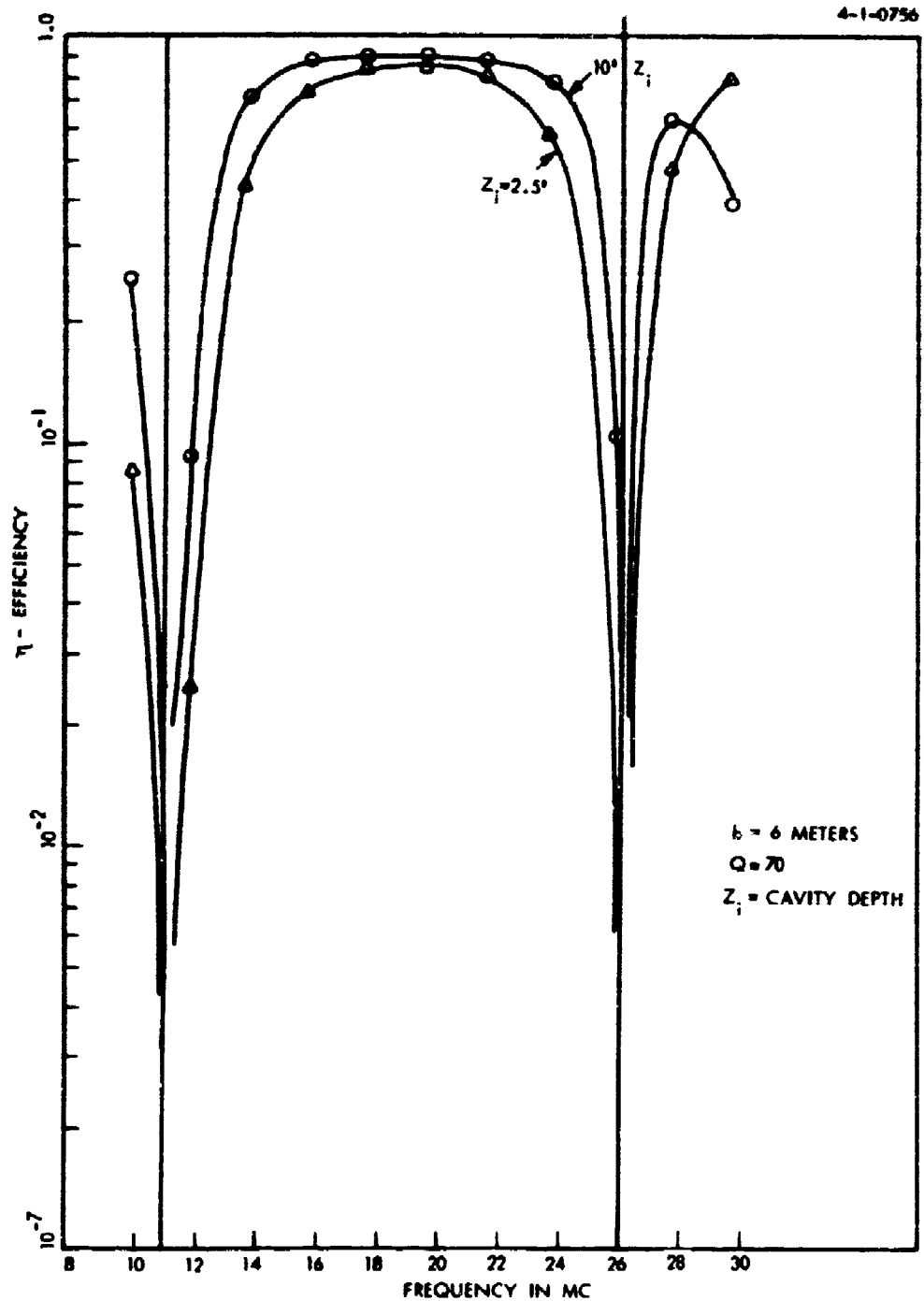


Figure 2-13. Efficiency of 40° Annular Slot Versus Frequency  
 With Backup Cavity Depth as a Varying Parameter.

Galejs and Row<sup>7</sup> and has been used for the computations. This analysis was originally designed for electrically small antennas. Only a linear field distribution across the slot was considered. At the higher frequencies the slot width may be a considerable fraction of the wavelength, and a different field distribution may result. It is therefore possible that the validity of the analysis in its present form is limited to the lower frequencies. Results of measurements indicate that good agreement between theory and measurements is reached up to the second cutoff frequency of the cavity. Above this cutoff frequency measured efficiencies are considerably lower than theoretically predicted. However this can have several reasons, and need not necessarily reflect on the invalidity of the analysis. It is well possible that greater losses in the antenna are incurred at the higher frequencies which were not accounted for. The results of the computation are therefore presented with this reservation.

Figure 2-14 shows the geometry of the model adopted for the debris analysis. The top hat is backed with a conducting cavity of radius  $b$  and depth  $z_1$ . The cavity is filled with a lossy dielectric with wave number  $k_1$  which also overlies the top hat to depth  $d$ . In practice this dielectric will be asphaltic concrete. The debris then is represented by a uniform layer of conductivity  $\sigma_d \gg \omega \epsilon_0$ . The space above the ground plane instead of being infinite is bounded at radius  $C$  by perfectly conducting cylindrical walls so that it forms a circular waveguide of diameter large compared to a wavelength. The reason for choosing a waveguide is that there are fundamental analytical difficulties in treating the problem of radiation into an inhomogeneous half space such as made up of conducting dielectric layers of finite thickness. It can be shown that the calculations of the slot admittance are made practicable if the slot is assumed to radiate into a wide waveguide instead of an inhomogeneous half space. Since the admittance of the waveguide of finite diameter approximates the admittance for an inhomogeneous half space and the fields in the vicinity of the slot are not affected

3-1-0430

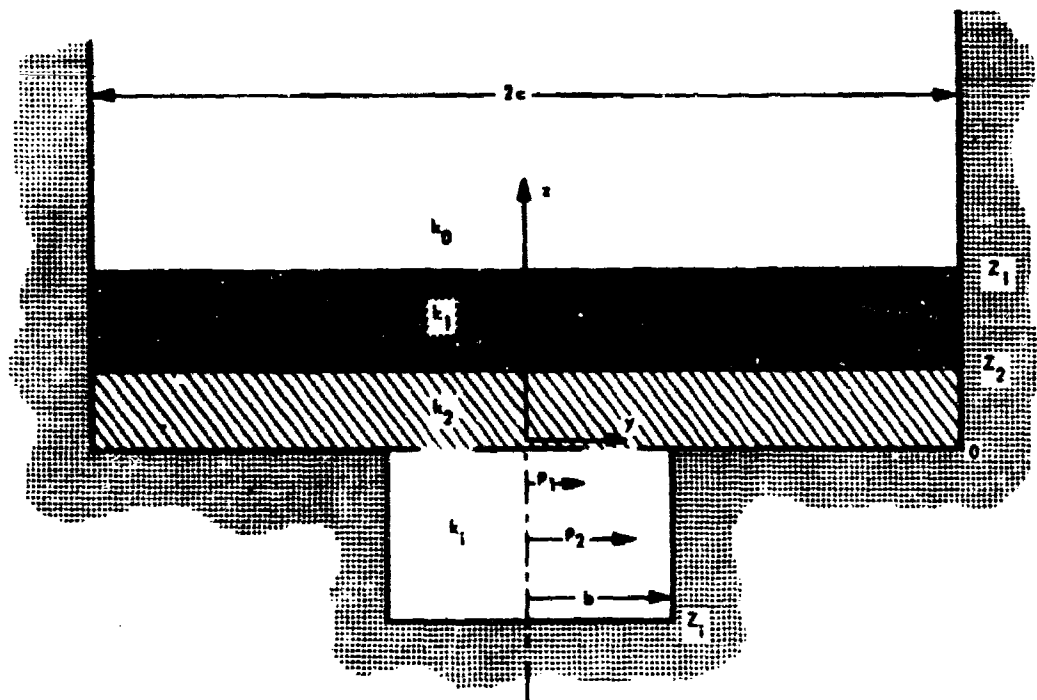


Figure 2-14. Slot Geometry Used for Analysis of Debris Effects.

by the presence of the waveguide walls, which are far removed from the slot, this geometry yields realistic susceptances and also realistic estimates of losses in the lossy dielectric and debris layers.

Using this model the slot admittance follows as

$$Y = \left\{ \frac{4\pi}{\left[ \log \frac{b}{a} \right]^2} \sum_{n=1}^{\infty} \frac{\sigma_2 + j\omega\epsilon_2}{\gamma_{n2}} \frac{1 + B_{n2}}{1 - B_{n2}} \left[ \frac{J_0(\lambda_n a) - J_0(\lambda_n b)}{\lambda_n c J_1(\lambda_n c)} \right]^2 \right. \\ \left. - \sum_{m=1}^{\infty} \frac{\sigma + j\omega\epsilon_1}{\gamma_m} \frac{1 + B_m}{1 - B_m} \left[ \frac{J_0(\lambda_m a) - J_0(\lambda_m b)}{\lambda_m b J_1(\lambda_m b)} \right]^2 \right\} = Y_o + Y_m$$

where

$$J_0(\lambda_m b) = J_0(\lambda_n c) = 0$$

The reflection coefficient  $B_m$  is determined from the requirement that  $E_\rho(\rho, z_1) = 0$ . This gives

$$B_m = e^{-2\gamma_m z_1}$$

The reflection coefficient  $B_{nj}$  are determined after matching the  $E_\rho$  and  $H_\phi$  components across the dielectric interfaces at  $z = z_1$  and  $z_2$ . A computation results in

$$B_{nj} = e^{-2\gamma_{nj} z_j} \left[ \frac{S_{nj} - D_{nj}}{S_{nj} + D_{nj}} \right]$$

where

$$S_{nj} = \left[ \frac{k_1 - 1}{k_j} \right]^2 \left[ e^{-2\gamma_{n(j-1)} z_j} + B_{n(j-1)} \right]$$

$$D_{nj} = \frac{\gamma_{n(j-1)}}{\gamma_{nj}} \left[ e^{-2\gamma_{n(j-1)} z_j} - B_{n(j-1)} \right]$$

and where  $j = 1$  or  $2$ . The computation starts by determining  $B_{n1}$  with  $B_{no} = 0$  (there are only outgoing waves for  $z > z_1$ ). This value of  $B_{n1}$  is then used for computing  $B_{n2}$ , which completes the determination of the slot admittance.

The radiation conductance  $G_R$  may be determined after computing the power flow for  $z > z_1$ .  $G_R$  is given by

$$G_R = 2\pi R_e \sum_n \frac{\gamma_{no}}{j\omega\epsilon_0} \left| \frac{A_{no}}{V} \right|^2$$

where

$$\frac{A_{no}}{V} = - \left[ \frac{e^{-\gamma_{n1} z_1} + B_{n1} e^{\gamma_{n1} z_1}}{e^{-\gamma_{no} z_1}} \quad \frac{e^{-\gamma_{n2} z_2} + B_{n2} e^{\gamma_{n2} z_2}}{e^{-\gamma_{n1} z_2} + B_{n1} e^{\gamma_{n1} z_2}} \right]$$

$$\left[ \frac{2(\sigma_2 + j\omega\epsilon_2)J_0(\lambda_n a) - J_0(\lambda_n b)}{(\log \frac{b}{a}) (1 - B_{n2}) \gamma_{n2} \lambda_n c J_1(\lambda_n c)} \right]$$

These formulas have been evaluated by a digital computer both for the annular slot antenna of Figure 2-1, and for the large Warrensburg antenna. The results for the 20 ft cavity radius antenna of Figure 2-1 are shown in Figures 2-6, 2-7, 2-8, and 2-11 for a 1 and 2 foot debris coverage together with curves for no debris coverage, marked "0" debris. For these computations a debris conductivity  $\sigma_d = 0.01$  mho/m and dielectric constant  $\epsilon_r = 6$  were taken.

Extensive measurements of soil conductivity in Warrensburg, Missouri, and comparison with other measurements (see Appendix A) indicate that these are realistic values for the frequency range 2-30 Mc. Following are the results of computations of debris effects for the 20 ft antenna Figure 2-1. Figure 2-6 shows the effect of a 1 foot and 2 foot debris coverage ( $\sigma = 0.01 \text{ mho/m}$ ) on the susceptance  $B_T$  of the antenna. The curves marked

$$\Delta_1 = (B_T)_0 \text{ debris} - (B_T)_{1 \text{ foot debris}} \text{ and}$$

$$\Delta_2 = (B_T)_0 \text{ debris} - (B_T)_{2 \text{ feet debris}}$$

indicate the change of susceptance by 1 foot and 2 feet debris coverage respectively. For 1 foot of debris  $\Delta_1$  is always negative. This means that the total susceptance with debris is positive almost over the whole frequency range, except at a frequency which is slightly greater than the cutoff frequency between (11.7 - 11.9 Mc). The change of sign of  $B_T$  at the second cutoff frequency disappears and the parallel resonance frequency ( $B_T = 0$ ) no longer exists. The debris therefore increases the capacity of the antenna. The same is true for the 2 foot debris coverage. The susceptance  $B_T$  remains positive at the first cutoff frequency, but changes sign at the second cutoff frequency. The parallel resonance frequency ( $B_T = 0$ ) is still present, but shifted to a higher frequency (~ 21.5 Mc).

Figure 2-8 shows the effect of debris on the radiation conductance. This is increasingly reduced with increasing height of debris. The reduction of  $G_R$  is roughly 40 percent for the 2 foot coverage at the high frequency end, and decreases to about 25 percent at 10 Mc.

Figure 2-7 illustrates the effect of debris on the total conductance  $G_T = G_R + G^-$ . At the cutoff frequencies  $G_T$  peaks up to high values. These peaks are hardly affected by the height of debris. Away from the cutoff frequencies  $G_T$  is much lower and is substantially increased as the debris cover increases.

Of particular interest is the effect of debris on the efficiency, which is calculated as  $\eta = G_R/G_T$ . This is shown on Figures 2-11 and 2-12. Both figures contain the same information, Figure 2-11 on a semilog scale, Figure 2-12 on a linear scale.

Considering the optimum frequency range between the two cutoff frequencies one finds that the reduction in efficiency between the maxima of the 0 and 1 foot debris curves is from 0.9 to 0.3 (i.e., about 5 db) and between the maxima of the 1 and 2 foot curves is from 0.3 to 0.15 (i.e., about 3 db). This indicates that the first foot of debris coverage causes the greatest degradation whereas additional debris coverage causes a relatively smaller degradation. In other words the degradation of efficiency is not proportional to debris thickness, but increases at a less than linear rate.

Looking now at the efficiency maxima at the frequencies below the first cutoff frequency one finds that the efficiency peak with zero debris is about  $1/3$  of the peak in the optimum range. Furthermore this peak is now reduced to  $1/6$  (by  $\sim 8$  db) by a 1 foot debris coverage, whereas the second foot of debris causes a further reduction of only 1.6 db. Thus the electrically small antenna suffers much more by debris, particularly for the first foot of coverage, than the larger antenna. This again points out that the optimum operating range is between the first and second cutoff frequencies.

Beyond the second cutoff frequency the curves show a very marked increase of efficiency which almost reaches the same level of the peak between first and second cutoff. It must be pointed out however, that these high efficiencies beyond the second cutoff frequency could not be measured with the Warrensburg antenna, so that it is questionable if such high efficiency are realizable in practice. There are a number of reasons explaining the lower efficiencies at the high end of the band which are discussed elsewhere in this report.

## 2.2 EXPERIMENTAL INVESTIGATION AND COMPUTATIONS FOR THE HF ANNULAR SLOT ANTENNA LOCATED IN WARRENSBURG, MISSOURI

### 2.2.1 Introduction

The results of our initial studies in the field of Hardened HF Antennas indicated that the annular slot antenna shown in Figure 2-15 has desirable electrical and mechanical properties (i.e., hardness capability to withstand high overpressures) warranting further study. Following the theoretical analysis of the performance of this antenna in the HF band as presented in Section 2.1 an experimental investigation of a full-scale HF annular slot (approximately 56 feet in diameter) in Warrensburg, Missouri, was carried out. The performance of the actual model is in close agreement with the theoretical predictions from approximately 2 - 15 Mc and deviates from theoretical prediction in the 15 to 30 Mc region. This section presents a detailed report of measured performance in the HF annular slot antenna in Warrensburg with and without a debris cover.

### 2.2.2 Annular Slot Computation

Based upon the theory for the annular slot antenna presented in Section 2.1 and using the physical parameters of the Warrensburg Antenna a theoretical solution for the efficiency and admittance of a full scale annular slot antenna was generated in the frequency range 2 - 30 Mc.

The parameters used for the computation are:

Average slot radius	$\rho = 28$ feet
Cavity depth	$Z_1 = 5$ feet
$Q_c$ representing all losses	$Q_c = 25$
Dielectric constant of asphaltic concrete	$\epsilon_R = 3.65$

Debris constants used in the computer solution were obtained from the debris measurements made in Warrensburg. The measured value of debris conductivity varied from approximately  $10^{-3}$  to  $30 \times 10^{-3}$  mho/m from 2 to 30 Mc.



4-1-0705

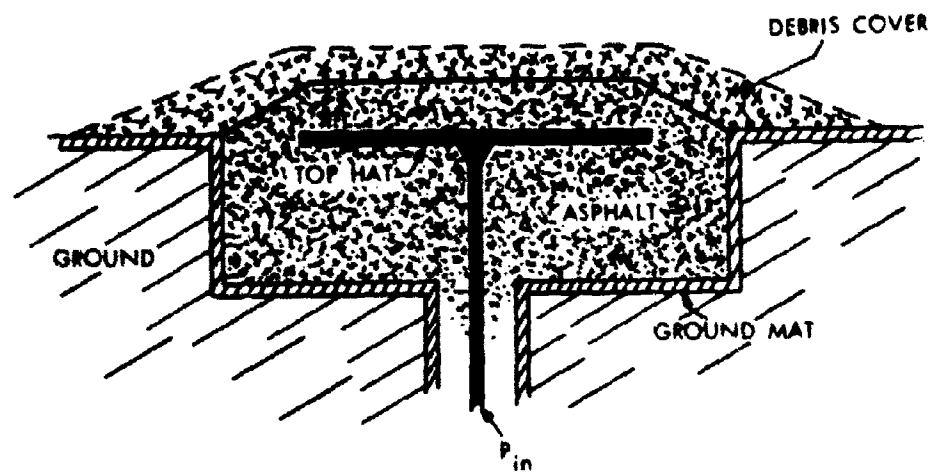


Figure 2-15. Configuration for a Hardened Annular Slot Antenna.

Computer solutions were generated for  $\sigma$  equal to 1.5, 5.5, 10 and 30 millimhos and then appropriate value based on the debris conductivities data plotted in Figure 2-13 in Section 2.2.6 were used to plot the theoretical efficiency versus frequency curve in Figure 2-21. A full uniform cover of debris having thicknesses of 12 and 24 inches was assumed in the theoretical computer solutions. This represents the worst possible debris loading condition, probably more pessimistic than reality. Studies in the area of debris loading indicate situations whereby the debris as a result of nuclear weapon would be randomly distributed in mounds of varying heights over the surface of the antenna. Some portions of the antenna would be loaded one, two, or several feet depending upon weapon yield and range, and others would be clear of debris. Operation of the antennas in such an environment would always be better than that under a full uniform debris layer. Measurements at Sylvania showed no degradation in the annular slot performance over the no debris case when only the top hat was covered with debris; i.e., the slot not covered. Degradation occurred only when the slot was covered with debris.

### 2.2.3 Discussion of Predicted Results

The results of computations using the parameters listed in Section 2.2 are presented in the following figures. Figures 2-16 and 2-17 present the inside conductance  $G_{in}$  due to cavity losses, and the inside susceptance  $B_{in}$  reflected by the cavity as a function of frequency. The series and parallel resonance conditions showing the cutoff frequencies and anti-resonance frequencies characterized by the maxima and minima of the conductance are clearly indicated.

Series resonance (cutoff) frequencies are at 6, 14, 22.6 Mc

Parallel resonance frequencies are at 11.5, 21, 30 Mc

The maximum conductances at the cutoff frequencies taken from Figure 2-16, and the effective  $Q_c$  computed from the bandwidth of these curves, together with effective characteristic impedance, computed from  $Q_c$  and  $G_L \text{ max}$

( $Z_0 \approx 4 Q_c / \pi G_L$ ) are listed in Table 1a.

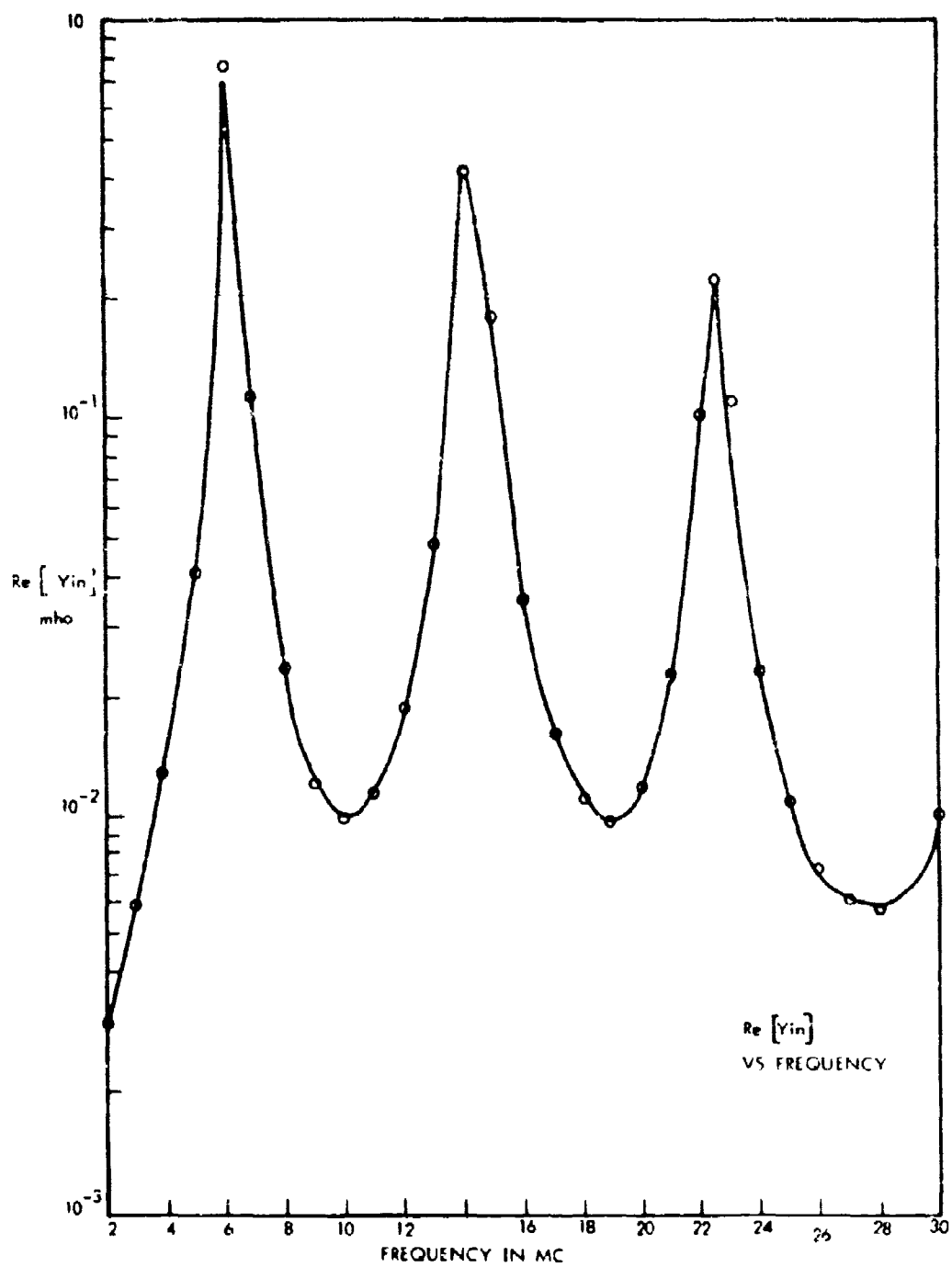


Figure 2-16. Computed Inside Conductance of Warrensburg Antenna Versus Frequency.

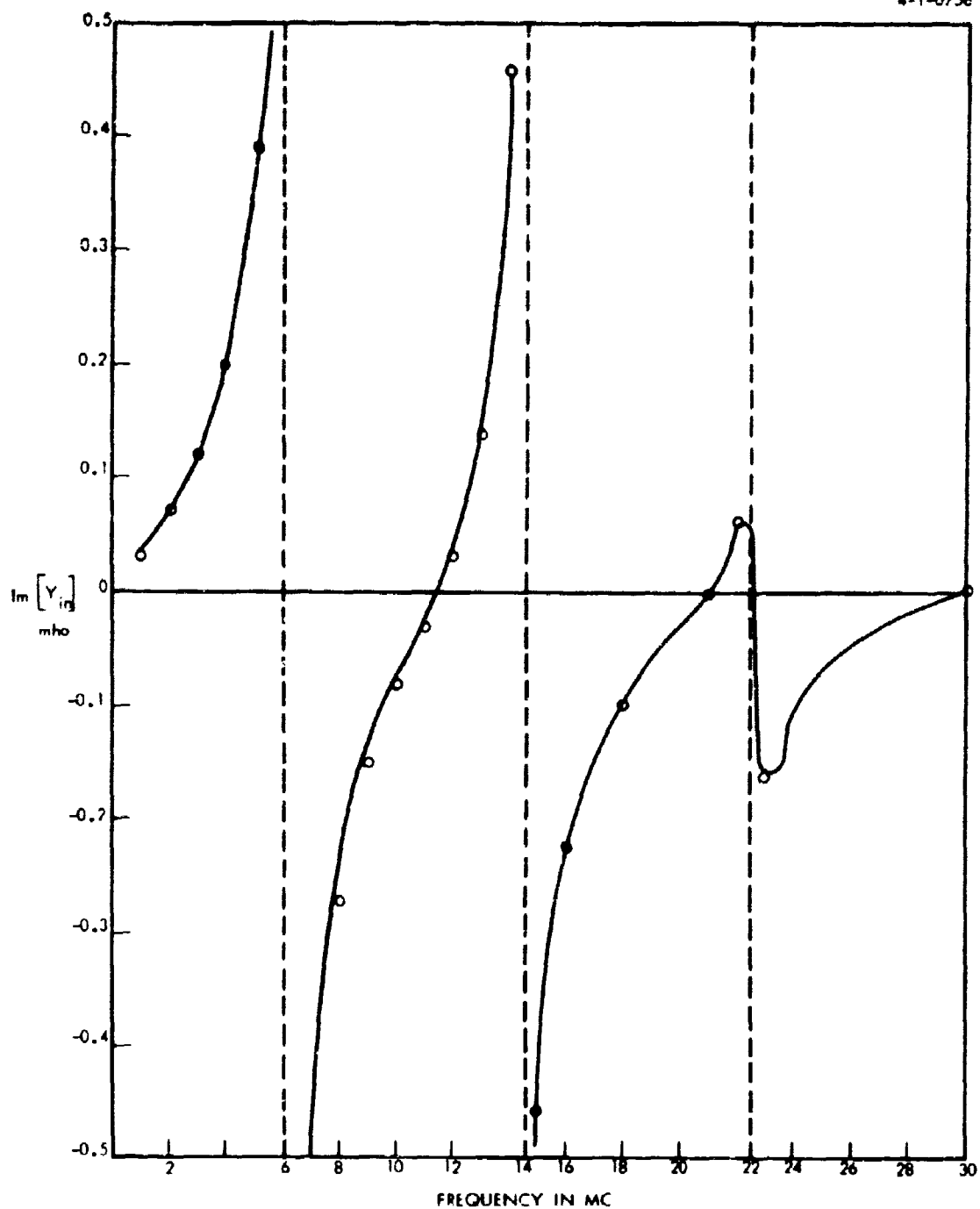


Figure 2-17. Computed Inside Susceptance of Warrensburg Antenna Versus Frequency.

TABLE Ia

$\underline{f_{co}}$	$\underline{G_{in}}$	$\underline{Q_c}$	$\underline{Z_o}$
Mc	mho		ohm
6	0.76	15	25
14	0.42	15	15
22.6	0.22	15	17

There is a great difference between the maximum and minimum conductances as seen from the curves in Figure 2-18, and the maximum conductance at the cutoff frequencies is quite high. The  $Q_c$  taken from the bandwidth of the G-curve is lower than the  $Q_c$  which was used for the computation ( $Q_c = 25$ ). It appears that  $Q_c$  when used for crude estimates should be about 1/2 of the cavity filler material.

Figures 2-18 and 2-19 show the conductance  $\text{Re}[Y_o] = G_o$  and susceptance  $\text{Im}[Y_o] = B_o$  which are due to the field outside the cavity. This outside admittance is affected by the cover of asphalt above the disk and the debris layer, whereas the inside admittance is not affected by these.

The outside conductance  $G_o$  shown in Figure 2-18, is practically identical with the radiation conductance, if no debris is present. The only difference stems from the losses in the asphalt cover above the disk. Debris increases the outside conductance by adding losses, due to dissipated power, to the radiation conductance.

Figure 2-19 shows the variation of the outside susceptance with frequency. It stems from the fringe capacity of the disk against the outside space. The susceptance curve shows a flat portion indicating a decrease of the fringe capacity with frequency in this range. The effect of debris is generally to increase the susceptance.

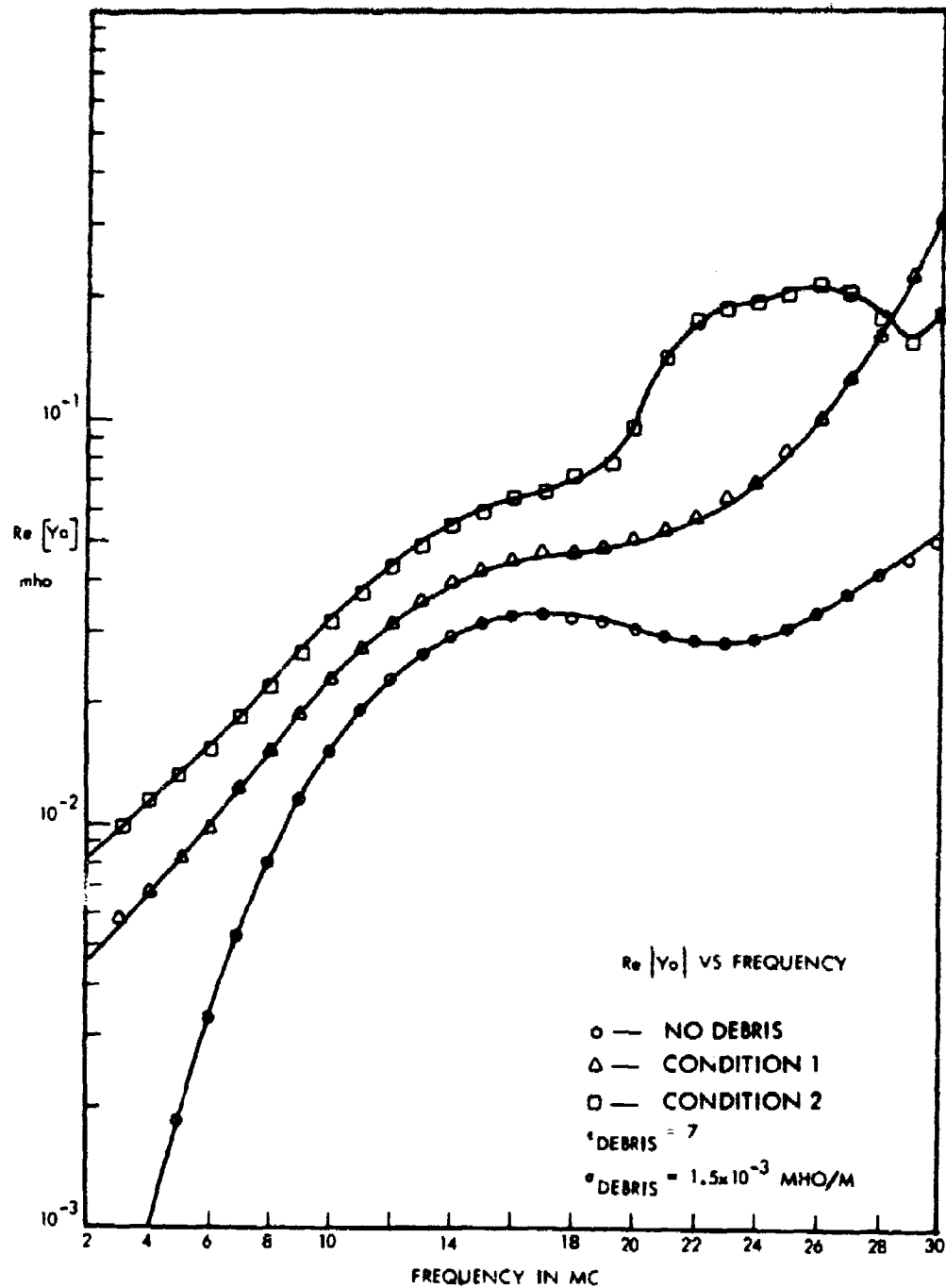


Figure 2-18. Computed Outside Conductance of Warrensburg Antenna.

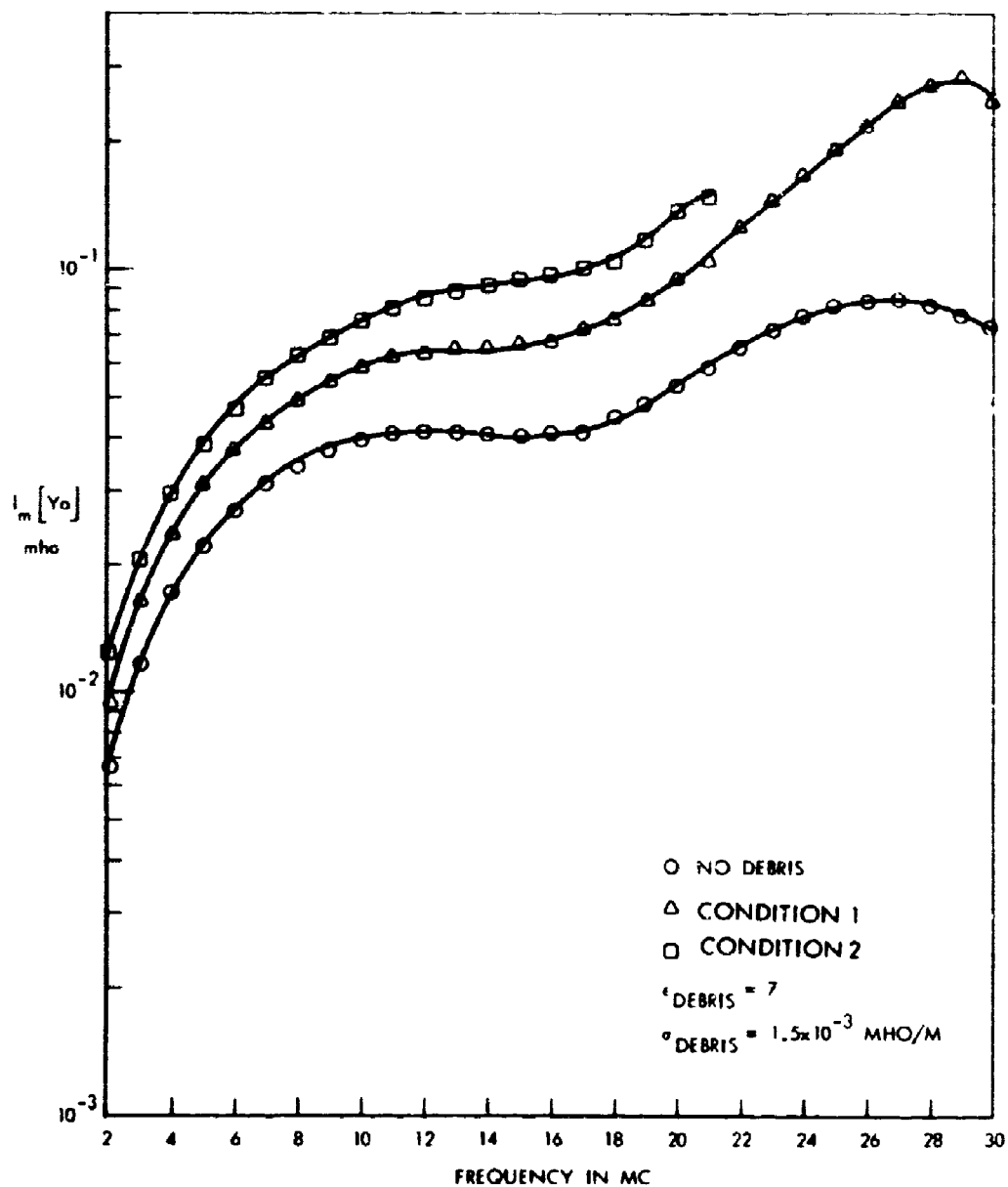


Figure 2-19. Computed Outside Susceptance of Warrensburg Antenna.

Figure 2-20 shows the variation of the radiation conductance  $G_R$  with frequency. The difference  $G_O - G_R$  represents the effect of debris and asphalt losses in the asphalt blanket above the disk. At low frequencies there is no effect of debris on  $G_R$ . At the higher frequencies the curves separate and  $G_R$  increases with thickness of debris cover. This increase of  $G_R$  with debris does not show up if the debris conductivity is chosen higher than it is here, as is apparent from a comparison with Figure 2-8 where the debris conductivity is 0.01 mho/m. It is doubtful if the increase of  $G_R$  as shown in Figure 2-20 is realistic or due to inaccuracy of the theory at higher frequencies resulting from idealizations in the assumptions.

The final result of this computation is presented in Figure 2-21 showing the variation of efficiency with frequency. Points of maximum efficiency and debris degradation are listed in Table Ib: The last two columns contain the radiation power factor and estimated efficiency at parallel resonance using the transmission line approximations and  $Q_c$  and  $Z_O$  listed in the preceding Table Ia. The maximum efficiencies range between ~ 60% to 80% without debris for the first two parallel resonance frequencies. Comparison with the crude estimate based on the simple transmission line mode indicates that the maximum efficiency can be estimated with a fair degree of accuracy if the effective loss  $Q_c$  is assumed about one-half of the  $Q$  of the dielectric filling the cavity. The first maximum of efficiency at 4 Mc is low since the cavity radius/wavelength ratio is low at this frequency and there does not exist a parallel resonance condition at this point, which would reduce the effective losses appearing across the slot. Degradation from debris is predicted as ranging from 1 to 10 db for a one foot debris cover, and increasing to 2 to 14 db for 2 feet of debris cover.

The versatility of the computer program permitted the theoretical investigation as to the effect of the thickness of the asphalt blanket for a 40 foot diameter annular slot optimized for operation from 10 to 30 Mc on the radiation efficiency. As shown in Figure 2-22, the efficiency of the antenna is essentially independent of asphalt blanket thickness whether or not a debris cover is present, thus the criterion for this parameter is



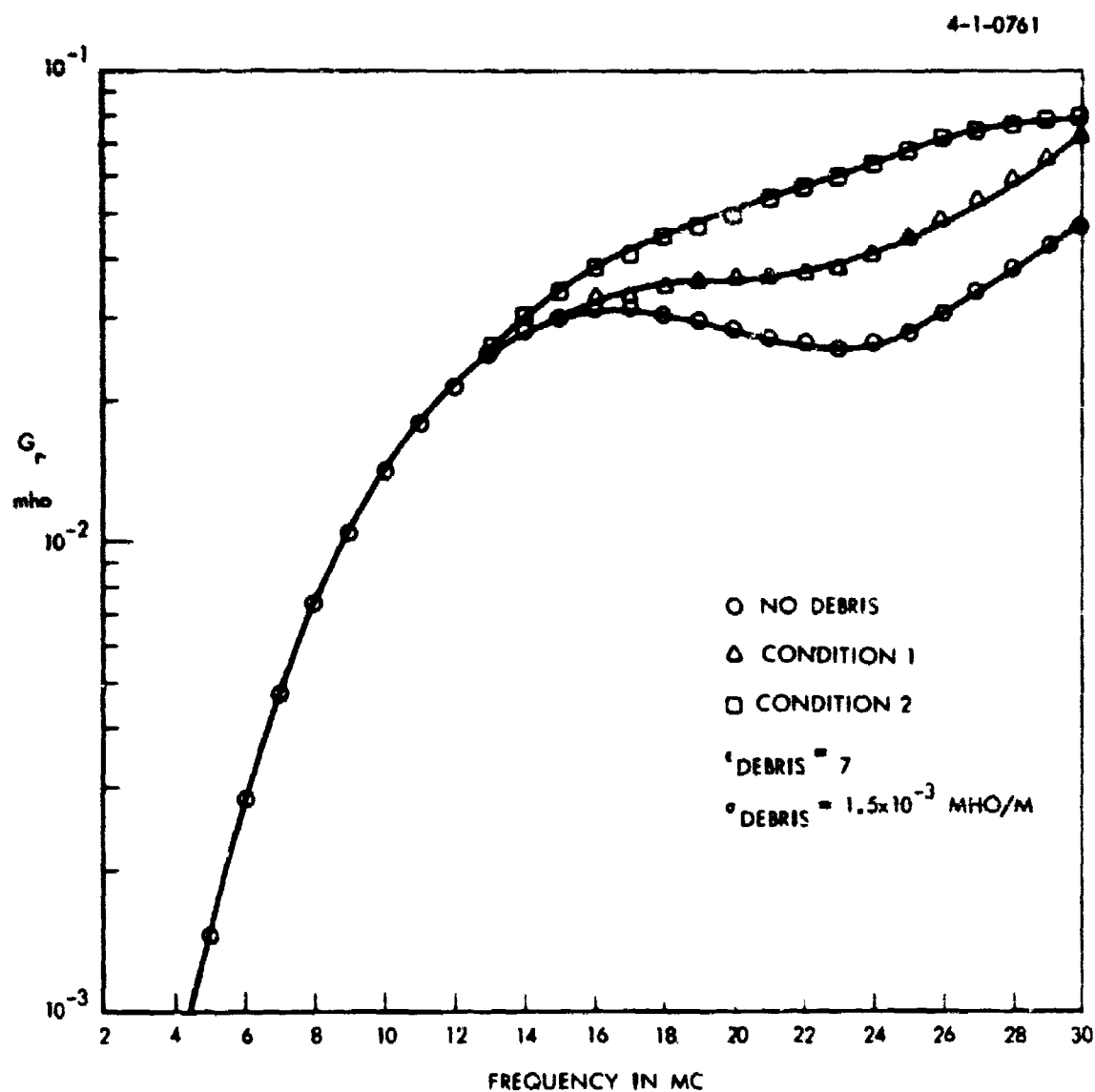


Figure 2-20. Computed Radiation Conductance of Warrensburg Antenna.

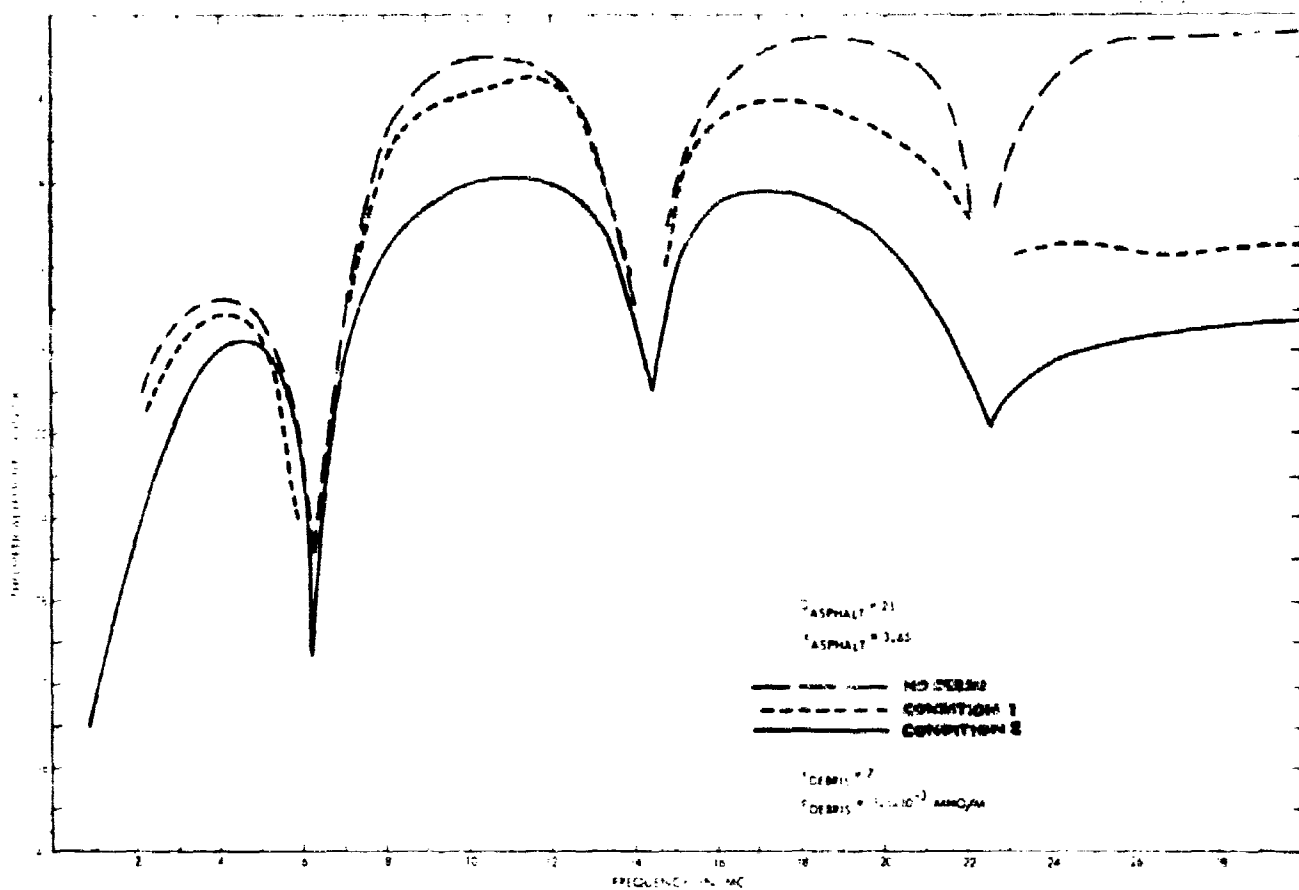


Figure 2-21. Theoretical Efficiency Versus Frequency.

Frequency	Efficiency	Degradation in $\eta$		Efficiency in Percent	Radiation Power Factor	Estimated Efficiency
	$\eta$ in db	1 ft debris $\eta$ degr	2 ft debris $\eta$ degr	$\eta$ no debris	P	$\eta$ est.
4 Mc	-13.5	-1 db	-2 db	4 1/2%		
10.5 Mc	-2.0	-1 db	-6 db	63%	0.255	74%
18.5 Mc	-1.4	-2.6 db	-7.5 db	72%	0.143	68%
26-27 Mc	-1	-10 db	-14 db	79%		

4-1-0779

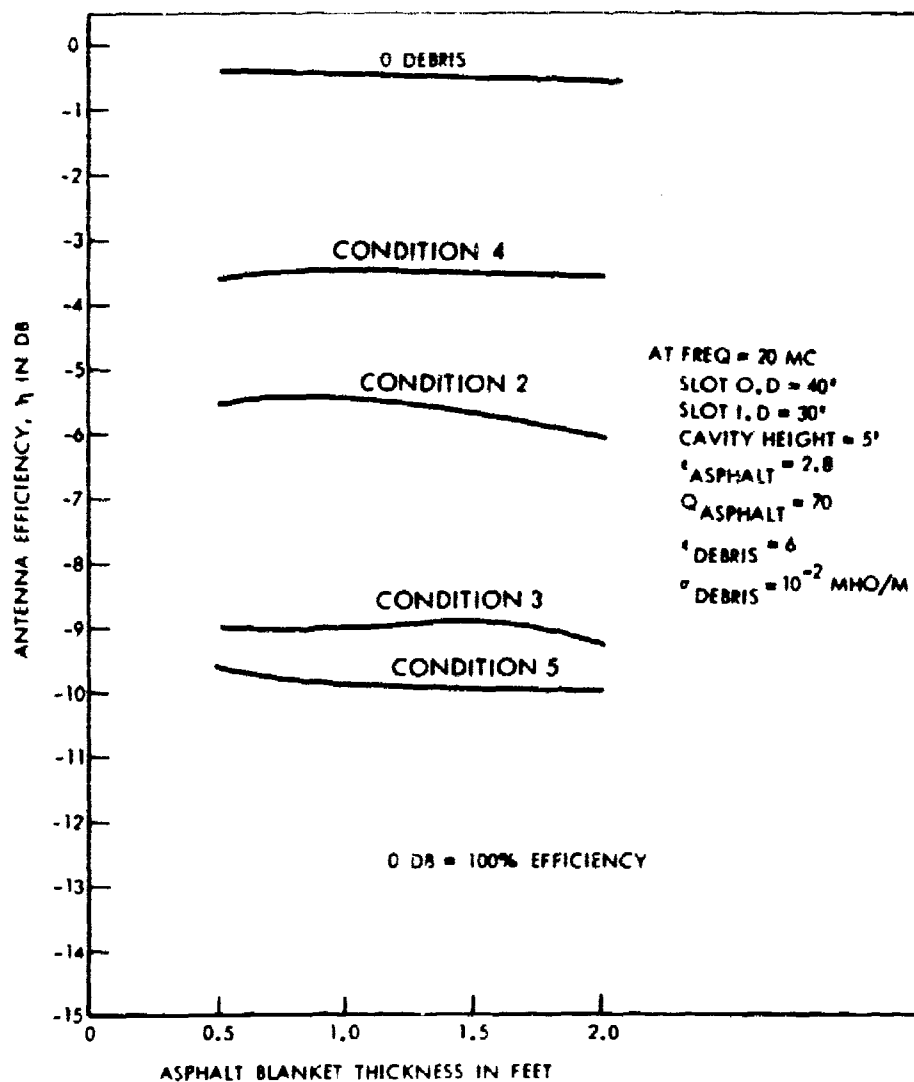


Figure 2-22. Annular Slot Antenna Efficiency Versus Asphalt Blanket Thickness.

determined by thermal ablation requirements. For a multiple hit capability, a two foot asphaltic blanket is indicated from theoretical ablative considerations.

Comparisons of the above mentioned predicted performance parameters with actual measurements for the annular slot in Warrenburg are presented in Sections 2.2.5 and 2.2.9.

#### 2.2.4 Warrensburg Antenna Site

The configuration and dimensions of the HF annular slot antenna are shown in Figure 2-23. The antenna consists of a ground mat 63 feet in diameter, a top hat 48 feet in diameter, and a slot width of 7.5 feet. Spacing between top hat and ground mat is approximately 4.5 feet.

The antenna is completely embedded in asphaltic concrete having a Q of 25 and a dielectric constant of 3.65. An access hole is provided in the center of the antenna for making connections from the underground coaxial feed cable to the antenna input terminals. A test shed located approximately 287 feet from the antenna feed point was used throughout this experimental program for exciting the antenna and performing input impedance measurements. The radiated field intensity along the ground was measured at a point 385 feet from the antenna. Figures 2-24 and 2-25 indicate the experimental test set-up at Warrensburg and expanded view of access hole. Photographs in Figures 2-26 and 2-27 show profile views of the annular slot antenna.

Electrical measurements made on the RG-220 coaxial feed cable indicated a physical cable length of 287 feet. Cable measurements also showed that the feed line is a multiple half wavelength (i.e., series resonant) at the following frequencies.

$$f_{SR \text{ in mc}} = 1.15 m \text{ where } m = 1, 2, 3, 4, \dots$$

The frequencies at which the line length is a multiple quarter wavelength or anti resonant is as follows:

$$f_{AR \text{ in mc}} = 0.575 n \text{ where } n = 1, 3, 5, 7 \dots (\text{odd integer})$$

Electrical line lengths were established for each of the interested frequencies in the HF band (2 to 30 Mc) and having the measured value of antenna input impedance at the shed (i.e.,  $Z_{shed}$ ), standard transmission line techniques were used to roll back the impedance toward the antenna terminals to establish the input impedance or  $Z_{ant}$ . Lumped LC networks or appropriate series capacitors were used to efficiently match the antenna for the field intensity measurements.

4-1-0708

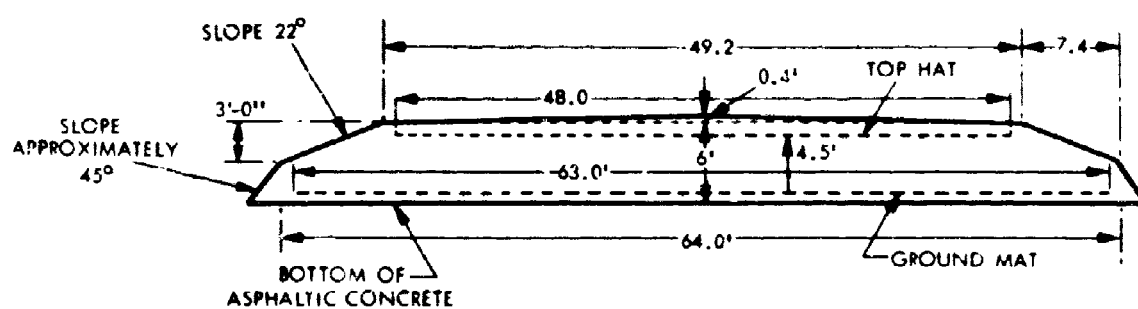


Figure 2-23. Configuration of the Warrensburg Antenna.

4-1-0709

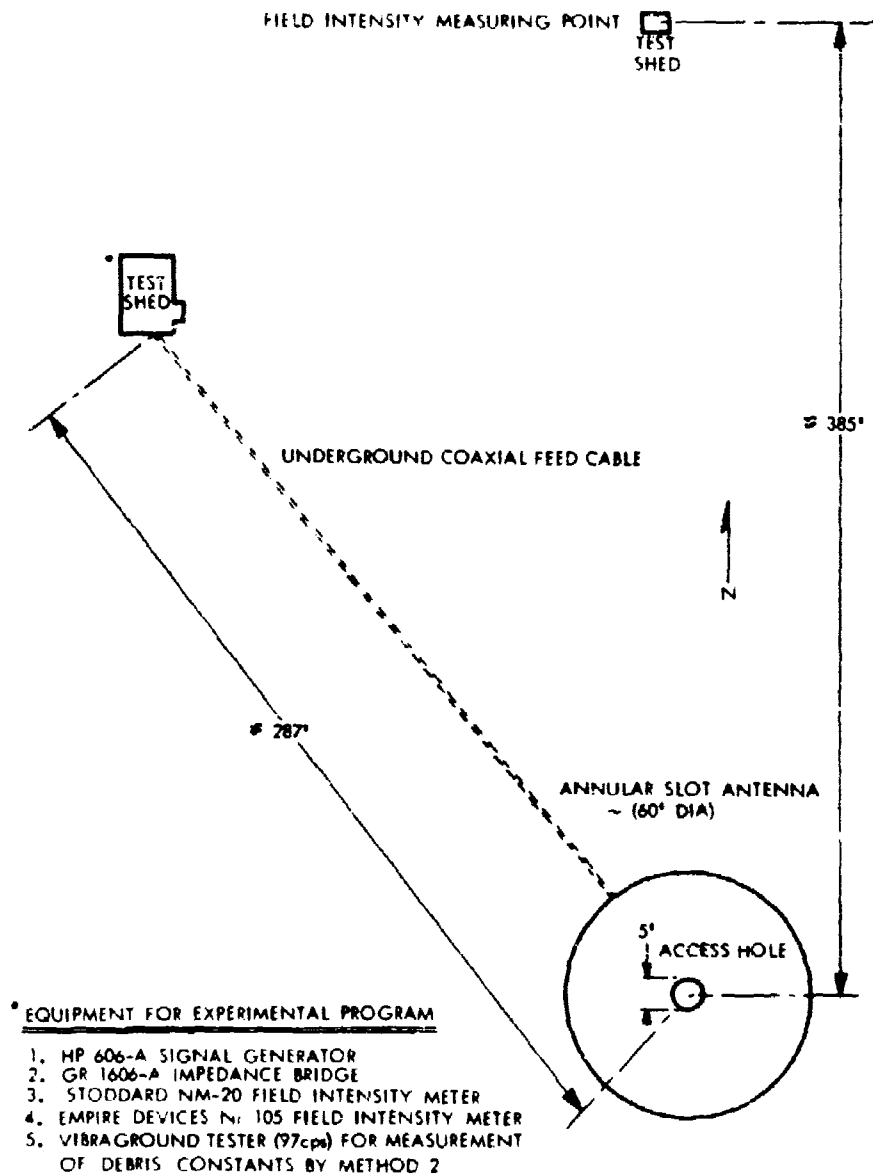


Figure 2-24. Experimental Set-up at Warrensburg.



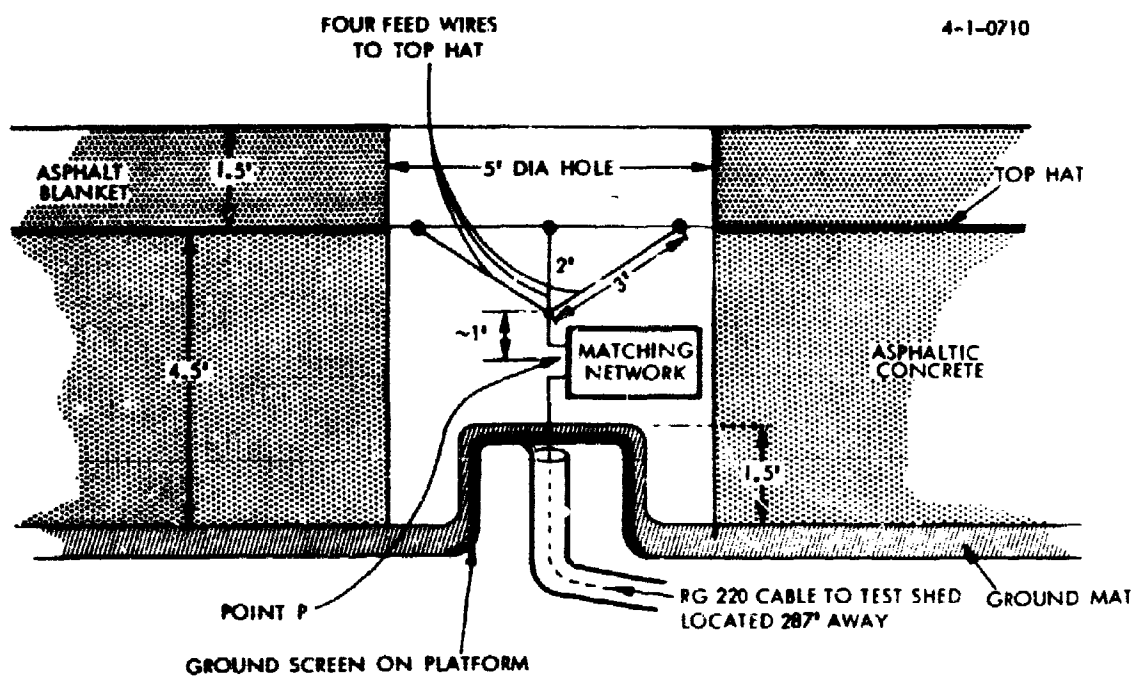


Figure 2-25. Expanded View of Access Hole Showing Electrical Connection to the Antenna.

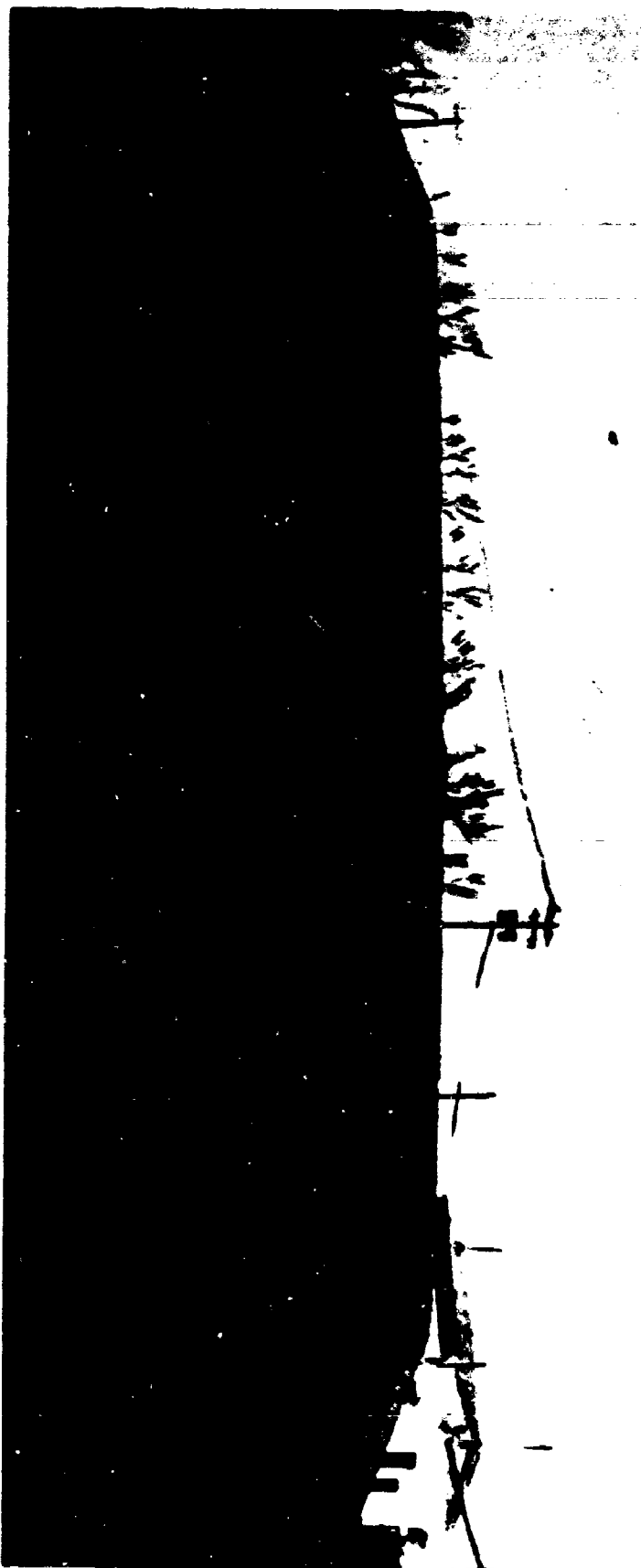
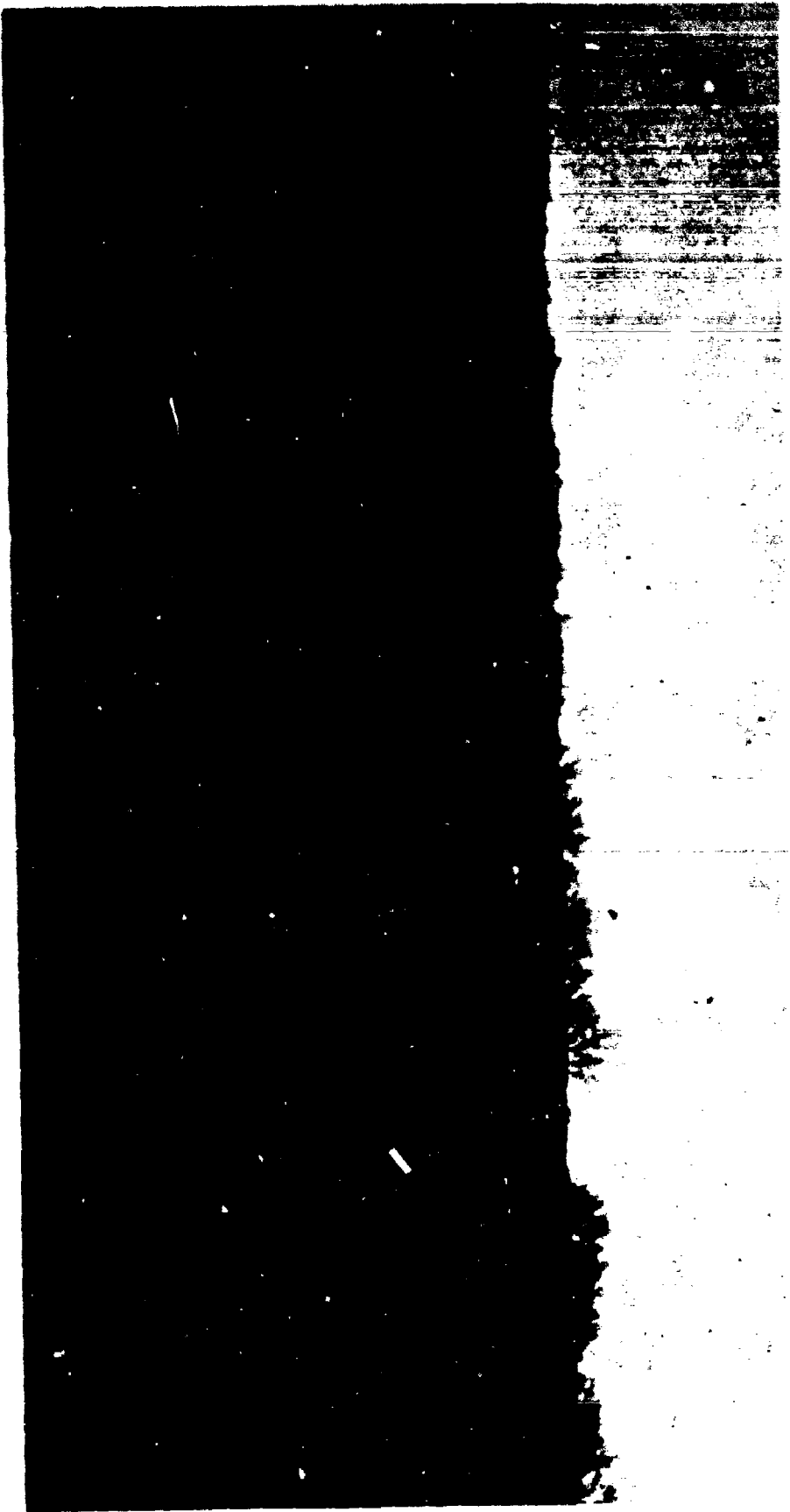


Figure 2-26. Profile of Annular Slot Looking in NW Direction.



**Figure 2-27. View of Antenna from Test Shed Looking in SE Direction.**

### 2.2.5 Measured Terminal Input Impedance and Field Intensity

Measurements were made as to the terminal input impedance, and radiated field intensity along the ground. These were made for the following conditions shown in Figure 2-28.

- (a) Antenna with no debris cover
- (b) Antenna under condition 1
- (c) Antenna under condition 2
- (d) Antenna under condition 3

The soil in the vicinity of the antenna was used to provide a debris cover for these measurements. Electrical measurements were made on random samples of the soil so as to establish debris parameters for the cover. A detailed discussion of the test procedure and tabulation of debris parameters for the HF region is given in Section 2.2.6 of this report.

Input impedance measurements for the antenna are presented in the Smith plots of Figures 2-29 through 2-34.

The field intensity as measured on the ground at the test point located 385 feet from the antenna is plotted in Figures 2-35 through 2-38. All curves have been referenced to the theoretical field strength at 385 feet for a short vertical monopole (of 100 percent efficiency) having a power input of 1 watt. This corresponds to a field intensity along the ground of 98 db above 1  $\mu\text{V/m}$ ; therefore, the left hand ordinate in Figures 2-35 through 2-38 is field strength along the ground in db referenced to a short vertical monopole.

The right hand ordinate for Figures 2-35 through 2-38 is the deviation from theoretical monopole (100 percent efficiency) for the Warrensburg annular slot antenna as derived from the computer solution and includes the effects of lobing (i.e., the K-factor discussed in Section 2). Taking the difference (in db) between the solid and the dotted curves of the field intensity plots provides the antenna efficiency, either theoretical or measured, for the antenna. For example, Figure 2-35 is a plot of the field intensity with no debris cover. At 12 Mc, we have

$E_1 = E_{\text{field}} = 92.2 \text{ db}$  measured for Warrensburg Antenna

$E_2 = E_{\text{field}} = 93.5 \text{ db}$  theoretical for Warrensburg Antenna

$E_3 = E_{\text{field}} = 96.4 \text{ db}$  for theoretical annular slot of 100 percent efficiency

(Theoretical Efficiency)  $\eta_{\text{theo.}} = E_2 - E_3 = (93.5 - 96.4) \text{ db} = - 2.9 \text{ db}$  or 51%

(Measured Efficiency)  $\eta_{\text{actual}} = E_1 - E_3 = (92.2 - 96.4) \text{ db} = - 4.2 \text{ db}$  or 39%

4-1-0711

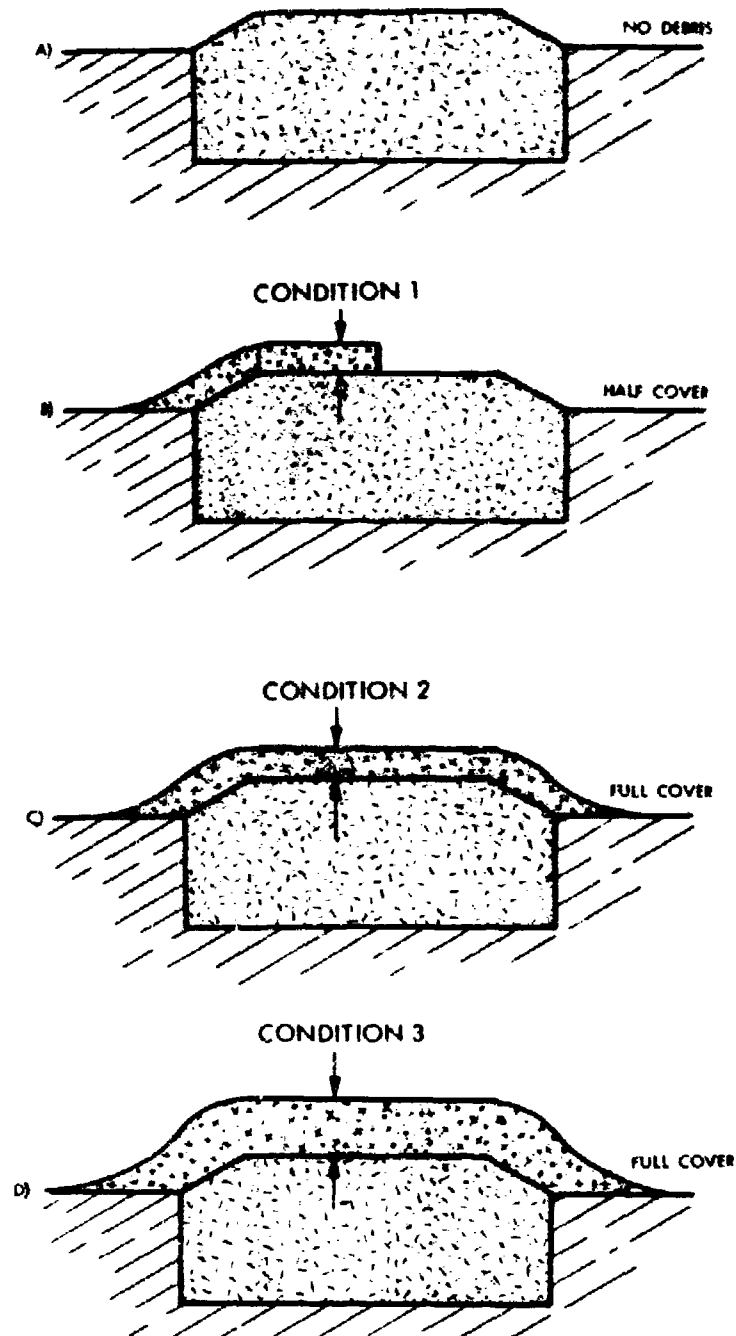


Figure 2-28. Conditions Under Which Antenna was Tested.

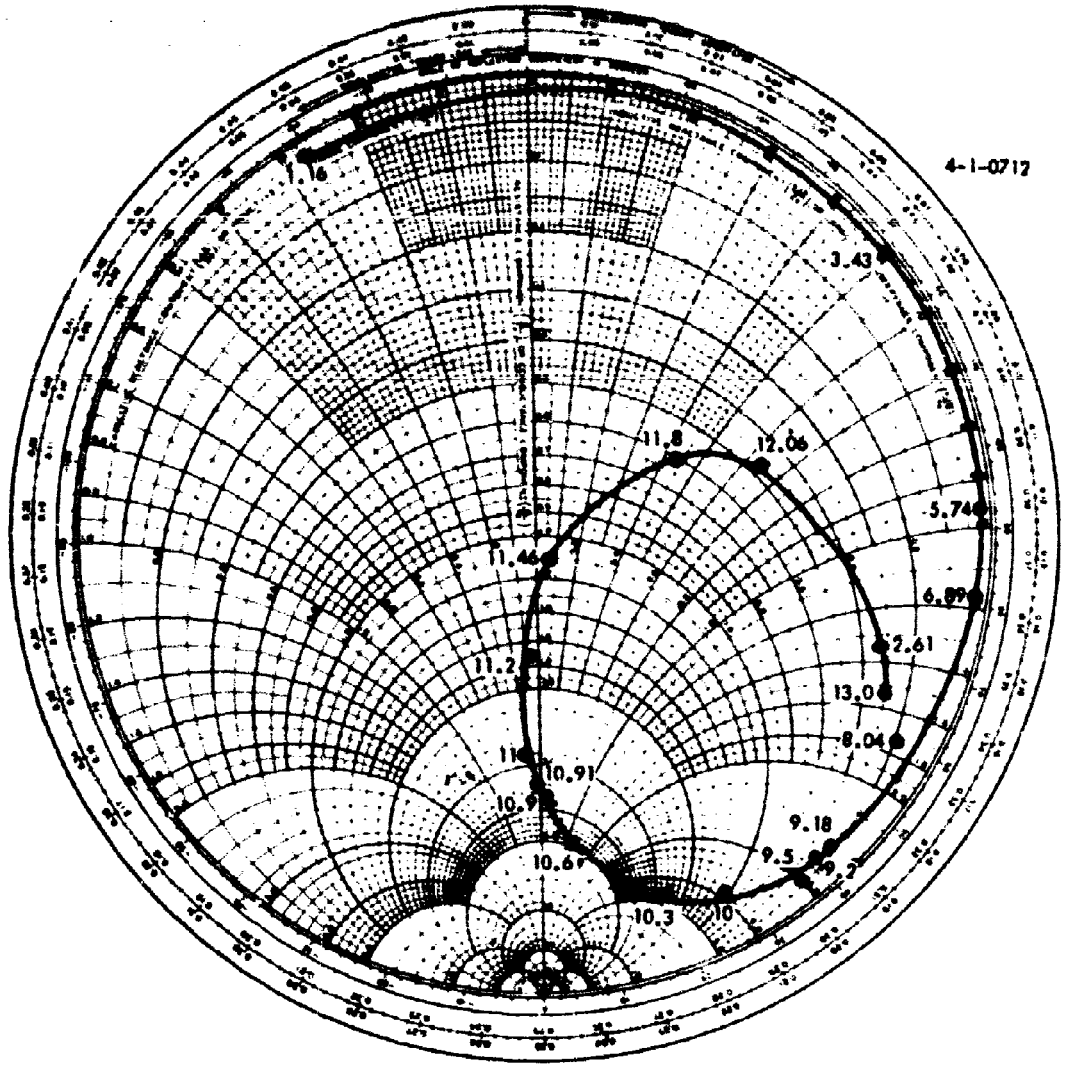


Figure 2-29. Terminal Impedance of Antenna, 1.16-13 Mc, No Debris.

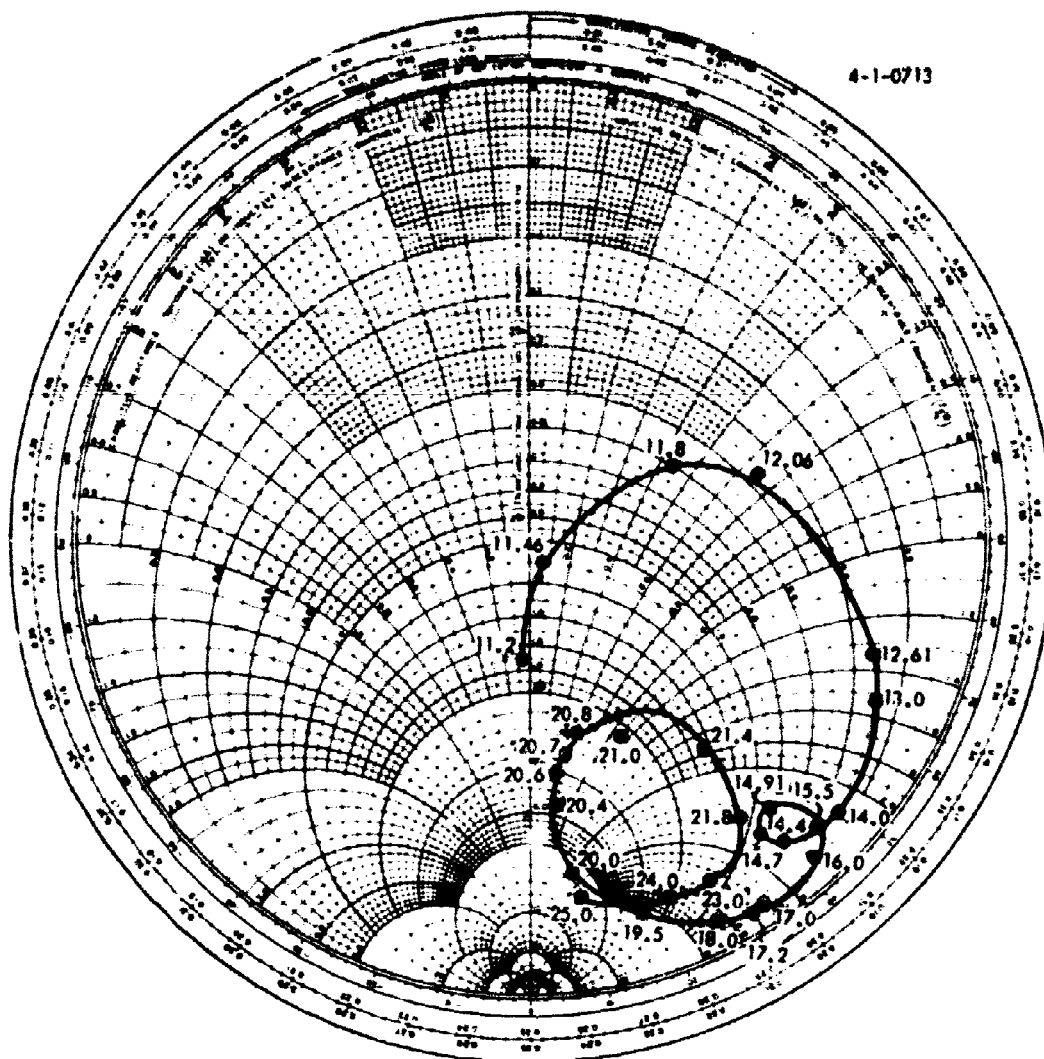


Figure 2-30. Terminal Impedance of Antenna, 11.2-25 Mc, No Debris.



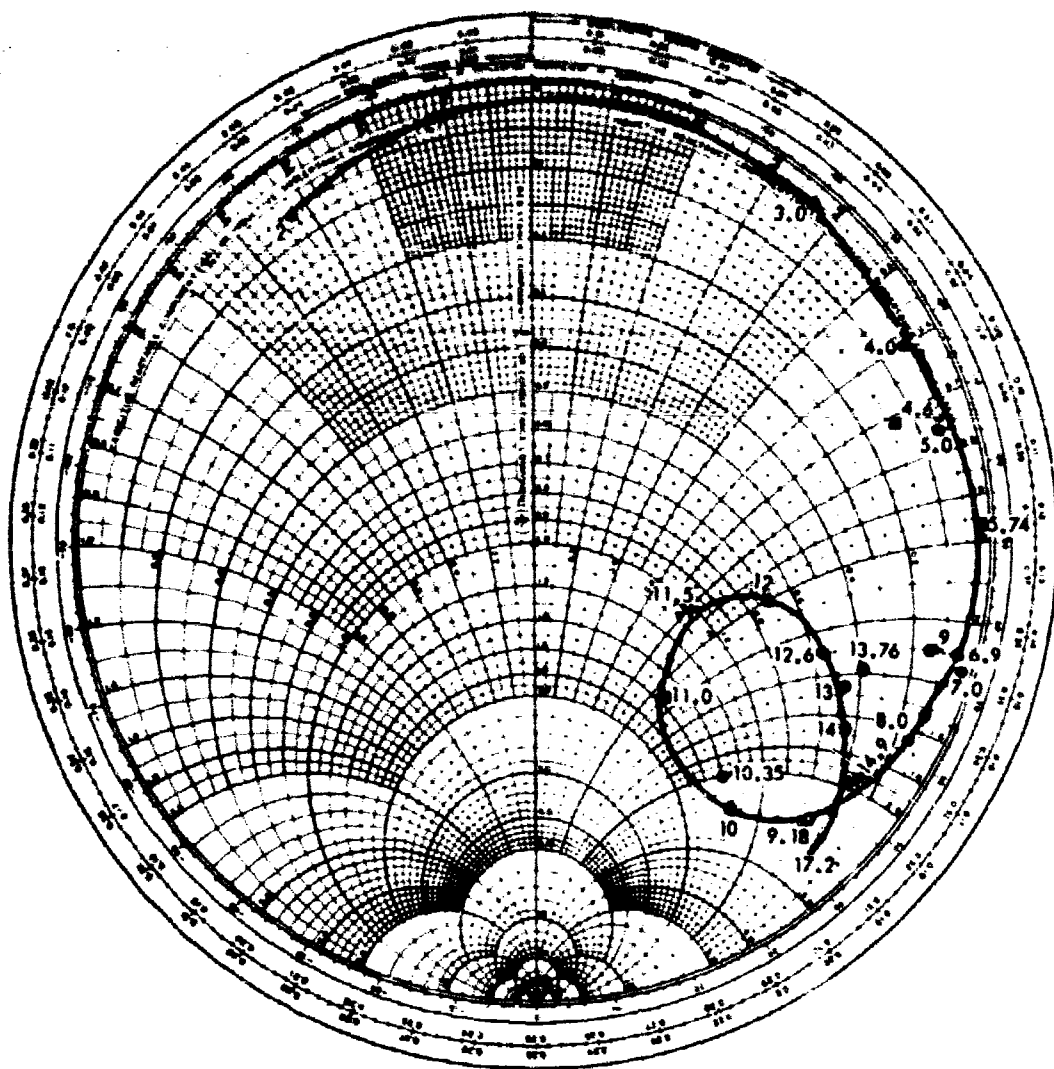


Figure 2-31. Terminal Impedance of Antenna, 2-17.2 Mc, Half Cover Condition 1.

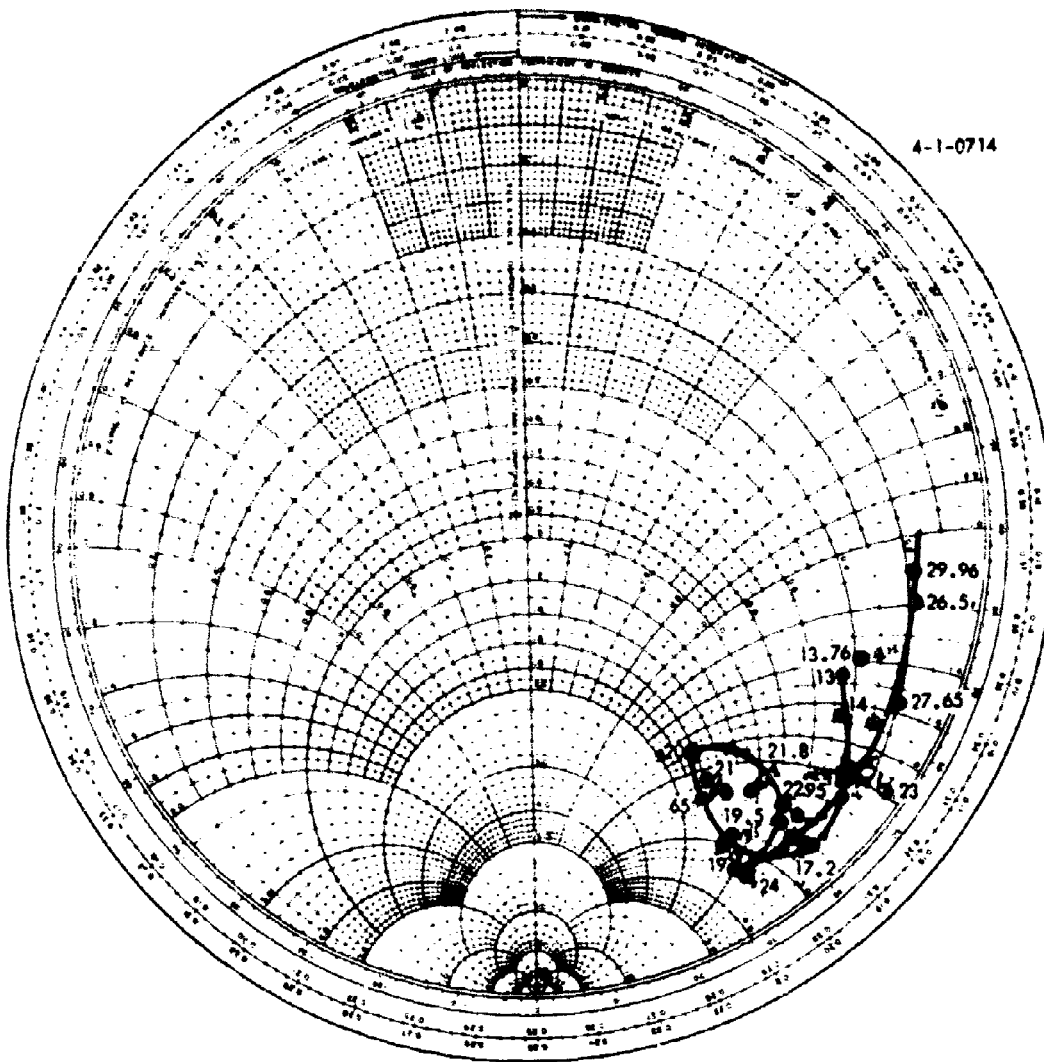


Figure 2-32. Terminal Impedance of Antenna, 13 - 29.96 Mc, Half Cover Condition 1.

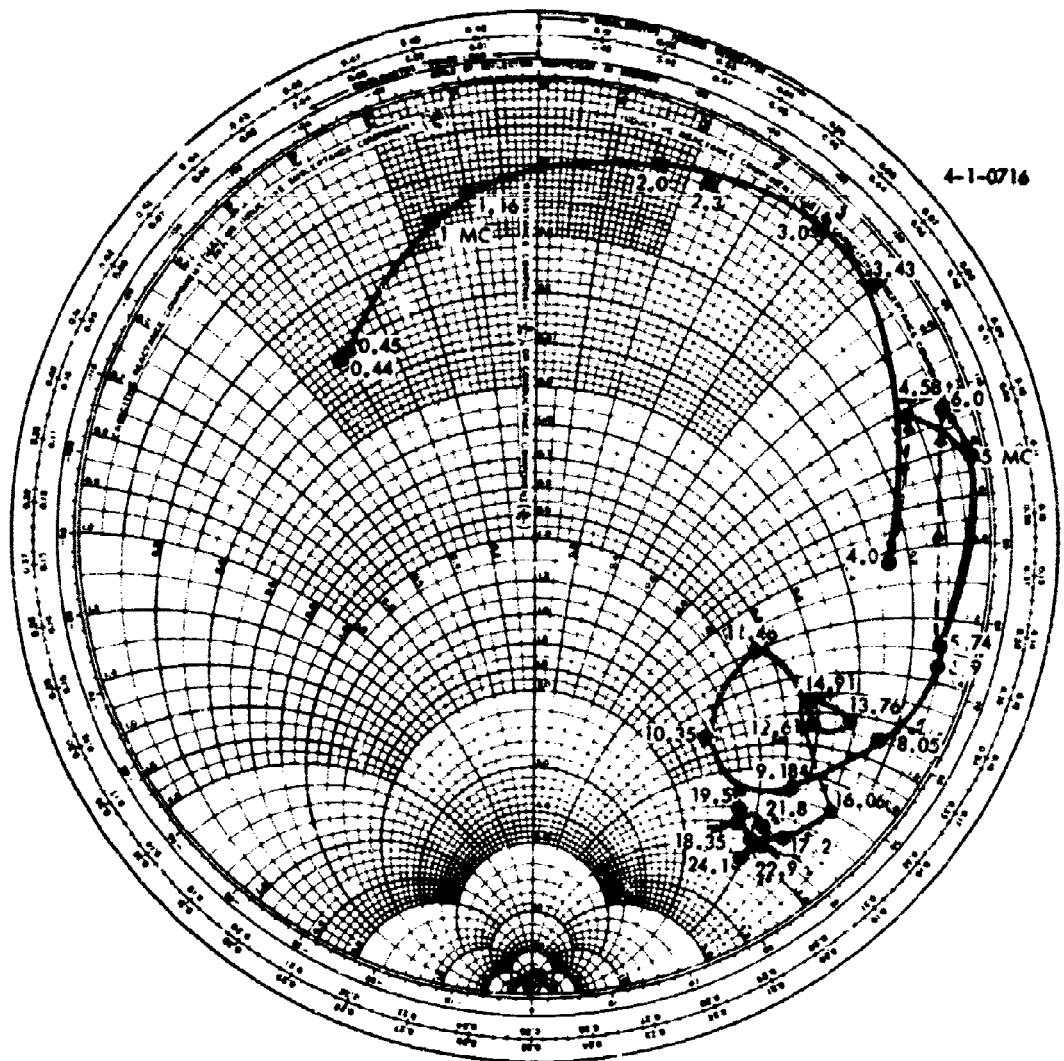


Figure 2-33. Terminal Impedance of Antenna, 0.44-24.1 Mc, Full Cover Condition 2.

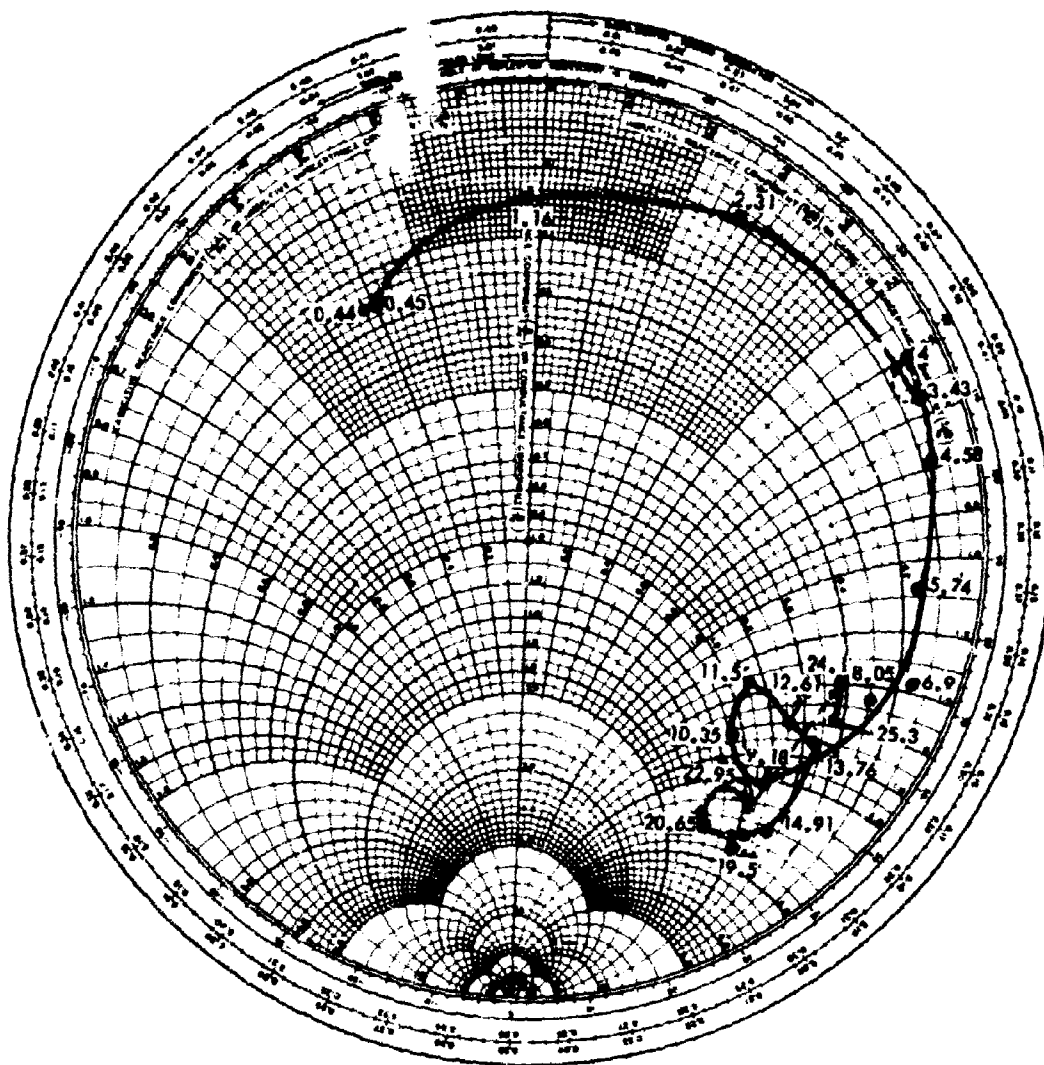


Figure 2-34. Terminal Impedance of Antenna, 0.44 - 24.1 Mc, Full Cover Condition 3.

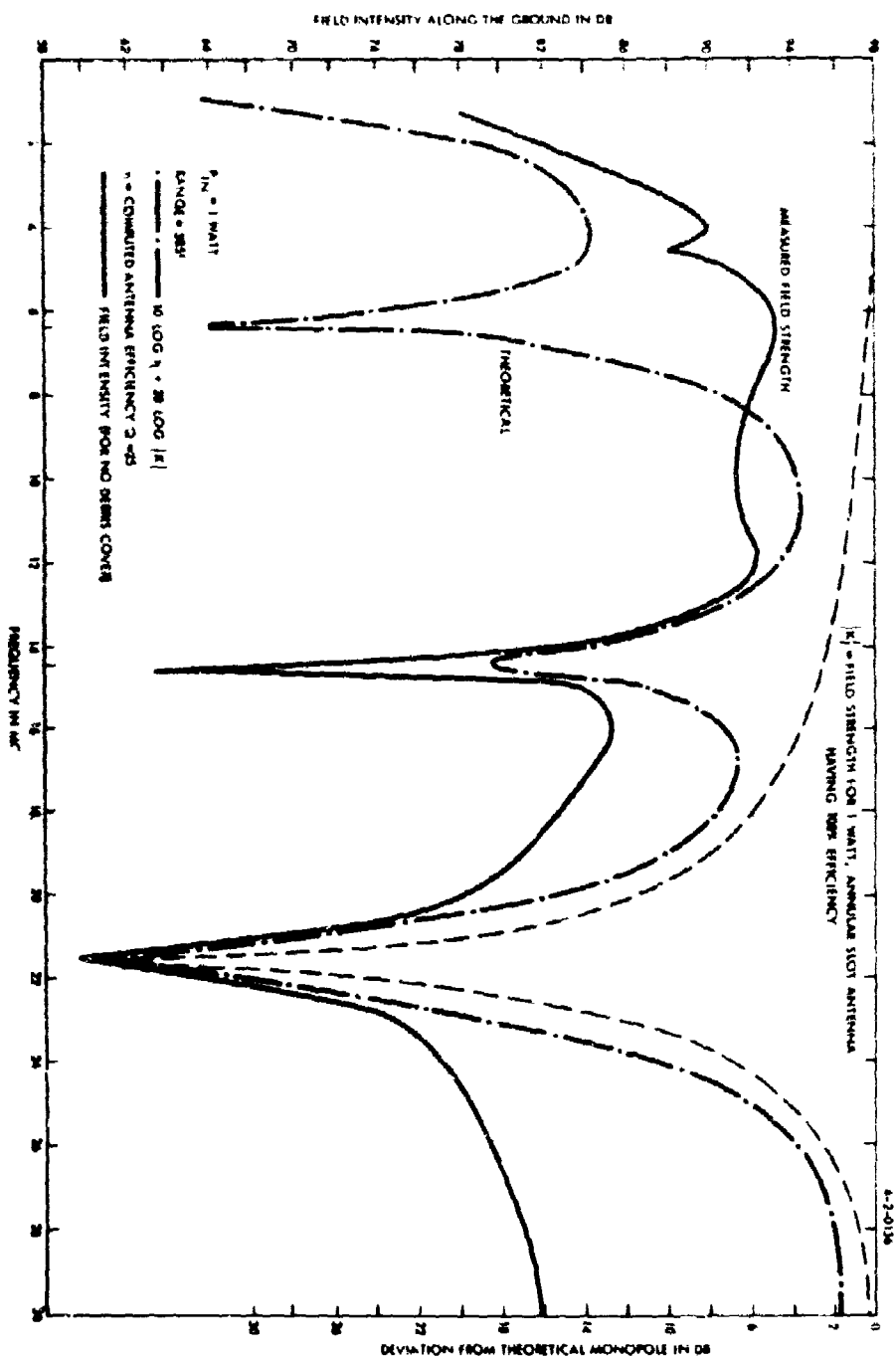


Figure 2-35. Theoretical and Measured Field Intensity Along the Ground

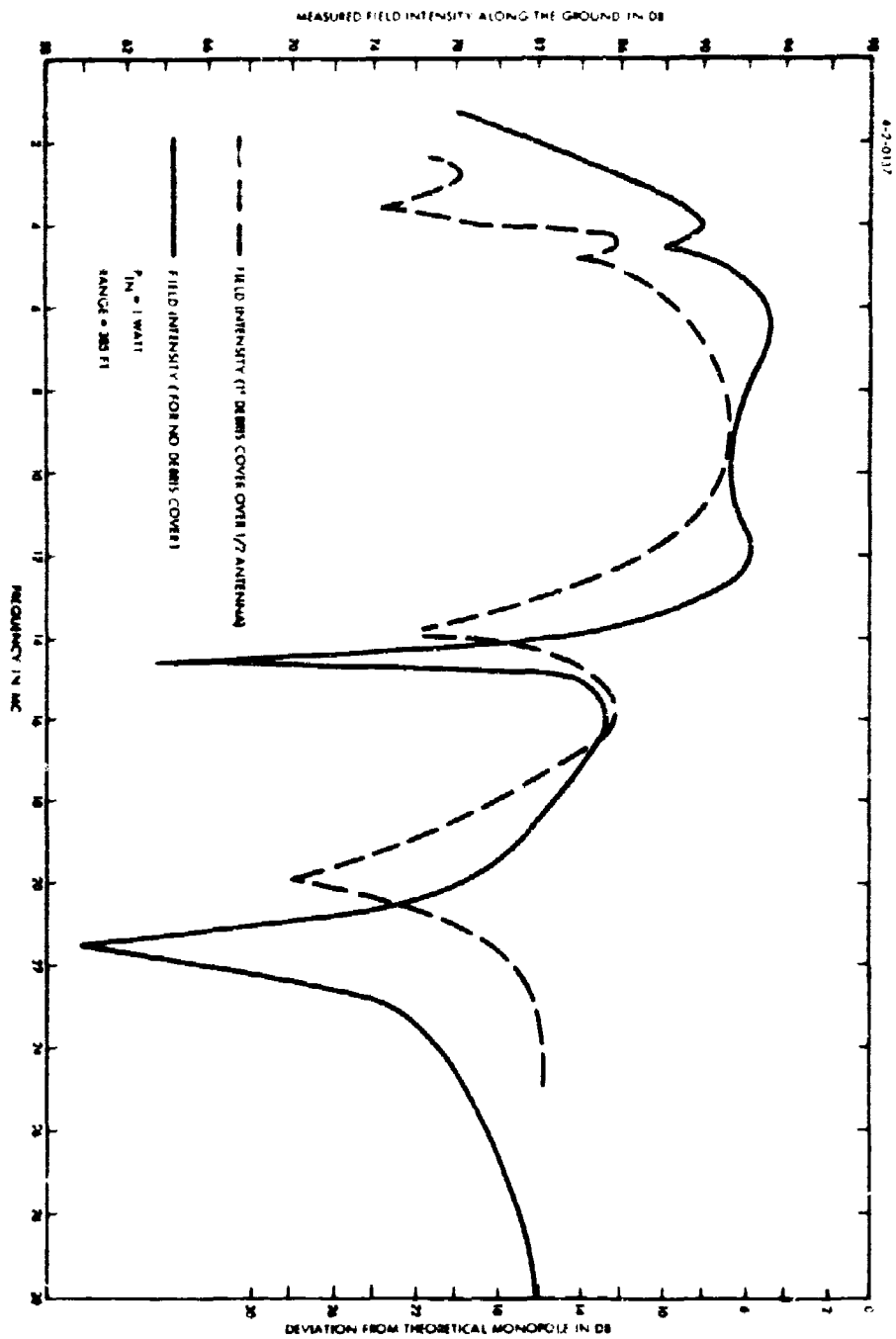


Figure 2-36. Measured Field Intensity Along the Ground Half Cover Condition 1.

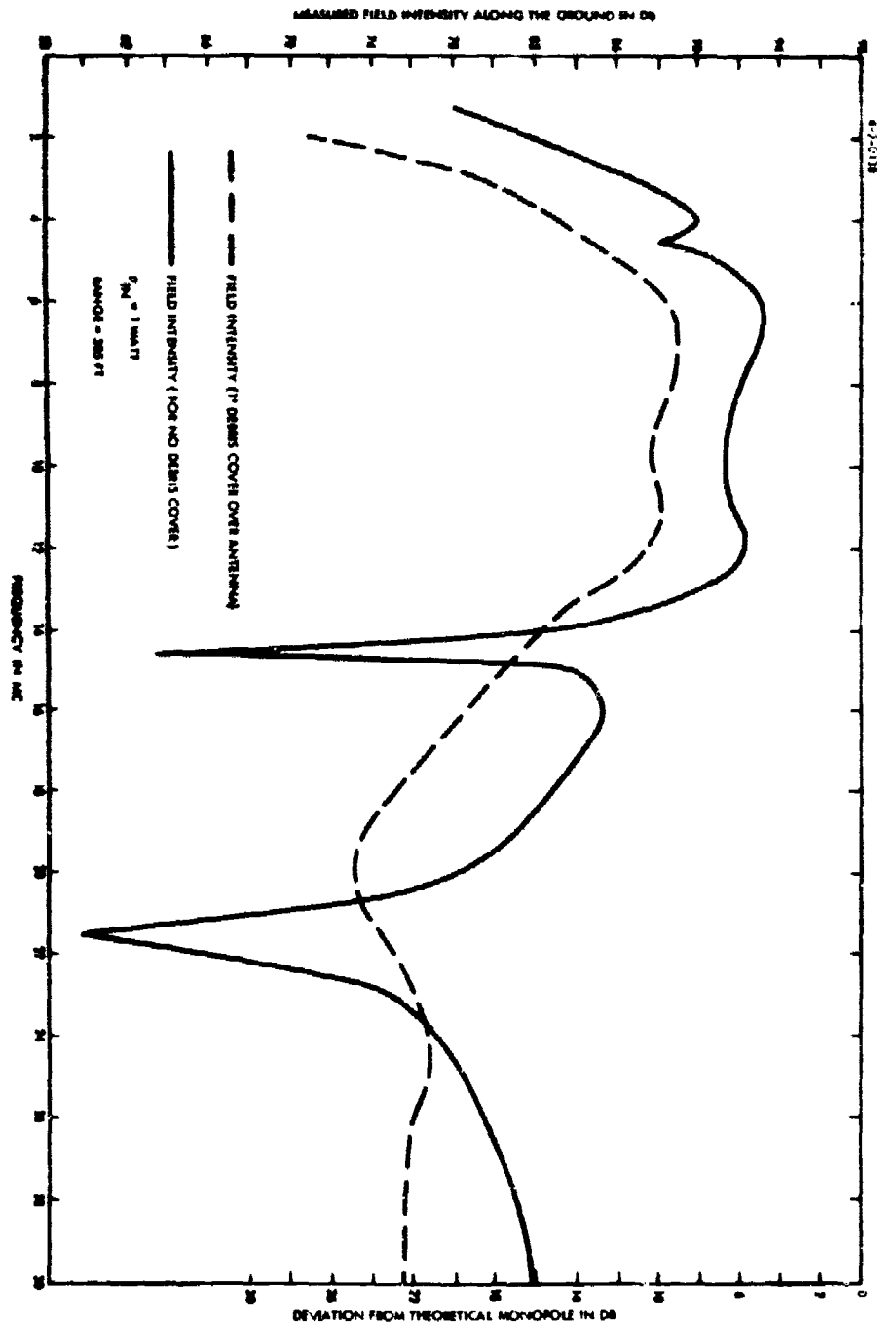


Figure 2-37. Measured Field Intensity Along the Ground Full Cover Condition 2.

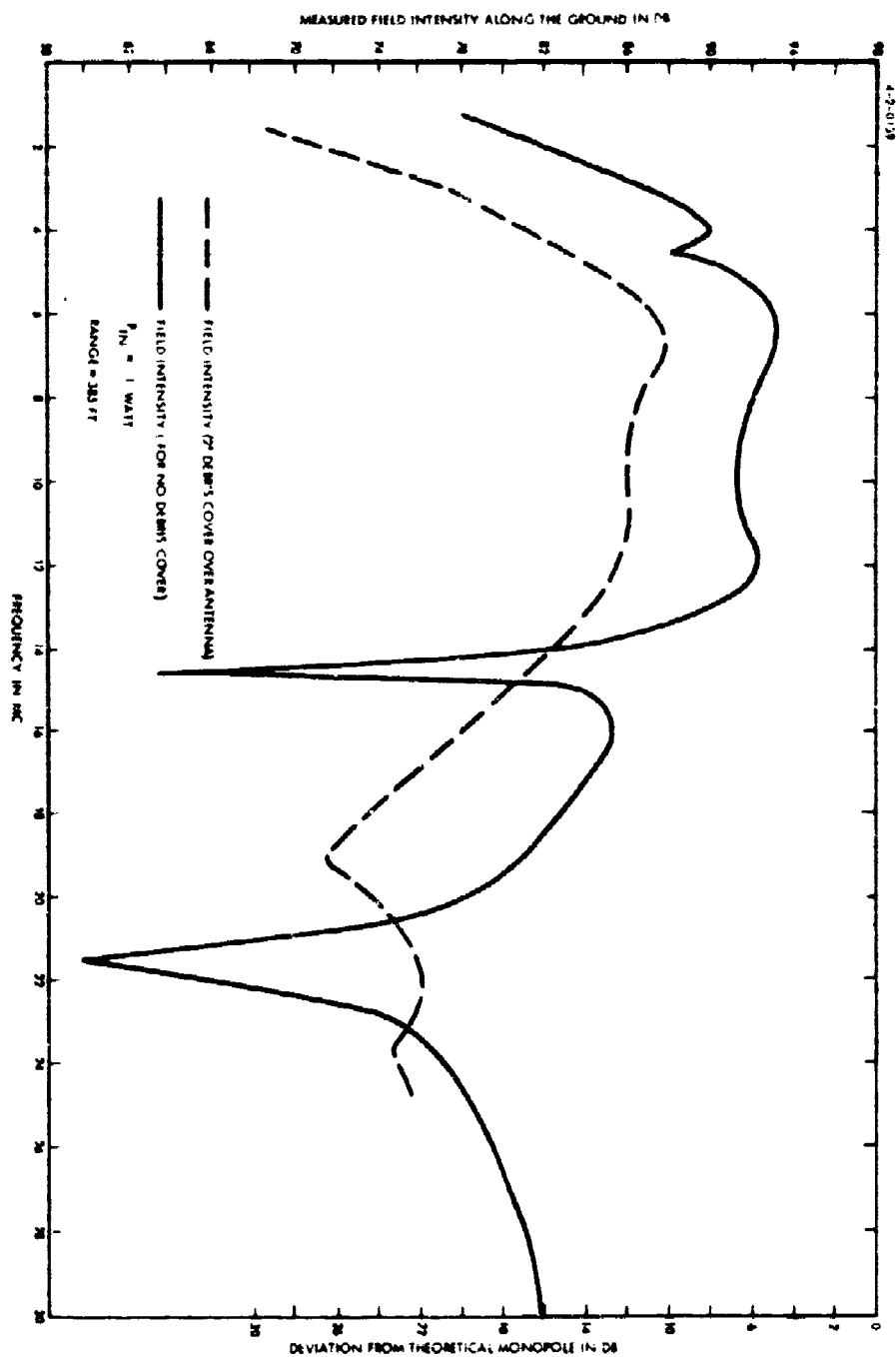


Figure 2-38. Measured Field Intensity Along the Ground Full Cover Condition 3.



### **2.2.6 Debris Characteristics at Antenna Site**

#### **2.2.6.1 Debris Measurement Technique**

The conductivity and dielectric constant of the ground surrounding the annular slot antenna in Warrensburg, Missouri were both measured by the impedance bridge technique. The soil in the immediate vicinity of the annular slot was used to provide a debris cover for the antenna. Basically, the debris parameter measurement technique consists of determining the impedance of the debris between two parallel plates of a capacitor. Figure 2-39 shows the basic setup. A GR type 1606A impedance bridge together with a NF 105 field intensity meter for the null indicator were used.

The debris measurements were made on samples taken from each of the four quadrants of the antenna top hat and at random from regions near the radiating slot. Measurements were made on samples taken from both the first and second 12 inch covers, in addition, the effects of soil compaction and rain were observed.

#### **2.2.6.2 Summary of Debris Parameter Measurements**

Figures 2-40 and 2-41 are plots of the actual reactance and resistance of the debris samples as measured on October 28, 1963 (first 12" cover) and October 29, 1963 (second 12" cover). The following should be noted.

##### **Sample**

- |    |  |
|----|--|
| 1  | is from SE quadrant of antenna                             |
| 2  | is from SW quadrant of antenna                             |
| 3  | is at random from vicinity of radiating slot               |
| 4  | is from NE quadrant of antenna                             |
| 5  | is from North half of radiating slot                       |
| 5' | is sample 5 after 0.13 inches of rain (2 hr rainfall)      |
| 6  | is from central region of antenna near the input terminals |

An initial calibration was made on the test set-up of Figure 2-39 with a dielectric of air and is presented below.

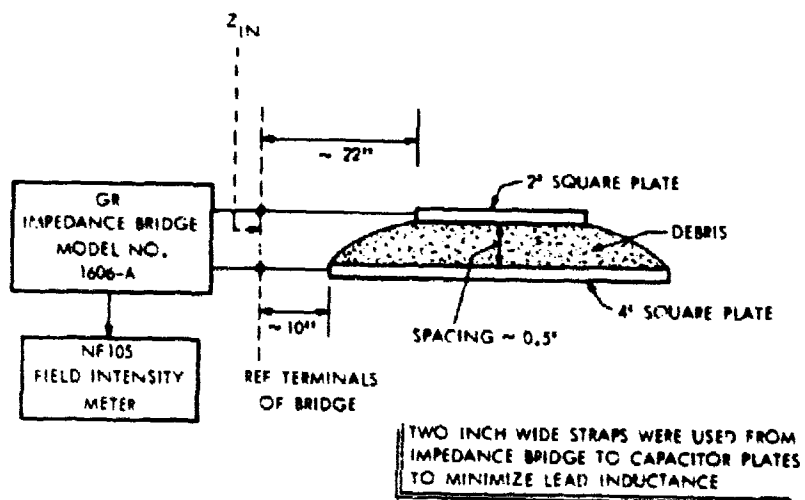


Figure 2-39. Technique for Measuring Debris Parameters.

4-1-0719

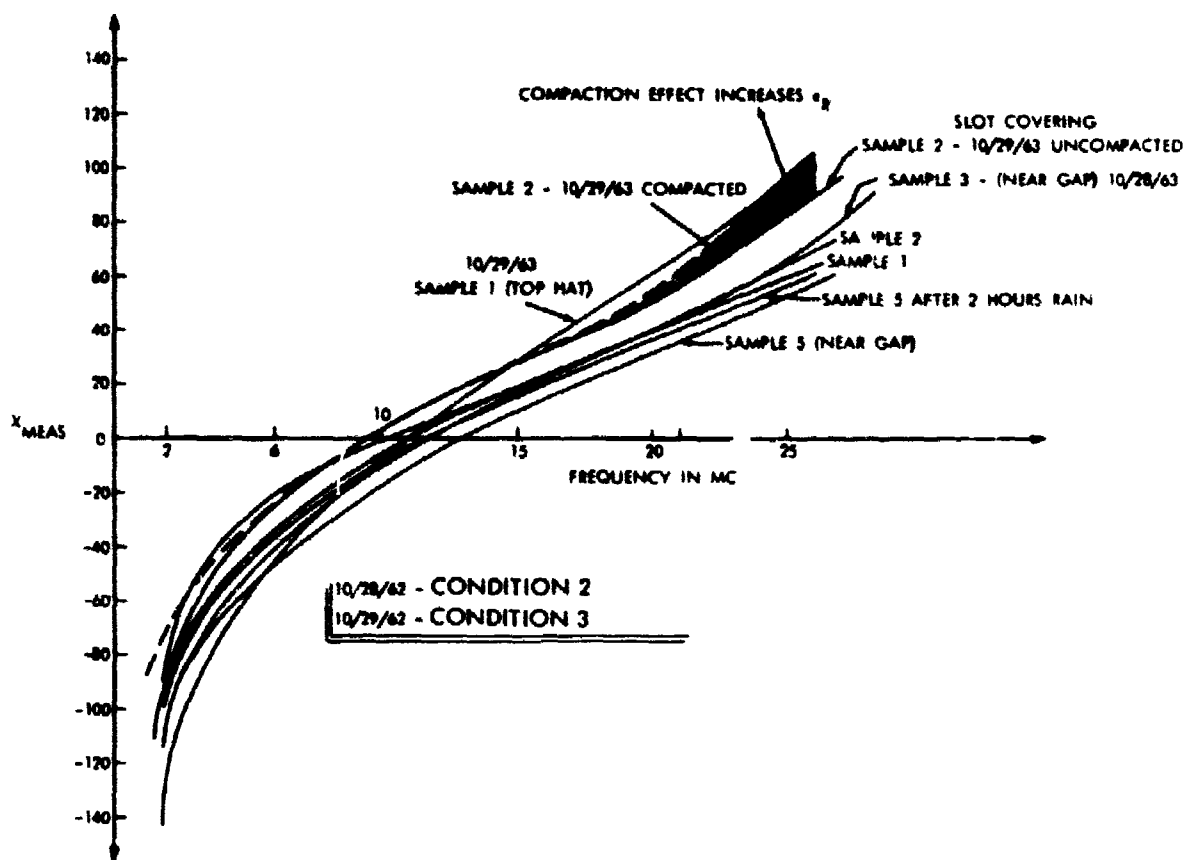


Figure 2-40. Plot of  $X_{debris}$  Versus Frequency for Debris Cover.

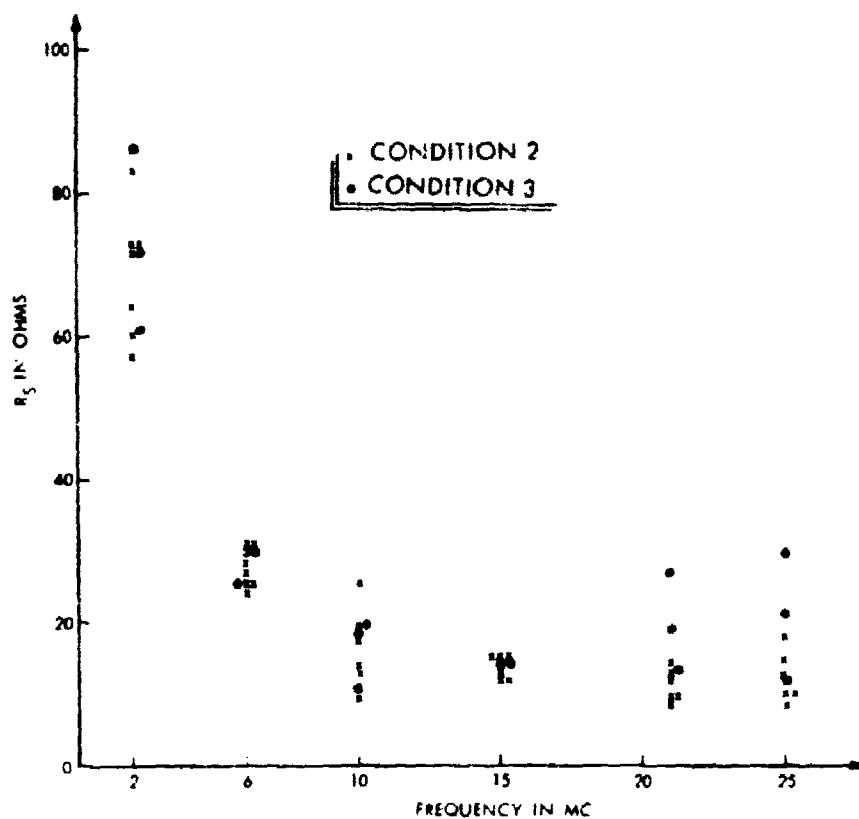


Figure 2-41. Plot of  $R_{\text{debris}}$  Versus Frequency for Debris Cover.

Frequency Mc	$Z_{in}$ (for air dielectric) ohms
2	0.1 - j952
6	0.3 - j308
10	0.3 - j175
15	2 - j96.7
21	1.8 - j47
25	1.75 - j19

These measurements were used to compute the effective series lead inductance in the circuit which had an average value of 0.383  $\mu$ h.

#### 2.2.6.3 Calculation of Debris Parameters and Summary of Debris Constants

The measured data of the reactance versus frequency for the parallel plate capacitor filled with debris approximates that of a series resonant circuit shown in Figure 2.42. From Figure 2-40, the rate of change of the reactance X versus frequency ( $\frac{dX}{d\omega}$ ) at resonance ( $\sim 11$  Mc) is 4.5 ohms/Mc, thus

$$L = \frac{1}{2} \frac{dX}{d\omega}$$

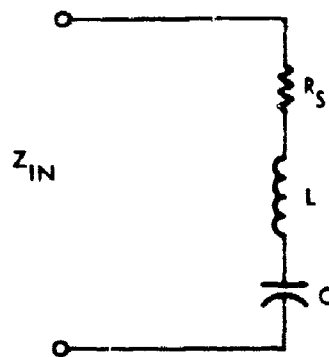
and for

$$\frac{dX}{df} = 4.5$$

$$L = \frac{1}{2} \left( \frac{1}{2\pi} \right) (4.5) = 0.358 \mu\text{h}$$

This value of series lead inductance closely correlates the previous calculations of L (within 7%) made from the impedance measurements in air. Having established a value for L, impedance measurements were made on the circuit in Figure 2-42 with debris as the dielectric in the parallel plate capacitor, C. Since the GR 1606A impedance bridge measures net reactance (i.e.,  $X_L - X_C$ ), it is necessary to add the reactance of the series inductance L to the measured reactance so as to obtain the corrected value

4-1-0721



WHERE

$R_S$  REPRESENT DEBRIS LOSSES

$L_S$  REPRESENT SERIES LEAD INDUCTANCE

$C$  REPRESENT DEBRIS CAPACITANCE

$Z_{IN} = R_S + j X_S$  AS MEASURED ON GR1606A BRIDGE

WHERE  $X_S = X_L - X_C$

Figure 2-42. Equivalent Circuit for Debris Measuring Circuit.

for  $X_C$ , the reactance of the debris loaded capacitor. Having  $X_C$ , the relative dielectric constant and  $Q$  of the debris is computed as follows:

$$\epsilon_R = \frac{X_{C(\text{air})}}{X_{C(\text{debris})}} \quad \left| \quad \text{for any frequency} \right.$$

where  $X_{C(\text{air})}$  at 2 Mc is 952 ohms, and

$$Q_{\text{debris}} = \frac{X_{C(\text{debris})}}{R_{S(\text{debris})}} = \frac{1}{\tan \delta}$$

where  $\tan \delta$  is the loss tangent of debris. Now the debris conductivity is found knowing  $\tan \delta$  from formula previously derived in Appendix A.

i.e.,

$$\sigma = \frac{\tan \delta}{60\lambda} \epsilon_R$$

where

$\sigma$  = mho/m is the debris conductivity

$\lambda$  = wavelength in meters

$\epsilon_R$  = relative dielectric constant

$\tan \delta$  = loss tangent of dielectric

Table II presents a computed summary of the debris parameters from the measured parameters of the first and second 12 inch debris cover. Figure 2-43 is a plot of the debris conductivity versus frequency from which the following can be concluded.

TABLE II

\*SUMMARY OF DEBRIS CONSTANTS COMPUTED FROM THE  
MEASUREMENTS AT WARRENSBURG, MISSOURI

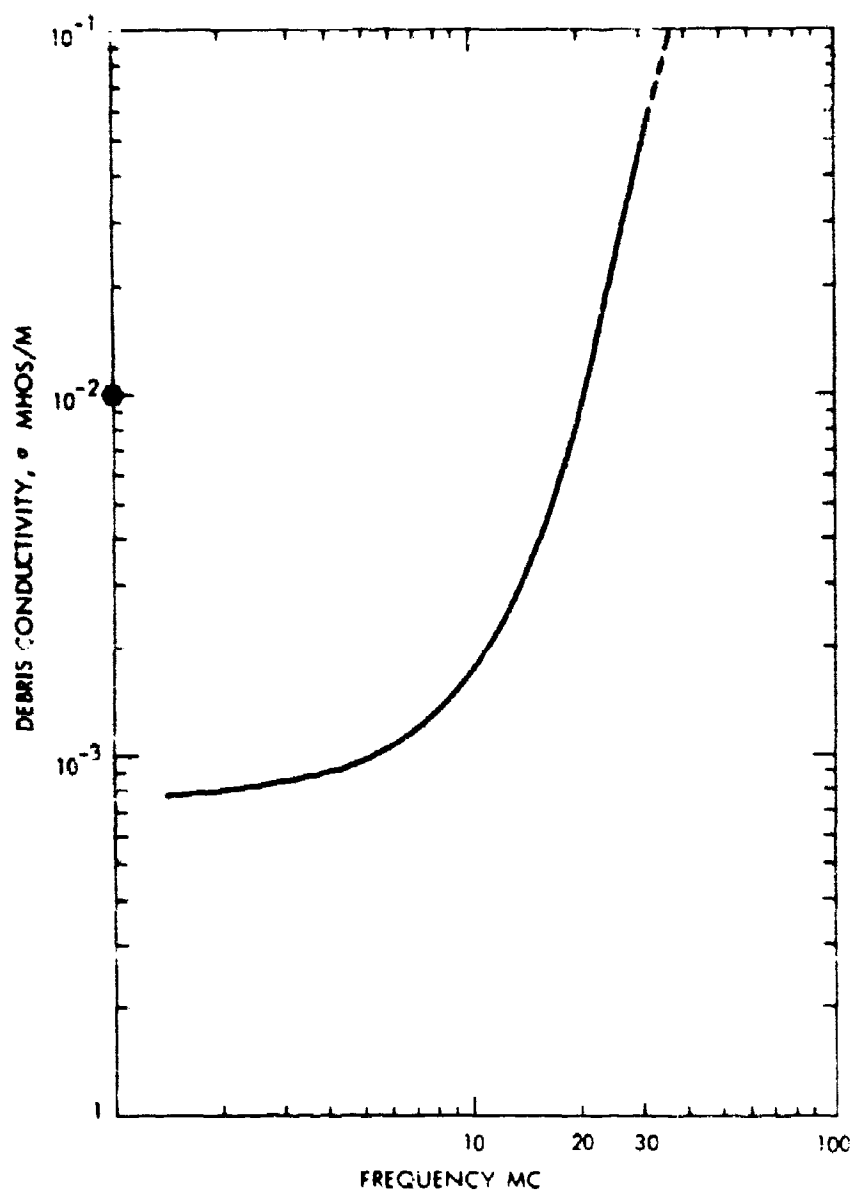
f	$\epsilon_R$	$Q_{\text{debris}}$	$\tan \delta$	$\sigma$
mc	-	-	-	mho/m
2	10	1.37	0.73	$0.8 \times 10^{-3}$
6	6	1.85	0.532	$1 \times 10^{-3}$
10	6	1.73	0.579	$1.9 \times 10^{-3}$
15	6	1.31	0.764	$3.9 \times 10^{-3}$
21	8.6	0.8	1.25	$1.25 \times 10^{-2}$
25	9.8	0.6	1.67	$2.5 \times 10^{-2}$

\*Where  $\epsilon_R$ ,  $Q_{\text{debris}}$ , and  $\sigma$  are average values of all samples measured at particular frequencies.

$$\tan \delta = 1/Q_{\text{debris}}$$



4-1-0722



●  $\sigma \sim 10^{-2}$  MHOS/M BY 97 CPS TEST

Figure 2-43. Debris Conductivity at Warrensburg Versus Frequency.

From

The Soil Conductivity is

2-6 Mc	$\sigma \sim 10^{-3}$ mho/m
6-10 Mc	$\sigma \sim 1.5 \times 10^{-3}$ mho/m
10-15 Mc	$\sigma \sim 3 \times 10^{-3}$ mho/m
15-20 Mc	$\sigma \sim 8 \times 10^{-3}$ mho/m
20-30 Mc	$\sigma \sim 3 \times 10^{-2}$ mho/m

The effects of rain on the debris parameters at Warrensburg, Missouri do not appear to be significant until a condition is reached whereby the soil becomes essentially a paste-like or heavy liquid. The measurements indicate an essentially negligible increase in the relative dielectric constant and series resistance after a 2 hour rainfall in which the total accumulated rain was 0.13 inches. Soil compaction by bull-dozer and walking over debris samples has the effect of increasing the dielectric constant,  $\epsilon_R$ , slightly.

#### 2.2.6.4 Conductivity Measurements by the 97 CPS Probe Technique

Debris conductivity measurements were made at 97 cps using the buried four electrode technique or Vibraground Tester shown in Figure 2-44. The separation between electrodes was 6 inches and the depth of burial was approximately 12 inches.

The summary of the debris parameters measured at 97 cps are listed in Table 3 where it is shown that the average measured value of debris conductivity was ten milli-mhos per meter ( $10^{-2}$  mho/m).

From above it can be concluded that measurements of debris conductivity by the 97 cps technique produces results that fall within the range of values measured by the impedance bridge technique from 2-30 Mc.

4-1-0723

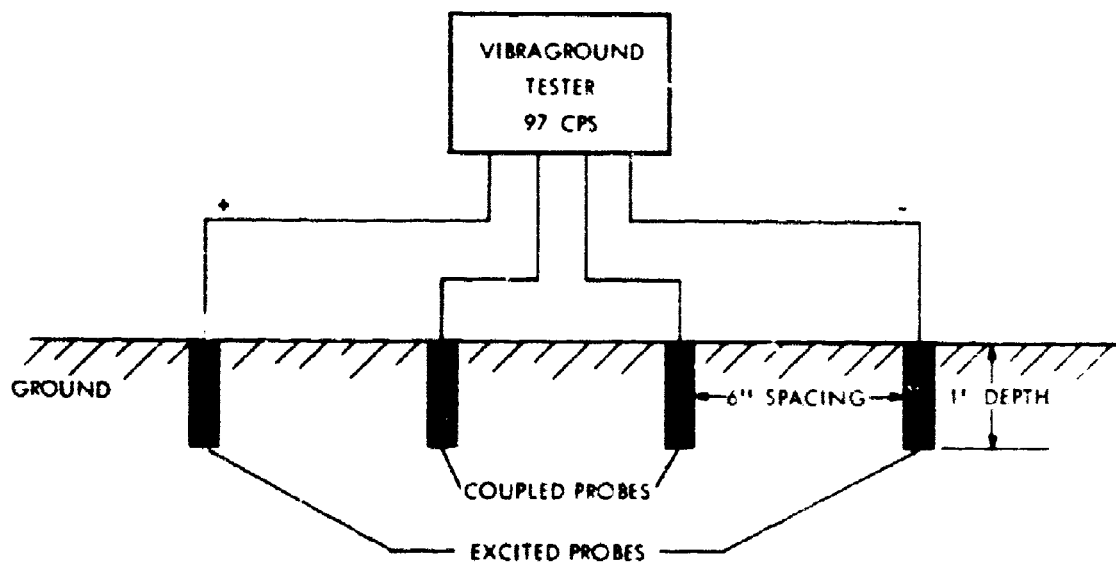


Figure 2-44. Debris Conductivity Measurements by Four Electrode Method.

TABLE III

f cps	Sample Tested	Depth of Probe inches	Separation (D) inches	$\bar{R}$	R avg	$\sigma$ mho/m
97	#5	12	6	90	$8.62 \times 10^3$	$1.16 \times 10^{-2}$
97	#4	12	6	100	$9.6 \times 10^3$	$1.04 \times 10^{-2}$
97	#4	6	6	150	$14.4 \times 10^3$	$0.7 \times 10^{-2}$

where

$$R_{avg} = D \bar{R} \times 191.51$$

D = Separation of probes in feet

$\bar{R}$  = Vibraground meter reading in ohms

and

$$\sigma = \frac{100}{R} \text{ mho/m}$$

### 2.2.7 Evaluation of Impedance Measurements of Annular Slot Antenna

#### Correlation of Theoretical and Measured Terminal Impedance of Antenna. No Debris.

The admittance of the annular slot antenna has been calculated by Galejs and Thompson<sup>3</sup>. The antenna is a cavity backed annular slot and it is assumed that the radiation or far field is due almost entirely to the fringing of the electric field maintained across the gap between the disk and the adjacent highly conducting ground. The admittance across the slot is calculated, i.e. the edge of the disk and the edge of the cavity are considered as terminals. In practice, however, such an antenna is fed from the center by inserting a coupling network between the center of the disk and the ground which forms the bottom of the cavity. In the Warrensburg antenna, the feed network at the center of the antenna consisted of a vertical wire-fan, length 1.2 meters, made of three wires which were connected to a coax feed cable. The ground screen was raised in the center and connected to the outer conductor of the feed cable. (See Figure 2-25).

The impedance of the antenna was measured at point P where the feed cable is connected to the raised ground screen. Since the impedance was measured in the center of the antenna, and was calculated at the slot it is necessary to establish the analytical relation between the impedances at the two terminal points. The following approach was chosen.

The antenna structure is considered a radial transmission line shown in Figure 2-45 which is formed by the disk (hat) and the ground plane with asphaltic concrete as the dielectric. The average radius between disk and end of cavity  $r_0 = \frac{\zeta_1 + \zeta_2}{2}$ . The inside radius  $r_1$  is the average radius of the wire-fan at the feed point. The transmission line is loaded at the outer end by the admittance ( $Y_{out}$ ) reflected to the slot plane by the outside space. This has been computed using the results of Galejs and Thompson analysis of the cavity backed annular slot.  $Y_{out} = G_R + j\omega C_S$  where  $G_R$  is the radiation conductance of the slot and  $C_S$  is the edge capacity of the disk against the surrounding ground. At the inner end (near the center) the radial transmission line is connected to the short fan-shaped line. This is considered as a linear transmission line of short length (corresponding to the physical length) and air as dielectric. The outside admittance

4-1-0724

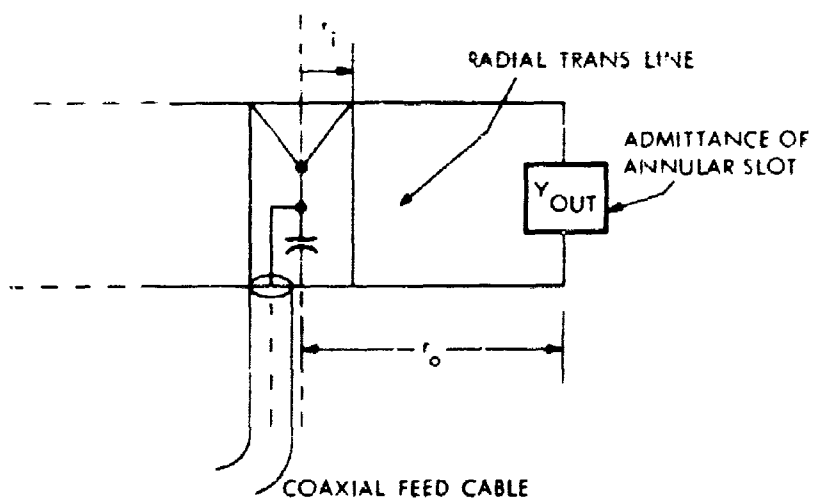


Figure 2-45. Radial Transmission Line Model for Annular Slot Antenna.

(load admittance) is transformed by the radial transmission line to the input admittance at radius  $r_1$ : which then is the load admittance for the short linear transmission line. This transformation is accomplished by the following relations<sup>4</sup> which are valid for the dominant E-type mode (i.e.,  $m=0$ ,  $n=0$ ).

$$Y'(r_1) = \frac{j + Y'(r_0) \zeta(x,y) \operatorname{ct}(x,y)}{\operatorname{Ct}(x,y) + j Y'(r_0) \zeta(x,y)} \quad (18)$$

where

$$\operatorname{ct}(x,y) = \frac{J_1(x) N_0(y) - N_1(x) J_0(y)}{J_0(x) N_0(y) - N_0(x) J_0(y)}$$

$$\operatorname{Ct}(x,y) = \frac{J_1(y) N_0(x) - N_1(y) J_0(x)}{J_1(x) N_1(y) - N_1(x) J_1(y)}$$

$$\zeta(x,y) = \frac{J_0(x) N_0(y) - N_0(x) J_0(y)}{J_1(x) N_1(y) - N_1(x) J_1(y)}$$

$$x = k_c r_1 \quad y = k_c r_0$$

$$Y'(r_1) = \frac{Y(r_1)}{Y_1} = Y(r_1) Z_1 = \frac{Z_1}{Z(r_1)}$$

$$Y'(r_0) = \frac{Y(r_0)}{Y_0} = Y(r_0) Z_0 = \frac{Z_0}{Z(r_0)}$$

$Z_1$  and  $Z_0$  are the characteristic impedances at the inner radius  $r_1$  and outer radius  $r_0$  respectively

$$z_1 = \frac{\zeta b}{2\pi r_1} ; \quad z_0 = \frac{\zeta b}{2\pi r_0}$$

$$\zeta = \sqrt{\frac{\mu}{\epsilon_c}}$$

where  $b$  is the distance between the two plates of the radial transmission line. The dielectric in the radial transmission line is asphaltic concrete which has losses which can be expressed by the  $Q$  - factor.  $k_c$  is therefore complex and is expressed by the complex dielectric constant which is given by

$$\epsilon_c = \epsilon_0 \epsilon_r \left( 1 - j \frac{\epsilon''}{\epsilon_r} \right)$$

$$\frac{\epsilon''}{\epsilon_r} = \frac{\sigma}{\omega \epsilon_0 \epsilon_r} = \frac{\sigma}{\epsilon_r} = \tan \delta = \frac{1}{Q}$$

$$k_c^2 = \omega^2 \mu_0 \epsilon_c = (\omega^2 \mu_0 \epsilon_0) \epsilon_r \left( 1 - j \frac{\epsilon''}{\epsilon_r} \right)$$

$$= (\omega^2 \mu_0 \epsilon_0) \epsilon_r \left( 1 - j \frac{1}{Q} \right)$$

$$k_c = k_0 \sqrt{\epsilon_r} \sqrt{1 - j \frac{1}{Q}} \approx k_0 \sqrt{\epsilon_r} \left( 1 - \frac{j}{2Q} \right) \quad \text{if } Q \gg 1$$

$$k_0 = \omega \sqrt{\mu_0 \epsilon_0} = \frac{2\pi f}{c_0} = \frac{2\pi}{\lambda_0}$$



Using these equations  $x$  and  $y$  are found to be

$$x = k_1 r_i = \frac{2\pi}{\lambda_0} \sqrt{\epsilon_r} r_i \left(1 - \frac{j}{2Q}\right)$$

$$x = \frac{\pi}{150} f_{mc} \sqrt{\epsilon_r} r_i \left(1 - \frac{j}{2Q}\right)$$

$$y = k_1 r_o = \frac{\pi}{150} f_{mc} \sqrt{\epsilon_r} r_o \left(1 - \frac{j}{2Q}\right)$$

For the characteristic impedances one need not use the complex dielectric constant since  $Q$  is large. Thus  $Z_i$  and  $Z_o$  are real:

$$Z_i = \frac{120 \pi b}{2\pi r_i \sqrt{\epsilon_r}} = \frac{60 b}{r_i \sqrt{\epsilon_r}}$$

$$Z_o = \frac{60 b}{r_o \sqrt{\epsilon_r}}$$

The constants were chosen to give best agreement with the measurements, and they are in agreement with the physical dimensions of the antenna. The relative dielectric constant of the asphaltic concrete is  $\epsilon_r$ , which varies between 3 and 4. A value of 3.65 was chosen since this agrees with the second notch of the field strength versus frequency curve at 14.6 Mc. The outer radius  $r_o$  is the average between disk and cavity radius. The inner radius  $r_i$  is not critical. A change of  $r_i$  between 0.1 and 1 meter hardly affects the impedances. The following values are used for the computations:

$$r_i \sqrt{\epsilon_r} = 0.3$$

$$r_o \sqrt{\epsilon_r} = 15.9$$

$$r_i = 0.157 \text{ m}$$

$$r_o = 8.35 \text{ m}$$

$$\text{(The average outer radius is } \frac{7.3 + 9.6}{2} = 8.45 \text{ m)}$$

$$b = 1.37 \text{ m}$$

$$\epsilon_r = 3.65$$

$$Q = 25$$

With these data the characteristic impedance at the outer radius

$$Z_o = \frac{60 b}{r_o \sqrt{\epsilon_r}} = \frac{82.6}{15.9} = 51.9 \text{ ohms}$$

and the characteristic impedance at the inner radius

$$Z_i = \frac{60b}{r_i \sqrt{\epsilon_r}} = \frac{82.6}{0.3} = 276 \text{ ohms}$$

The efficiency of the annular slot antenna, using the radial line technique, is calculated from the basic line equation:

$$V(r) = V(r_o) [Cs(x,y) - j Z_o I(r_o) sn(x,y)]$$

$$ZI(r) = Z_o I(r_o) cs(x,y) - j V(r_o) Sn(x,y)$$

$$\eta = \frac{|V(r_o)|^2 G_R}{|V(r)|^2 \text{Re}\{Y(r)\}}$$

where

$V(r_o)$  is the voltage at the outer radius  $r_o$ , and  $|V(r_o)|^2 G_R$  is the radiated power,  $V(r)$  is the voltage at the inner radius  $r_i$ , and  $Y(r_i)$  the input admittance at this point and  $|V(r_i)|^2 \text{Re}\{Y(r_i)\}$  is the input power.

The input admittance  $Y(r_i)$  and the normalized input admittance  $Y'(r_i)$  are related by

$$Y(r_i) = \frac{Y'(r_i)}{Z} \quad ; \quad Y'(r_i) \text{ is given by Equation (18)}$$

$$V(r_i) = V(r_o) [Cs(x,y) - j Y'(r_o) sn(x,y)]$$

$$= V(r_o) F(x,y)$$

Thus

$$\eta = \frac{G_R}{F(x,y)^2 \text{Re}\{Y(r_i)\}}$$

Best agreement between measured and theoretical impedances was achieved by using a short linear line in series with the radial transmission line. The product of characteristic impedance and line length of the linear line was chosen so that the calculated reactance was equal to the measured reactance at the frequency of 3.43 Mc. At this frequency the input reactance of the radial line is -8.0 ohms, and the measured reactance is + 21.3 ohms. Thus the linear line should give a reactance of  $21.3 + 8 = 29.3$  ohms at  $f = 3.43$  Mc. The reactance of the line is

$$Z_{tg} \beta l \approx Z \beta l = \frac{Z 2\pi l}{\lambda} = \frac{Z 2\pi}{300} \cdot f l$$

$$\text{Thus } Z l = \frac{29.3}{2\pi} \frac{300}{3.43} = 408 \text{ ohm meters}$$

The physical length of the linear line is 1.2 m

$$\text{Hence } Z = \frac{408}{1.2} = 340 \text{ ohms}$$

The value of the characteristic impedance corresponds to the average characteristic impedance of the wire fan which constitutes the line.

The equivalent circuit which was used to calculate the input impedance is shown in Figure 2-46.

The radial line is loaded at the outer end with the outside admittance  $Y_{out} = G_R + j\omega C_s$  of the cavity. The radius  $r_o = \frac{r_1 + r_2}{2}$  is the average between disk and cavity edge. The impedance  $(R + jX)$  at a small radius  $r_1$  is calculated by radial transmission line theory. This impedance  $(R + jX)$  is the load for the short linear line which transforms the load impedance to the input impedance  $(R_1 + jX_1)$  using conventional transmission line theory (Smith Chart). The result of this computation is given in the following Table IV and is plotted on the Smith Chart (Figures 47 and 48) together with the measured impedance (referenced to an impedance of 50 ohm). It can be seen that the agreement between theory and measurement up to a frequency of about 13 mc is very good, in particular with respect to the reactance. At the low frequencies the theoretical resistance values are smaller than the measured values. This could possibly be due to the fact that the actual Q value of the radial line, which is determined by ground losses and dielectric losses

4-1-0725

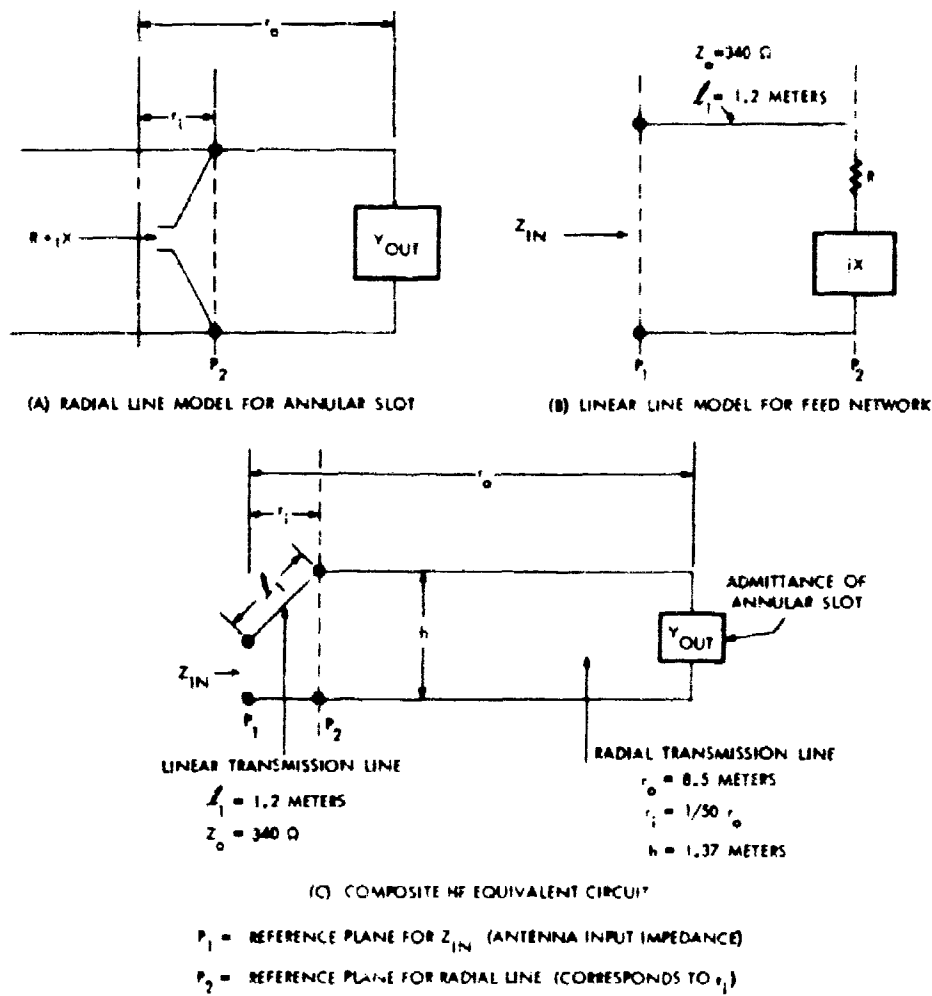


Figure 2-46. Equivalent for Computing Antenna Input Impedance for Radial Line Model.

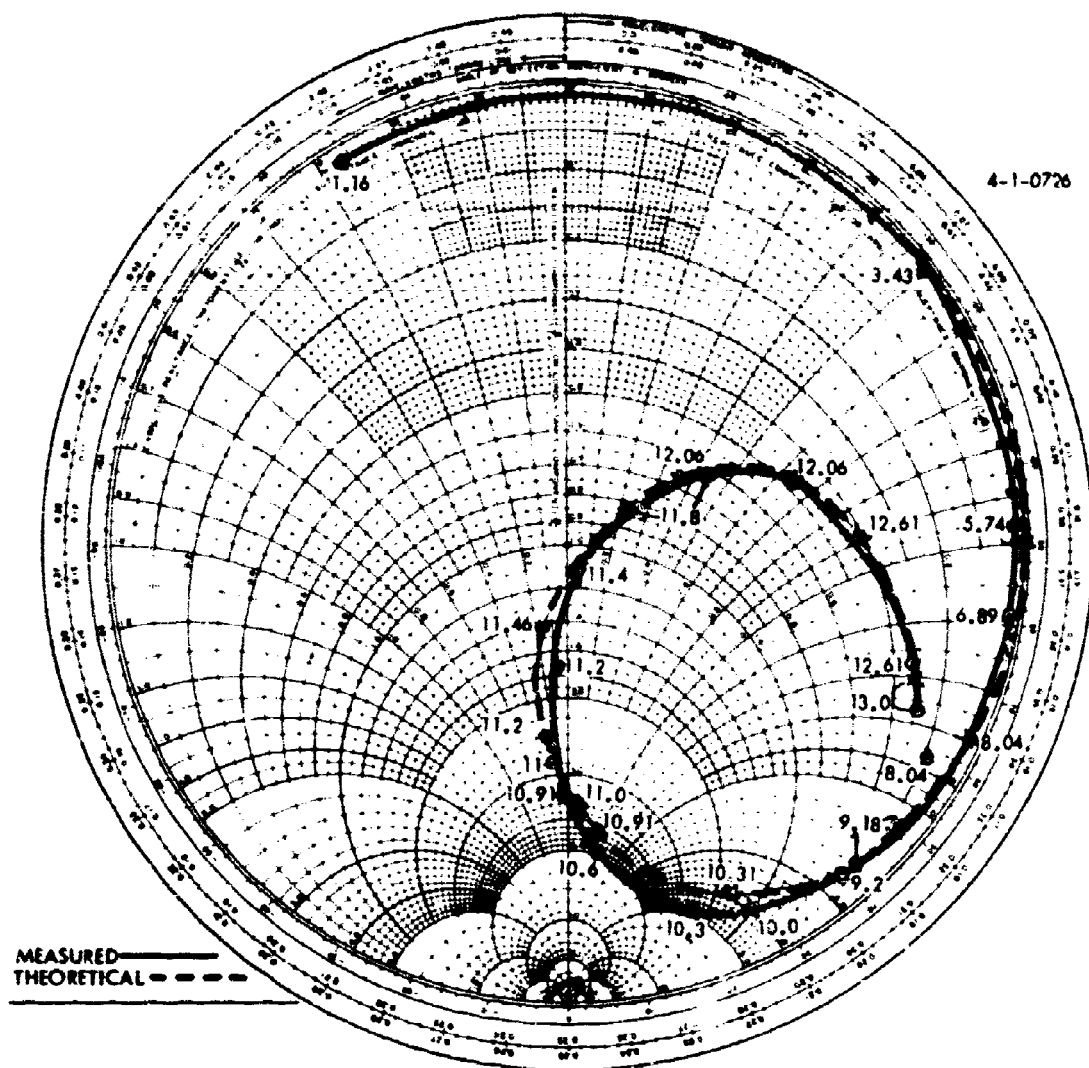


Figure 2-47. Input Impedance Versus Frequency for Radial Line - 1.16 to 13 Mc.

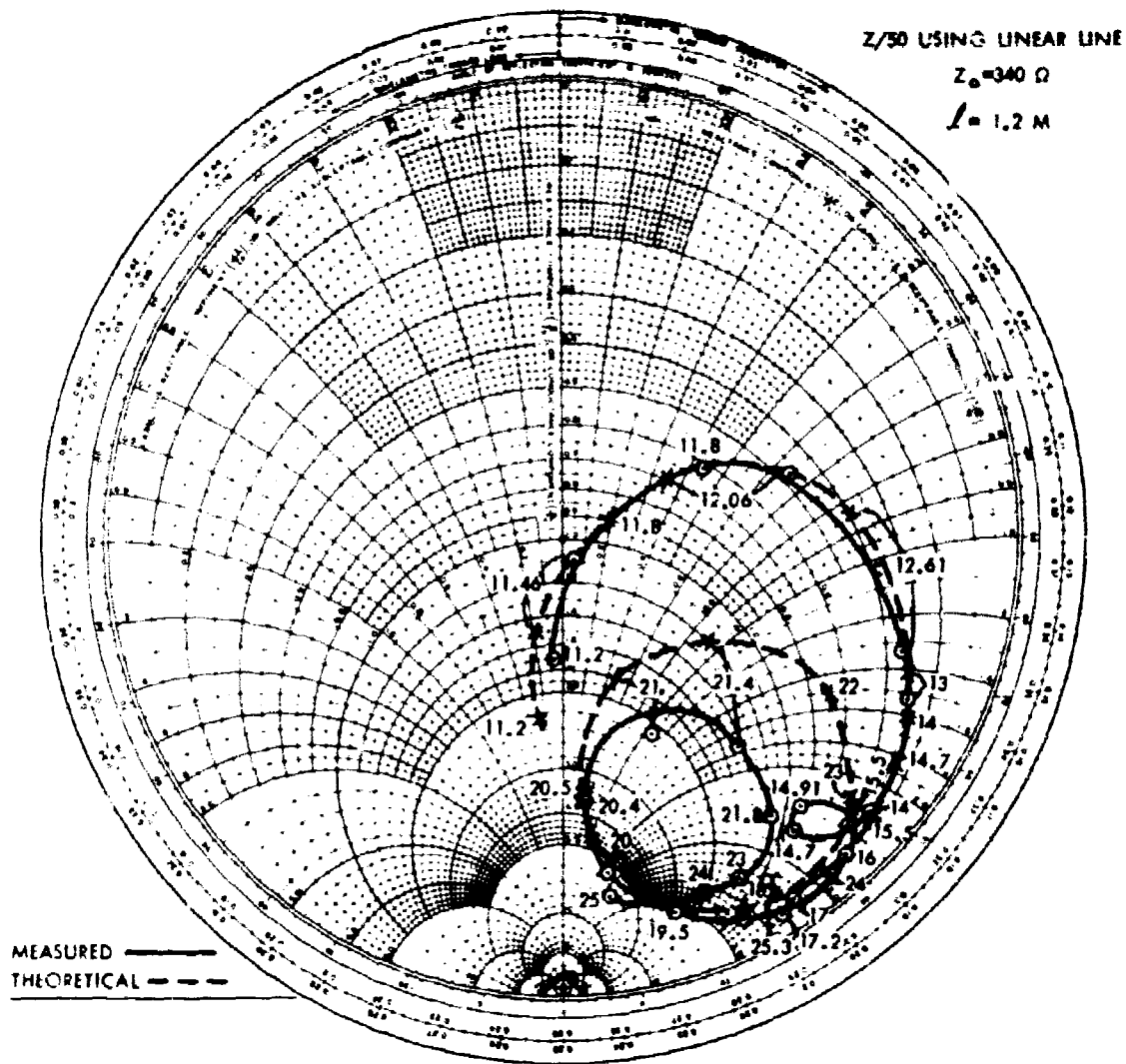


Figure 2-48 Input Impedance Versus Frequency for Radial Line - 11.2 to 25.3 Mc.

TABLE IV

CALCULATED INPUT IMPEDANCE OF THE ANNULAR SLOT

$\epsilon$	$G_R$	$C_s$	$R$	$X$	$R_1$	$X_1$	$\frac{R_1}{50}$	$\frac{X_1}{50}$
3.41	$.061 \times 10^{-2}$	$1.412 \times 10^{-2}$	.225	- 8.03	.23	+ 24	.005	+ .48
5.74	.293	2.58	.537	- 1.86	.60	+ 49	.01	+ 1.0
8.04	.551	3.125	2.39	+ 10.8	2.4	+ 82	.05	+ 1.6
9.18	.868	3.53	8.21	+ 29.7	8.2	+ 106	.16	+ 2.12
10.31	1.252	3.835	63.6	+ 87.3	76	+ 190	1.56	+ 3.8
10.91	1.468	3.96	214.5	- 10.6	210	+ 47	4.2	+ .94
11.0	1.90	4.10	180	- 52.6	177	+ 14	3.55	+ .29
11.2	1.96	4.12	135	- 95.8	120	- 14	2.4	- .27
11.46	2.064	4.11	83.7	- 103	75	- 10	1.5	- .20
11.8	2.232	4.10	48.1	- 70.8	44	+ 8.5	.88	+ .17
12.06	2.32	4.12	34.1	- 80.4	34	+ 17	.68	+ .34
12.61	2.51	4.12	20	- 64.3	20.5	+ 41	.41	+ .82
13	2.64	4.10	15.4	- 56.4	15	+ 68	.30	+ 1.4
14	2.92	4.04	10.4	- 42.7	14	+ 78	.28	+ 1.6
14.7	3.07	4.02	9.35	- 35.6	12	+ 92	.24	+ 1.84
16.0	3.27	4.05	10.3	- 23	14	+ 119	.28	+ 2.40
18.0	4.26	4.42	23.7	+ 7.7	34	+ 176	.68	+ 3.56
20.0	3.03	5.28	58.2	+ 40.2	227	+ 150	4.55	+ 3.0
21	2.91	5.86	18*	+ 30.7	95	+ 24	1.9	+ .48
22	2.83	6.49	136	- 156	34	+ 75	.68	+ 1.5
23	2.82	7.10	47.0	- 131	22	+ 109	.44	+ 2.18
24	2.80	7.64	24.9	- 102	18.5	+ 142	.37	+ 2.85
25.1	3.16	8.12	19.0	- 76.1	27.0	+ 187	.54	+ 3.74

$$Y_0 = G_R + j C_s$$

\*\* See figure 34 for definition of  $\mu$ ,  $X$ ,  $R_1$ ,  $X_1$

in the asphaltic concrete, is different from that chosen for the computation ( $Q_c = 25$  was chosen). Theoretical reactance is somewhat slipping behind the measured reactance in particular at the higher frequencies. Between 14 and 16 Mc the measured impedance forms a small loop on the Smith Chart. This does not show up in the theoretical curve and it is not clear what causes this loop. It might perhaps be a higher mode of the radial line, which starts propagating. The third loop of the measured curve (20-25 Mc) has a smaller radius and is shifted to higher resistances and reactances than the corresponding theoretical loop in this frequency range. The shift to higher resistances is probably due to a lower  $Q$  in this band. Measurements indicate that the actual  $Q$  drops to 5 and below at the high end of the band, thus explaining higher input resistances and lower efficiency. The increasing slipping of the reactances with increasing frequency seems to indicate that the outer radius  $r_o$  of the radial line is a little bit too small. A small increase in  $r_o$  will have an effect on the input reactance which increases with frequency. It would hardly be noticeable at low frequencies but have an appreciable effect at high frequencies. So it is possible that a slightly larger  $r_o$  will produce better agreement between theoretical and measured data. From this comparison of theoretical and measured data the following conclusions are drawn:

The input impedance of the annular slot antenna can be predicted with a fair degree of accuracy by using a model shown in Figure 2-46 consisting of a radial transmission line which is loaded at its outer end with the outside admittance of the cavity, and is connected close to the center of the line with a short linear transmission line. The constants of the radial line are determined by the average outer radius  $r_o = \frac{r_1 + r_2}{2}$ , the inner radius  $r_1$ ,

which is very small ( $r_1, r_o \sim \frac{1}{50}$  or less, not critical), the height of the disk above the ground, and the dielectric constant and  $Q$  factor of the dielectric which fills the cavity. The characteristic impedance and length of the linear transmission line are corresponding to the average diameter of the wire which makes up the line, and to the physical length of this wire, which is about equal to the distance between the top hat and ground of the antenna. For this case,  $Z_o$  was taken equal to 340 ohms and the length of line was 1.2 meters.

Further study is required to determine the effects of debris on the antenna impedance. Debris coverage will affect the outside slot admittance and possibly the attenuation and characteristic impedance of the radial transmission line.



## 2.2.8 Measured Properties of Asphaltic Concrete

### 2.2.8.1 Q Factor

A calculation of the asphaltic Q of the antenna was made from a measurement of the input impedance at 440 kc. A GR-1606 A impedance bridge was connected across the input antenna terminals in the access hole of the antenna for these measurement.

Thus

$$\begin{aligned}Z_{in} &= R - jX_C \\&= 2 - j50\end{aligned}$$

and

$$Q_{\text{asphalt}} = \frac{X_C}{R} = \frac{50}{2} = 25$$

The antenna at these frequencies represents a parallel plate capacitor having a capacitance of 6900 $\mu$ pf.

Another measurement of asphaltic Q was made in the HF region. A small screen was placed over the top of the antenna and impedance measurements were made as to the capacitance of this plate to the top hat of the antenna. The results of these measurements are plotted in Figure 2-49, and indicate a close correlation to the measurements at 440 kc. Another interesting point shown in this figure is the roll off of the asphaltic Q beyond 12 Mc. This may be a contributing factor as to the low efficiency exhibited by the antenna beyond 15 Mc, and is probably due to the cracks developing in the antenna asphalt blanket, especially in the vicinity of the central access port. This cracking may be due to the bulldozers and associated construction equipment used to put on and take off the debris cover on the Sylvania investigations of the annular slot antenna for the minuteman program.

### 2.2.8.2 Dielectric Constant

The calculation of the dielectric constant of the asphaltic concrete was made from the antenna input impedance measurements at 440 kc and the measurement of the second notch in the field intensity versus frequency curve (Figure 2-35).

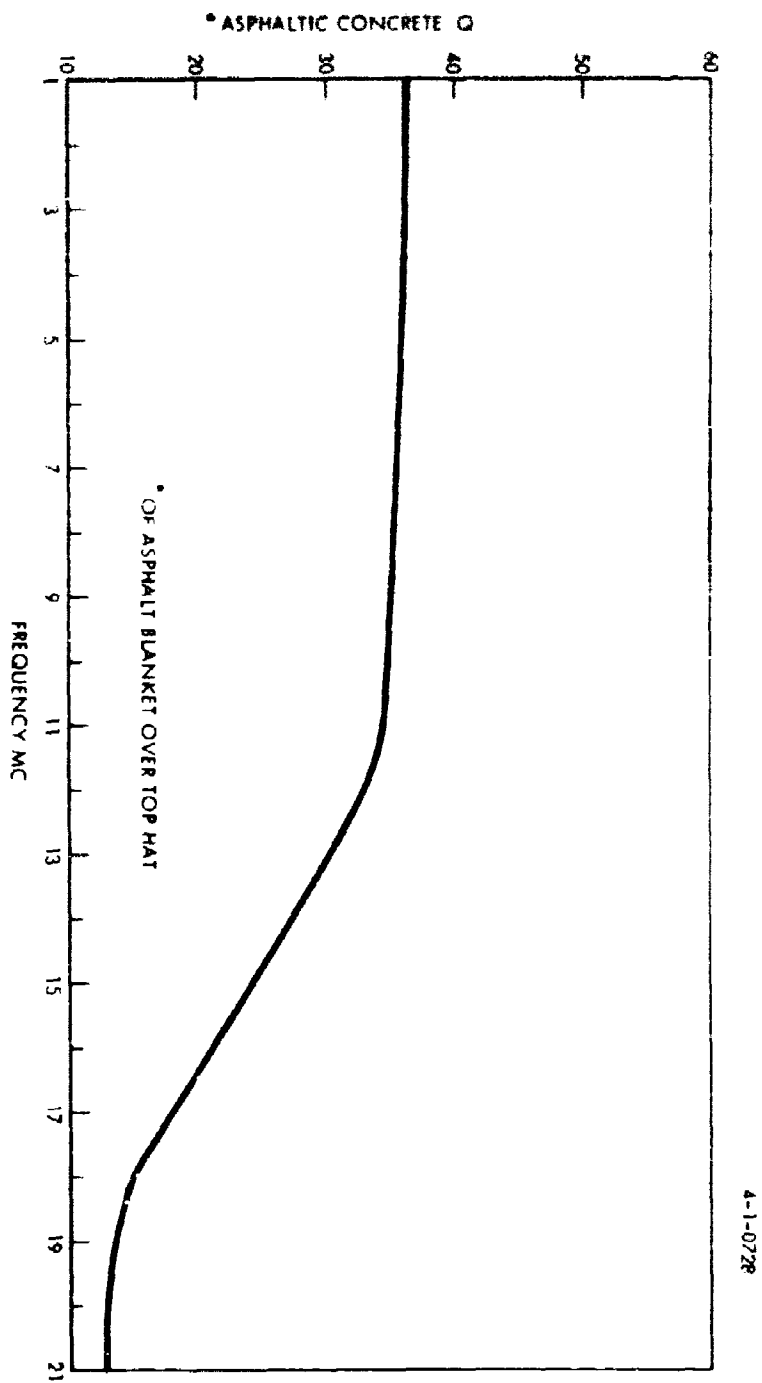


Figure 2-49. Asphaltic Q Versus Frequency.

Now the antenna input impedance measurement at 440 kc indicated the following:

$$Z_{in} = 2 - j50$$

from which the capacity of the antenna embedded in asphalt is 6900  $\mu\mu\text{f}$ , or 4 times that of the antenna with a dielectric constant of unity (i.e., capacitance in air).

From Section 1.3, Admittance of the Annular Slot Antenna, Equation (2.12), the notches in the efficiency and field intensity curves versus frequency occur when

$$\frac{b}{\lambda} = \frac{\text{Roots of } J_0(\lambda_a b)}{2\pi \sqrt{\epsilon_1}} = \frac{a_1}{2\pi \sqrt{\epsilon_1}}$$

where

$a_1 = 2.403$  for 1st notch,  $= 5.52$  for 2nd notch,  $= 8.65$  for 3rd notch

$b$  = outer radius of annular slot,

$\lambda$  = wavelength

$\epsilon_1$  = dielectric constant of asphaltic concrete

Considering the second notch which was measured at 14.6 Mc, we find that for an  $\epsilon_1$  (asphaltic concrete dielectric constant) of 3.65, the theoretical and measured notches coincide -- i.e.,

$$\epsilon_1 = \left[ \frac{v_{air} a_1}{2\pi b f} \right]^2$$

where

$a_1 = 5.52$  at second notch

$v_{air} = 1000 \times 10^6$  ft/sec (velocity of propagation in air)

$b = 31.5$  ft

$f = 14.6$  Mc

thus

$$\epsilon_1 = \frac{5.52 \times 1000}{2\pi \times 31.5 \times 14.6} = (1.91)^2 = 3.65$$

The value of dielectric constant as measured in the HF range was used in the computer program for evaluating the theoretical performance of the annular slot antenna.

### 2.2.9 Analysis of Data and Conclusions

A comparison of theoretical predictions and the measured parameters of the annular slot antenna in Warrensburg, Missouri yields the following conclusions:

#### 2.2.9.1 Notches in Efficiency

The predicted notches in the efficiency from 2 to 30 Mc were observed. They are due to the multiple series resonant frequency of the back-up cavity at which point the cavity presents a low impedance across the radiating annular slot. The predicted and measured notches are as follows:

<u>Measured <math>f_{\text{notch}}</math></u>	<u>Predicted <math>f_{\text{notch}}</math></u>	<u>Comments</u>
4.5 to 5 Mc	6 Mc	Shift in position of measured notch may be attributed to antenna lead in series inductance slight changes in both asphaltic dielectric constant and effective radius of radiating slot.
14.6 Mc	14.6 Mc	Both notches coincide for an average radius of 28 feet, and an asphaltic dielectric constant of 3.65.
21.6 Mc	21.6 Mc	Both notches coincide for an average antenna radius of 28 feet. This null is due to the sky wave effect or shift in elevation of the main lobe of the antenna at the upper end of the HF band.

#### 2.2.9.2 High Efficiency

The predicted regions of high efficiency in between the notches were measured. For an asphaltic Q of 25, the actual antenna efficiency curve approximates the predictions from 2 to 15 Mc; above 15 Mc, the assumption such as uniform excitation of the annular slot both radially and

circumferential, constant asphaltic Q do not hold; therefore a greater deviation exists between theoretical predictions and actual measurements.

The Warrensburg antenna appears to be an optimum physical design from 3.5 to 13.5 Mc where the efficiency, with no debris cover, is equal to or greater than 10 percent. From 5.5 to 12.5 Mc the efficiency, with no debris, is greater than 25 percent and approaches 40 percent. These efficiencies are for a measured asphaltic Q of 23; if the asphaltic Q were 70, antenna efficiencies in the order of 85 to 90 percent would have been possible.

#### 2.2.9.3 Performance of Antenna Under a Debris Cover

The effects of debris having measured parameters from  $10^{-3}$  to  $30 \times 10^{-3}$  mho/m were observed under conditions 1, 2, and 3. Measurements were made as to the field strength at a point 385 feet from the antenna. The reference used throughout these tests was the computed field strength at 385 feet for a short vertical monopole (100 percent efficiency) having a power input of 1 watt, or a theoretical field strength along the ground of 98 db above 1 microvolt/meter. Tables V and VI summarize some of the significant data taken from the field intensity plots in Section 2.2.5.

From the above, and curves in Section 2.2.5, it can be concluded that:

- (a) Antenna degradation due to debris is a minimum at frequencies for which the antenna dimensions are optimized, i.e., a diameter-to-wavelength ratio ( $D/\lambda$ ) of 0.9 to 1.
- (b) Debris degradation is very low in the optimized frequency range under condition 1; i.e., approximately -1 db.
- (c) Debris degradation is greatest under condition 2; condition 3 appears to degrade the antenna slightly, i.e., approximately 0 to -2 db.
- (d) Debris degradation is more severe at frequencies for which  $D/\lambda$  approaches 0.25. Thus in the frequency range of 2-4 Mc, degradation increases from -7 db at 4 Mc to -18 db at 2 Mc.
- (e) At 25 Mc or the upper end of the band, the antenna efficiency appears to be lower than in the 5.5 to 12.5 region by approximately 14 db (with no debris). The deterioration in antenna efficiency at the upper end of the band indicates either an increase in total antenna losses or conversion of the uniform excitation of the slot. Increased loss at the upper end of the band may be attributed to a decrease in asphaltic Q and increased ground losses. Further investigation is required into this effect.

TABLE V

\*MEASURED FIELD INTENSITY ALONG THE GROUND FOR WARRENSBURG ANNULAR SLOT ANTENNA

FREQ. mc	WITH NO DEBRIS db	WITH DEBRIS COVER			LOSSLESS ANTENNA SLOT** ANTENNA WITH NO DEBRIS db
		CONDITION 1 db	CONDITION 2 db	CONDITION 3 db	
2	82	75	64	64	98
4	90	87	83	81	98
8	92	91	88.5	86.5	97.5
10	91.5	90.2	87.5	86	97
16	85.5	85.5	76	78	94.6
25	78.5	82	76.5	75.5	93.6

\*Field Strengths are for an Rf antenna input power of 1 watt at a range of 385 feet

\*\*Theoretical field strength for a 100 percent efficient antenna

TABLE VI

## EFFICIENCY OF THE ANNULAR SLOT ANTENNA

Freq.	No Debris Percent	*Debris Cover			Comments
		CONDITION 1 Percent	CONDITION 2 Percent	CONDITION 3 Percent	
2	2.5	0.5	0.04	0.04	for asphaltic cavity $Q \approx 25$
4	16	8	3.2	2	
6.5	36	20	12.2	10.7	
8	28	22	12.5	8	
10	28	16.7	11.2	8.5	
12	39	12.5	12.5	8	
16	12.5	12.5	11.2	8	
20	12.5	3.2	3.2	5	
25	3.2	7.2	2	1.6	



Debris degradation in vicinity of 25 Mc is only 2 db for condition 2.

- (f) Debris cover has the effect of damping out and shifting the location of the notch frequencies.

### 2.3 DESIGN PROCEDURE FOR THE ANNULAR SLOT ANTENNA

Measurements have indicated that the optimum frequency range of operation of an annular slot antenna is between the first and second cutoff frequencies. Operation below the first cutoff frequency is possible with decreased efficiency. The radius of the cavity, therefore, is chosen so that the second cutoff frequency is slightly above the upper end of the frequency band in which the antenna is supposed to operate.

The cutoff frequencies are determined by  $bk_1 = R_n$  where  $R_n$  are the roots of  $J_0(x)$

$$k_1 = \frac{2\pi}{\lambda} \sqrt{\epsilon_{1r}} = \frac{2\pi \sqrt{\epsilon_{1r}}}{300} \quad f_c = \frac{\omega \sqrt{\epsilon_{1r}}}{300}$$

$\epsilon_{1r}$  = dielectric constant of cavity filler material  
(asphaltic concrete)

With  $f_c$  given as approximate 1.05  $f$  to 1.1  $f$  the cavity radius  $b$  is obtained as follows: [ $f_n$  = highest operating frequency]

where

$$\text{and } b = \frac{R_n}{k_1} = \frac{300}{2\pi f_c} \frac{R_n}{\sqrt{\epsilon_{1r}}} = \frac{47.7 R_n}{f_c \sqrt{\epsilon_{1r}}}$$

For the second cutoff frequency  $R_2 = 5.52$  and  $b = \frac{263}{\sqrt{\epsilon_{1r}}} \frac{1}{f_2}$  [m]

with  $f_2$  in Mc. (second cutoff frequency)

This is the cavity radius which gives optimum efficiency between the first two cutoff frequencies, whose ratio

$$f_2/f_1 = R_2/R_1 = 5.52/2.403 = 2.3$$

The maximum efficiency occurs between  $f_1$  and  $f_2$ , namely at the first parallel resonance frequency. The efficiency at this frequency (without debris cover) can be crudely estimated by using the equivalent linear transmission line operating in the  $\lambda/2$  mode with maximum voltage at the open end. The Q of this line can be estimated from the Q of the dielectric which fills the cavity. With asphaltic concrete  $Q_c$  will range approximately from 25 to 50.

The characteristic impedance  $Z_o$  of the antenna circuit can be estimated by considering the cavity as an radial transmission line, whose characteristic impedance at any radius  $r$  is given as

$$Z_r = \sqrt{\frac{\mu_o}{\epsilon_o \epsilon_r}} \frac{h}{2\pi r} = \frac{60h}{\sqrt{\epsilon_r} r}$$

where  $h$  = distance between disk and ground.

An approximate value of the effective characteristic impedance of the equivalent line is obtained by using an average radius  $r \approx \frac{b}{2}$ . The depth  $h$  of the cavity has to be estimated. Normally a depth between 1 and 2 m is adequate. The greater depth will give a slightly increased efficiency, but the cost increases approximately proportional with  $h$ .

Having chosen  $h$  one obtains  $Z_o \approx \frac{120 h}{\sqrt{\epsilon_r} b}$ .

The radiation conductance  $G_R$  of the annular slot antenna depends on the average slot radius  $\rho = (a+b)/2 = b - \frac{w}{2}$ , where  $w$  is the slot width. This has to be estimated. A first choice of  $w$  equal to one to two times the cavity height will be adequate in most cases. Thus the average slot radius  $\rho_o$  is fixed and the radiation conductance  $G_R$  can be obtained from Figure 2-2

using  $x = \frac{2\pi\rho_o}{\lambda} = \frac{\pi\rho_o f}{150}$ .

At the parallel resonance frequency  $f_p$  the efficiency has a maximum.  $f_p$  is estimated as the geometric mean between the adjacent cutoff frequencies:  $f_p = \sqrt{f_1 f_2}$ . At this frequency the radiation power factor is obtained from  $Q_c$ ,  $Z_o$ , and  $G_R$  as

$$P = \frac{2}{\pi} G_R Z_o, \text{ and, with } pQ_L = \frac{1}{\pi} G_R Z_o Q_c$$

the efficiency

$$\eta_{\max} = \frac{1}{1 + (pQ_L)^{-1}}$$

This is the maximum efficiency occurring at the parallel resonance frequency  $f_p$ . The efficiency drops to practically zero at the cutoff frequencies. Below  $f_1$  it increases again, reaches a maximum, which is much lower than the main maximum, and then decreases rapidly approaching zero for very low frequencies. However, experiments show that the null at the first cutoff frequency is not as deep as predicted by theory, but actually is hardly observable, so that practically the efficiency decreases monotonically from the main maximum as the frequency is decreased.

Having determined  $b$  and  $\rho_o$  the radiation pattern obtained with this  $\rho_o$  in the operating frequency range has to be examined with respect to the elevation angle of the lobe maximum, the directivity on the ground and in direction of the lobe maximum. The following points are of interest:

Zero ground field will be obtained when

$$x = \frac{2\pi\rho_o}{\lambda} = \frac{\pi f_o \rho_o}{150} = 3.83$$

i.e., at a frequency  $f_o = \frac{3.83 \times 150}{\pi \rho_o}$  [Mc]

Combining this with  $\rho_o = \frac{150 R_2}{\pi f_2 \sqrt{\epsilon_{1r}}}$

one obtains the following relation between  $f_o$  and  $f_2$

$$\begin{aligned} \frac{f_o \rho_o}{f_2 \rho_o} &= \frac{150 \times 3.83}{\pi \cdot 150 \cdot R_2} \pi \sqrt{\epsilon_{1r}} = \frac{3.83}{5.52} \sqrt{\epsilon_{1r}} \\ &= 0.695 \sqrt{\epsilon_{1r}} \end{aligned}$$

Thus for  $\sqrt{\epsilon_{1r}} \geq \frac{1}{0.695}$ , or  $\epsilon_{1r} \geq 2.07$   $f_o \geq f_2$ . If  $\epsilon_{1r} > 2.07$  the frequency which gives zero ground field is greater than the second cutoff frequency and therefore is outside the frequency range of interest.

The quantity  $x = 2\pi\rho_o/\lambda$  which determines the directivity at any frequency  $f$  is given by  $x = \frac{\pi f \rho_o}{150}$

The directivity  $g$  at the frequencies of interest and the elevation angle of the lobe maximum can be found from Figure 2-5.

Having determined the pattern characteristics for a known cavity radius  $\rho_o$  one has to examine if the pattern characteristics (lobe elevation angle directivity) meet the required specifications especially with regard to propagation requirements.

This procedure establishes the approximate cavity radius  $b$  and average slot radius  $\rho_o$  and maximum obtainable efficiency if the highest operating frequency is given. It was necessary to estimate the cavity depth  $h$ , and slot width  $w$  from practical considerations. With the data then a computer solution for the efficiency variation over the whole frequency band of interest should be made, in order to obtain an exact knowledge of the frequency

dependence of the antenna with the chosen parameters. The results have to be compared with the specified requirements, and if necessary, changes in the parameters  $a$ ,  $b$ ,  $h$  and the material  $Q_c$  have to be made until the required performance is achieved.

The design procedure is summarized in the following table.

Cavity Dimensions and Maximum Efficiency

<u>Given</u>	Highest operating frequency $f_n$ and Operating frequency range
--------------	--

Choose

Dielectric	
$\epsilon_{lr}$	.8 - 3.8
$Q_c$	25 - 50
Cavity Depth $h$	1 - 2 m
Slot Width $w$	$w = (1 \text{ to } 2) h$

Determine

Second Cutoff Frequency	$f_2 \approx 1.05 f_n$
First Cutoff Frequency	$f_1 = f_2 / 2.3$
Parallel Resonance Frequency	$f_p = \sqrt{f_1 f_2}$
Cavity Radius	$b = \frac{263}{\sqrt{\epsilon_{lr} f_2}}$
Disk Radius	$a = b - w$
Average Slot Radius	$\rho_0 = b - w/2$

Effective Characteristic  
Impedance

$$Z_o = \frac{120 h}{\sqrt{\epsilon_{1r}} b}$$

$$x = \frac{\pi f \rho_o}{150} \text{ at } f = f_p$$

$$x_p = \frac{\pi f_p \rho_o}{150}$$

Radiation Conductance  
at  $f = f_p$

$$G_R = F(x) \text{ from Figure 2-2}$$

Radiation Power Factor  
at  $f = f_p$

$$p = \frac{2}{\pi} G_R Z_o$$

$pQ_L$  at  $f = f_p$

$$pQ_L = \rho Q_c / 2$$

Max. Efficiency at  
 $f = f_p$

$$\eta_p = \frac{1}{1 + (pQ_L)^{-1}}$$

Computer Solution for  $\eta$  over the frequency range to determine exact performance.

### Pattern Characteristics

Ground Null Frequency  $f_o$

$$f_o / f_2 = 0.695 \sqrt{\epsilon_{1r}}$$

Frequency  $f_g$  where lobe lifts  
off the ground,  $x_g = 1.85$

$$f_g = \frac{x_g \cdot 150}{\pi \rho_o} ; \epsilon_m = 0$$

$$g_m = g_o = 2.4$$

Directivity at highest operating  
frequency  $f_n$

$$x_n = \frac{\pi f_n \rho_o}{150}$$

Directivity at  $f = f_p$

$$x_p = \frac{\pi f_p \rho_o}{150}$$

$$\left. \begin{array}{l} \epsilon_m \\ g_m \\ g_o \end{array} \right\} \text{ from Figure 2-5} \\ \text{with appropriate } x.$$

An example will illustrate this design procedure.

### Cavity Dimensions and Maximum Efficiency

Highest Operating Frequency

$$f_n = 25 \text{ Mc}$$

Choice

$$\epsilon_1 = 2.8 \quad Q_1 = 50$$

$$h = 1.5 \quad w = 1.5 \text{ m}$$

Determine

$$f_2 = 25.1.05 = 26.2 \text{ Mc}$$

$$f_1 = 26.2/2.3 = 11.4 \text{ Mc}$$

$$f_p = \sqrt{26.2 \times 11.4} = 17.3 \text{ Mc}$$

$$b = 263/\sqrt{2.8 \times 26.2} = 6 \text{ m}$$

$$a = 6 - 1.5 = 4.5 \text{ m}$$

$$\rho_o = 6 - 0.75 = 5.25 \text{ m}$$

$$Z_o = 120 \times 1.5/\sqrt{2.8 \times 6} = 17.9 \text{ ohm}$$

$$x_p = \frac{\pi 17.3 \times 5.25}{150} = 1.9$$

$$C_R = 18 \times 10^{-3} \text{ mho}$$

$$p = \frac{2}{\pi} 18 \times 17.9 \times 10^{-3} = 0.205$$

$$pQ_L = 0.205 \times 25 = 5.1$$

$$\eta_p = \frac{1}{1 + (5.1)^{-1}} = \frac{1}{1.196} = 0.84$$



### Pattern Characteristics

Ground Null Frequency

$$f_o = 26.2 \times 0.695 \times \sqrt{2.8}$$

$$= 30.5 \text{ Mc}$$

Frequency  $f_g$  where lobe lifts off  
the ground,  $e^m = 0$

$$f_g = \frac{1.85 \times 150}{\pi \times 6} = 17 \text{ Mc}$$

$$x_g = 1.85 ; g_m = g_o = 2.4$$

Directivity at  $f = f_g$

$$g_o = g_m = 2.4$$

Directivity at  $f = f_n$

$$\text{where } x_n = \frac{\pi \times 25 \times 5.25}{150} = 2.75$$

$$\left\{ \begin{array}{l} e_m = 47^\circ \\ g_m = 2.7 \\ g_o = 1.5 \end{array} \right.$$

Directivity at  $f = f_p$

$$\text{where } x_p = 1.9$$

$$\left\{ \begin{array}{l} e_m = 15^\circ \\ g_m = 2.4 \\ g_o = 2.4 \end{array} \right.$$

The complete solution for this design

$$b = 6.0 \text{ m}$$

$$a = 4.5 \text{ m}$$

$$h = 1.5 \text{ m}$$

is shown in Figures 2-6, 2-7, 2-8, 2-9, 2-11, and 2-12.

## SECTION 3

### LOG SPIRAL ANTENNA

#### 3.1 INTRODUCTION

The equiangular spiral antenna represents a relatively simple structure exhibiting some very interesting and desirable properties in the HF region. Investigations by Dyson<sup>8,9,10</sup> and others<sup>11,12</sup> at UHF and microwave frequencies have demonstrated the essentially frequency independent radiation and impedance characteristics over bandwidths in the order of 10:1. The design of the antenna is specified entirely by angles and its performance appears to be independent of frequency. The equiangular log spiral antenna has the property that the specifications for the highest and lowest frequencies of operation are independent; i.e., the highest usable frequency is generally determined by the inner diameter of the spiral and the lowest usable frequency is determined by the outer diameter of the antenna.

The two-arm planar log spiral antenna provides a circularly polarized bidirectional beam on the axis of the antenna. This is shown in Figure 3-1. A four-arm planar spiral, on the other hand, with appropriate feed system produces a more desirable radiation pattern for HF communication. A typical radiation pattern for a four-arm log spiral operating in this so-called "Second Mode" is also shown in Figure 3-1.

#### 3.2 DESIGN PROCEDURE

The equiangular spiral shown in Figure 3-2 may be defined by the equation  $\rho = k e^{a\phi}$  where  $\rho$  and  $\phi$  are the polar coordinates of a point on the spiral. The constant,  $a$ , controls the rate of spiraling about the origin and  $k$  determines the radius  $\rho$  or size of the terminal region.

A physical antenna is generated by considering the following curves:

$$\rho_1 = k e^{a\phi}$$

and

$$\rho_2 = k e^{a(\phi-\delta)} = K\rho_1$$

4-1-0766

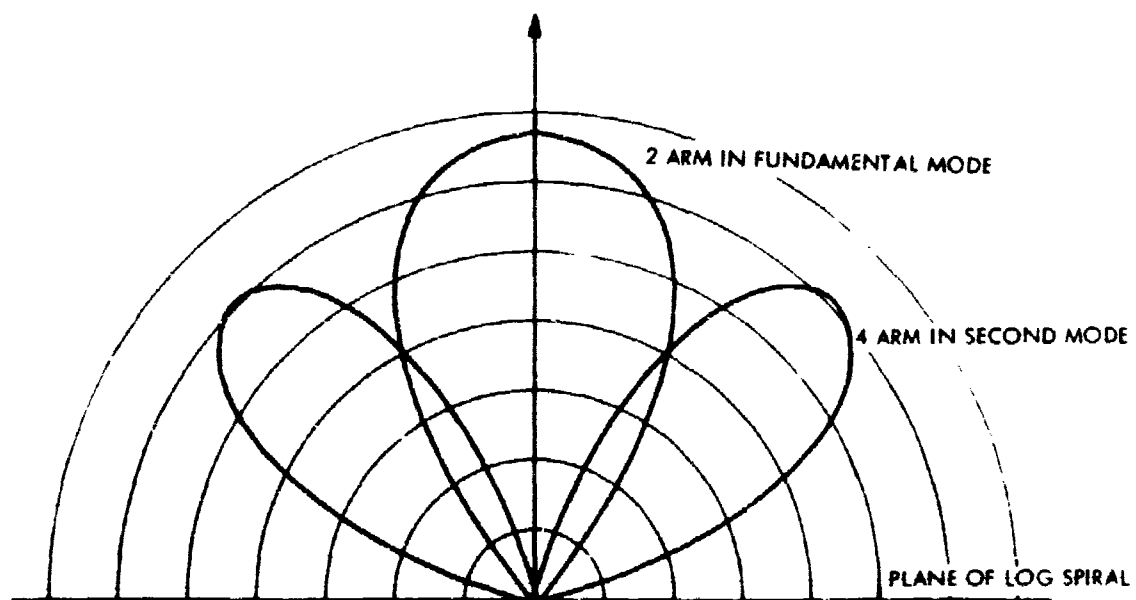


Figure 3-1. Radiation Pattern of Log Spirals.

4-1-0767

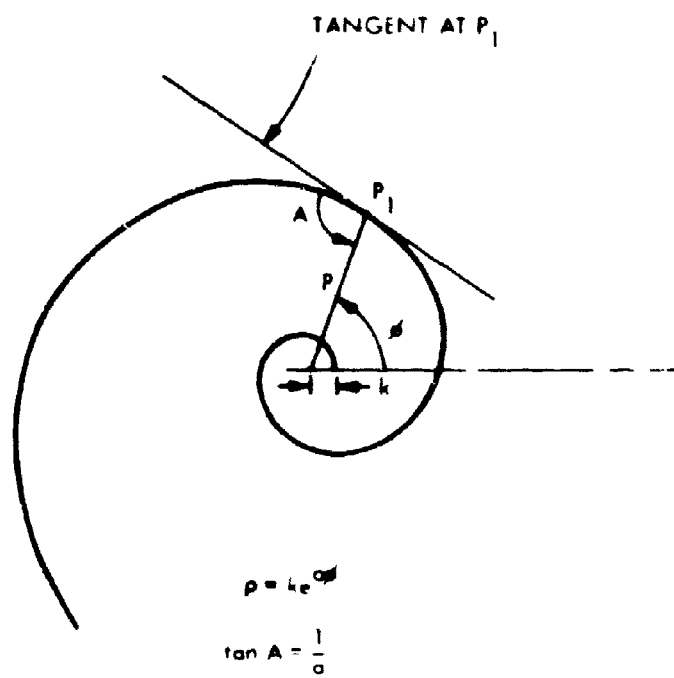


Figure 3-2. Parameter for Equiangular Spiral.

where

$$K = e^{-a\delta} = \frac{\rho_2}{\rho_1} \ll 1$$

Thus if we consider an antenna with a conductor having its edges specified by  $\rho_1$  and  $\rho_2$  (which is  $\rho_1$  rotated through an angle  $\delta$ ), the arm width is immediately specified by the fixed rotation angle  $\delta$ .

A planar balanced spiral consisting of four such conductors represents one form of the spiral antenna capable of operation in the second mode.. Another form of this antenna consists of a spiral slot cut in a large conducting sheet. An appropriate backup cavity is required to support such a structure and limit the radiation to that hemisphere above the ground. The configuration of such a backup cavity should be such that the basic properties of the log spiral in air are not radically disturbed.

Design criteria for the spiral geometry based upon Sylvania scale model tests at 90 Mc is as follows:

$$\rho_1 = 0.05 \lambda e^{0.3\phi}$$

$$\rho_2 = 0.9 \rho_1$$

where

$$\text{Outer diameter} = \frac{2\lambda}{\pi} \quad (\text{determine the lowest usable frequency of operation } f_1)$$

$$\text{Inner diameter} = \frac{\lambda}{3\pi} \quad (\text{determine highest usable frequency of operation } f_2)$$

$$\lambda = \text{wavelength in asphaltic concrete at } f_1$$

$$\text{Backup Cavity Height} = 5' \quad (\text{in asphaltic concrete})$$

Using these relations, a 45 foot (OD) and 7.5 foot (ID) log spiral would theoretically cover the frequency range of 8 to 30 Mc at maximum efficiency.

The spiral slot antenna has been found to be the most useful form since it permits the feeding of such a balanced structure in a completely balanced

manner by embedding the coaxial feed cable in the ground plane. Figure 3-3 shows this technique as used in the experimental evaluation of scale model of the HF spiral. Dyson refers to this method of feed as the "infinite balun." Figure 3-4 shows the technique that should be used to excite the four arms of a spiral slot antenna operating in the second mode.

### 3.3 RADIATION PATTERN

The antenna radiation patterns are relatively insensitive to the number of turns used although there may be optimum ranges of operation. Good patterns are generally obtained for spirals in the order of 1 to 1.5 turns.

The log spiral radiates a circularly polarized field (axial ratio - 2:1) for frequencies in which the spiral arm length is equal to or greater than a wavelength. For frequencies such that the spiral arms are short in terms of  $\lambda$ , the radiated field is linearly polarized. This would be the case for frequencies below  $f_1$ . In the vicinity of  $f_2$ , the terminal region of the spiral becomes the radiator and since this approaches a half wave dipole, the radiated field in the vicinity of  $f_2$  becomes linearly polarized.

### 3.4 INPUT IMPEDANCE

The input impedance of a log spiral antenna converges rapidly as the spiral arm length exceeds a wavelength and is generally a function of the factor  $K = \frac{\rho_2}{\rho_1}$ . In general, for conduction arm or slot spirals, the antenna is rarely mismatched by more than 3:1 to a 50 ohm line and as exhibited in the Sylvania experimental program, the VSWR is usually less than 2:1 over the operating frequency range.

This feature of the log spiral antenna is outstanding in that once the design of the antenna is established, operation over a broad frequency band is possible without the use of matching networks. In addition, the constant input impedance characteristic of the log spiral appears to be maintained under the effects of a debris cover; in the experimental program at Sylvania, for a 10 ft diameter spiral, the input impedance improved with debris loading.

### 3.5 EXPERIMENTAL INVESTIGATION OF THE LOG SPIRAL ANTENNA

The experimental investigation of the log spiral during Phase 2 was concerned with the measurement of input impedance, bandwidth, field intensity, and the effects of debris on these parameters.

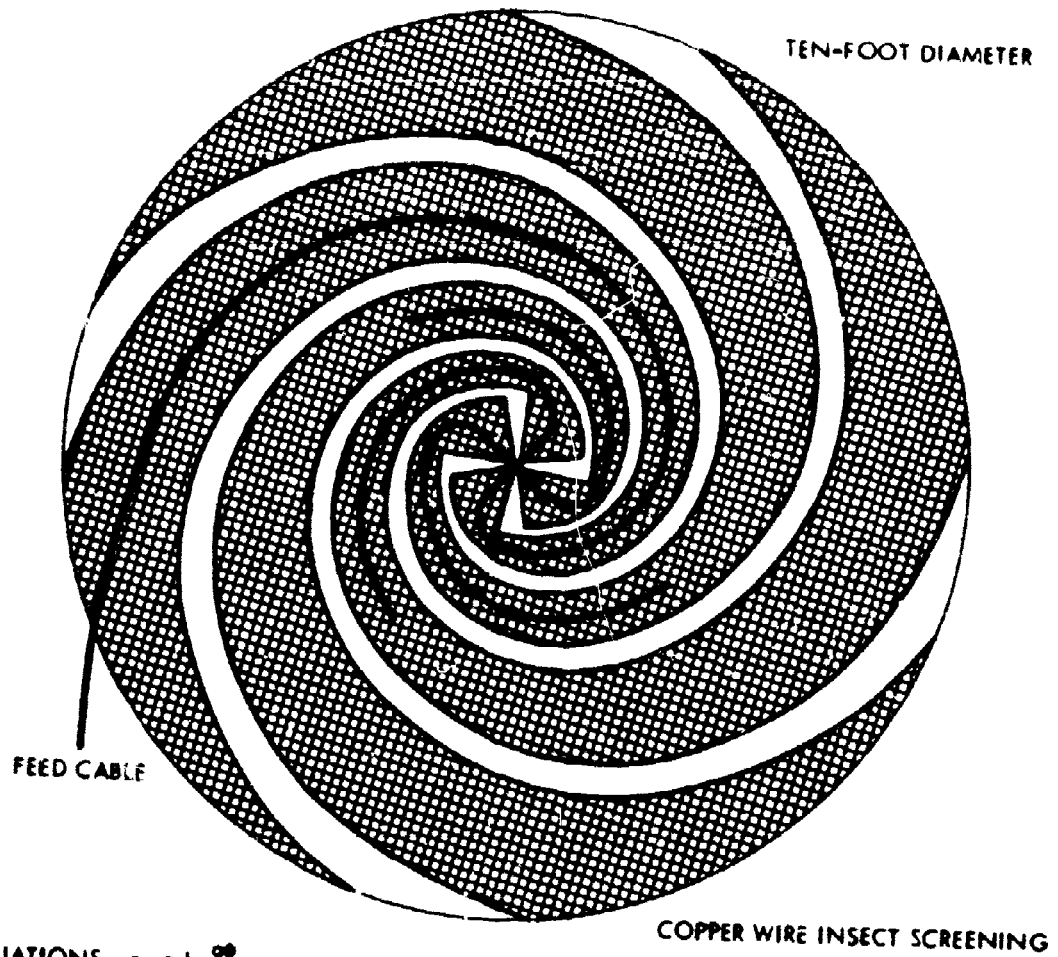
Measurements made at 90 Mc on random samples of the farm loam used as a debris cover indicated an average conductivity of  $3 \times 10^{-3}$  mho/m and a relative dielectric constant of 3.3. Appendix F contains a discussion of the test procedure and tabulation of debris measurements at Waltham, Massachusetts.

The log spiral scale model used in the experimental program is shown in Figure 3-5. It is 10 feet in diameter and was fabricated from copper wire insect screening attached to a plywood form. Design details together with appropriate equations for each spiral slot arm and feed cable are shown in Figure 3-3.

The four-arm spiral slot antenna investigated at Sylvania (Figure 3-5) was placed over an 18-inch backup cavity and is shown in Figure 3-6. Additional construction details are given in Appendix B.

An infinite balun feed arrangement is shown in Figure 3-3 together with an expanded view of the central region in Figure 3-4. Dummy cables (RG-8/U short circuited at both ends) were used to maintain structural symmetry on the other three arms.

4-1-0739



EQUATIONS -  $p_1 = k e^{a\theta}$

$$p_2 = K p_1$$

$$k = .05 \lambda_1 \text{ FOR DIA OF SPIRAL} = \frac{2\lambda_1}{\pi}$$

$$\lambda_1 = 200 \text{ INCHES FOR } f = 60 \text{ MC}$$

$$a = 0.3$$

$$K = 0.9$$

HEIGHT ABOVE EDGE OF  
BACK UP CAVITY  $\approx 4^\circ$

Figure 3-3. Log Spiral Antenna.





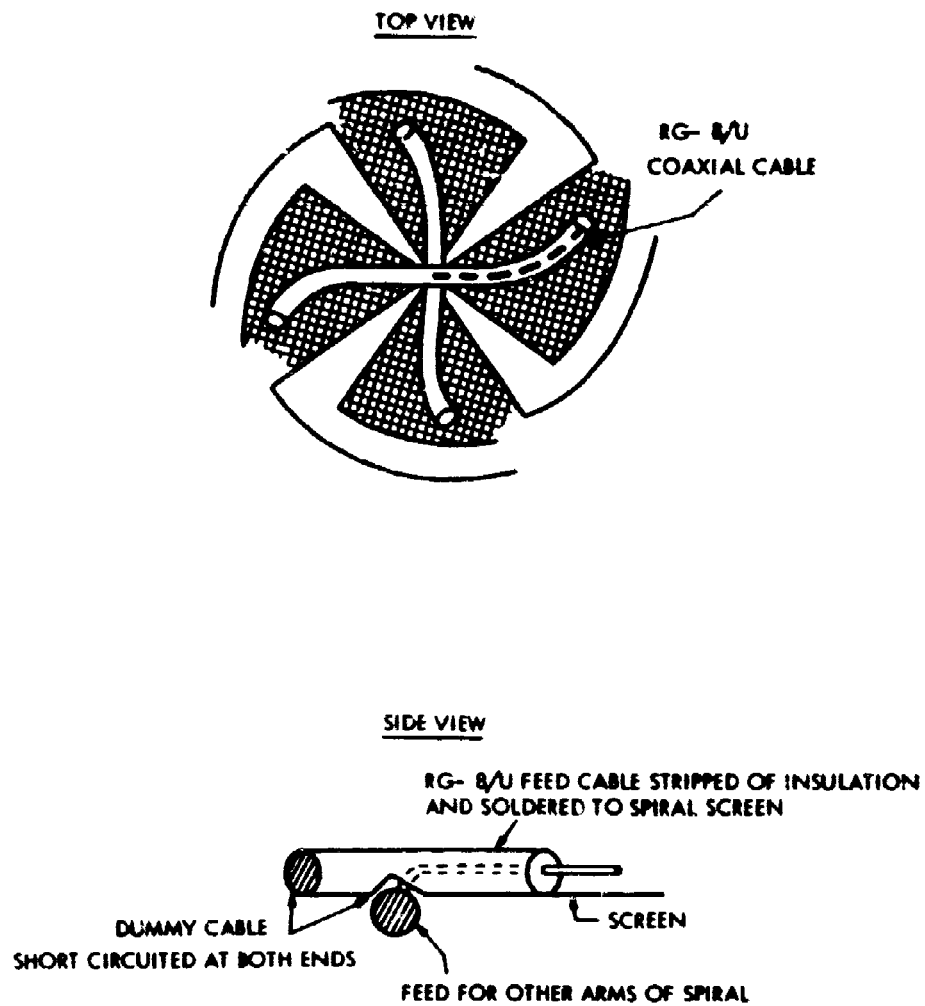
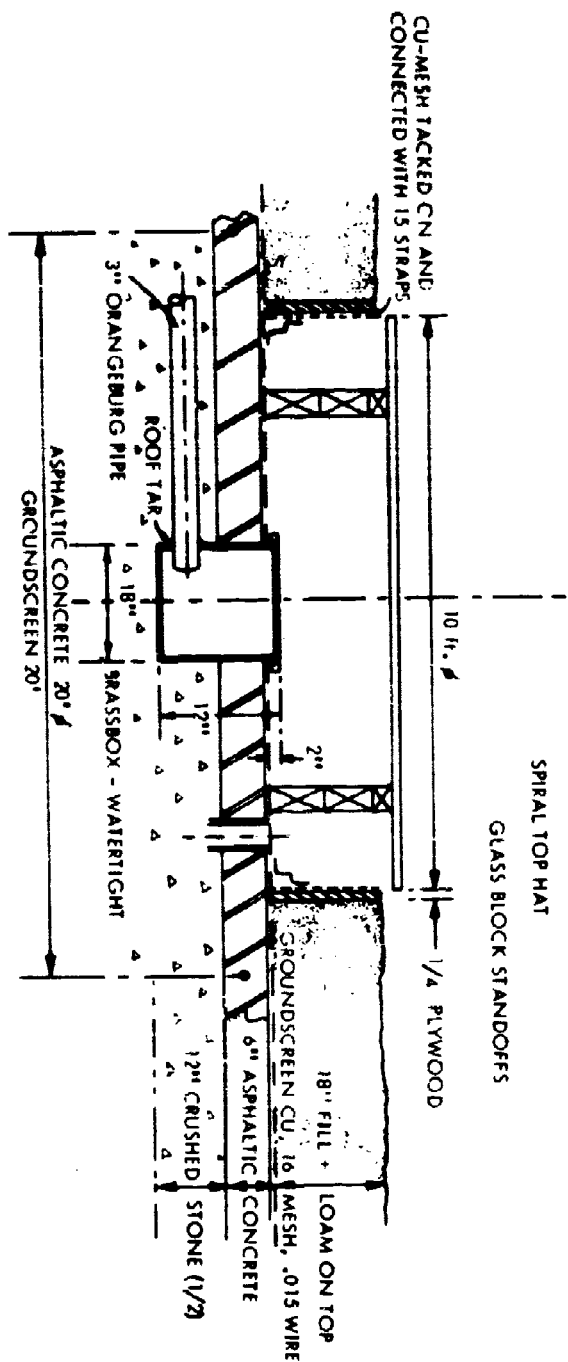


Figure 3-4. Log Spiral Antenna Feed Arrangement.



Figure 3-5. Photo of Scale Model of HF Spiral.



4-1 0768

Figure 3-6. Cross-section Log Spiral Antenna and Back-up Cavity.

Input impedance measurements on the four-arm spiral antenna from 95 to 120 Mc are shown in the Smith plot of Figures 3-7, 3-8, and 3-9, for no debris and for conditions 20 and 21. Figure 3-10 presents a composite plot of these conditions where it can be seen that the measured input impedance with no debris closely approximates the design criterion of 50 ohms. Loading the log spiral antenna with debris improved the input impedance match to a 50-ohm line.

The debris cover was placed on a plywood platform spaced approximately 6 inches above the plane of spiral by glass blocks. This spacing served to simulate the isolation effects of an asphaltic blanket placed over an actual antenna to protect it from the ablative effects of a nuclear weapon.

Because of the weather conditions existing during the experimental program, soil was packed in 50 pound bags and stored at above freezing temperatures until actually used. The log spiral was tested under two debris blankets, the only difference being in the way the debris bags are placed over the antenna (completely random) and the distribution of the glass blocks underneath the plywood platform supporting the debris (also random).

The radiated field intensity from the spiral antenna was measured at seven stations situated on a circle 53 feet from the center of antenna site. These stations are shown in Figure 1-3. A plot of the elevation pattern of the log spiral at station 6 is shown in Figure 3-11 for the vertically polarized component of electric field,  $E_v$ . Bandwidths of approximately  $20^\circ$  were measured for  $E_v$  with and without debris (first cover). The field intensity under condition 21 increased by 3 db over the no-debris and is due to a conversion of energy from the horizontally polarized component  $E_h$ , to the  $E_v$  component. This fact is illustrated in the data plotted in Figure 3-12 where

$E_v$  is the vertically polarized electric field with no debris

$E_{vd}$  is the vertically polarized electric field with full cover of debris (second cover)

4-1-0775

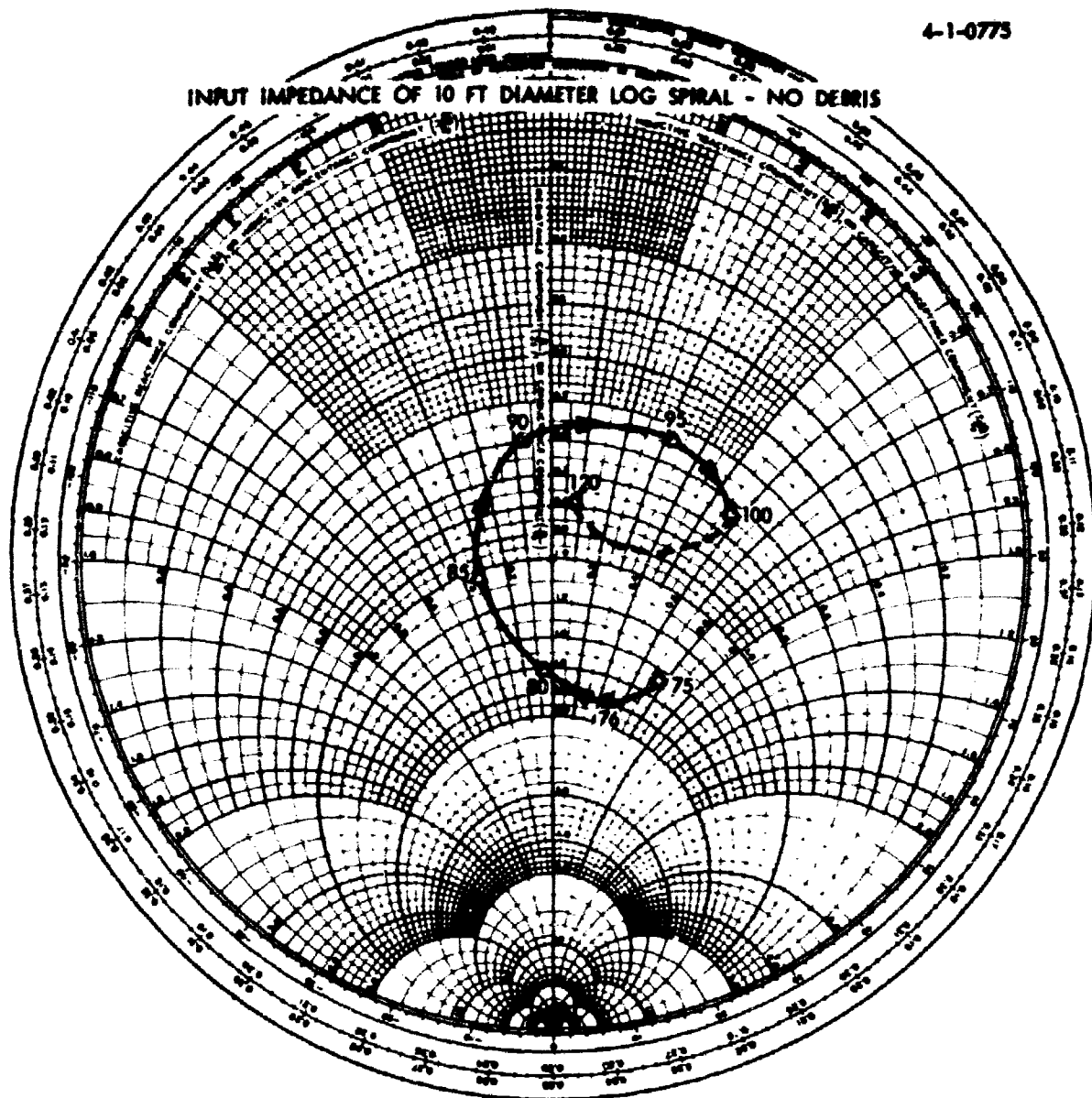
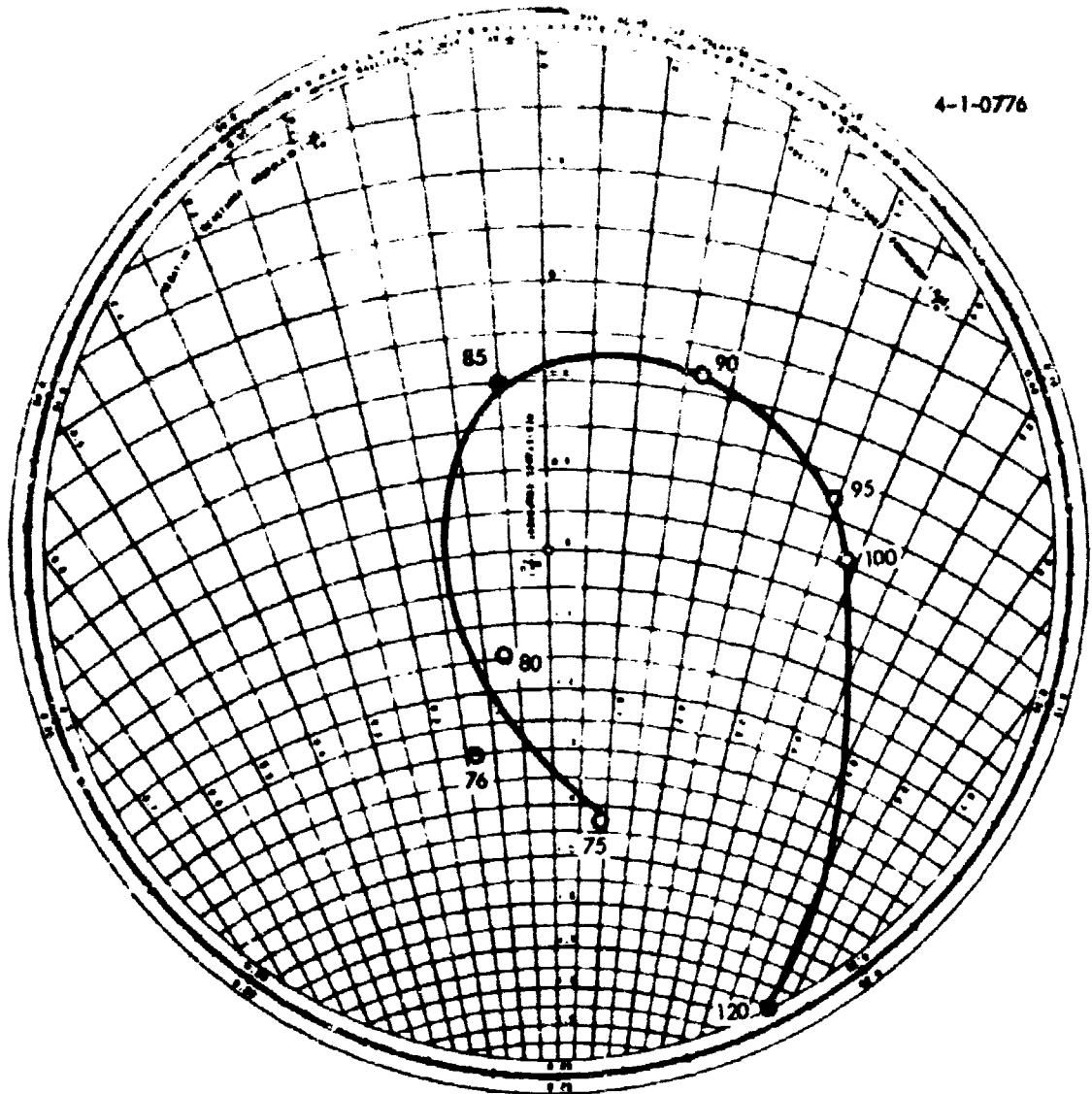


Figure 3-7. Input Impedance of 10<sup>0</sup> Diameter Log Spiral No Debris.



LOG SPIRAL ANTENNA IMPEDANCE DEBRIS CONDITION # 20 (1/2 COVER)

Figure 3-8. Input Impedance of 10<sup>8</sup> Diameter Log Spiral Half Cover of Debris.

4-1-0777

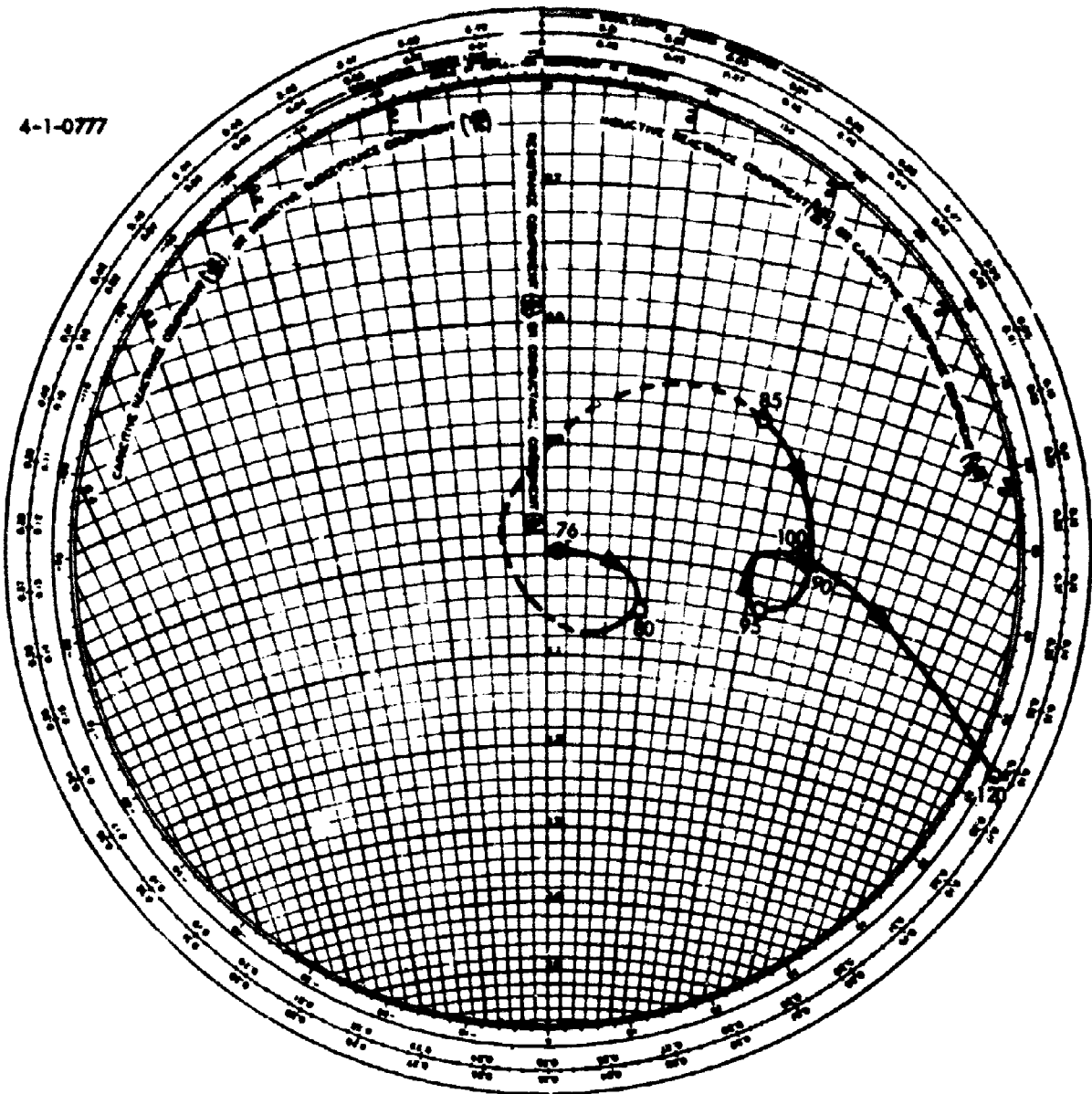


Figure 3-9. Input Impedance of 10" Diameter Log Spiral Full Cover of Debris.



4-1-0778

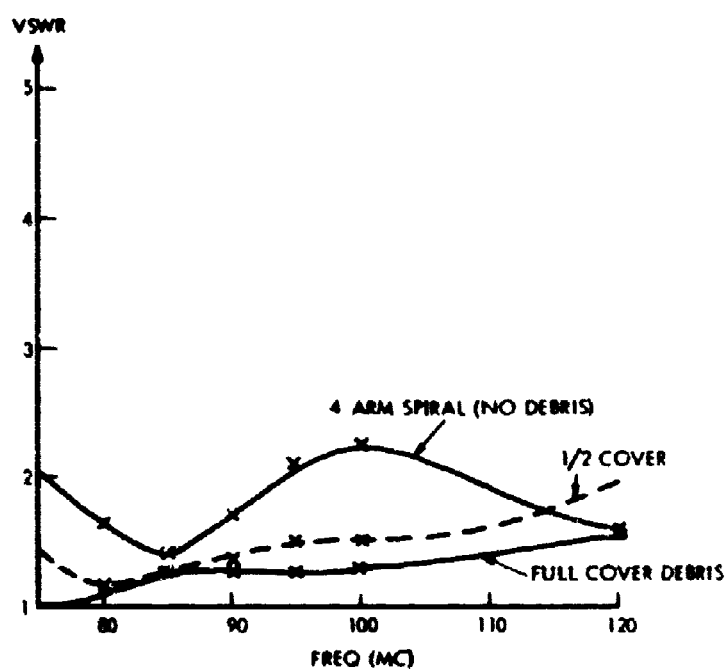


Figure 3-10. VSWR Versus Frequency for Log Spiral With and Without Debris.

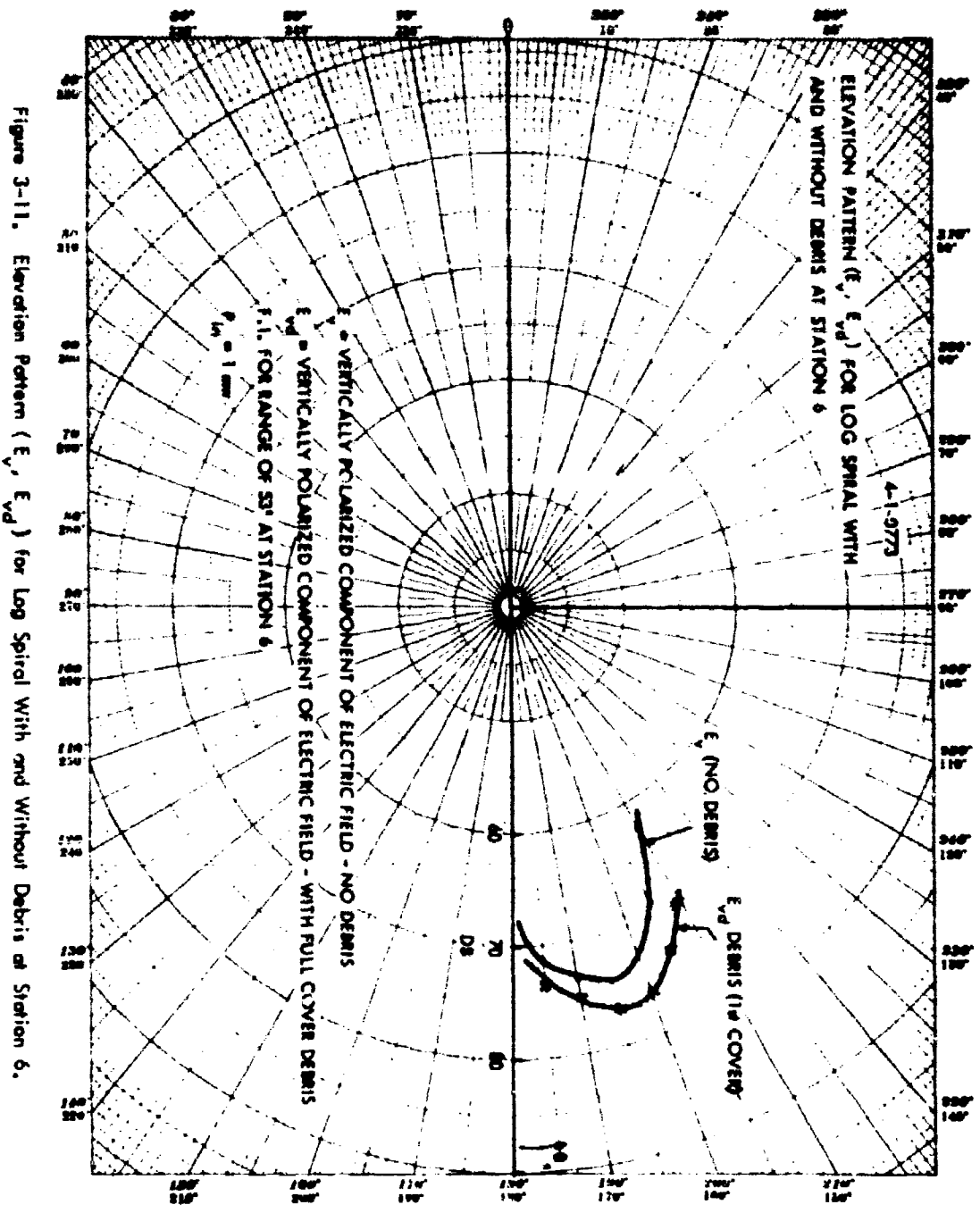


Figure 3-11. Elevation Pattern ( $E_v$ ,  $E_{vd}$ ) for Log Spiral With and Without Debris at Station 6.

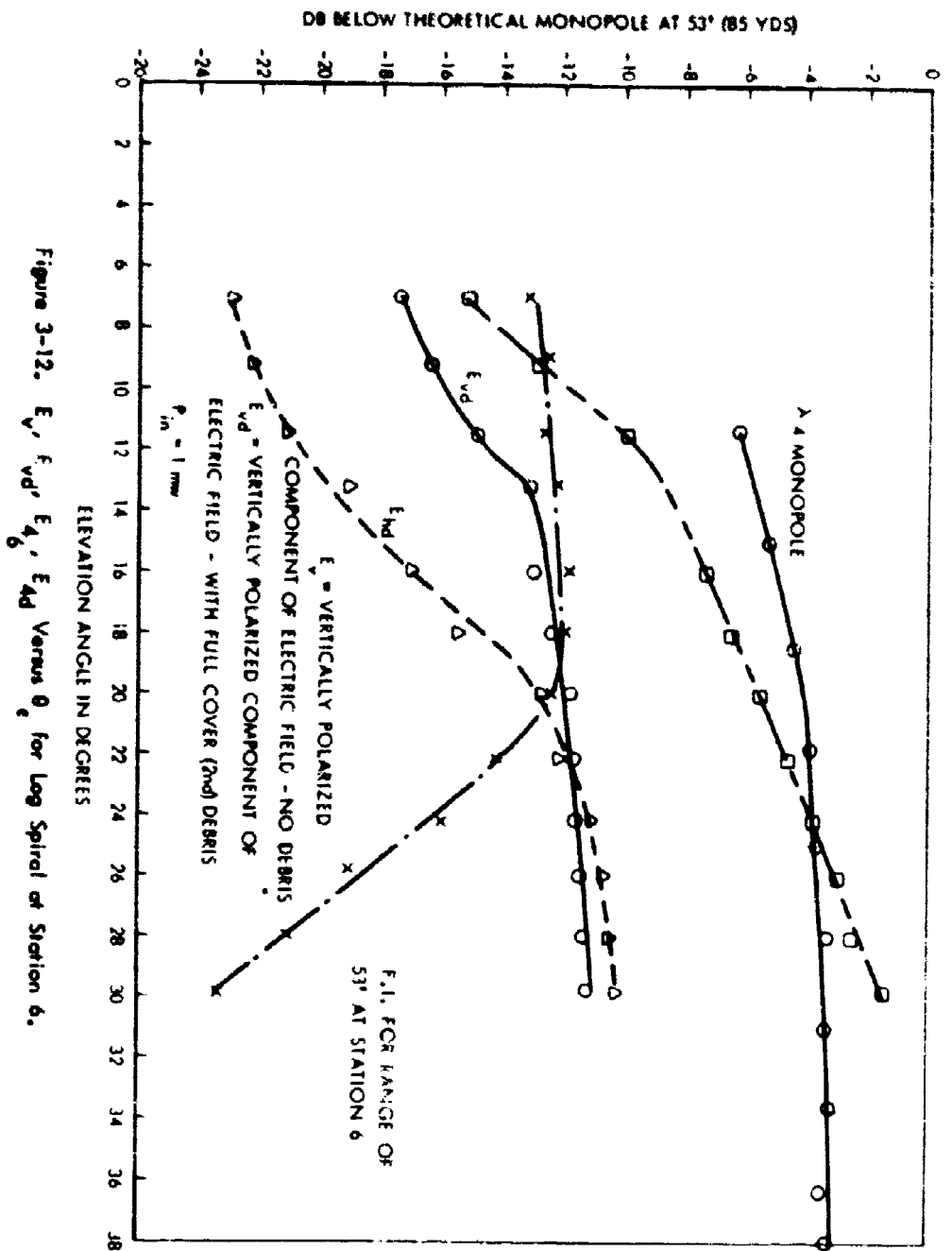


Figure 3-12.  $E_v$ ,  $E_h$ ,  $E_{vd}$ ,  $E_{hd}$  Versus  $\theta$  for Log Spiral at Station 6.

$E_H$  is the horizontally polarized electric field with no debris

$E_{Hd}$  is the horizontally polarized electric field with full cover of debris (second cover)

The ordinate in Figure 3-12 is normalized to the field intensity which would be received from a 100 percent efficient  $\lambda/4$  monopole over a perfect ground ( $\sigma = \infty$ ) at a range of 53 feet. Its magnitude would be 85.7 db above 1  $\mu\text{V/m}$  for an input power of 1 milliwatt. This is a standard reference used throughout this report.

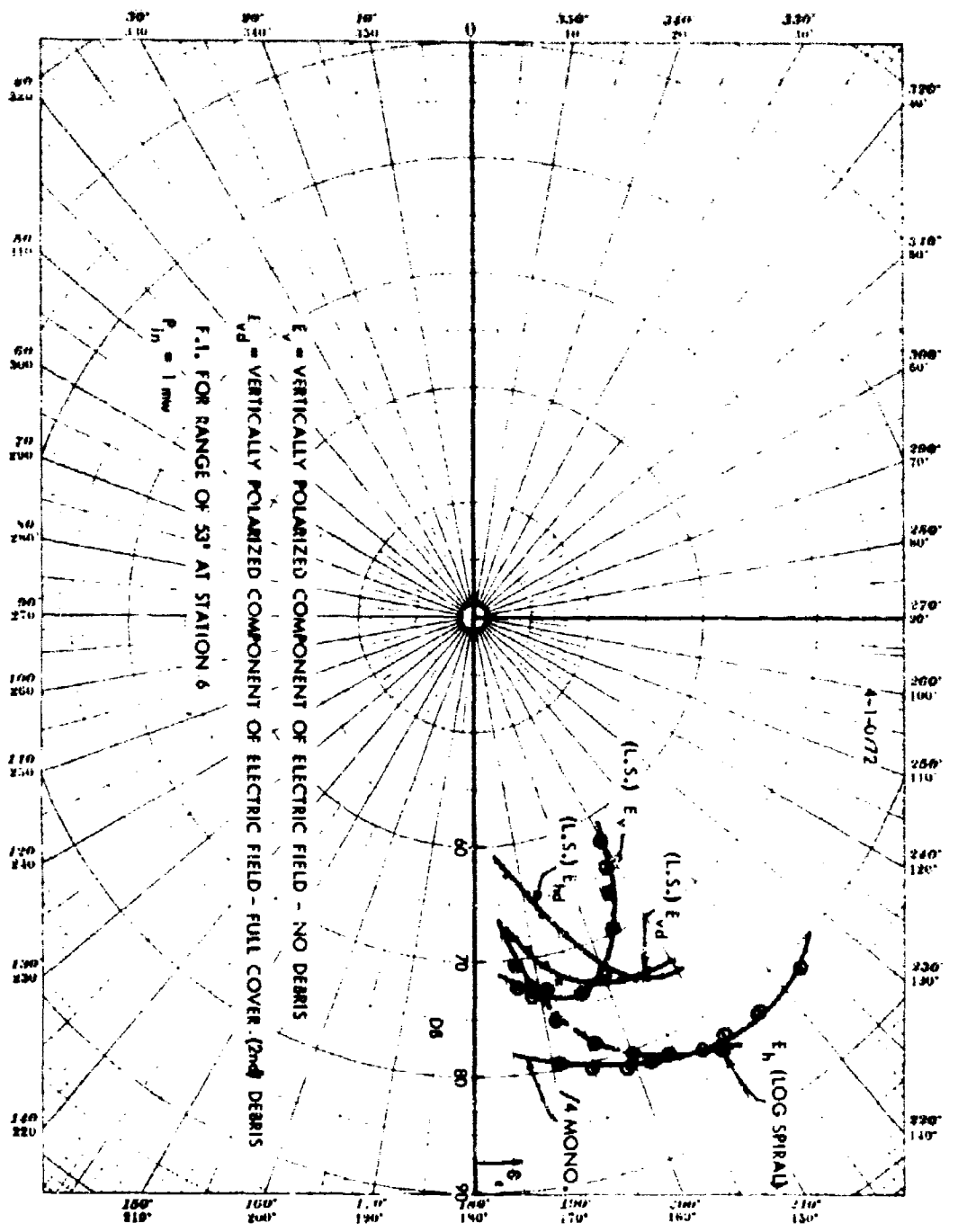
Referring to Figure 3-12 we see that loading the log spiral with full layer of debris (second cover) had the following effects at station 6:

- (1) Magnitude of  $E_H$  decreased approximately 8 to 10 db for elevation angles of 7 to 30 degrees.
- (2) Magnitude of  $E_V$  decreased slightly at low elevation angles (7 to 13°) and then remained essentially constant to 30°. It can be seen that  $E_{Vd}$  at an elevation angle of 30° is greater than  $E_V$  (no debris case) by 12 db.
- (3) Circularity ratio ( $E_V/E_H$ ) improved significantly with debris loading especially at the higher elevation angles where its value was unity.

An elevation pattern taken at station 6 indicates the change occurring in the radiation pattern of a spiral under second debris cover. These patterns are plotted (Figure 3-13) from data of Figure 3-12 and correspond to a full debris cover at a range of 53 feet. The radiated field intensity received from the  $\lambda/4$  reference monopole at station 6 is also plotted in Figure 3-13.

Figures 3-14 and 3-15 summarize the measured field intensity at stations 5 and 1 for the log spiral (with and without debris) and the reference  $\lambda/4$  monopole. The measured data of  $E_H$  versus  $\theta_e$  at these stations followed the same behavior as at station 6; i.e., it decreased with debris loading

Figure 3-13. Elevation Pattern for Log Spiral and  $\lambda/4$  Monopole With and Without Debris.



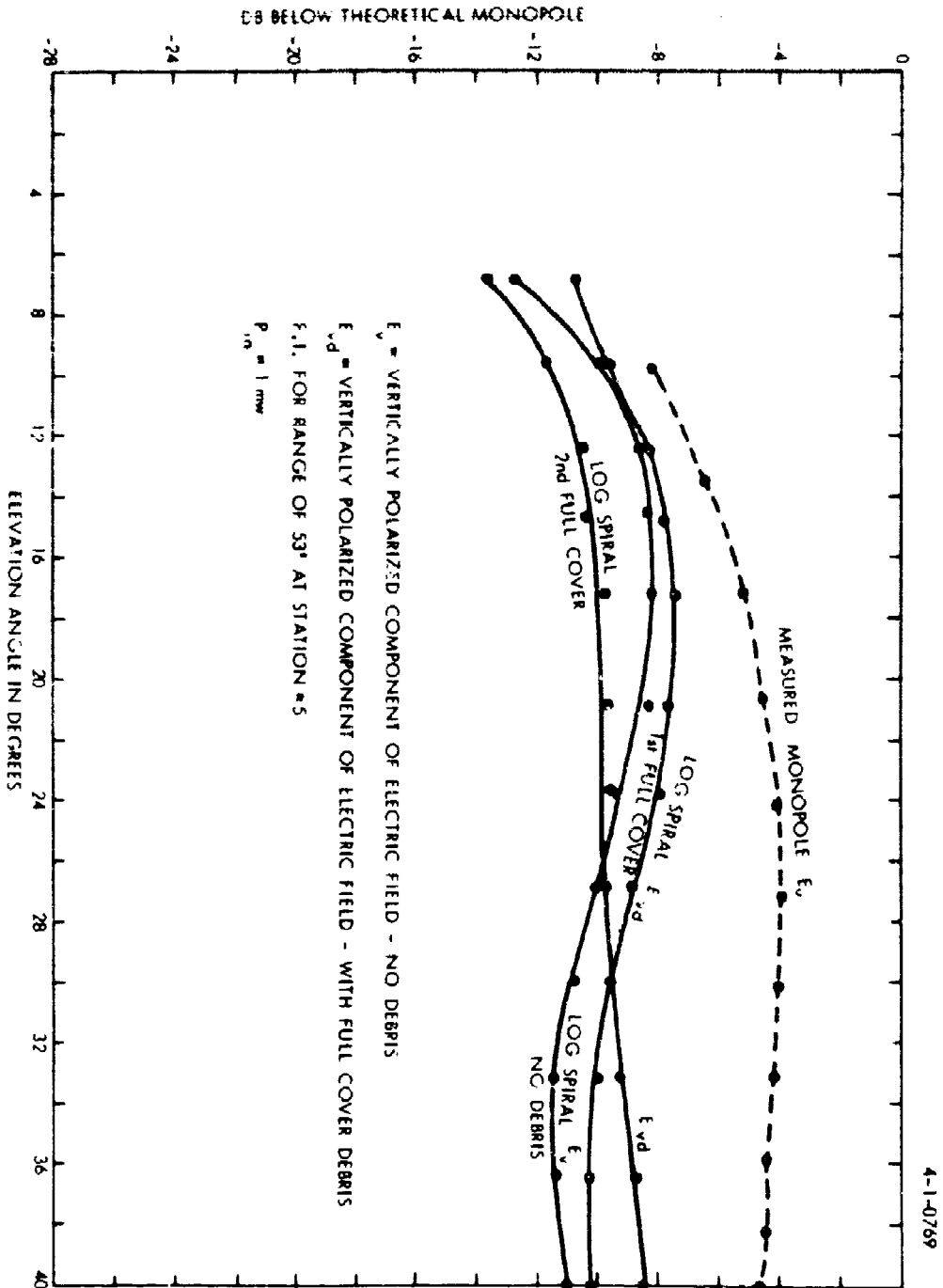


Figure 3-14. Measured Field Intensity Versus Elevation Angle for Log Spiral at Station 5  
With and Without Debris.

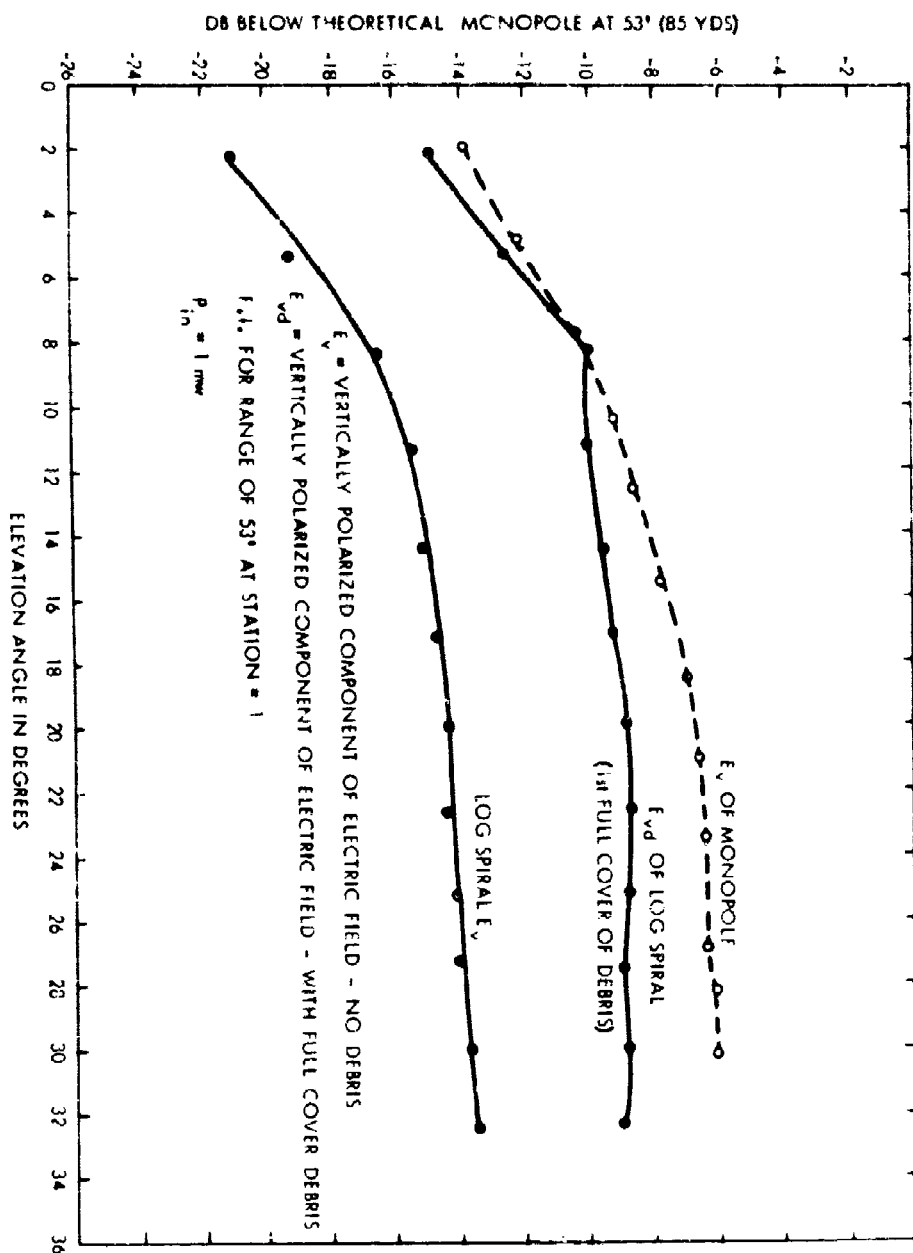


Figure 3-15. Measured Field Intensity Versus Elevation Angle for Log Spiral at Station 1  
 With and Without Debris.

whereas in Figures 3-14 and 3-15  $E_v$  increased with debris loading. This was consistently observed during the experimental program and appears to be a characteristic of the log spiral antenna.

The azimuthal radiation pattern of the log spiral (for  $E_v$ ) at a fixed elevation angle of approximately  $18^\circ$  is shown in Figure 3-16 together with that of the reference monopole. These field intensity plots were made at 90 Mc with an antenna input power of 1 milliwatt. For the case of a log spiral operating under a debris cover, radiated field was only monitored at stations 1, 5, and 6. Referring to Figure 3-16 we see that the log spiral exhibits lobing in the azimuthal plane with an increased gain over a monopole ( $\sim 4$  db) at  $\theta_{Az}$  of  $45^\circ$  to  $90^\circ$ , a null at  $\theta_{Az}$  of zero and a second maximum at  $\theta_{Az}$  equal to  $-45^\circ$ . Debris loading appears to fill in the null in the azimuthal pattern without significantly affecting the second maximum in the NW quadrant.

### 3.6 SUMMATION OF EXPERIMENTAL RESULTS

The experimental investigation of the 10 ft diameter log spiral antenna with backup cavity with and without debris resulted in the following conclusions.

#### 3.6.1 Input Impedance

The measured input impedance closely correlated theoretical predictions over the frequency range used in the test program. The input VSWR from 7 to 120 Mc decreased with debris loading as shown below and approached a matched condition ( $Z_0 = 50$  ohms)



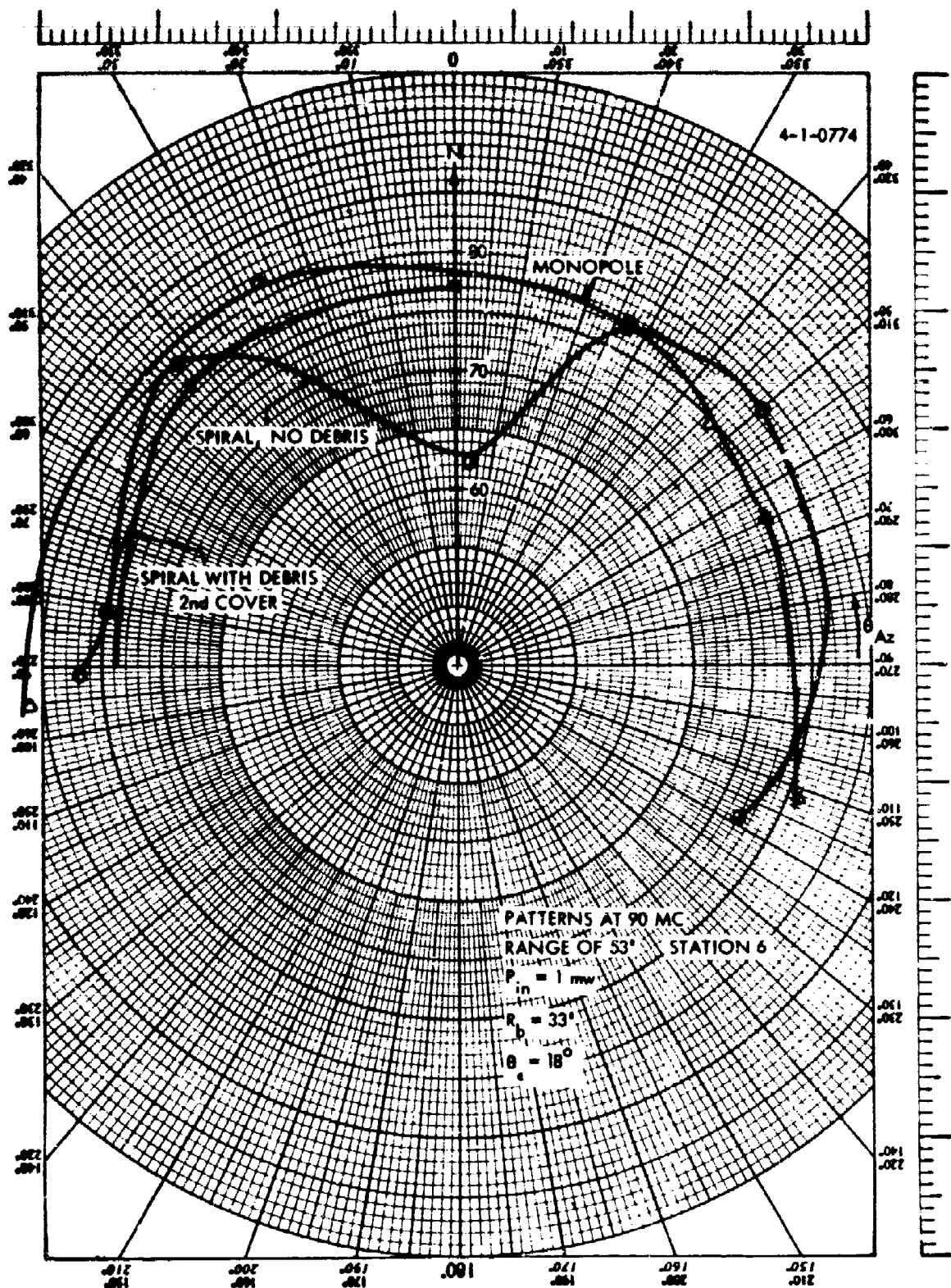


Figure 3-16. Azimuthal Plots of Log Spiral (With and Without Debris) and the Reference  $\lambda/4$  Monopole.

TABLE VII

Frequency	No Debris	Input VSWR	
		Full	Debris* Cover
Mc	-	-	-
75	2	1	
80	1.65	1.1	
90	1.70	1.2	
100	2.25	1.25	
110	1.9	1.4	
120	2	1.5	

\*  $\sigma$  debris  $\sim 2$  to  $3.3 \times 10^{-3}$  mho/m  
 $\epsilon_R \sim 3.5$

80 to 100 Mc frequency band

### 3.6.2 Radiation Pattern

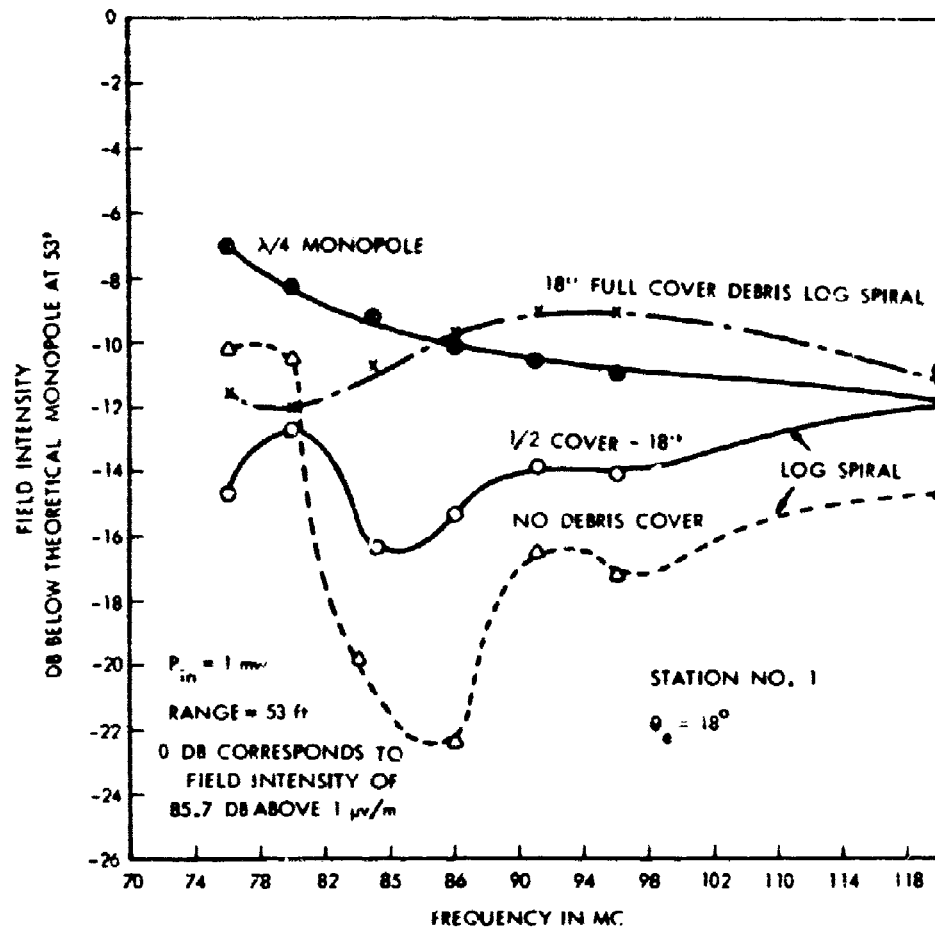
The log spiral exhibited lobing in both the azimuth and elevation planes for the no debris case. The antenna gains taken from azimuthal patterns (Figure 3-16) are as follows

Frequency	$\theta_{Az}$	Gain over $\lambda/4$ Monopole	Comments
Mc		db	
90	45° to 90°	4	for $P_{in} = m\omega$ , $R = 53$ ft
90	0° N	-16	and no debris.
90	-45°	-1	Reference for $\theta_{Az}$ is true north.

The elevation patterns for  $E_v$  and  $E_H$  indicate a beamwidth of approximately 20°. Under debris loading, the following effects were noted in the radiation patterns at 90 Mc.

- (a) In general, the vertically polarized electric field component  $E_v$ , remained the same or increased significantly. (Thus, debris loading appears to enhance  $E_v$ .)
- (b) In general, the horizontally polarized electric field component  $E_H$ , decreased --i.e., the energy being converted into vertically polarized component,  $E_v$ .
- (c) Beamwidths of the  $E_v$  and  $E_H$  components in elevation are not affected significantly by debris; i.e., BW is 20° with and without debris.
- (d) No azimuthal lobing was observed at monitoring stations. The null in pattern at station 1 (under no debris case) was filled in under the debris loaded condition.

The effects of debris loading on the log spiral versus frequency are shown in Figure 3-17. These results are for field intensities measured at station 1 and at an elevation angle of 18 degrees. This figure clearly shows the increase in the vertically polarized E field intensity ( $E_v$ ) with debris loading. It can be seen that under a full cover of debris, the gain of the log spiral is approximately 1 to 2 db over a  $\lambda/4$  monopole from 86 to 118 Mc. At 90 Mc, the vertically polarized component increased approximately 3 db with a half cover of debris, and 7 db with a full cover of debris over the no debris case.

Figure 3-17. Log Spiral Antenna  $E_v$  Versus Frequency Station 1.

## SECTION 4

### LINEAR SLOT

#### 4.1 LINEAR SLOT ANTENNA BACKED BY A RECTANGULAR CAVITY

Slot type antennas as used in the microwave field, provide an antenna which can be mounted flush with the ground and therefore can be made extremely hard, capable of withstanding very high overpressures. Basically it is possible to use a long slot in a conducting screen which is placed on the ground surface and separates the lossy ground from the lossless air. By exciting the slot by a current source which lies in the interface between the two media an electric field is set up across the slot, producing a radiation field. An antenna of this type has been analyzed by J. Galejs<sup>13</sup>. The radiation efficiency of the slot is very low (less than 1/10%) due to the high ground losses. Therefore this type of slot antenna is not useful for the application at hand. However, much higher radiation efficiencies are possible in a slot antenna backed by a cavity, as has been shown by J. Galejs<sup>14</sup>.

The basic configuration of the rectangular cavity-backed linear slot antenna is shown in Figure 4-1. The upper surface of the cavity (length  $x_0$ , width  $y_0$ ) is flush with the ground surface. The depth of the cavity is  $z_0$ . A horizontal slot, parallel to the longer side of the cavity ( $x_0$ ), is placed in the upper surface. The slot width is  $d$ , and the distance from the edge is  $y_c$ . The slot position in the upper surface is arbitrary; i.e., the coordinate of the slot center ( $y_c$ ) can vary from  $d/2$  to  $y_0/2$ :

$$\frac{d}{2} \leq y_c \leq \frac{y_0}{2},$$

Of particular interest are the positions

$$y_c = \frac{d}{2} \quad \text{slot at one side of cavity}$$

$$y_c = \frac{y_0}{2} \quad \text{slot in middle of cavity}$$

4-1-0779

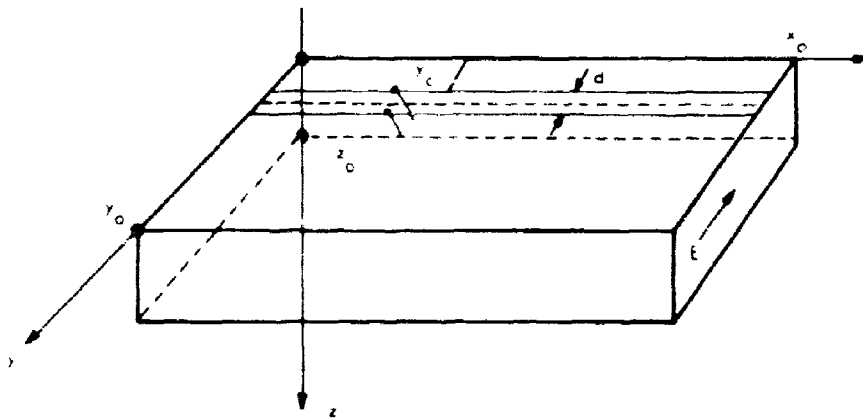


Figure 4-1. Cavity Backed Linear Slot Antenna in Air.

The source is applied either across the slot in the middle (at  $x = \frac{x_0}{2}$ ) or by a vertical E probe in center (or to one side) or by a loop at one side of the cavity. The electric field is excited across the slot in the y-direction. The cavity acts as a waveguide which is shorted at one end, operating in the fundamental  $TE_{10}$  mode. The direction of propagation is either in the z-direction or y-direction depending on the excitation and position of the slot. The predominant components of the E field are  $E_y$  and  $E_z$ , respectively. One propagating mode is obtained when  $x_0 < \lambda < 2x_0$  if the cavity is filled with air. When the cavity is filled with a dielectric of relative dielectric constant,  $\epsilon_r$ , the guide wavelength is reduced to

$$\lambda_g = \frac{\lambda_0}{\sqrt{\epsilon_r - \left(\frac{\lambda_0}{\lambda_c}\right)^2}}$$

with

$$\lambda_c = \frac{\lambda}{\sqrt{\left(\frac{m}{2x_0}\right)^2 + \left(\frac{n}{2y_0}\right)^2}}$$

For the  $TE_{10}$  mode,  $\lambda_c = 2x_0$  and  $\lambda_g = \frac{\lambda_0}{\sqrt{\epsilon_r - (\lambda_0/2x_0)^2}}$ . The cutoff wavelength is given by  $\sqrt{\epsilon_r} = \lambda_0/2x_0$ ;  $\lambda_0 = \sqrt{\epsilon_r} 2x_0$ . In order that the  $TE_{10}$  mode can exist the operating frequency must be greater than the cutoff frequency  $f_c$ ; i.e.

$$f \geq \frac{c_0}{\lambda_0} \geq \frac{c_0}{2x_0 \sqrt{\epsilon_r}} = f_c = \frac{f_{c0}}{\sqrt{\epsilon_r}} \quad \text{where}$$

$f_{c0} = \frac{c_0}{2x_0}$  is the cutoff frequency in the air-filled cavity. When the cavity is filled with a dielectric material with a dielectric constant of  $\epsilon_r$ , the cutoff frequency is reduced by  $1/\sqrt{\epsilon_r}$ . Thus for a given operating frequency the cavity cross section can be reduced to  $(1/\sqrt{\epsilon_r})^2 = 1/\epsilon_r$ .



## 4.2 DESIGN OF ANTENNA

We consider two designs which yield optimum efficiency. In one case the slot is at the edge of the cavity, in the second configuration, it is in the center. In order to get optimum efficiency the cavity is designed to operate at a frequency which is above the first cutoff frequency, so that the  $TE_{10}$  mode can propagate. When the slot is in the center the direction of propagation is in the z-direction. Optimum efficiency of the cavity would be obtained if the cavity depth could be made one fourth of the guide wavelength  $\lambda_g$ . Considering a frequency of 10 Mc (wavelength of 100 feet in air), a quarter wave depth would be  $25/\sqrt{\epsilon_r} = 15$  feet using a fill material with a dielectric constant of 2.8. However it is possible to achieve good efficiencies with considerably smaller cavities which are designed to operate close to resonance.

The design of such a cavity is as follows: The condition for propagation of the  $TE_{10}$  mode is:

$$\lambda_0 = \frac{c_0}{f_0} < 2x_0\sqrt{\epsilon_r}$$

Choosing a design frequency of  $f_0 = 10\text{Mc}$ , we get  $x_0 > c_0/f_0 \cdot 2\sqrt{\epsilon_r} = 10^9/10^7 \cdot 2\sqrt{\epsilon_r} = 50/\sqrt{\epsilon_r}$  feet. The length of the cavity  $x_0$  must be greater than 50 feet for air, and greater than  $50/\sqrt{2.8} = 30$  feet for asphalt ( $\epsilon_r = 2.8$ ). We choose  $x_0 = 60/\sqrt{\epsilon_r} = 36$  feet (or 60 feet for air).

The width  $y_0$  and depth  $z_0$  are chosen so that the cavity is resonant at the design frequency  $f_0 = 10\text{Mc}$ . The terminal susceptance  $B$  of the slot measured between two points in the middle of the slot is then zero. For a certain slot width there is a combination of  $y_0$  and  $z_0$  which makes the cavity resonant. Table VIII (for an air-filled cavity) shows data for various cavity widths  $y_0$  which yield a resonant cavity. The slot width is small (1/4 foot). The slot position is either in the middle of the top surface ( $y_c = y_0/2$ ) or at one end ( $y_0 = d/2$ ). The table shows that resonant cavities can be obtained with cavities of depths of less than 5 feet. The cavity volume is always smaller

TABLE VIII  
CAVITY DATA VERSUS CAVITY WIDTH  $y_o/\lambda_o$  AIR FILLED CAVITY

$\frac{y_o}{\lambda}$	$z_o/x_o$		Cavity Vol. $\times 10^3$		BW/ $f_o$		(BW/Vol) $\times 10^5$	
	$Y_c = \frac{Y_o}{2}$	$\frac{d}{2}$	$\frac{Y_o}{2}$	$\frac{d}{2}$	$\frac{Y_o}{2}$	$\frac{d}{2}$	$\frac{Y_o}{2}$	$\frac{d}{2}$
0.42	0.05	-	12.6	-	0.16	-	1.3	-
0.40	0.055	0.016	13.2	3.85	0.17	0.036	1.3	0.95
0.30	0.08	0.04	14.4	7.2	0.18	0.08	1.3	1.1
0.28	-	0.05	-	8.4	-	0.09	-	1.1
0.20	0.12	0.09	14.4	10.8	0.19	0.12	1.32	1.1
0.10	0.10	0.17	12	10.2	0.16	0.12	1.33	1.2

if the slot is on the side but the efficiency is also less. An estimate of the efficiency is obtained by considering the relative bandwidth of the cavity which is tabulated in Table VIII. The bandwidth near resonance is defined as  $8W = f_2 - f_1$ , where the susceptance  $|B|$  of the slot is twice the conductance  $G$  at  $f_1$  and  $f_2$ . There is a maximum of bandwidth for a cavity width  $y_0$  approximately  $0.2 \lambda_0$ . The maximum bandwidth is greater if the slot is in the center of the cavity, and also the bandwidth per unit volume is greater in this case. We find, therefore, that within the range of parameters considered, the cavity with the slot in the center appears to offer a better utilization of the cavity volume and therefore may be somewhat more economical.

The bandwidth of the slot can be increased by increasing the slot width. At the same time the depth of the cavity must be increased to obtain resonance. But the percent increase in bandwidth is greater than the percent increase in volume so that the bandwidth per unit volume is increased as the slot is made wider. The maximum obtainable bandwidth for a resonant cavity (air filled) with a slot width of 1/4 ft is 12% with a volume of  $10.8 \times 10^3 \text{ ft}^3$  (Table VIII, slot on one side). As the slot width is increased to 2 feet the maximum bandwidth increases to 30% and the volume doubles. Thus we have the situation that the volume has to be increased if the slot is increased, and as a result a greater bandwidth is obtained.

When the cavity is filled with dielectric material all dimensions of the cavity are reduced by  $1/\sqrt{\epsilon_r}$ . The slot length is therefore reduced and radiation conductance, which is determined by the slot area, is reduced. This reduction of  $G_R$  can be compensated within certain limits by increasing the slot width; i.e., by maintaining a constant slot area. Furthermore, the  $Q$  of the cavity is reduced if it is filled with dielectric material due to the dielectric losses. In air the  $Q$  of the cavity is determined by the radiation conductance and the ground losses, which are small. The  $Q$  of the dielectric cavity is determined by the radiation conductance and the total loss conductance. The  $Q_L$  resulting from the losses is determined by the dielectric fill material, as when asphaltic concrete is recommended. Practical experience with asphalt-filled antennas indicates that the  $Q_L$  is in the range of 50 to 70.

### 4.3 EFFICIENCY CONSIDERATIONS

The efficiency of the slot antenna is determined in the same manner as has been used with the annular slot antenna, using the basic relation between bandwidth and radiation power factor  $p$  that is valid for every tuned circuit or cavity:

$$p = \frac{\Delta\omega}{\omega_0}$$

where  $\Delta\omega/\omega_0$  is the relative bandwidth of the cavity which is only loaded with radiation conductance.

The efficiency

$$\eta = pQ_T = \frac{pQ_L}{1+pQ_L} = \frac{1}{1 + 1/pQ_L}$$

$$\eta = \frac{1}{1 + \frac{1}{\frac{\Delta\omega}{\omega_0} Q_L}}$$

The efficiency that is obtained with a bandwidth of 10% and say a  $Q_L = 50$  is therefore

$$\eta = \frac{1}{1 + \frac{1}{0.1 \times 50}} = \frac{5}{6} = 0.83 \text{ or } 83\%$$

and with a bandwidth of 2%; i.e.,  $p = 0.02$

$$\eta = \frac{1}{1 + \frac{1}{0.02(50)}} = \frac{1}{2} \text{ or } 50\%.$$

We can now proceed to design the cavity for an operating frequency of 10 Mc. The cavity is filled with asphaltic concrete to obtain the necessary hardness. The  $Q$  of the cavity due to losses is taken as  $Q_L = 50$ . The depth

of the cavity is chosen at about 5 feet, since this is a depth which will yield a bandwidth which is not far removed from the maximum obtainable bandwidth, while on the other hand, it keeps the volume and hence cost within practical limits.

Design A. The slot is in the center of the cavity as shown in Figure 4-2. The dimensions of the cavity in air having a depth of 5 feet are taken from Table VIII and compiled in Table IX. The dimensions are then reduced by  $1/\sqrt{\epsilon_r} = 0.6$  for asphaltic concrete-filled cavity and the slot width increased to 2 feet in order to obtain optimum bandwidth.

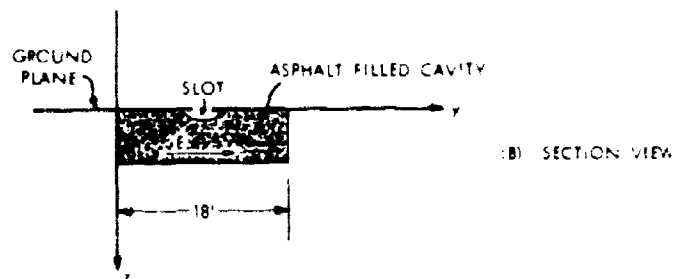
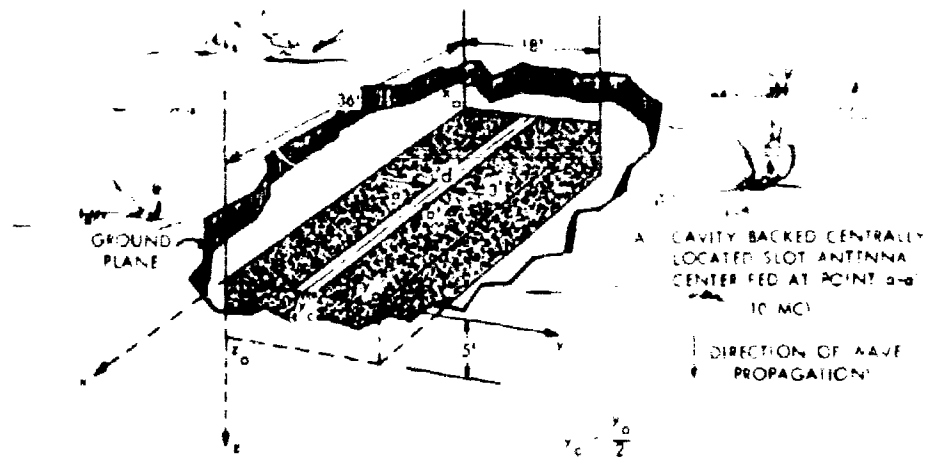
Design B. The slot is at the end of the cavity (See Figure 4-3), and the slot width is taken equal to the cavity depth. In this manner a folded cavity is obtained. The wide slot gives a z-component (vertical component), of the electric field at the slot edges. This field can propagate in the y-direction. To obtain optimum efficiency the width  $y_0$ , which is not actually the depth of the cavity because y is the propagation direction, should be approximately 1/4 wavelength. The design data are listed in Table X.

These two antennas provide high efficiency with a comparatively low volume (120 cubic yards).

#### 4.4 SUMMARY

The rectangular slot backed by a rectangular cavity is very suitable for use as a hardened antenna, capable of withstanding severe nuclear weapons effects. The size of the antenna designed for a frequency of 10 Mc is in the order of 18 x 36 feet and the depth need not exceed 5 feet, yielding a cavity volume of 120 cubic yards. The bandwidth of this antenna is in the order of 10% to 15%, but with a suitable tuning and matching network at the feed point it may be operated over a broad frequency range of approximately 2:1. There will be changes in the operating mode as the frequency is increased and the cutoff frequencies of the higher cavity modes are exceeded. This will cause changes in the radiation pattern and variations in the terminal impedance which have to be further examined. The radiation pattern of the slot operating in the dominant mode is similar to that of a vertical loop. It is

4-1-0572



NOTES: 1.  $x_0 \sim 0.6\lambda$

$d, z_0$  ARE OPTIMIZED FOR MAXIMUM ANTENNA EFFICIENCY FOR A GIVEN VOLUME

2. TYPICAL DESIGN - 10-20 MC - ASPHALT FILLED CAVITY

$x_0$	36"	$y_0$
$y_0$	18"	$z_0$
$z_0$	5"	

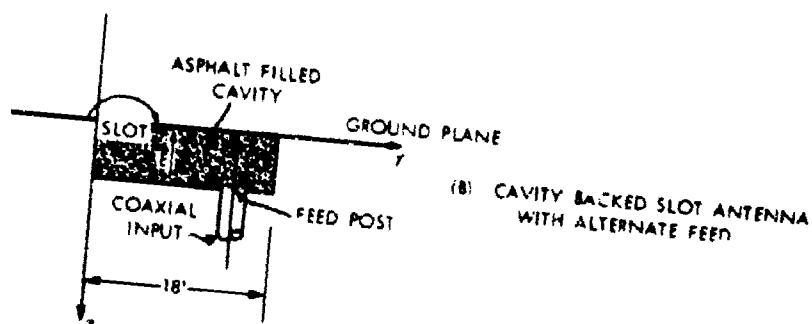
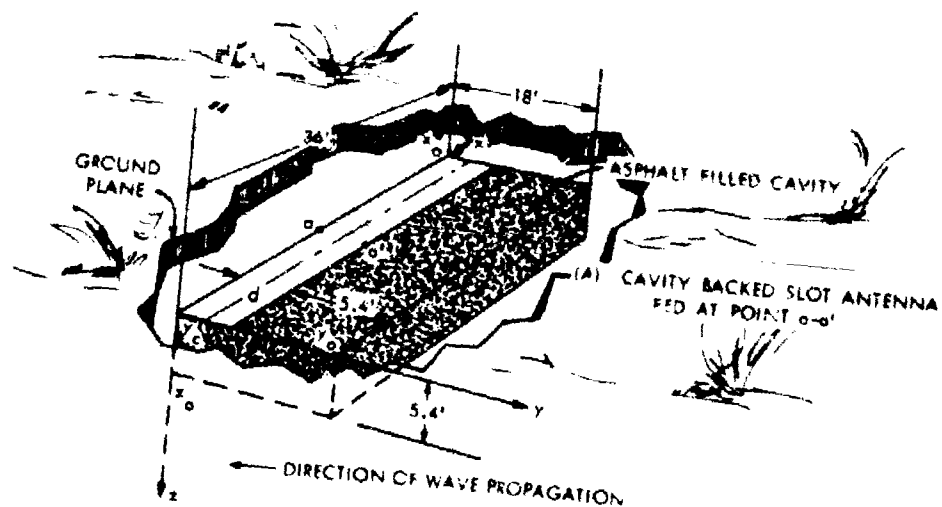
8W ~ 15 PERCENT

Figure 4-2. Configuration of Linear Slot Centrally Located - (10-20 mc).

TABLE IX

	Air	Asphalt
Cavity length $x_0$	60 ft	36 ft
Cavity width $y_0$	30 ft	18 ft
Cavity depth $z_0$	8 ft	5.0 ft
Slot width $W$	1/4 ft	2 ft
Cavity Volume	$14.4 \times 10^3$ cub. ft	$3.25 \times 10^3$ cub. ft
Bandwidth $\Delta\omega/\omega_0$	0.18	0.16
QL	150	50
Efficiency	95%	89%

4-1-0573



- NOTE: 1.  $x_0 \approx 0.6\lambda$   
 $d, z_0$  ARE OPTIMIZED FOR MAXIMUM ANTENNA EFFICIENCY  
 FOR A GIVEN VOLUME  
 2. TYPICAL DESIGN - 10 MC (ASPHALT FILLED CAVITY)  
 $x_0 = 36'$   
 $y_0 = 18'$   
 $z_0 = d = 5.4'$   
 $y_c = d/2$   
 BANDWIDTH AT PARTICULAR  
 FREQUENCY ~ 15 PERCENT

Figure 4-3. Configuration of Linear Slot at End of Cavity (10-20 mc).



TABLE X

	Air	Asphalt
Cavity length $x_o$	60 ft	36 ft
Cavity width $y_o$	30 ft	18 ft
Cavity depth $z_o$	4 ft	5.4 ft*
Slot width $w$	1/4 ft	5.4 ft*
Cavity volume $x_o y_o z_o$	$7.2 \times 10^3$ cubic ft	$3.5 \times 10^3$ cubic ft
Bandwidth $\Delta\omega/\omega_o$	0.08	0.09
$Q_L$	150	50
Efficiency	92%	82%

\*The depth was increased from  $4/\sqrt{\epsilon_r} = 2.5$  ft to 5.4 ft in order to increase the bandwidth and efficiency.

figure  $\pi$  shaped on the ground and vertically polarized, thus providing directional radiation (see Figure 4-4). It is possible to obtain omnidirectional radiation by using a square cavity (same depth) and providing two slots at right angles, crossing at the center of the cavity. The two slots are fed separately at the center by two transmission lines with a phase shift of  $90^\circ$  between the two feed voltages.

The construction of the cavity-backed slot antenna is simple. The walls of the cavity are made from heavy copper mesh, and it can be filled with asphaltic concrete of high dielectric quality and high strength; thus a linear slot represents an extremely hardened antenna in the HF band. The upper surface of the cavity with the slot's covered with a layer of asphalt of at least 12 to 13 inch thickness, to provide protection against thermal radiation effects.

#### 4.5 EXPERIMENTAL INVESTIGATIONS

##### 4.5.1 Scale Model

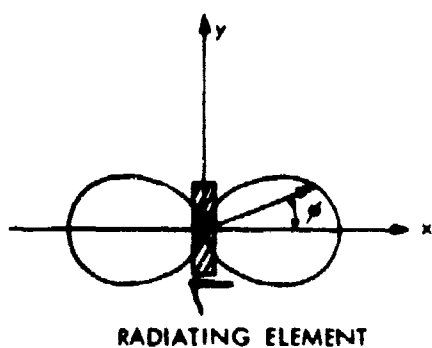
The scale model of the linear slot antenna used in the experimental program is shown in photograph Figure 4-5. Design center frequency for the antenna was 90 Mc. The model, details of which are given in Appendix B, utilized a telescopic feed probe centrally located within a rectangular back-up cavity and provisions were incorporated for varying the slot aperture. Glass blocks in the back-up cavity were used to support the top cover.

Debris loading of the antenna consisted of the placement of debris on a wooden platform 6 inches above the plane of the antenna aperture which as in the case of the log spiral simulates the isolation which would be provided by an asphaltic blanket in an actual antenna.

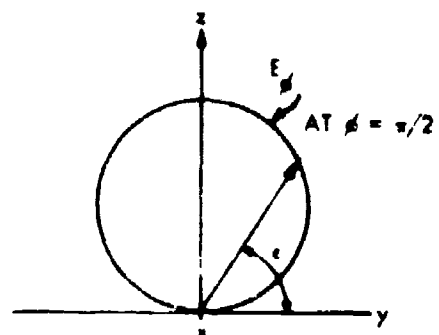
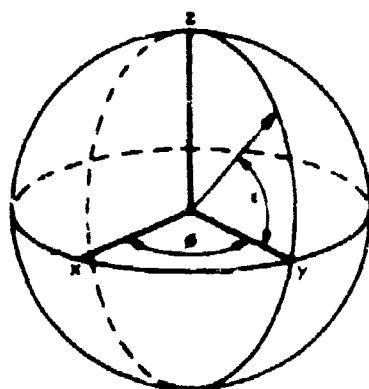
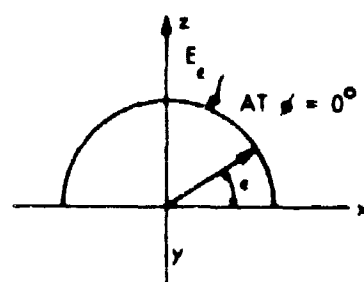
Two cases of debris loading were considered

- (a) uniform cover over one half the aperture (condition 20, HC)
- (b) uniform cover over the whole aperture and designated full cover (condition 19).

AZIMUTH PATTERN (HORIZONTAL)



ELEVATION PATTERN (VERTICAL)



NOTE:  $E_v$  IS VERTICALLY POLARIZED COMPONENT OF FAR FIELD  
 $E_h$  IS HORIZONTALLY POLARIZED COMPONENT OF FAR FIELD

Figure 4-4. Radiation Pattern of Linear Slot.

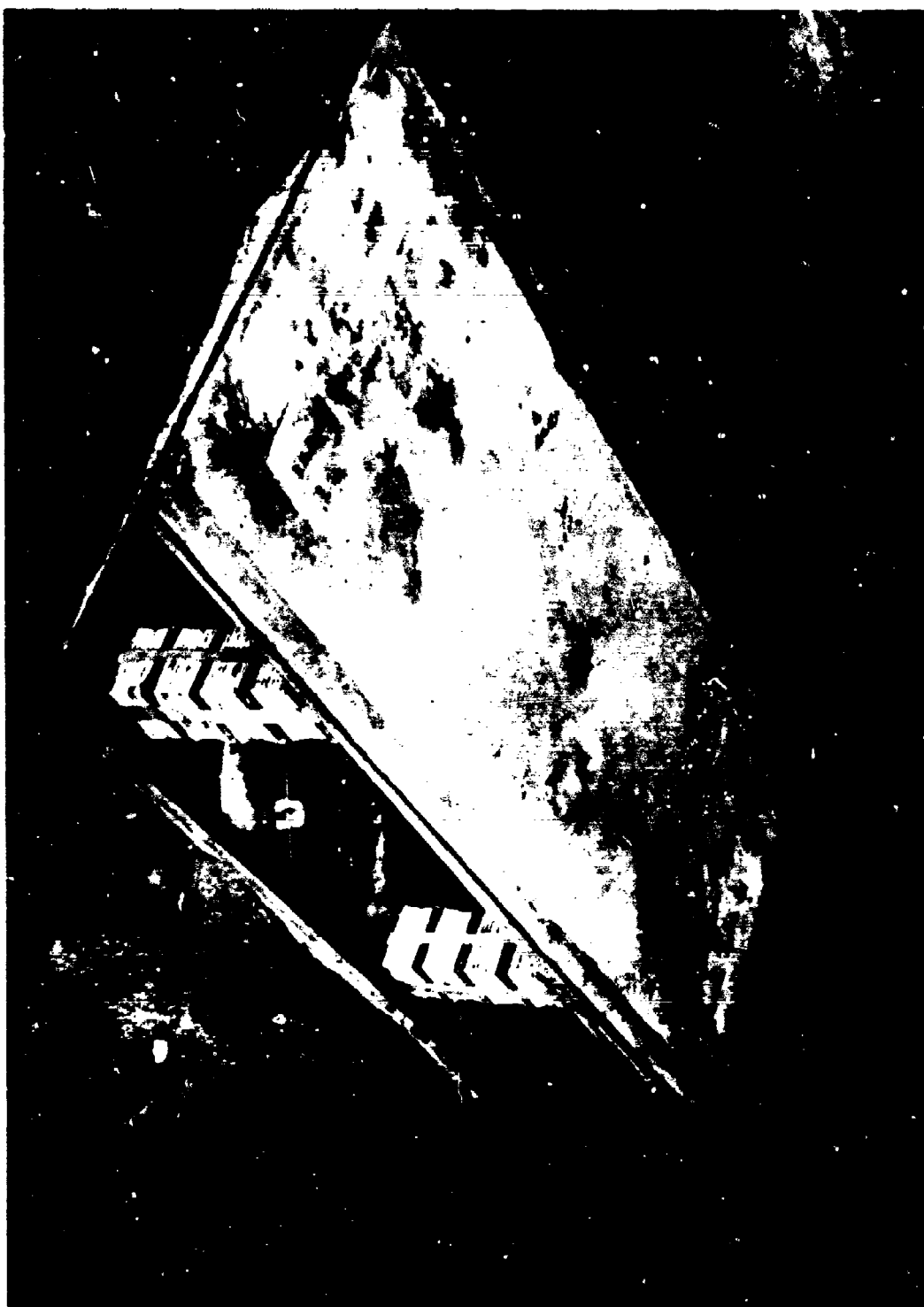


Figure 4-5. Photo of Linear Slot Scale Model Antenna.

#### 4.5.2 Input Impedance Considerations

- a) Tables XI and XII, Figures 4-6, 4-7, and 4-8 summarize the input impedance and VSWR from 75 to 100 Mc. Appendix C contains a detailed summary of the experimental setup and impedance roll-back techniques used at Sylvania for measurement and calculation of antenna input impedance.
- b) Experimental investigations indicate that the input impedance is not critical to slot aperture variations in the order of 6 to 13 inches. However, it was a function of the feed probe position when the probe was centrally located.
- c) Without debris, for  $VSWR \leq 2:1$  (no tuning or matching network):  
Bandwidth = 84 to 91 Mc, or about 10 percent for 88 Mc.
- d) With debris, VSWR (from 84 to 91 Mc) increased to 10:1.
- e) With appropriate tuning and matching network, can achieve the following performance with and without debris:
  - without debris,  $VSWR \leq 2.5$  to 1 from 75 to  $> 100$  Mc
  - with condition 20 HC debris,  $VSWR \leq 2.5$  to 1 from 75 to  $> 100$  Mc
  - with condition 19 FC debris,  $VSWR \leq 3.4$  to 2.5 from 75 to 85 Mc
  - $VSWR \leq 2.5$  to 1 from 85 to  $> 100$  Mc.

#### 4.5.3 Field Intensity Measurements

##### (a) Radiation Pattern

The azimuthal radiation pattern at a fixed elevation angle of 18 degrees as a function of frequency is shown in Figure 4-9, and exhibits that expected from such an antenna (i.e., a figure-eight pattern in azimuthal plane). Appendix C contains details of experimental setup used to perform the field intensity measurements.

##### (b) Gain over an actual $\lambda/4$ monopole.

f	Gain	$\theta_{Az}$ for max.
76 Mc	1 db	70° from plane of antenna
85 Mc	2 db	90° from plane of antenna
90 Mc	-1 db	125° from plane of antenna

##### (c) Antenna Bandwidth

Field Intensity versus frequency at Station 1, which is approximately 90° to the plane of the linear slot, is shown in Figure 4-10, indicates the following characteristics.

- (1) Without Debris, antenna exhibits gain greater than a  $\lambda/4$  monopole from 78 to 92 Mc with peak field intensity occurring at 85 Mc.
- (2) With condition 20 HC of debris, the peak in the field intensity versus frequency curve shifts to 90 Mc. In general the measured field intensity decreased approximately 2 db from the no-debris case. Comparing the linear slot field intensity with that of the monopole, it is seen that debris degradation is approximately 0 to 2 db from 78 to 92 Mc.
- (3) With condition 19 FC of debris, the peak in the field intensity curve shifts from the no-debris case to 90 Mc. In general, the measured field intensity equals that of the  $\lambda/4$  monopole from 76 to 86 Mc, was greater than the monopole from 85 to 97 Mc, and reached a peak value 4 db above the monopole at 90 Mc.

**TABLE XI**  
**NORMALIZED ANTENNA INPUT IMPEDANCE ( $Z_o = 50$  ohms)**

Freq. Mc	No Debris		Condition 19 Debris		Condition 20 Debris	
	$Z_A/Z_o$		$Z_A/Z_o$		$Z_A/Z_o$	
	R	X	R	X	R	X
75	0.45	-1.7	1.0	-2.9	1.4	-2.6
80	0.5	-1.11	0.85	-2.7	1.4	-2.6
85	1.08	-0.62	0.70	-2.41	1.22	-2.55
90	1.7	-0.5	0.55	-2.00	0.75	-2.1
95	2.5	-1.15	0.49	-1.70	0.61	-1.91
100	1.7	-1.9	0.45	-1.38	0.48	-1.71

TABLE XII  
VSWR ANTENNA INPUT ( $Z_0 = 50$  ohms)

Freq. Mc	No Debris	Condition 19	Condition 20
75	9.0	10.0	6.9
80	4.7	10.0	6.2
85	1.81	10.0	7.0
90	1.9	9.1	7.8
95	3.3	8.2	8.0
100	4.2	6.7	8.8



4-1-0780

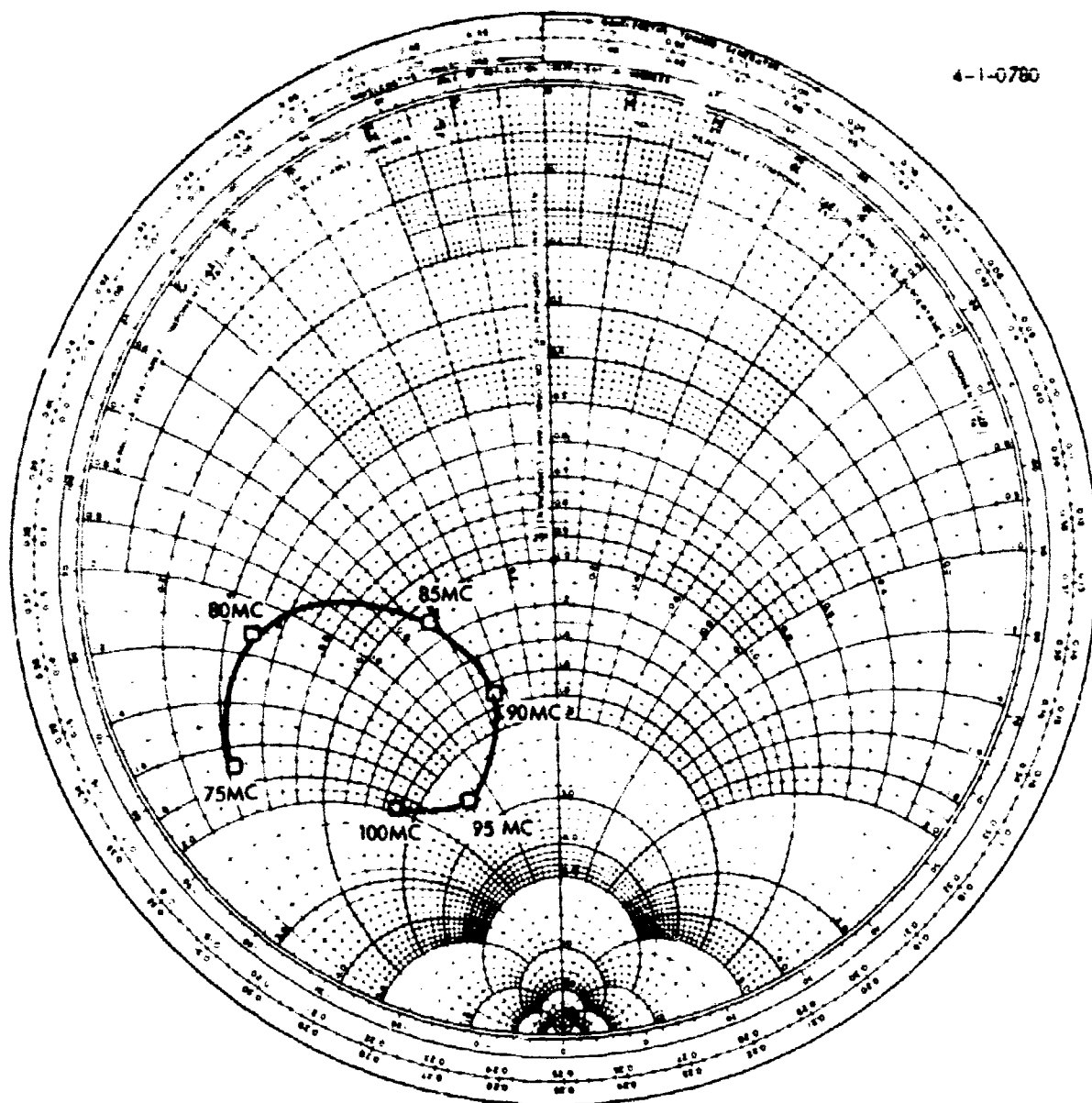


Figure 4-6. Linear Slot Input Impedance Versus Frequency (No Debris).

4-1-0781

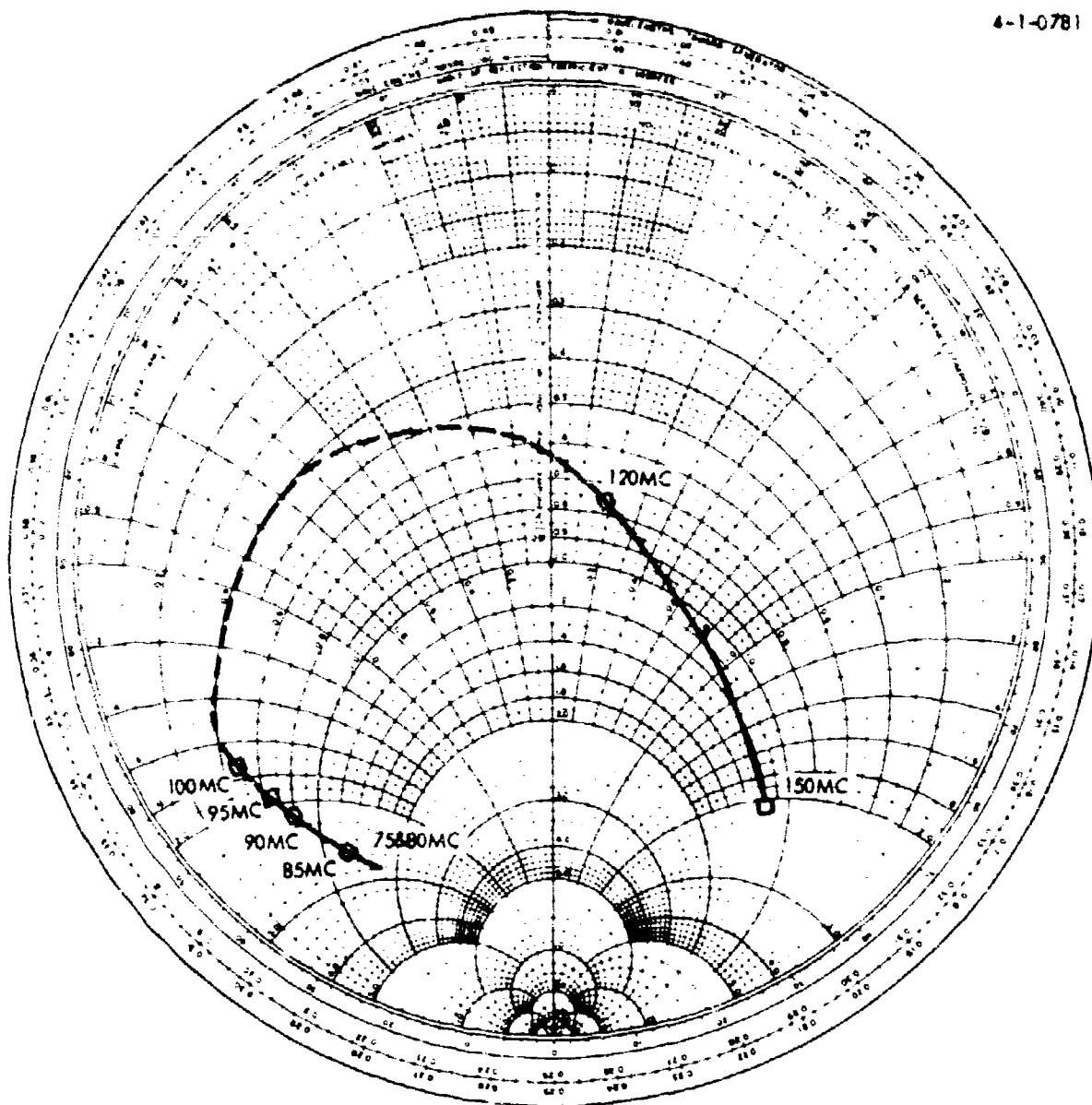


Figure 4-7. Linear Slot Input Impedance Versus Frequency

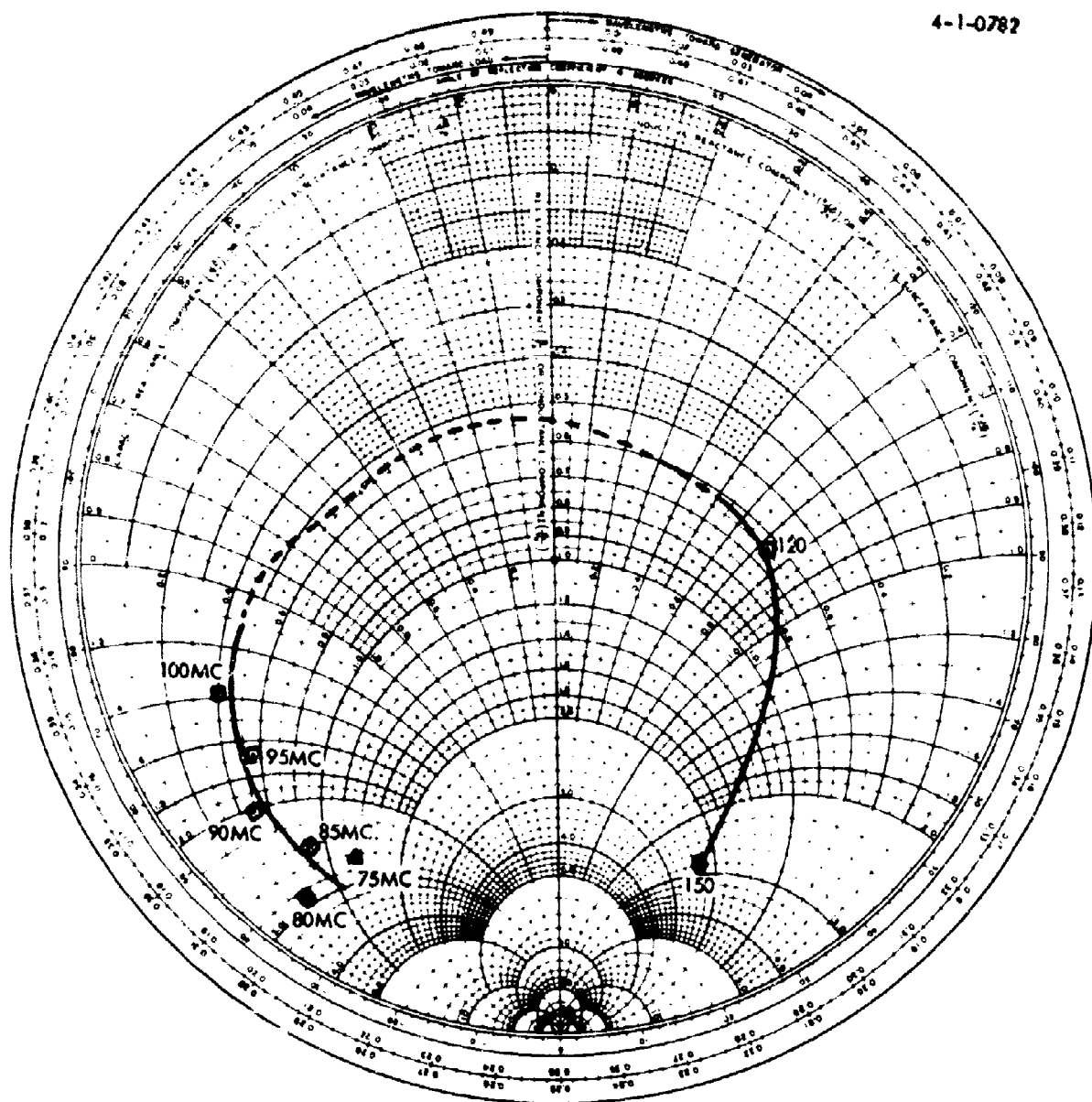


Figure 4-8. Linear Slot Input Impedance Versus Frequency

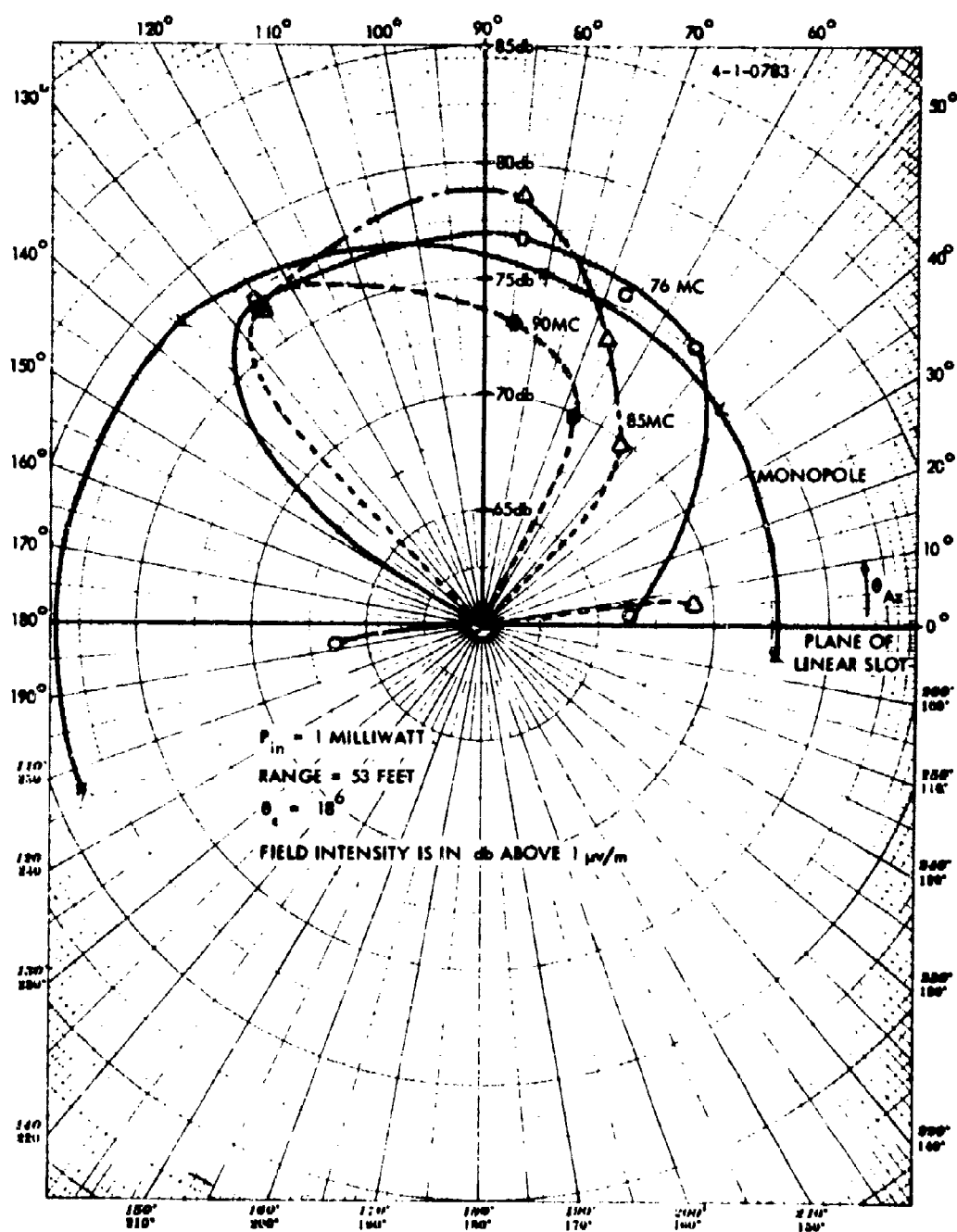


Figure 4-9. Linear Slot and Reference Monopole Azimuthal Patterns ( $\theta_s = 18^\circ$ ).

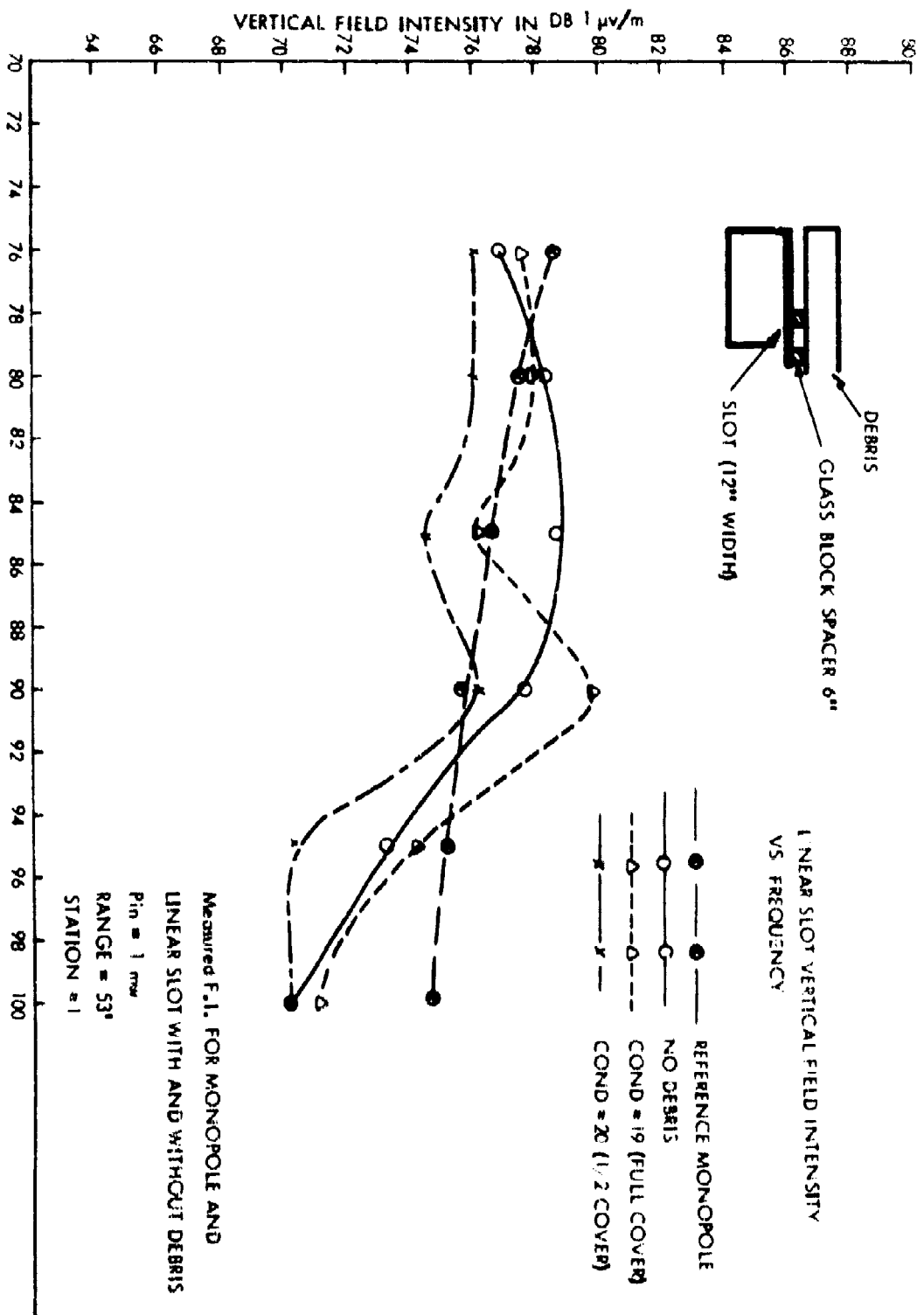


Figure 4-10. Field Intensity Versus Frequency for Linear Slot Model at Station 1.

## SECTION 5

### THE WIRE SLOT ANTENNA

#### 5.1 INTRODUCTION

The Wire Slot Antenna (WSA) consists of a vertical wire slot mounted above a conducting plane. (Figure 5-1a.) The two vertical wires form two vertical monopoles which are connected by a horizontal wire serving as a feed line for the second grounded monopole. The other monopole is directly connected to the coaxial feed cable.

The two monopoles are the principal radiators of the vertically polarized fields. The cavity is excited by the monopoles and apparently acts as a resonator which contributes essentially to the radiation field. This combination of a pair of vertical monopoles within a cavity or trough in which they are placed, constitutes the mathematical model on which the following analysis is based.

#### 5.2 ANALYSIS OF THE WSA

The basic dimensions of the WSA are as follows:

- $w$  = distance between the two vertical wires (monopoles)
- $h$  = height of the wire slot or height of each monopole above the ground plane; i.e., depth of cavity
- $a, b$  = length and width of cavity

We consider first the current distribution and input impedance of the antenna. The two monopoles are connected at the top by a horizontal wire of length  $w$ , parallel to the ground plane, which acts as a transmission line feeding the second monopole from the top, whereas the first monopole is fed from the base-end; i.e., from the bottom. Thus we have the following equivalent circuit in Figure 5-1b.

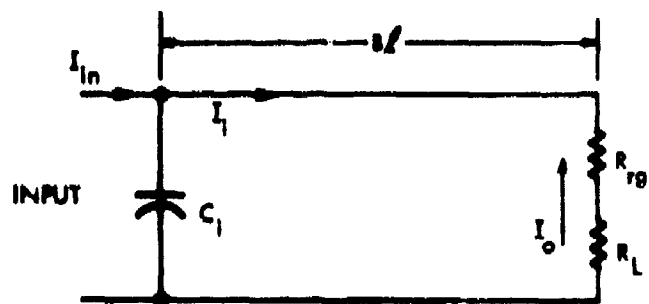
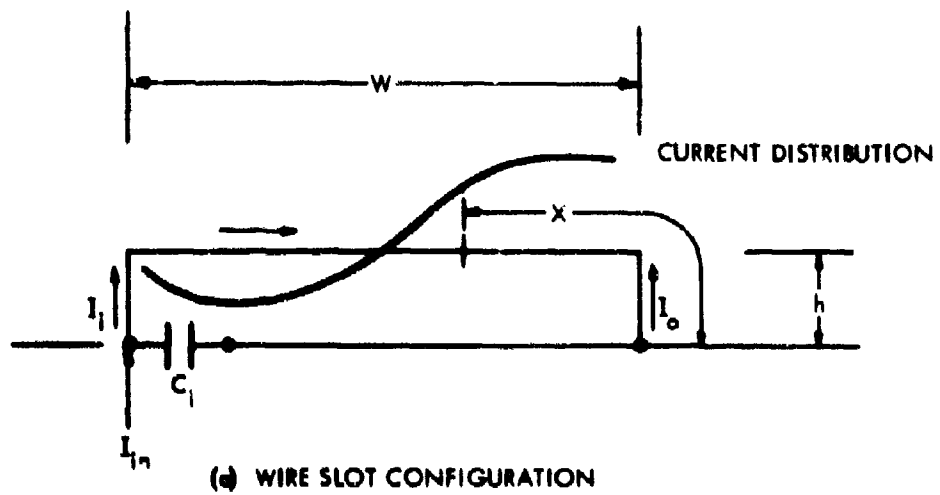


Figure 5-1. Wire Slot Antenna.

The grounded radiator carries the current  $I_0$ . This current varies sinusoidally along the length of the line, since the attenuation along the line is negligible, and the far end of the line is grounded, so that a standing wave along the horizontal wire is obtained; i.e.,  $I = I_0 \cos \beta x$ . The current maximum  $I_0$  is at the grounded end and the input current at the feed point is  $I_{in} = I_0 \cos \beta(w + 2h)$  with  $\beta = \frac{2\pi}{\lambda}$

Since  $\beta(w + h) > \frac{\pi}{2}$ , the current reverses its phase at the point  $\beta x = \frac{\pi}{2}$ , so that both  $I_{in}$  and  $I_0$  are flowing in the same direction (upward); i.e., they are in phase. The lead through connector at the feed point has a certain capacity  $C_1$  which shunts the feed cable. Parallel to this capacitor is the transmission line which has the impedance  $Z_0$ . The characteristic impedance is that of a wire of radius  $r$  at height  $h$  above a metal plane.

Thus

$$Z_0 = 138 \log_{10} \frac{2h}{r}$$

For

$$\frac{2h}{r} = 100, Z_0 \approx 280 \text{ ohm}$$

which correlates reasonably well with the measured impedance of the model (315 ohms). The reactance of the shorted line is  $j A_0 \tan \beta(w + 2h) = j Z_0 \tan \beta \ell = j X_{in}$ ,  $\ell = w + 2h$ . The resistive part of the input impedance is determined by the radiation resistance and loss resistance of the antenna. Of particular interest are the first series and parallel resonances of the antenna. These occur when

$$\tan \beta_1 \ell = 0 ; \quad \beta \ell = \pi$$

Series Resonance

and

$$Z_0 \tan \beta_2 \ell = \frac{1}{\omega_2 C_1}$$

Parallel Resonance



The model WSA antenna has following parameters

$$w = 1.55 \text{ m} ; \quad h = 0.25 \text{ m} ; \quad l = w + sh = 2.05 \text{ m}$$

$$\text{Series resonance frequency} \quad f_s = f_1 = 76 \text{ Mc} ; \quad \lambda_1 = 3.95 \text{ m}$$

$$\text{Parallel resonance frequency} \quad f_p = f_2 = 925 \text{ Mc} ; \quad \lambda_2 = 3.24 \text{ m}$$

$$\text{Characteristic Impedance} \quad Z_c = 315 \text{ ohm}$$

$$\text{Effective length} \quad \beta_1 l_e = \frac{2\pi}{\lambda_1} \quad l_e = \frac{2\pi}{3.95} \quad l_e = \pi$$

$$l_e = \frac{3.95}{2} = 1.98 \text{ m},$$

which is quite close to the actual length

$$l = 2.05 \text{ m}.$$

$$\text{Electrical length} \quad \beta_2 l_e = \frac{2\pi}{3.24} \times 1.98 = 1.23 \pi \text{ or } 220^\circ$$

$$\text{Capacitance} \quad \omega_2 C_1 = \frac{1}{Z_o \tan \beta_2 l_e} = \frac{1}{315 \tan 220^\circ} = \frac{1}{264}$$

$$\text{Capacity} \quad C_1 = \frac{10^6}{264} \times \frac{1}{185 (\pi)} = 6.5 \mu\mu\text{F}$$

### 5.3 RADIATION PATTERN AND RADIATION RESISTANCE

The radiation pattern of two vertical monopoles which are fed in phase and are separated by the distance  $w$  is obtained as the product of the pattern of a single monopole, and the group pattern of the two monopoles.

$$ED = 60 I_0 F_m(x) \times G(\phi, \psi)$$

$D$  = distance from antenna

$\phi$  = elevation angle

$\psi$  = azimuth angle measured from plane of wire slot

$I_0$  = current in the grounded monopole

$$I_{in} = p I_0 ; p = \cos \beta \ell = \frac{I_{in}}{I_0}$$

The pattern function of one monopole is

$$F_m(x) = \beta \ell \cos \phi \text{ (over perfect ground)}$$

The group pattern function for the case of equal phase in both radiations is

$$G(\phi, \psi) = \sqrt{(1+p)^2 - 4p \sin^2\left(\frac{\beta w}{2} \cos \phi \cos \psi\right)}$$

The maximum of  $G$  is at  $\phi = 0^\circ$ ;  $\psi = 90^\circ$ ,  $G_{\max} = G(0^\circ, 90^\circ) = (1+p)$

The minimum of  $G$  in the ground plane is at  $\phi = 0^\circ$ ;  $\psi = 0^\circ$ ,

$$G_{\min} = G(0^\circ, 0^\circ) = \sqrt{(1+p)^2 - 4p \sin^2\left(\frac{\beta w}{2}\right)}$$

The ratio of the square of the field intensities on the ground plane ( $\phi = 0$ ), at the azimuth angles  $\psi = 90^\circ$  (maximum) and  $\psi = 0$  (minimum) is

$$K^2 = \frac{|G(0^\circ, 90^\circ)|^2}{|G(0^\circ, 0^\circ)|^2} = \left[ 1 - \frac{4p \sin^2(\beta w/2)}{(1+p)^2} \right]^{-1}$$

The radiation resistance of a single short monopole of height  $h$  over perfect earth referred to the current  $I_0$  is

$$R_{ro} = 40(\beta h)^2 = 40 \times 4\pi^2 \left(\frac{h}{\lambda}\right)^2 = 160\pi^2 \left(\frac{h}{\lambda}\right)^2$$

The effective height is equal to the actual height in this case, since the horizontal feed wire acts as a top load for each of the monopoles, so that the current is practically uniform on the antenna.

The radiation resistance of the group referred to the current  $I_0$  in the grounded monopole is

$$R_{rg} = R_{ro} [1 + p^2 + 2pS]$$

$S$  is a function of  $(\beta w)$  for the case of equal phase of the two radiator currents. It is determined by the mutual coupling between the two monopoles.

The current  $I_0$  in the grounded radiator, to which the radiation resistance is referred, is given by the total input power  $P_T$  and the total resistance in the circuit, which is the sum of the radiation resistance  $R_r$  and the loss resistance  $R_L$ :

$$I_0^2 (R_{rg} + R_L) = P_T ;$$

$R_L$  can be estimated from the  $Q_L$  of the transmission line:

$$Q_L = \frac{\pi Z_0}{2R_L} \quad \text{for the half-wavelength line}$$

$$R_L = \frac{\pi Z_0}{2Q_L} \quad \text{with } Q_L = 150 \text{ and } Z_0 = 315 \text{ ohm}$$

$$R_L = \frac{\pi \times 315}{300} = 3.3 \text{ ohm}$$

This is approximately the loss resistance of the model antenna.

The efficiency of the antenna is

$$\eta = \frac{R_{rg}}{R_{rg} + R_L} ; \quad \text{The radiated power is } P_r = I_o^2 R_{rg}.$$

Thus,

$$I_o = \sqrt{P_r / R_{rg}}$$

and the field intensity on the ground is

$$\begin{aligned} (ED)_o &= 60(\beta l) G(\phi, \psi) \sqrt{P_r / R_{rg}} \\ (ED)_o &= \frac{60 \beta h}{\sqrt{40} \beta h} \frac{G(\phi, \psi)}{\sqrt{1 + p^2 + 2pS}} = \frac{30}{\sqrt{10}} \frac{G(\phi, \psi)}{\sqrt{1 + p^2 + 2pS}} \\ &= 9.5 \frac{G(\phi, \psi)}{\sqrt{1 + p^2 + 2pS}} \quad \text{for } P_r = 1 \text{ Watt.} \end{aligned}$$

In the direction  $\phi = 0$  ;  $\psi = 90^\circ$  (broadside direction) the field is

$$DE(0, 90) = 9.5 \frac{G(0, 90)}{\sqrt{1 + p^2 + 2pS}} = 9.5 \frac{1 + p}{\sqrt{1 + p^2 + 2pS}}$$

and in the endfire direction  $\phi = 0^\circ$  ;  $\psi = 0^\circ$

$$\begin{aligned} DE(0, 0) &= 9.5 \frac{G(0, 0)}{\sqrt{1 + p^2 + 2pS}} = \frac{9.5 \sqrt{(1+p)^2 - 4p \sin^2(\beta w/2)}}{\sqrt{1 + p^2 + 2pS}} \\ &= DE(0, 90)/K \end{aligned}$$

$$\frac{DE(0, 90)}{DE(0, 0)} = K \text{ as indicated above.}$$

The field intensity of the single top loaded vertical monopole over perfect ground is obtained for  $p = 0$ , and  $G(\phi, \psi) = 1$ . The current  $I_0$  of the monopole is  $I_0^2 R_{ro} = P_r$

$$I_0 = \sqrt{P_r / R_{ro}}$$

Thus

$$DE(0)_{\text{mono}} = 60 \times \beta l \sqrt{P_r / R_{ro}} = 9.5 \text{ Volt for } P_r = 1 \text{ Watt}$$

The field intensity ratio of the monopole pair to the single monopole for equal radiated power is in direction  $\phi = 0$  ;  $\psi = 90^\circ$

$$\left[ \frac{(ED)_{90^\circ}}{(ED)_{\text{mono}}} \right]^2 = \frac{(1+p)^2}{1+p^2 + 2pS} = G_o \text{ (Directivity of WSA in the broadside direction)}$$

and in direction  $\phi = 0^\circ$  ;  $\psi = 0^\circ$  or endfire direction,

$$\begin{aligned} \left[ \frac{(ED)_{0^\circ}}{(ED)_{\text{mono}}} \right]^2 &= \left[ \frac{(ED)_{90^\circ}}{(ED)_{\text{mono}}} \right]^2 \frac{1}{K^2} \\ &= \frac{(1+p)^2}{(1+p^2 + 2pS)} \frac{1}{K^2} \end{aligned}$$

Table XIII lists relative field intensities and radiation resistances as calculated with the preceeding expressions for the conditions of the model antenna:

TABLE XIII

f Mc	$\lambda_m$ meters	$w/\lambda$	$\beta l$	$p =$ $\cos \beta l$	$360^\circ (\frac{w}{\lambda})$
65	4.60	0.336	$161^\circ$	0.944	$121^\circ$
70	4.28	0.362	$172^\circ$	0.991	$130^\circ$
76	3.95	0.393	$187^\circ$	0.993	$141.4^\circ$
80	3.75	0.413	$197^\circ$	0.957	$149^\circ$
85	3.53	0.440	$209^\circ$	0.873	$158^\circ$
90	3.33	0.465	$222^\circ$	0.743	$167^\circ$
95	3.16	0.491	$234^\circ$	0.593	$177^\circ$

f Mc	2S	$1+p^2 + 2pS$	$R_{ro}$	$R_{rg}$	$R_{rs}$ ohm	$G_o$
65	0.5	2.36	4.65	11.0	2.95	2.0 db
70	0.35	2.33	5.40	12.6	3.2	2.3 db
76	0.11	2.09	6.3	13.2	3.3	2.8 db
80	0	1.92	7.0	13.4	3.5	3.0 db
85	-0.15	1.63	7.9	12.9	3.7	3.3 db
90	-0.30	1.33	8.9	11.9	3.9	3.6 db
95	-0.40	1.11	9.9	11.0	4.3	3.6 db

TABLE XIV

f	$\frac{(ED)_{90^\circ}}{(ED)_{0^\circ}} = K$	20 log K	$\left[ \frac{(ED)_{90^\circ}}{(ED)_{\text{mono}}} \right]^2$	$\left[ \frac{(ED)_{0^\circ}}{(ED)_{\text{mono}}} \right]^2$
76	3.11	9.9 db	2.8 db	2.8 - 9.9 = - 7.1 db
90	5.8	15.3 db	3.6 db	3.6 - 15.3 = -11.7 db

f	$\frac{1}{\omega C_1}$	$Z_o$	$R_L$	$*Q_L$	$R_{rg}$ ohm	$R_{rs}$ ohm
76	312 $\Omega$	315 $\Omega$	3.3 $\Omega$	150	13.2	3.3
90	264 $\Omega$	315 $\Omega$	4.0 $\Omega$	150	11.9	3.9

\*  $Q_L$  is an assumed value that characterizes the losses in the WSA. For a WSA imbedded in asphalt,  $Q_L$  is approximately 50.

Table XIV contains the essential data at the two resonance frequencies for the monopole pair, without consideration of the back cavity or trough. Considering the two resonance frequencies the following facts are observed for the theoretical monopole pair model. The pattern is roughly a figure  $\infty$  shape at both frequencies, with the maximum broadside to the plane of the wire slot. The minimum radiation along the ground, or at low elevation angles, is in the plane of the wire slot, and the ratio  $E_{\max}/E_{\min} = E(90^\circ)/E(0^\circ) = K$ . at series resonance ( $f = 76$  Mc,  $K = 9.9$  db) the ratio is smaller than at parallel resonance ( $f = 90$  Mc,  $K = 15.3$  db). This means that the pattern pulls in more at 90 Mc than at 76 Mc. In both cases the broadside field intensity of the wire slot is greater than that of the omnidirectional monopole. The increase in field intensity is larger at 90 Mc (3.5db) than at 76 Mc (2.7 db). There is not much change in the radiation resistance of the wire slot at the two resonance frequencies.

#### 5.4 DISCUSSION OF MEASURED FIELD INTENSITY (WSA)

Analyzing the measured patterns and input impedances of the WSA the following observations are made and summarized in Table XV.

The input impedance Smith Chart plot Figure 5-2 shows clearly a series resonance frequency at 76.3 Mc and a parallel resonance frequency at about 92 Mc. The purely resistive impedances at these frequencies are 5 ohms and approximately 2600 ohms respectively. The azimuthal patterns are different at the two resonance frequencies. At 76 Mc the pattern is almost circular, but at 90 Mc the pattern has the expected figure  $\infty$  shape. Measurements over a flat ground, instead of the cavity, showed an increase in field intensity and radiation resistance at the resonance frequencies. Table XV summarizes certain results of measurements used for comparison with the theory (since the pattern is slightly serrated, average values for  $E(90^\circ)$  in the broadside direction were used for this comparison).



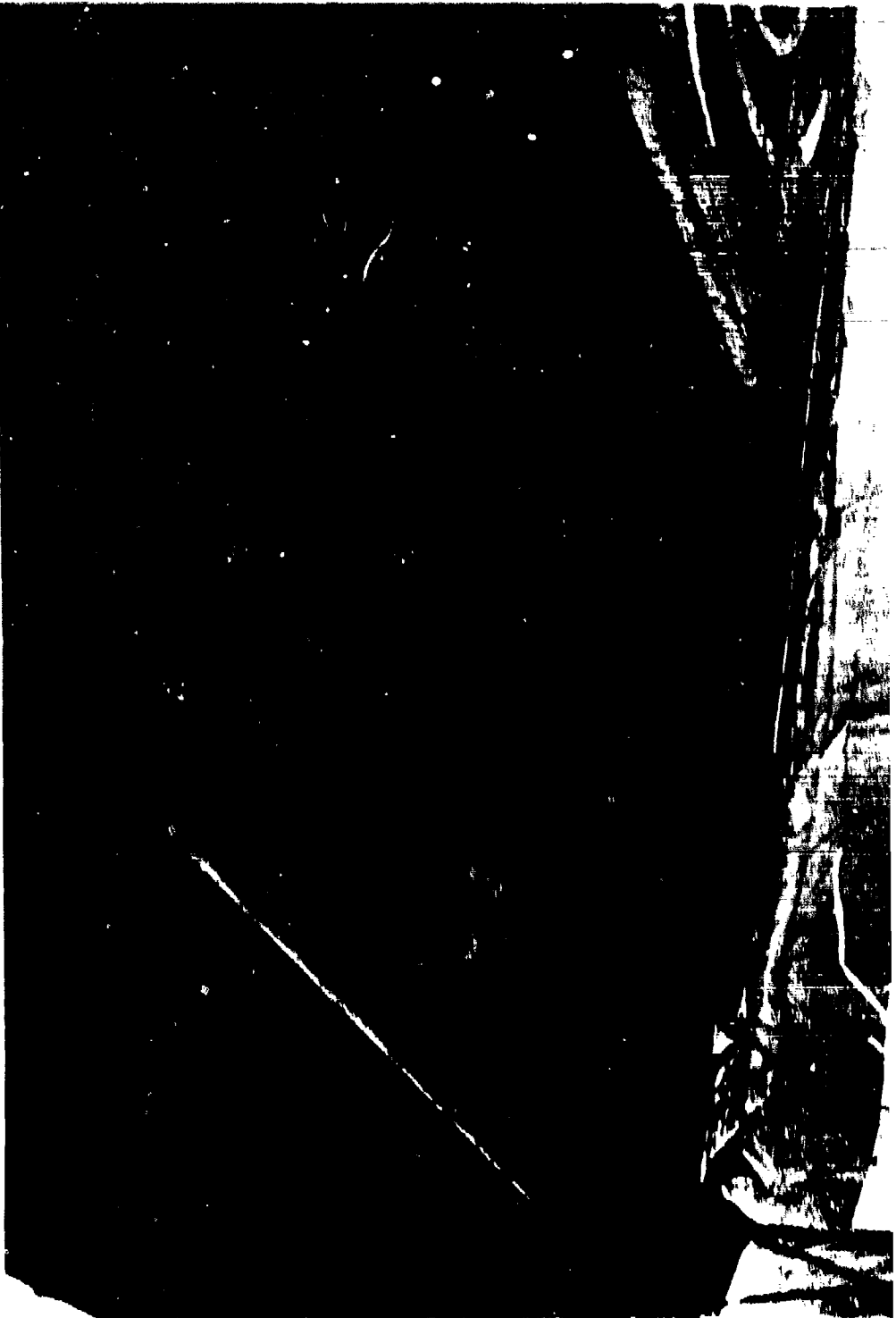


Figure 5-2. Photo of Scale Model Wing Star Airplane.

TABLE XV  
MEASURED DATA (AVERAGES)  
WIRE SLOT ANTENNA IN TROUGH

Frequencies	E(0)	E(90)	$\frac{E(90)}{E_M}$	$\frac{E(0)}{E_M}$	$\frac{E(90)}{E(0)} = K$	$R_{in}$
WS 76 Mc	72 db	70 db	-7 db	-7 db	0 db	5 ohm
Mono	79 db	77 db				
WS 90 Mc	89 db	81.5 db	+4.5 db	-10 db	+14.5 db	2500 ohm

WIRE SLOT ANTENNA ABOVE FLAT GROUND

Frequencies	$\frac{E(90)}{E(0)}$ (Flat) (Trough)	$\frac{E(90)}{E_M}$ (Flat)	$R_{in}$
76 Mc	+ 6.5 db	- 0.5 db	8 ohm
90 Mc	+ 3.5 db	+ 8 db	2500 ohm

### 5.3 EVALUATION OF WSA PERFORMANCE

Comparing measured and theoretical data, as derived from the monopole pair model, without cavity effects, yields the following evaluation at the two resonance frequencies.

a) Parallel Resonance,  $f = 92.5$  Mc

At the parallel resonance frequency the theoretical and measured pattern shapes of the wire slot agree well, as shown in the table below

	<u>Theoretical</u>	<u>Measured</u>
$G_o = \frac{E(90)}{E_M} = + 3.6$ db		+ 4.5 db
Data at $f=90$ Mc		
$\frac{E(0)}{E_M} = - 11.7$ db		- 10 db
$K = \frac{E(90)}{E(0)} = 15.3$ db		14.5 db

The ratio  $E(90)/E(0)$  is almost the same in both cases. Also the directivity  $G_o$  and the ratio  $E(0)/E_M$  agree within measurement accuracy ( $\pm 1$  db).

From this agreement of the patterns the conclusion is drawn that the monopole pair model is a reasonably good representation of the wire slot at the parallel resonance frequency. In particular this indicates that the currents in the two vertical legs of the wire slot are in phase, that the current ratio  $I_2/I_1 = I_o/I_1 \cdot p \approx 0.74$ , and that the space phase angle  $\beta w$  is determined by the physical separation  $w$  of the two radiators. The pattern is mainly generated by these two currents and the horizontal wire does not have an appreciable effect on the vertical component of the far field patterns.

From the agreement between calculated and measured pattern, and directivity  $G_o$  it is concluded that the radiation resistance at the parallel resonance frequency of the WSA is as calculated in Table XIV.  $R_{rg} = 11.9$  ohm. This radiation resistance is referenced to the base current ( $I_o$ ) in the grounded monopole. The total radiated power is, therefore,  $P_r = I_o^2 R_{rg}$ .

The input resistance and efficiency of the WSA at parallel resonance are calculated with the aid of an equivalent circuit. (Figure 5-1b.) The radiation resistance  $R_{rg}$  is placed at the end of a transmission line of electrical length  $\beta l = 220^\circ$ . In series with it is the loss resistance which represents the sum total of all losses in the antenna. At the input of the line, where the feed cable is connected, the current  $I_1$  is flowing. No attenuation is assumed on the line, thus

$$I_1 = I_o \cos \beta l = p I_o = -0.766 I_o$$

The line at its input terminals represents an impedance

$$Z_1 = j Z_o \tan \beta l + \frac{(R_{rg} + R_L)}{\cos^2 \beta l}$$

The inductance of the line is in resonance with the input capacity  $C_1$ , which is formed by the lead-through connector. The input impedance at parallel resonance is ohmic and given as:

$$\begin{aligned} Z_{in} &= \frac{X_1^2}{R_1} = \frac{Z_o^2 \tan^2 \beta l}{(R_{rg} + R_L) \cos^2 \beta l} \\ &= \frac{Z_o^2 \sin^2 \beta l}{(R_{rg} + R_L)} = 2600 \text{ ohm} \end{aligned}$$

since  $Z_{in}$  was measured as 2600 ohm.

Hence

$$R_{rg} + R_L = \frac{Z_o^2 \sin^2 \beta l}{2600} = \frac{315^2 \times 0.643^2}{2600} = 15.8 \text{ ohm}$$

$$R_L = 15.8 - R_{rg} = 15.8 - 11.9 = 3.9 \text{ ohm}$$

This is in close agreement with the estimated loss resistance of 4 ohm, using a line  $Q_L$  of 150.

The efficiency is then

$$\eta = \frac{R_{rg}}{R_{rg} + R_L} = \frac{11.9}{15.8} = 0.75 \text{ or } 75 \text{ percent.}$$

Measurements of the WSA over a flat ground screen without a cavity, as shown in Table XV, illustrate the influence of the cavity. Over flat ground the directivity in the broadside direction is increased by approximately 3 db. However the radiation resistance is hardly changed and the efficiency is somewhat increased.

b) Series Resonance,  $f = 76 \text{ Mc}$

The situation is different at the series resonance frequency (76 Mc). We find that the radiation pattern is practically circular, that the field intensity of the wire slot is considerably lower than that of the monopole, and that the input impedance is quite low. This different behavior as compared with the predictions based on the model is attributed to the influence of the cavity.

Comparing the measured and calculated patterns shows that the field intensity ratio of the wire slot in the endfire direction ( $\psi = 0^\circ$ ) and the monopole agree in both cases. However, the broadside field intensity is at the same low level as the endfire field intensity, indicating a circular pattern and low efficiency, since the broadside field intensity is much lower than that of the monopole. Table XVI shows the comparison between theoretical pattern and measured pattern.

TABLE XVI

	<u>Theoretical WSA</u>	<u>Measured WSA</u>
	$\frac{E(0)}{E_M} = -7.1 \text{ db}$	-7 db
$G_o =$	$\frac{E(90)}{E_M} = +2.8 \text{ db}$	-7 db
	$\frac{E(90)}{E(0)} = 9.9 \text{ db}$	0 db

From this discrepancy of the patterns the conclusion is drawn that the currents and fields excited in the cavity produce a far field which is also figure  $\infty$  shaped with opposing phase so that the total radiated field has a circular form. The radiation resistance is therefore equal to that of a short vertical omnidirectional monopole. The radiation resistance of one of the two vertical radiators of the wire slot is  $6.3\Omega$ . This radiator represents the reference monopole to which the wire slot antenna is compared. The field intensity produced by the WSA is 7 db below the reference monopole. This is due to a reduction of the effective height of the WSA and is apparently caused by the opposing currents in the cavity or trough walls. The radiation resistance  $R_{rg}$  of the WSA referred to the current in one of the two radiators is therefore reduced by 7 db from the original value of  $6.3 \text{ ohm}$ :  $R_{rg} = \frac{6.3}{5} = 1.3 \text{ ohm}$ . The measured input impedance is  $Z_{in} = 5 \text{ ohm}$ .

The equivalent circuit representing the losses and radiated power is the same as used before in the case of parallel (Figure 5-1b) resonance. The line length is now one-half wavelength. The line is terminated with  $R_{rg}$ , which is now very much smaller than in the case of parallel resonance, and by the loss resistance  $R_L$ , which has approximately the same value as before. Since the line is  $\lambda/2$  long, the line impedance at the input terminals is equal to the terminating impedance:  $Z_1 = R_{rg} + R_L$ . The capacity  $C_1$  has practically no effect at this frequency since its reactance is high compared to  $Z_1$ . Thus  $Z_{in} = R_{rg} + R_L = 5 \text{ ohm}$  (measured). This yields  $R_L = 5 - R_{rg} = 5 - 1.3 = 3.7 \text{ ohm}$ .

The efficiency of the WSA at the series resonance frequency is

$$\eta = \frac{R_{rg}}{R_{rg} + P_L} = \frac{1.3}{5} = 0.25 \text{ or } 25 \text{ percent.}$$

Measurements of the WSA over a flat ground screen at the series resonance frequency as shown in Table XV indicate the significant influence of the trough. Directivity under these conditions is increased by 6.5 db so that the broadside field intensity is approximately equal to that of the  $\lambda/4$  monopole. The radiation resistance for the WSA over a flat ground plane is computed to be approximately 5 ohms resulting in an antenna efficiency of 80 percent. This calculation assumes a reduction of the loss resistance to 3 ohms due to the elimination of the trough.

The radiation pattern for the WSA above a flat ground screen exhibits directivity and conforms to theoretical predictions.

## 5.6 WIRE SLOT EXPERIMENTAL INVESTIGATION

### 5.6.1 Scale Model

The scale model of the wire slot in a trough is shown in the photograph of Figure 5-2. Appendix B contains additional details as to the design and construction of the model antenna. The frequency for which the total perimeter of the slot (i.e., width + 2 (height), or  $w + 2h$ ) is a half wavelength at approximately 76 Mc.

The antenna consists of two vertical sections (or  $\lambda/16$  in height) which act as vertical radiating monopoles connected by a horizontal feed line. An insulator is utilized to isolate the input terminal wherever the second vertical radiator is grounded to the trough screening.

Input impedance and field intensity measurements were made under the following conditions of debris loading:

- (a) Condition 1, uniform debris cover over one-third of the wire slot and trough. This simulates the loading of one of the vertical monopoles.
- (b) Condition 5, debris cover centered over one-half the wire slot trough. This simulates the loading of the complete wire slot antenna; i.e., the 2 vertical monopoles and horizontal feed line.
- (c) Condition 12, uniform debris cover over the entire wire slot trough.

The debris covers discussed above were placed on a 3/4" plywood platform which covered the entire wire slot and trough. Debris as for the other model antennas had the following characteristics in the test frequency range.

$$\sigma \text{ debris} \sim 3 \times 10^{-3} \text{ mho/m}$$

$$\epsilon \text{ debris} \sim 3.5$$

#### 5.6.2 Input Impedance Measurements

Figures 5-3, 5-4, 5-5 are Smith chart input impedance plots from 75 to 110 Mc. From these curves, the following characteristics are observable:

- (a) The input impedance of the wire slot in a trough versus frequency appears to follow the same pattern with and without debris, however with debris loading, it tends to spiral in a clockwise direction and shrink toward the origin of the Smith Chart.
- (b) The antenna exhibits two frequencies at which the input impedance is resistive; i.e., approximately 76 Mc where the antenna is series resonant and at 92 Mc where it is antiresonant. These frequencies are shifted down approximately 3 percent with debris loading.
- (c) In air (without debris), the above resonant frequencies are related to the frequency ( $f_d$ ) for which the wire slot perimeter ( $w + 2H$ ) is a half-wavelength; i.e.,

$$f \text{ series resonance} = 1.05 f_d$$

$$f \text{ antiresonance} = 1.25 f_d$$



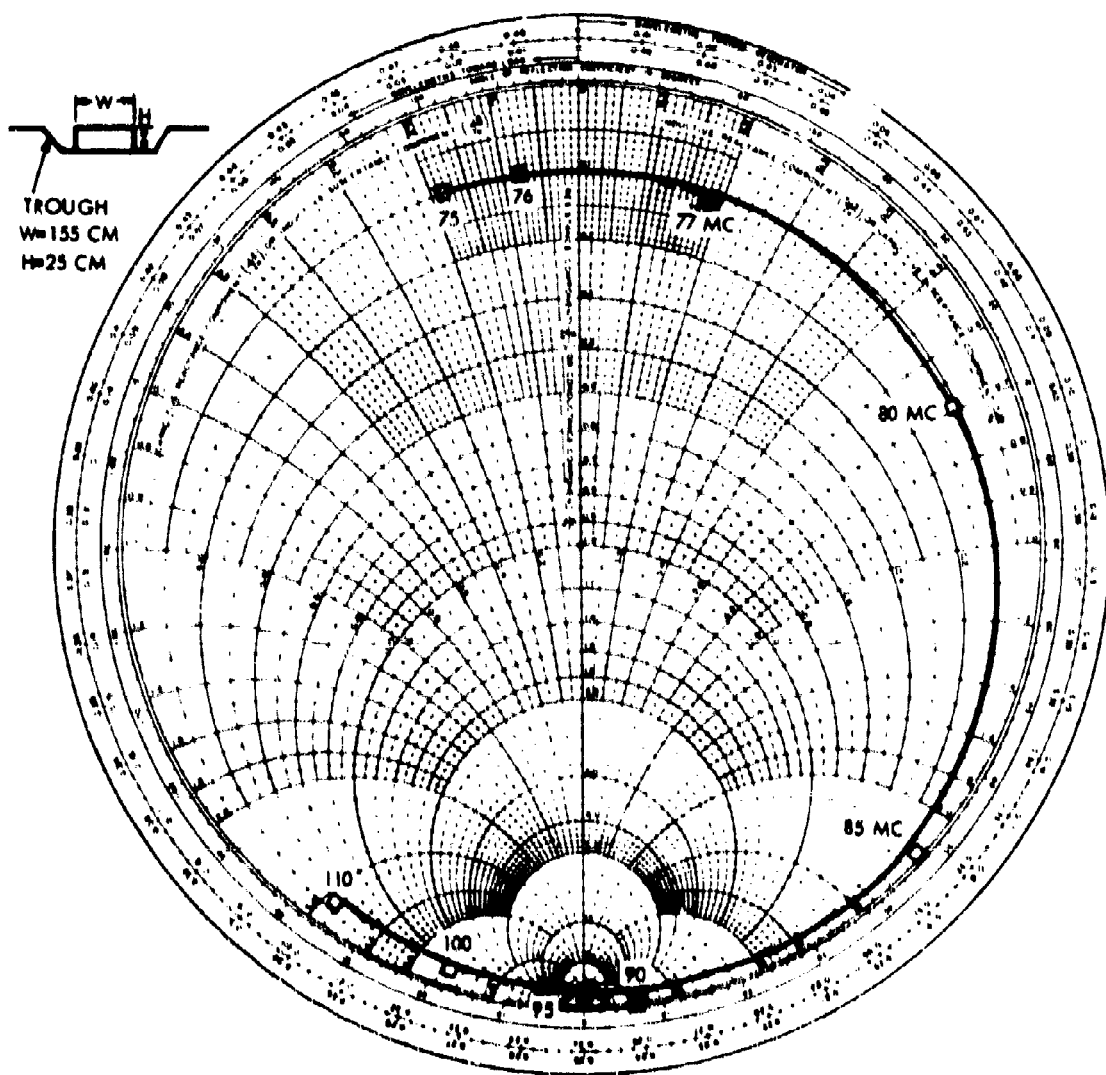


Figure 5-3. Smith Plot of Input Impedance vs Frequency.

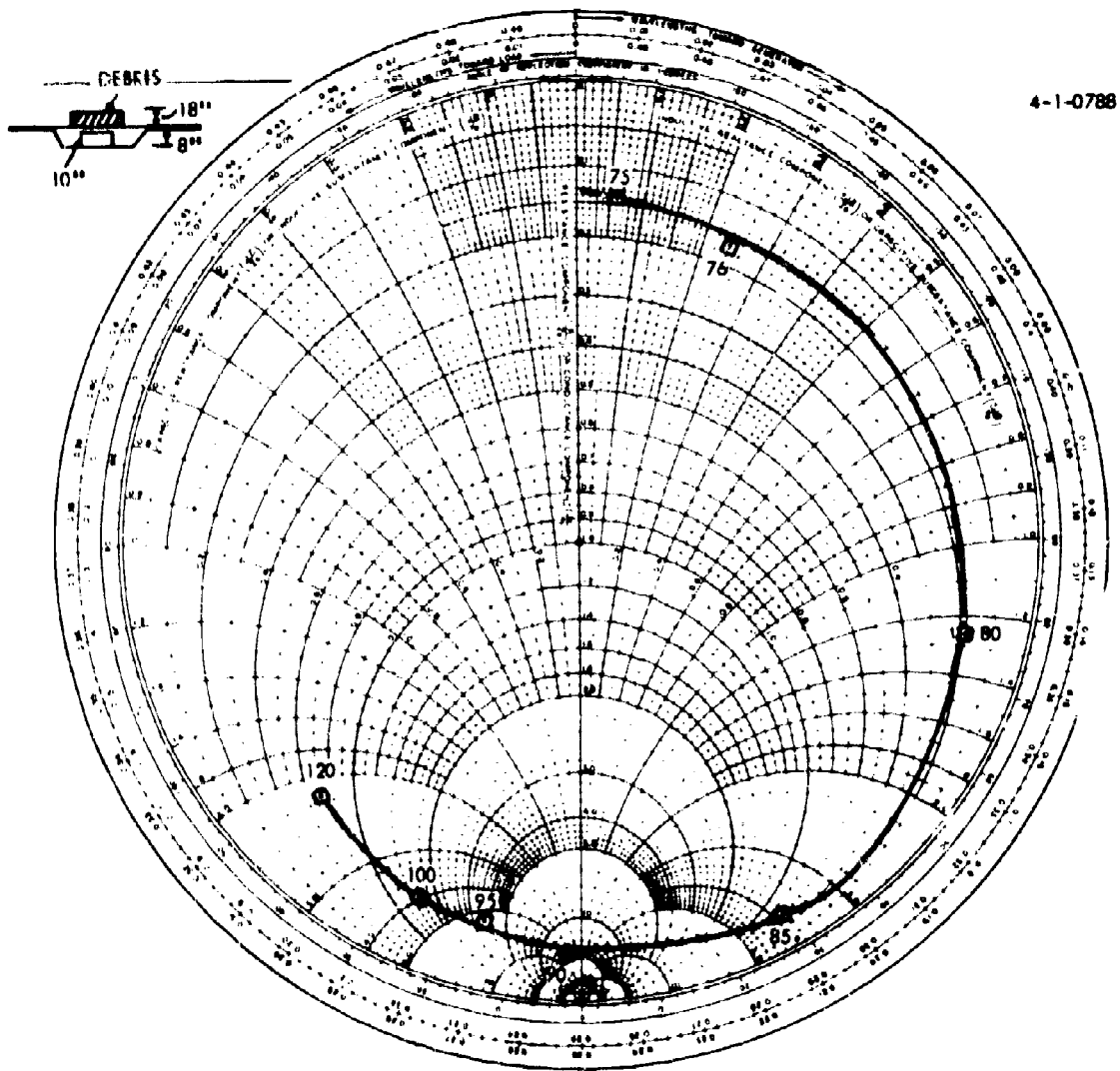


Figure 5-4. Smith Plot of Input Impedance vs Frequency.

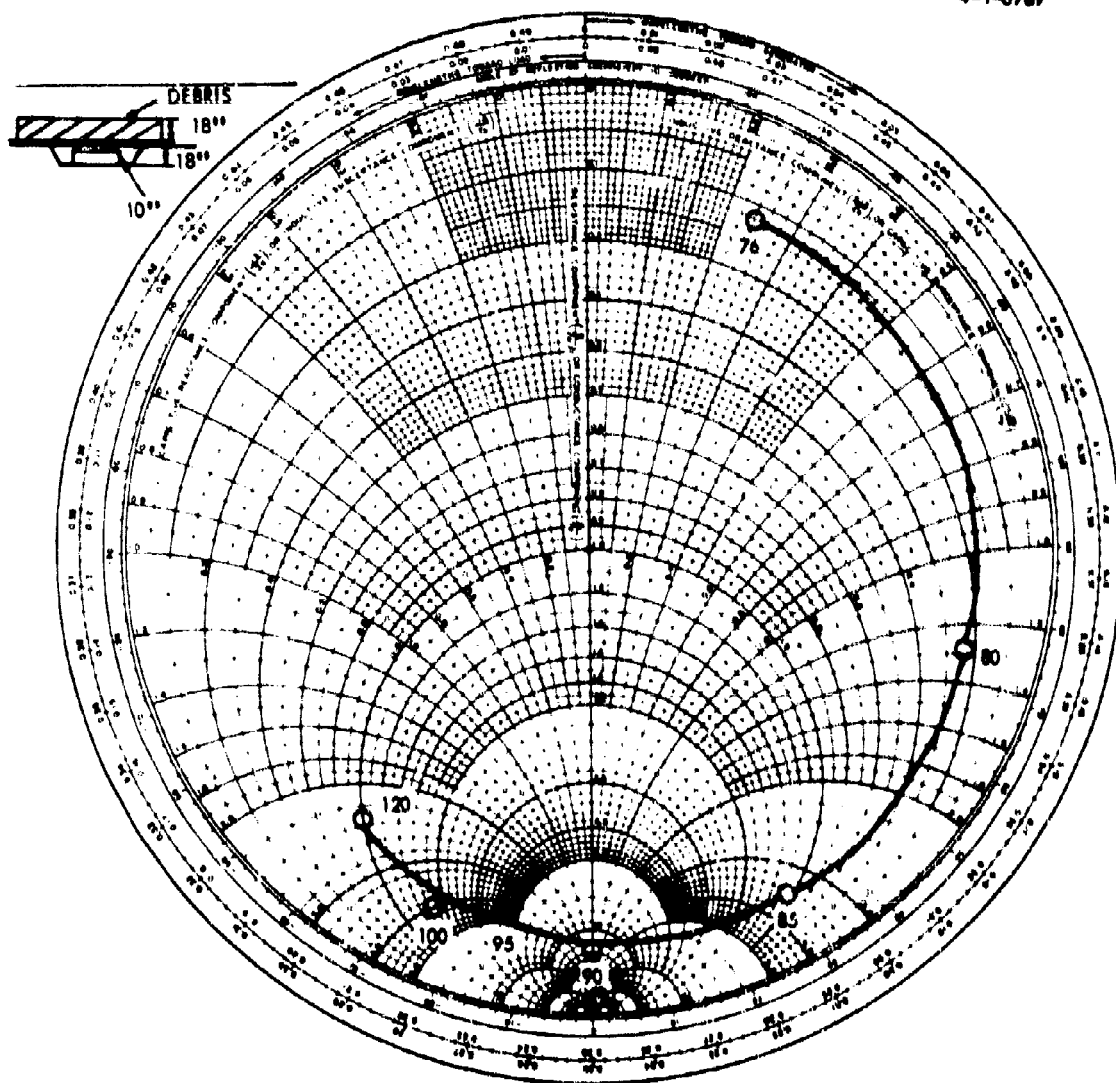


Figure 5-5. Smith Plot of Input Impedance vs Frequency.

It should be noted that the antiresonant frequency is determined by the resonance of the input terminal capacitance with the wire slot loop inductance, thus the above factor of 1.25 will depend upon the wire slot configuration. Approximate limits of this factor are 1.1 to 1.4.

- (d) Bandwidth of the Wire Slot Antenna - Without Debris  
For input VSWR  $\leq 1$  BW ~ 4 percent at 76 Mc. BW ~ 15 percent at 90 Mc which, as will be shown in the next section was approximately the center frequency of the optimum band of operation extending from 83 to 95 Mc. (i.e., where the wire slot exhibits maximum gain over a  $\lambda/4$  monopole.)
- (e) Bandwidth of the Wire Slot Antenna - With condition 12 full cover of debris. Under this condition, bandwidth and optimum band of operation are not significantly changed over the no debris case. Thus far

Input VSWR  $\leq 2:1$

BW ~ 4 percent at 76 Mc

BW ~ 15 percent at 90 Mc

Optimum Band of Operation ~ 85 to 95 Mc

### 5.6.3 Field Intensity Measurements

#### (a) Radiation Pattern

The azimuthal radiation pattern at a fixed elevation angle of  $18^\circ$  at 76 and 90 Mc together with a  $\lambda/4$  monopole (at 90 Mc) are shown in Figure 5-6. Patterns measured were as expected for this antenna. Averaging the measured field intensity in the broadside direction ( $\theta = 90^\circ$ ) between the azimuth angles  $70^\circ$  to  $135^\circ$ , the gain of the wire slot antenna compared to the monopole is as follows:

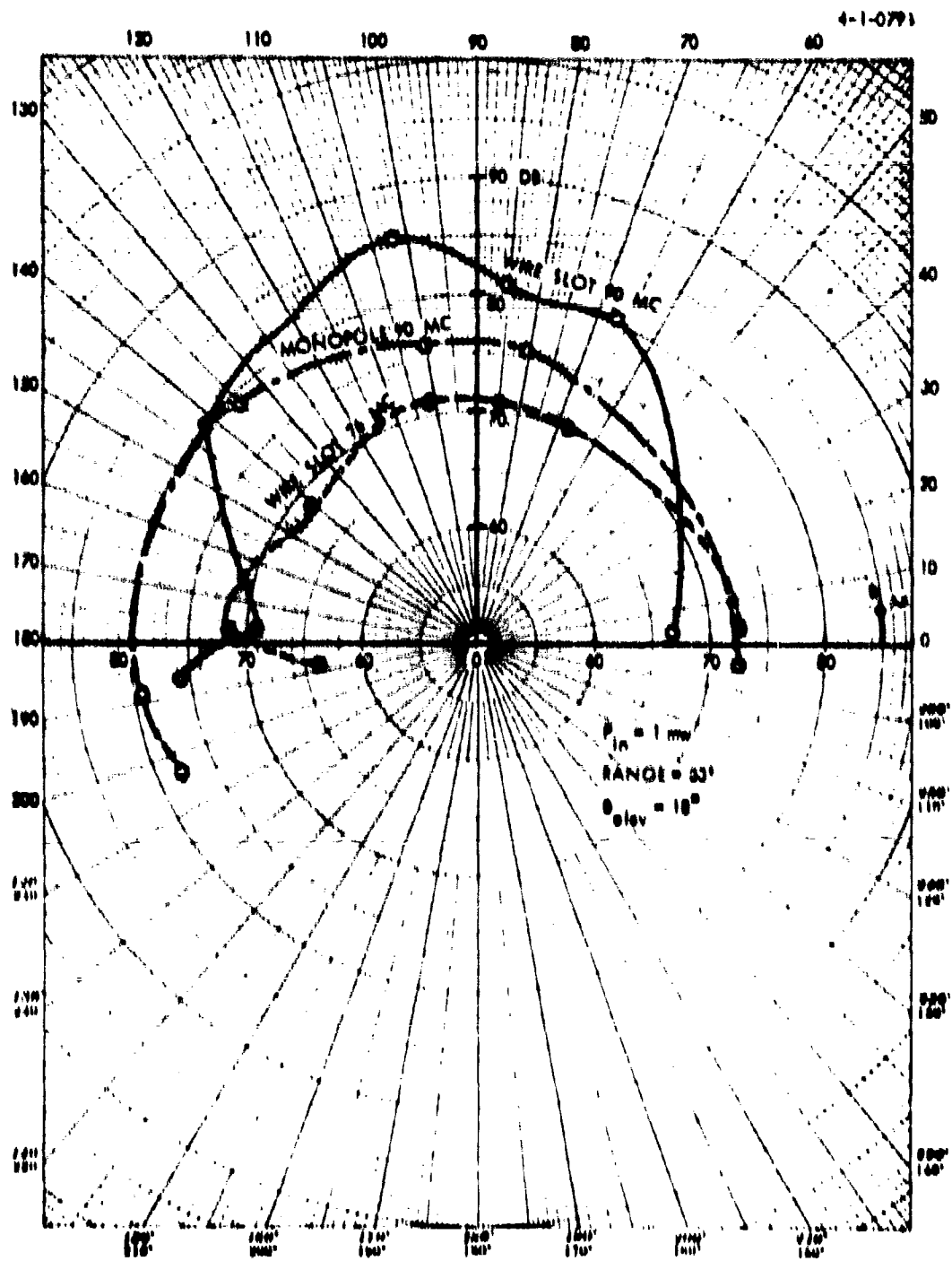


Figure 5-6. Field Patterns In Azimuth for Wire Slot at 76 and 90 Mc and Monopole at 90 Mc.

Average Field Intensity*			
Frequency	Mono	Wire Slot	Gain
76 Mc	77 db	70 db	-7 db
90 Mc	77 db	81.5 db	+4.5 db

(b) Field Intensity versus Frequency - With and Without Debris

The field intensity versus frequency at station 1, located approximately  $90^\circ$  (i.e., broadside) to the plane of the wire slot is shown in Figure 5-7. It is seen that the wire slot exhibits gain in this particular direction over a  $\lambda/4$  monopole from 80 to 115 Mc.

These values for field intensity are useful for determining the variations with frequency and the effects of debris on the wire slot antenna.

Under condition 1, the entire curve of field intensity versus frequency is shifted up in frequency and raised approximately 2 db over the no debris case. Under conditions 5 and 12 the field intensity is reduced in the order of 8 db at the antiresonance frequency and degraded approximately 2 db at the series resonance point. These results are summarized in the table below:

---

\* Monopole Field Intensity also averaged from  $\theta_{Az}$  of  $70^\circ$  to  $135^\circ$ .  
 $P_{in} = 1 \text{ mw}$   
 Range = 53 feet

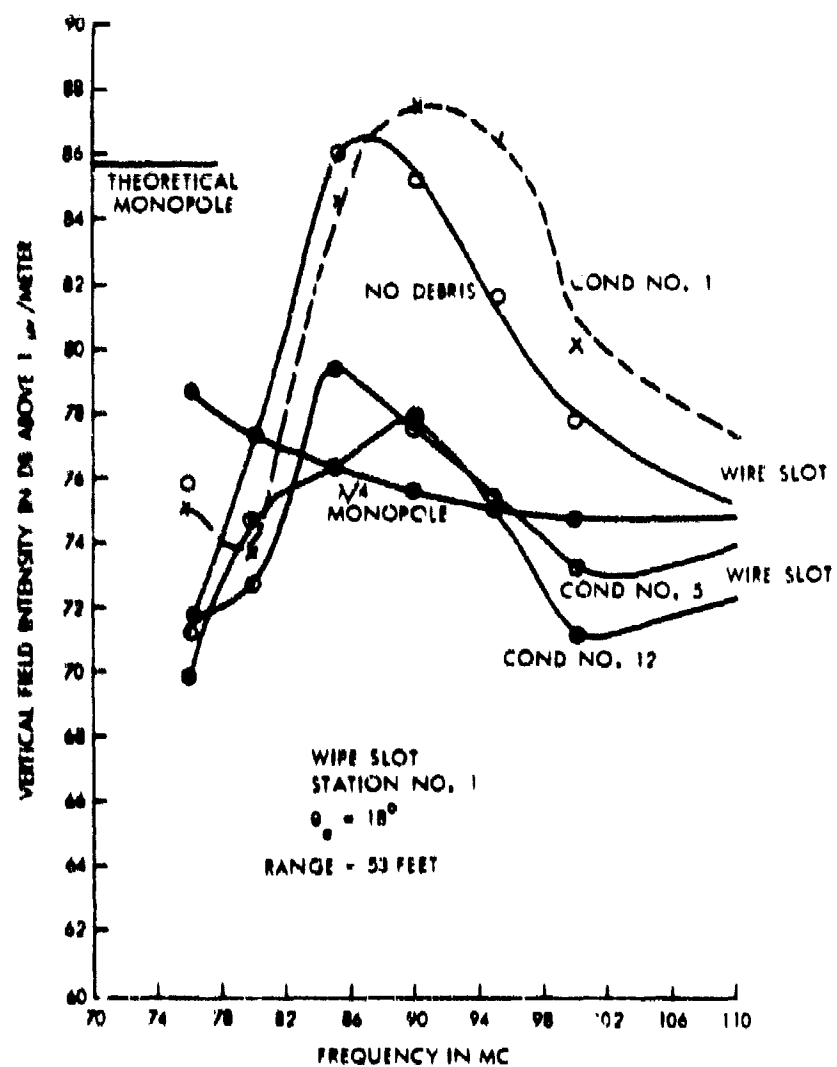


Figure 3-7. Field Intensity vs Frequency - - Monopole and Wire Slot with and without Debris.

Frequency Mc	Wire Slot* Field Intensity		Debris Degradation
	No Debris	Full Cover	
76	72 db	70 db	- 2 db
90	86 db	78 db	- 8 db
100	78 db	71 db	- 7 db

\* For  $P_{in} = 1 \text{ mw}$   
Range = 53 ft





## SECTION 6

### BURIED WIRE ANTENNA

#### 6.1 INTRODUCTION

At the low end of the HF band, in the frequency range from 2 Mc to about 6 Mc, the wavelength is long, so that large structures are required to obtain reasonable efficiencies. In addition there is the problem of high loss factor ( $\tan \delta \gg 1$ ) of debris which may cover the antennas, causing considerable degradation of efficiency. In order to reduce costs antenna structures have been developed which have a small volume, and which can be directly embedded in the ground to provide the necessary hardness. A linear wire antenna naturally uses up very little physical volume and has been used submerged in the earth.

The basic element of this type of antenna is an insulated wire which is buried in the ground parallel to the surface of the earth. The length of the wire can vary. The burial depth of the wire is determined by the hardening requirements.

The earth in which the antenna is placed is a lossy medium which causes considerable losses of the electromagnetic energy. A bare wire imbedded in the earth would have very high losses. The attenuation constant of a current flowing on the wire would be as large as that of the surrounding earth. An insulated wire provides an efficient way of reducing the attenuation on the wire and of establishing a linear current distribution in a lossy medium. Two types of current distribution can be distinguished. If such a wire is center-fed, and is insulated at the extremities, it will have a sinusoidal current distribution, provided its length is not too large. This is the standing wave type antenna. The traveling wave type antenna uses a traveling wave current distribution, which is obtained by terminating the wire in such a manner through a resistor, that no reflections take place at the ends. The fields immediately surrounding the antenna excite the interface ground-air immediately above the antenna and produce a field above and on the surface which then propagates in the upper half-space in air.

The theory of operation of the buried antenna deals with two major problem areas. The first category involves the propagation along the antenna wire, the second category involves the coupling of the energy of the buried antenna into the air-medium above. The following sections will deal with the theory and application of buried wire antennas, dividing the subject into the two categories of standing wave antennas and traveling wave antennas.

## 6.2 BURIED HORIZONTAL WIRE ANTENNAS WITH STANDING WAVE CURRENT DISTRIBUTION

This section deals with buried horizontal half-wave dipole antennas of various configurations. The dipoles are open ended so that a standing wave exists and the current along the antenna has a sinusoidal distribution.

The radiation pattern and efficiency of single dipoles and dipole arrays buried a few feet in the ground have been investigated. The arrays include the linear array, the Z-type array (both directional), the grid array and the circular array (both omnidirectional).

### 6.2.1 Impedance Properties of the Buried Dipole Antenna

The antenna wire can be treated like a coaxial cable when the surrounding earth represents the outer conductor. The axial propagation characteristics can be described by the propagation constant  $\Gamma = \alpha + j\beta$  along the wire, and the characteristic impedance  $Z_0$  of the insulated wire.  $\alpha$  is the attenuation constant. The phase constant

$$\beta = \frac{2\pi}{\lambda_c} = \left(\frac{2\pi}{\lambda_0}\right) \left(\frac{\lambda_0}{\lambda_c}\right) = k \frac{\lambda_0}{\lambda_c}$$

describes the wavelength  $\lambda_c$  on the wire, and  $k = 2\pi/\lambda_0$  describes the wavelength  $\lambda_0$  in air for a given frequency  $f$ .

$\alpha$  and  $\beta$  are a function of the wire diameter  $a$ , the insulation diameter  $b$ , the skin depth  $\delta$  of the earth surrounding the wire, the dielectric constant  $\epsilon_r$  of the wire insulation, and the burial depth  $h$ . Typical values of  $\alpha$  and  $\beta$ , together with other data, are tabulated in Table XVII for the frequency range 2-30 Mc, using the following data:

# CONDUCTING EARTH

Burial depth:  $h = 1 \text{ m}$

Conductor diameter:  $2a = 0.05 \text{ m}$

Insulation diameter:  $2b = 0.018 \text{ m}$  :  $b/a = 3.36$

Dielectric constant  
of insulation:  $\epsilon_r = 2.25$

Earth conductivity:  $\sigma = 0.01 \text{ mho/m}$

Earth dielectric constant:  $\epsilon_g = 6$

Loss tangent of earth:  $\tan \delta = p = p_0 / \epsilon_g$

$$= 60d\lambda_0 / \epsilon_g = \lambda_0 / 10$$

$$\text{Skin depth in earth: } = \frac{\lambda_0}{2\pi} \sqrt{\frac{1}{30d\lambda_0}} = \frac{\lambda_0}{2\pi} \sqrt{\frac{2}{p_0}}$$

TABLE XVII. SINGLE ELEMENT ALONE

$l_{mc}$	$\lambda_{om}$	$\lambda [m]$	$1/k = \lambda_o/\lambda_c$	$\lambda_c/2 [m]$	$a/l$	$R_{in} [dB]$
2	150	3.55	3.45	21.8	0.066	23.5
4	75	2.51	3.38	11.1	0.070	24.2
10	30	1.60	3.30	4.55	0.0705	24.0
20	15	1.12	3.18	2.35	0.071	23.4
30	10	0.92	3.12	1.61	0.070	22.4

The buried dipole has a length  $l = \lambda_c/2$ . The wire wavelength is determined by  $\beta/k = \lambda_o/\lambda_c$ . The table shows that the ratio of air wavelength to wire wavelength is approximately 3.3 and does not vary very much with frequency. Thus the wavelength on the cable is approximately 1/3 of the wavelength in air. The column  $\lambda_c/2$  gives the length of the half-wave dipole, which is the basic antenna element.

$\alpha/\beta = \alpha(\lambda_c/2\pi)$  indicates the attenuation over  $(\lambda_c/2\pi)$  of wire length. This quantity also does not vary much with frequency and is approximately 0.07. The attenuation on the wire is low due to the insulation of the wire from the ground. If the wire were directly imbedded in the earth the  $\alpha/\beta$  ratio would be approximately 1, just as it is in the earth.

The input impedance at the feed point in the center of the wire is purely resistive, if the wire length is made approximately  $\lambda_c/2$ .  $R_{in}$  is approximately 23  $\Omega$  and does not vary much with frequency, if the length is made  $\lambda_c/2$  for each frequency. On the other hand, the input impedance of the dipole behaves quite similarly to that of a dipole in air if the frequency is changed and the length is kept constant. Both resistance and reactance vary widely, as long as not more than one or two wavelengths are on the wire. The fluctuations of impedance decrease as the frequency is increased and the wire is 2 - 3 wavelengths long and more. This provides a possibility to make the antenna broadbanded.

The data in Table XVII pertains to a single dipole buried in the ground. These data change if the dipole is used in an array, due to mutual coupling of elements. The mutual coupling is detrimental to the antenna efficiency since it increases the input impedance of each element. However, the mutual coupling decreases rapidly with increased spacing between wires and becomes negligible for spacing between elements of more than 3 skin depths. On the other hand mutual coupling becomes significant as the spacing becomes less than one skin depth. A good approximation of the mutual coupling effects for a large loosely coupled array is obtained by considering each element as if it were in an infinite array of uniformly spaced elements, which are fed with

TABLE XVIII. SINGLE ELEMENT IN ARRAY

$f_{mc}$	$\lambda_{om}$	$\delta[m]$	$\beta/k = \lambda_o/\lambda_c$	$\lambda_c/2[m]$	$(\alpha/\beta) \infty$	$R_{in}[\Omega] \infty$
2	150	3.55	3.45	21.8	0.10	35.6
4	75	2.51	3.38	11.1	0.10	35.6
10	30	1.60	3.30	4.55	0.09	30.8
20	15	1.12	3.18	2.35	0.085	27.8
30	10	0.92	3.12	1.61	0.081	26.0

equal currents. Table XVIII shows the data of one element in an infinite array. Only  $\alpha$  and  $R_{in}$  are different from the values obtained for a single element alone. The change of  $\beta$  and therefore of  $\lambda_c$  (wavelength on the wire) is small under the stated conditions.

### 6.2.2 Radiation Characteristics and Efficiency of Single Element

The coupling of the RF energy from the buried antenna into the upper half-space is accomplished by the near zone field of the buried dipole. This field at the interface produces a field in the lossless air half-space which is quite similar to the field produced by a horizontal dipole at the interface air-ground, the only difference being an exponential term  $e^{-\gamma_1 h}$  which multiplies the field of the buried dipole and causes an exponential decay with burial depth  $h$ . (The radiation field of a horizontal dipole over a lossy half-space according to K.A. Norton<sup>16</sup> is as follows.

The far zone fields of a horizontal dipole at the interface as well as those of a buried horizontal dipole have horizontally and vertically polarized components. Using a cylindrical coordinate system  $(\rho, \phi, z)$  with the origin at the interface, the  $+z$  axis vertical pointing upward, and the  $\phi$ -coordinate measured from the dipole axis, the three components of the far zone field are as follows:

$$E_{+z} \sim C \cos \phi \frac{\sqrt{n^2 - 1}}{n^2} \quad n = \text{refractive index}$$

$$E_{\rho} \sim C \cos \phi \cdot \frac{1}{n^2} \quad \frac{E_{\rho}}{E_{+z}} = \frac{1}{\sqrt{n^2 - 1}}$$

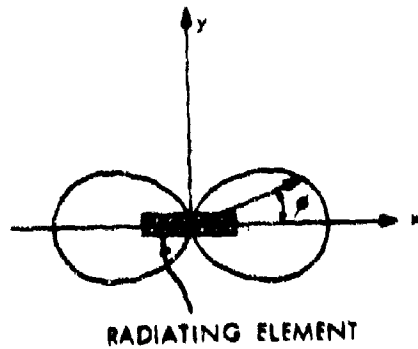
$E_{\phi}$  is negligible

In the direction of the dipole axis ( $\phi = 0$ ) both  $E_{+z}$  and  $E_{\rho}$  are maximum, in the direction perpendicular to the dipole ( $\phi = \pi/2$ ) both components are zero, (see Figure 6-1). The azimuthal pattern on the ground plane is given by the  $\cos \phi$  function, i.e., it is figure 00 shaped

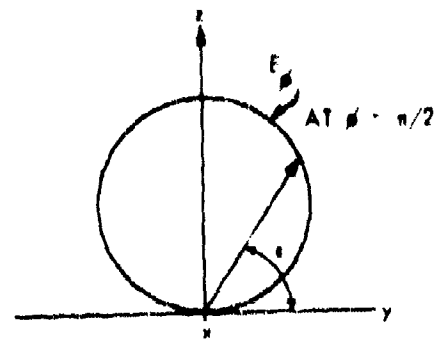
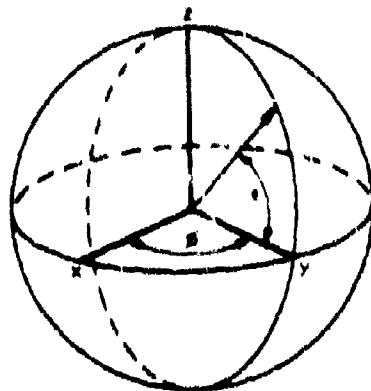
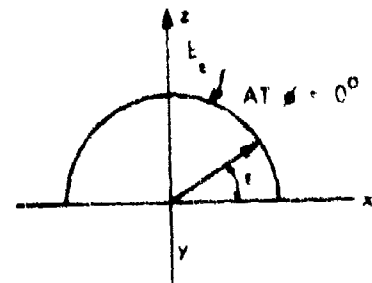


4-1-0582

AZIMUTH PATTERN (HORIZONTAL)



ELEVATION PATTERN (VERTICAL)



NOTE:  $E_v$  IS VERTICALLY POLARIZED COMPONENT OF FAR FIELD  
 $E_h$  IS HORIZONTALLY POLARIZED COMPONENT OF FAR FIELD

Figure 6-1. Radiation Pattern for a Single Buried Horizontal Dipole.

with the maximum in the direction of the dipole axis. Since the  $E_\theta$  component on the ground is small the field on the ground is vertically polarized. Above the ground the  $E_\theta$  is no longer negligible and the field therefore has a horizontal component. This becomes apparent from an inspection of the elevation pattern. In the vertical plane ( $\phi = 0$ ) the elevation pattern is semi-circular. There is no appreciable  $E_\theta$  component in the  $\phi = 0$  plane, and the field is therefore polarized in this plane; i.e., vertically polarized. In the vertical plane perpendicular to the dipole axis ( $\phi = \pi/2$ ) there is only an  $E_\theta$  component indicating horizontal polarization.  $E_\theta$  in this plane varies with  $\sin \theta$  of the elevation angle and is zero on the ground and maximum in the vertical direction. The pattern has circular shape as shown in Figure 6-1, and the field is horizontally polarized in this plane.

Comparing the radiation pattern as described with that of a small vertical loop antenna one readily sees that both are identical. The earth currents flowing from one side of the dipole to the opposite side together with the current on the antenna wire give this effect. The directivity gain of the horizontal buried dipole is therefore 1.75 db with respect to an isotropic radiator over perfect ground radiating into a hemisphere, and 4.75 db with respect to an isotropic radiator in free space which radiates into the full sphere.

It is interesting to compare the far-zone field of a horizontal dipole at the interface ground-air with the far-zone field of a short vertical dipole at the interface. The radiation pattern is shown in Figure 6-2. This dipole produces on the ground a vertical field component

$$\sqrt{E_{+z}} = C$$

and a radial field component

$$\sqrt{E_r} = \frac{\sqrt{n^2 - 1}}{n^2} (\sqrt{E_{+z}}) = \frac{\sqrt{n^2 - 1}}{n^2} C$$

The ratio of the field components is determined by the refractive index  $n$  between ground and air:

4-1-C583

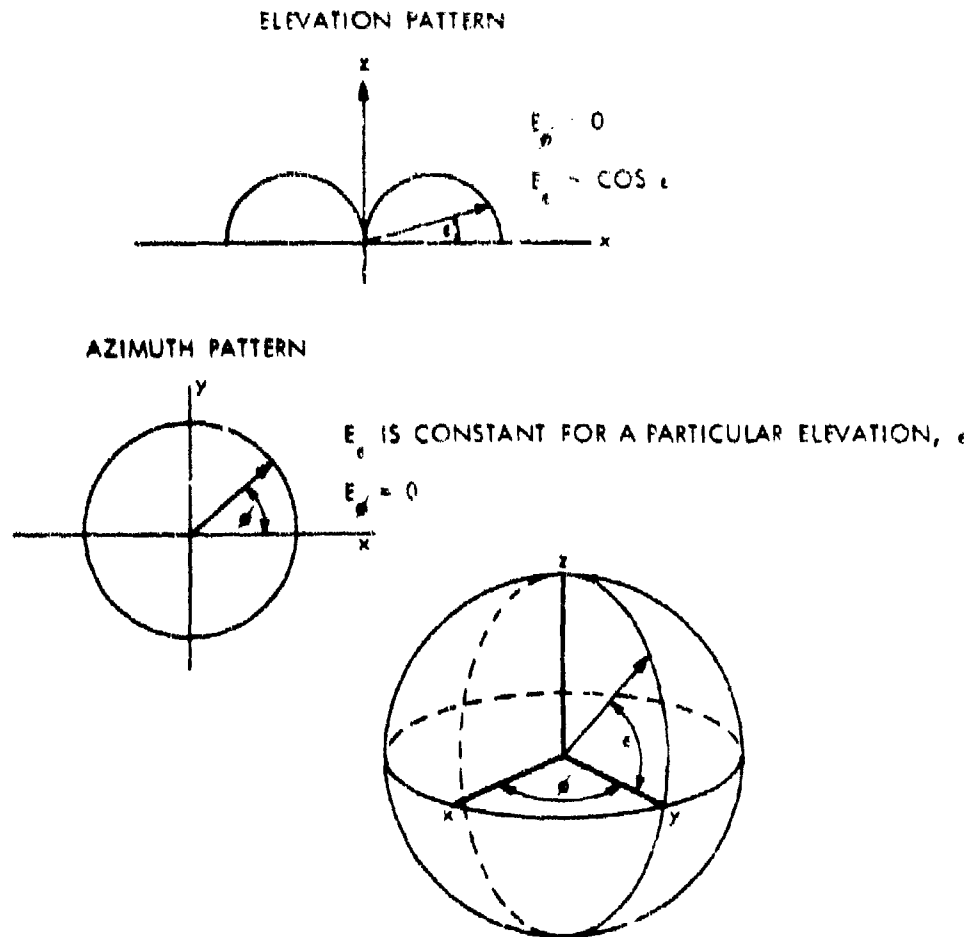


Figure 6-2. Radiation Pattern of a Short Vertical Monopole Over Perfect Ground.

$$\frac{vE_r}{vE_z} = \frac{\sqrt{n^2 - 1}}{n^2}$$

The field below the interface has also two components. The radial component, being parallel to the interface, is the same as above the surface. The vertical component

$$vE_{-z} = \frac{vE_r}{\sqrt{n^2 - 1}}$$

$$\frac{vE_r}{vE_{-z}} = \sqrt{n^2 - 1}$$

and

$$\frac{vE_{+z}}{vE_{-z}} = n^2.$$

Comparing the radial component of the vertical dipole ( $vE_r$ ) and the z-component of the horizontal dipole ( $H_{+z}$ ) shows that

$$H_{+z} = vE_r \cos \phi = \frac{\sqrt{n^2 - 1}}{n^2} vE_{+z} \cos \phi$$

$$H_{+r} = H_{+z} \frac{1}{\sqrt{n^2 - 1}} = \frac{vE_r \cos \phi}{\sqrt{n^2 - 1}} = vE_{-z} \cos \phi$$

and

$$H_{-z} = \frac{1}{n^2} H_{+z} = \frac{vE_r \cos \phi}{n^2}.$$

The result is that the vertical field component ( $H_{+z}$ ) of the horizontal dipole is equal in strength to the radial component ( $vE_r$ ) of the vertical

dipole times  $\cos \phi$ . But this radial component of the vertical dipole is less than the vertical component ( $\sqrt{E_z}$ ) of the vertical dipole by the factor  $\sqrt{n^2 - 1/n^2}$  since  $|n^2| > 1$ . The refraction term  $\sqrt{n^2 - 1/n^2}$  is a result of the boundary conditions at the interface. If  $n^2$  is very large, as is the case for low frequencies and high soil conductivities, then the field of the horizontal dipole is greatly reduced compared with the field of the vertical dipole. On the other hand, at high frequencies  $n^2 \sim \epsilon_g$  ( $\epsilon_g$  dielectric constant of the ground) and the refraction term is

$$\frac{\sqrt{\epsilon_g - 1}}{\epsilon_g} \sim \frac{\sqrt{5 - 1}}{5} = \frac{2}{5} \quad \text{for } \epsilon_g = 5$$

Summarizing the preceding considerations the following result is obtained:

For all practical purposes the ground wave field from a buried horizontal dipole is obtained from the ground wave field of a vertical dipole above the interface by multiplying the field components of the vertical dipole with the pattern factor  $\cos \phi$  and the depth factor  $e^{-\delta h}$  (due to the burial depth), and applying the refraction term  $\sqrt{n^2 - 1/n^2}$  to the vertical component.

The refractive index  $n$  is the ratio of the propagation constants of the ground and air

$$n^2 = \frac{\gamma_1^2}{\gamma_0^2} = \epsilon_g - j \sigma / \omega \epsilon_0 = \epsilon_g (1 - jp)$$

$p = \tan \delta$  is the loss tangent of the soil in which the antenna is imbedded.

$$p = \frac{\sigma}{\omega \epsilon_0 \epsilon_g} = \frac{60 \sigma \lambda_0}{\epsilon_g}$$

The skin depth  $\delta$ , which determines the attenuation due to burial depth  $h$  of the dipole, is given by

$$\delta = \frac{\lambda_0}{2\pi} \sqrt{\frac{1}{30\sigma\lambda_0}} = \frac{\lambda}{2\pi} \sqrt{\frac{2}{p}}$$

The refraction term  $|\sqrt{n^2 - 1}|/|n^2|$  and the loss through burial (in db) for a burial depth of 1 m are listed in Table XIX for the frequency range 2 - 30 Mc, using  $\sigma = 0.01$  mho/m and  $\epsilon_g = 6$ . The square of these quantities are given in db since this determines the launch efficiency of the antenna. Adding the refraction loss and the exponential loss through burial gives the total loss. This is the minimum loss of the buried dipole. The actual loss will always be somewhat larger than this minimum loss due to small ground losses in the immediate vicinity of the insulated antenna wire. This will be discussed in the following section.

The total minimum loss depends on the frequency, the soil constants, and the burial depth. At a certain frequency there will be a minimum loss as can be seen from the table. This is around 20 Mc for 1 foot burial depth and amounts to approximately -13 db, and it occurs between 15 and 20 Mc for a burial depth of 1 m, amounting to approximately -18 db. These numbers represent the absolute minimum loss which one buried dipole can have under the given conditions (soil  $\sigma = 0.01$  mho/m,  $\epsilon_g = 6$ ). Clearly this is a very low efficiency. But one has to consider that this antenna is extremely simple since it is only one insulated wire of comparatively short length. Also the efficiency can be increased by arraying a number of these dipoles as well be discussed in the following section.

### 6.2.3 Buried Dipole Efficiency

The launch efficiency of the horizontal buried dipole antenna is conveniently defined by comparing the ground wave field of this antenna with that of an ideal short vertical monopole above the interface. The vertical monopole is chosen as comparison antenna because its

TABLE XIX  
REFRACTIVE BURIAL LOSSES

$f_{mc}$	$n^2$	$20 \log \frac{\sqrt{n^2 - 1}}{ n^2 }$	Burial Loss		Refractive and Burial Loss	
			$h=1 \text{ ft}$	$h=1 \text{ m}$	$h=1 \text{ ft}$	$h=1 \text{ m}$
2	$6(1 - j15)$	-19.5db	-0.75db	-2.4db	-20.3db	-21.9db
4	$6(1 - j7.5)$	-16.6	-1.1	-3.5	-17.7	-20.1
10	$6(1 - j3)$	-12.9	-1.7	-5.4	-14.6	-18.3
20	$6(1 - j2)$	-10.5	-2.4	-7.7	-12.9	-18.2
30	$6(1 - j1)$	-10.4	-2.9	-9.4	-13.3	-19.8

radiation characteristics are similar to the horizontal buried monopole, and also the polarization is vertical on the ground for both antennas. The vertical fields of the buried antenna and the vertical monopole above the earth are compared when the antennas are fed with the same power. This defines the launching efficiency of the buried antenna as

$$\eta = \left| \frac{E_{zh}}{E_{zv}} \right|^2$$

The ideal vertical monopole of short length  $l$ , with triangular current distribution, has an input resistance equal to its radiation resistance of  $40\pi^2 (l/\lambda)^2$ . The ground wave field of such a monopole is

$$E_{zv} \cdot D \approx 3\pi \sqrt{P} \cdot F$$

where  $P$  is the input power in watts and  $F$  the ground wave attenuation factor. Using this the launch efficiency of the buried horizontal dipole is

$$\eta = \left( \frac{20}{\pi} \right)^2 \left| \frac{\sqrt{n^2 - 1}}{n^2} \right|^2 \frac{|f(\phi)|^2}{R_{in}} e^{-2h/\lambda}$$

$$f(\phi) = \frac{k \cos \phi}{I_0} \int_{-l/2}^{l/2} I(x) e^{ikx \cos \phi} dx$$

$f(\phi)$  is the pattern-length factor

$h$  is the burial depth

$I_0$  is the antenna base current

$l$  is the length of the buried dipole



$R_{in}$  is the input resistance of the buried dipole

$I(x)$  is the current distribution of the dipole antenna

$\frac{\sqrt{n^2 - 1}}{n^2}$  is the refraction term, as discussed in the previous section

The refraction term and the exponential term are the main contributors to the efficiency. In addition one has the  $|f(\phi)|^2/R_{in}$  term which depends on the antenna length.  $R_{in}$  for a single element alone is different from  $R_{in}$  of one element in an array. In the latter case  $R_{in}$  is larger, due to mutual coupling between elements. However, the increase is small if the elements are more than 1-1/2 skin depth spaced. In Table XX and Table XXI the efficiencies for a single element alone, and a single element in an array respectively are listed. The efficiency of an n-element array is obtained by multiplying the element-in-array efficiency with the number of elements:

$$\eta_{array} = \eta_{1 \text{ array}} \times n$$

In the tables, also,  $\eta_{10}$  is listed.  $\eta_{10}$  is the efficiency of the element due to all effects except the exponential term  $e^{-2h/\delta}$ . The overall efficiency is

$$\eta_1 = \eta_{10} \times e^{-2h/\delta}$$

and for the array

$$\eta_{1 \text{ array}} = \eta_{10 \text{ array}} \times e^{-2h/\delta}$$

The efficiency of the buried dipole is the gain (in this case the gain is negative and therefore represent a loss) compared to an ideal monopole or small vertical loop over perfect ground. Since the latter



TABLE XX . EFFICIENCY OF SINGLE ELEMENT ALONE

$f_{mc}$	$\frac{A}{\lambda_0}$	$\eta_{10}$	Burial Loss $h = 1 \text{ m}$	Overall Eff. $\eta_1$
2	0.145	-22.3 db	-2.4 db	-24.7 db
4	0.148	-19.2	-3.5	-22.7
10	0.152	-15.4	-5.4	-20.8
20	0.157	-12.7	-7.7	-20.4
30	0.160	-12.2	-9.4	-21.6

TABLE XXI. EFFICIENCY OF SINGLE ELEMENT IN ARRAY

$\epsilon_{mc}$	$\epsilon/\lambda_0$	$\eta_{10}$ array	Burial Loss $h = 1$ m	Overall Eff. $\eta_1$ array
2	0.145	-24.1 db	-2.4 db	-26.5 db
4	0.148	-20.9	-3.3	-24.4
10	0.152	-16.4	-5.4	-21.8
20	0.157	-13.3	-7.7	-21.0
30	0.160	-12.9	-9.4	-22.3

has a gain of  $3 + 1.75 = 4.75$  db over an isotropic radiator in free space (radiating into the full sphere) the gain (or loss) with respect to this isotropic radiator is

$$g_{db} = \gamma_{db} + 4.75 \text{ db}$$

#### 6.2.4 Buried Dipole Array

In order to improve the efficiency, and also to change the radiation pattern, an array of dipoles can be used. The simplest arrangement to improve the efficiency is an array of closely spaced identical parallel dipole elements. In the lossy ground the mutual coupling between parallel array elements is negligible if the distance between them is larger than 2-3 skin depths. As long as the array width is not greater than about  $1/4$  air wavelength, the radiated pattern in air is essentially that of a single element. For  $n$  identical elements with negligible coupling, therefore, the gain due to arraying is directly proportional to  $n$ . The essential thing is that, in the case of negligible coupling, the input resistance of each element in the array is the same as it is for the element alone. Therefore, if  $n$  elements are fed in parallel the input power to each element will be  $1/n \cdot P_T$  ( $P_T$  = total input power to  $n$  elements). The current in one element  $I_1$  is then  $I_1 = \sqrt{P/nR_{in}}$ . The total radiated field is proportional to  $nI_1 = \sqrt{Pn/R_{in}}$  and the radiated power is proportional to  $\sqrt{Pn/R_{in}}$  or  $n$  times larger than the radiated power of one element for the same input power.

As the array width increases when many elements are used, the radiation pattern will change and the realized pattern gain will be somewhat less than  $n$ .

As an example consider an array of 27 elements arranged in 3 rows of 9 elements each, as shown in Figure 6-3. For a frequency of 10 Mc, an element spacing of  $2\lambda = 3$  m, and a burial depth of 1 m, the element length would be 4.55 m, and the total area  $20 \times 24$  m. The array would

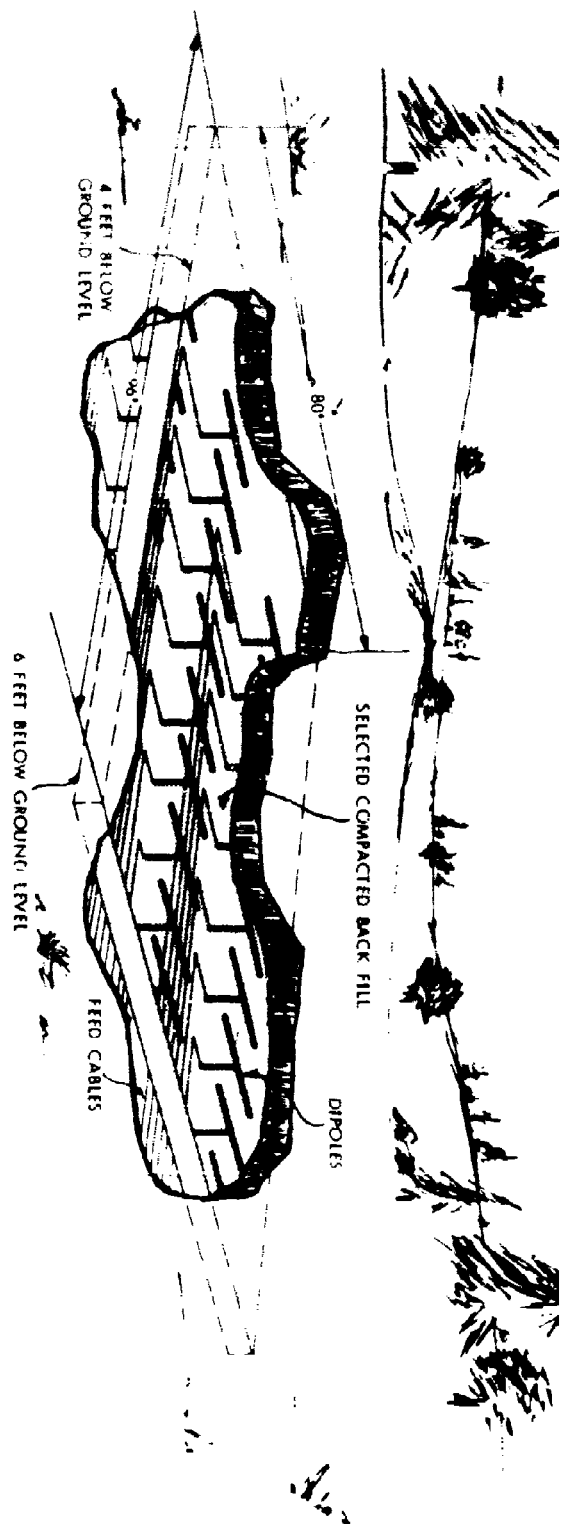


Figure 6-3. Buried Horizontal Dipoles - Rectangular Array.

have a gain of approximately  $-21.8 + 10 \log 27 = -21.8 + 14.3 = 7.5$  db compared to a vertical monopole, or  $-7.5 + 4.75 = -2.8$  db with respect to an isotropic radiator. The efficiency can be increased by decreasing the burial depth. Decreasing the burial depth to  $1/2$  m would decrease the burial loss by about 2.7 db, so that the gain with respect to the isotropic radiator would be approximately 0 db.

The radiation pattern of this array is that of a single buried element; i.e., it is figure  $\infty$  shaped on the ground.

To reduce the number of feed cables, the array shown in Figure 6-4 can be used. Three elements are connected in series and arranged in Z shape. Only the middle element of each Z is connected to a feed cable. Thus the number of feed cables is reduced to  $1/3$ .

A unidirectional pattern can be obtained by placing a second array at a distance of  $1/4$  air wavelength behind the first array and feeding it with a current which is  $90^\circ$  shifted in phase with respect to the first array. This gives a slight increase in directive gain since the back radiation is eliminated.

Generally speaking all the arraying techniques of linear antennas in air can be applied. Instead of combining single elements into an array, it is preferable to combine groups or elements into arrays. It is necessary to space the groups at distances of  $\lambda_0/4$  to  $\lambda_0/2$  of the air wavelength to obtain radiation pattern changes. This is so because each antenna element excites the ground vertically above it, so the phase differences between these secondary ground sources is equal to the phase differences in the element currents. The pattern in space is now generated by the superposition of the ground sources according to their space phase shifts which are proportional to  $d/\lambda_0$ . The air wavelength is, however, much larger than the wavelength on the antenna wire. Therefore,

$$\frac{d}{\lambda_0} = \frac{d}{\lambda_c} \frac{\lambda_c}{\lambda_0} = \frac{d}{\lambda_c} \cdot \frac{f_0}{f} \quad \text{where } \frac{\lambda_c}{\lambda_0} \approx \frac{1}{3}$$

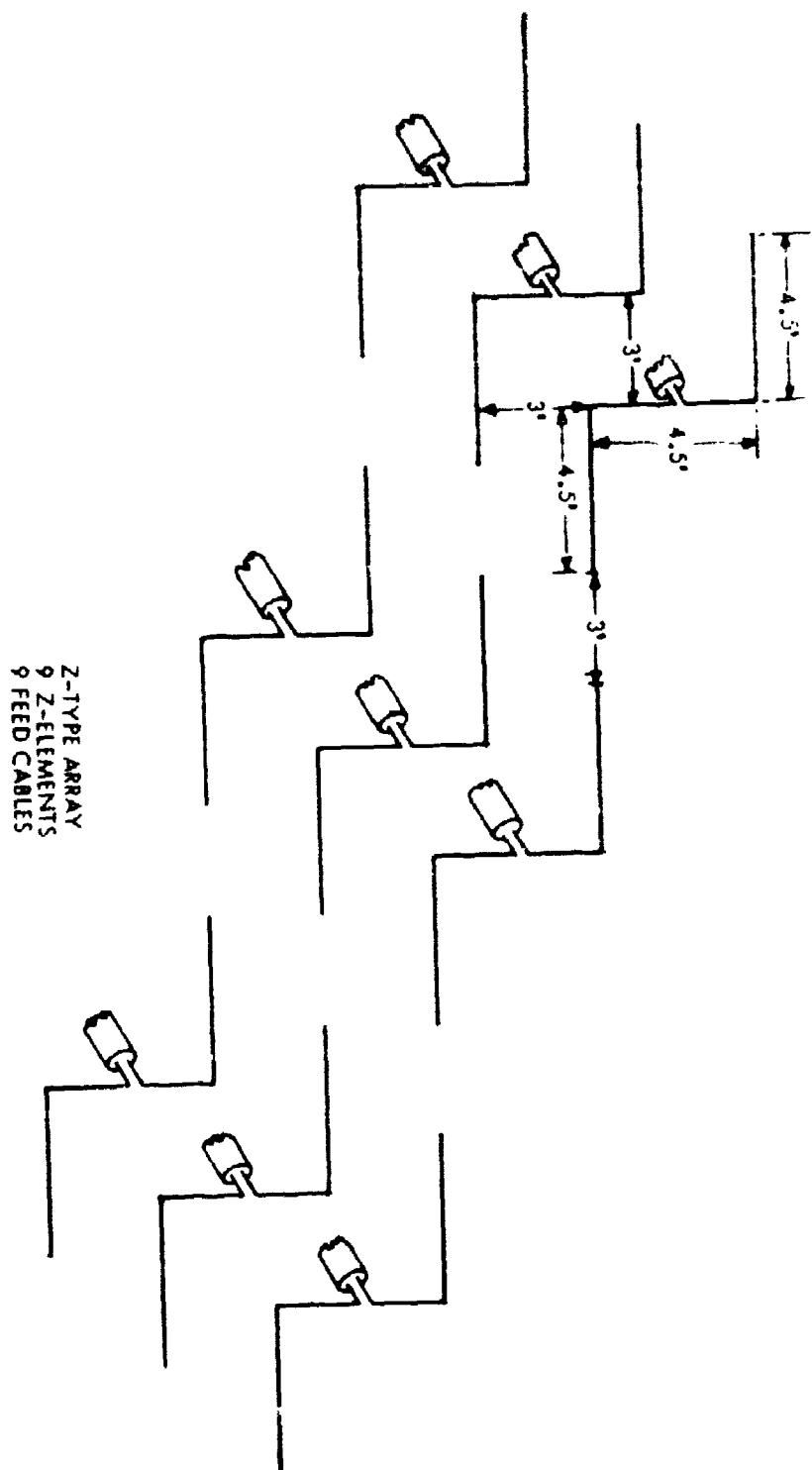


Figure 6-4. Buried Horizontal Dipoles - Z-type Array.



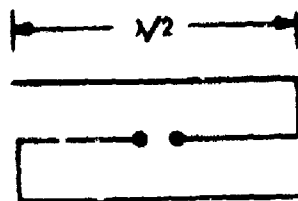
### 6.2.5 Omnidirectional Patterns

To obtain an omnidirectional pattern one can use two elements, or two groups of elements, positioned at right angles and fed with quadrature currents. This is shown in Figure 6-5b using two folded dipoles. The feed arrangement producing the  $90^\circ$  phase shift with a quarter wave line is indicated in Figure 6-5c. For equal currents in both parts the azimuthal pattern is circular and the elevation pattern is semicircular. This is then an isotropic radiator radiating equally strong in all directions of the upper hemisphere. If a total of  $2n$  elements are used,  $n$  elements in each group, then each group has  $1/2$  of the total input power and its gain is  $n/2$ . The total gain of the antenna with  $2n$  elements is therefore  $n$ ; i.e., equal to the element number of one group. This means a loss of 3 db in gain.

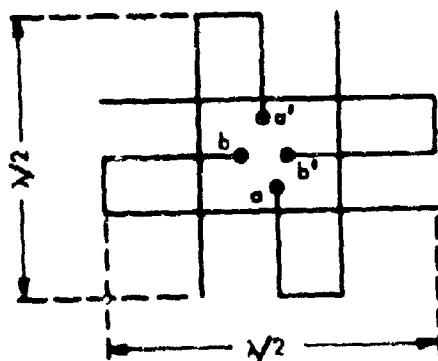
Another, more efficient arrangement is a circular array with dipole elements arranged in a radial position on a circle of about  $1/2$  air wavelength diameter or larger, as shown in Figure 6-6. The elements are fed so that the currents in all elements at a certain moment flows in the direction away from the center of the circle. Then the currents in opposite elements (such as A and B) flow in opposite directions and therefore have a space phase shift of  $180^\circ$ . If the diameter of the circle is one half air wavelength then the fields of the two elements add on the ground surface, but cancel in the vertical direction to the plane. This type of array is a circular array with all element currents in phase. The radiation pattern is given by

$$E \sim J_1(kr \cos \epsilon)$$

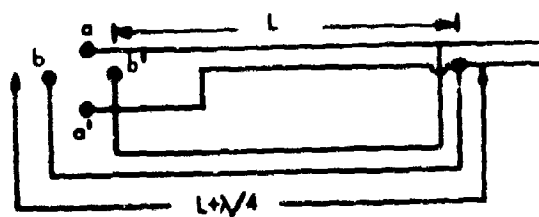
where  $\epsilon$  is the elevation angle,  $k = 2\pi/\lambda$ , and  $J_1$  is the Bessel function of the first order. The pattern is omnidirectional in azimuth. The polarization is vertical. The vertical radiation pattern is determined by  $J_1$ , and varies as the radius  $r$  of the circle is changed. If  $kr = 2\pi r/\lambda_0 = 1.84$ ;  $2r = 1.84 \lambda_0/\pi = 0.585 \lambda_0$ , according to the first maximum of  $J_1$ , then maximum radiation is along the ground plane (for  $\epsilon = 0^\circ$ ). The pattern is shown in Figure 6-7. If  $kr = 2\pi r/\lambda_0 = 3.83$ ;  $2r = 3.83 \lambda_0/\pi = 1.22 \lambda_0$ , according to the first root of  $J_1$ , then there is no radiation along the ground and the maximum radiation occurs at an elevation angle of  $61^\circ$ , as shown in Figure 6-7 (right side).



a. FOLDED DIPOLE - DIRECTIONAL



b. CROSS FOLDED DIPOLE PAIR - OMNIDIRECTIONAL



c. FEED FOR CROSSED PAIR

Figure 6-5. Feed Arrangements for Omnidirectional Pattern.

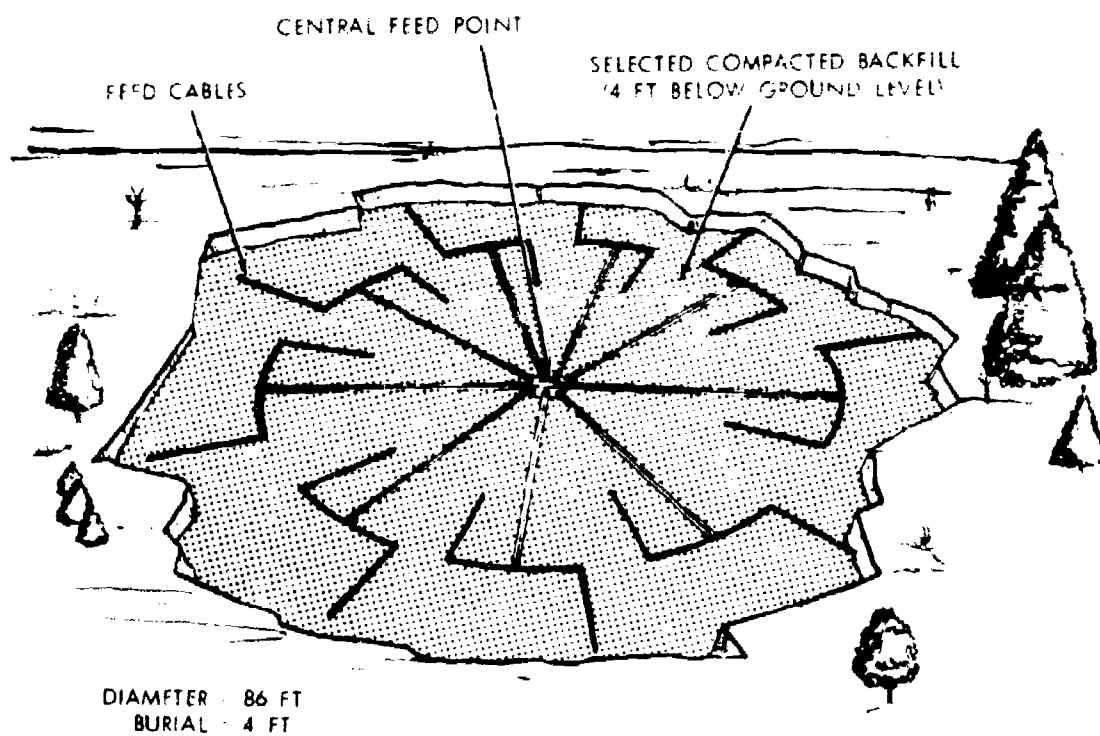


Figure 6-6. Buried Horizontal Dipoles - Circular Array.

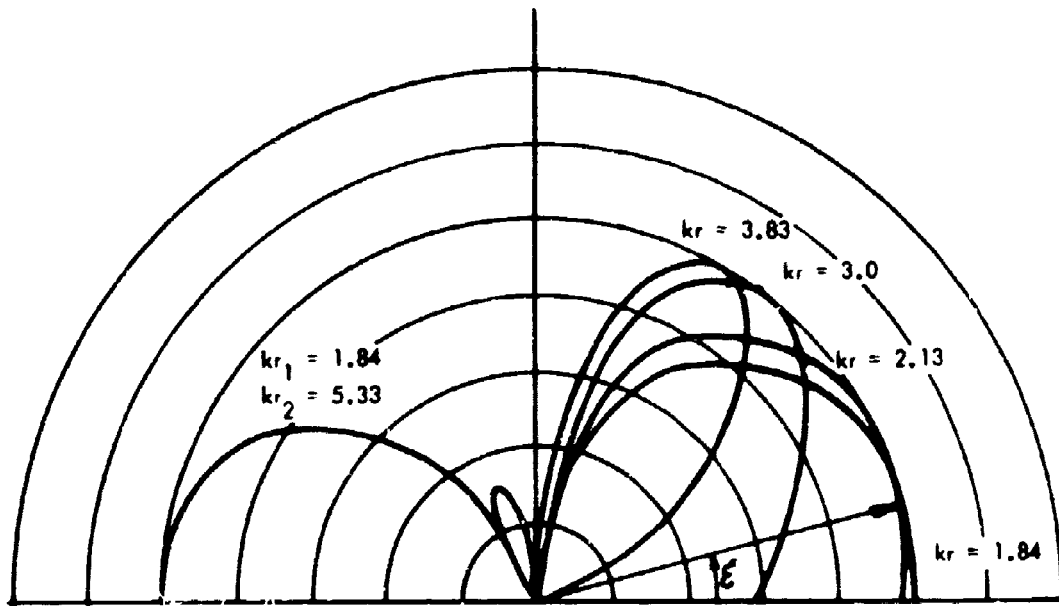


Figure 6-7. Radiation Pattern for Circular Array.

A maximum at  $30^\circ$  elevation can be obtained by choosing  $2\pi r/\lambda_0 = 2.13$ ,  
 $2r = 2.13 \lambda_0/\pi = 0.675 \lambda_0$ .

An advantage of this circular array is that the radiation in the vertical direction is always suppressed. This elimination of the vertical radiation, which is lost energy, results in an increase of directive gain in the vertical plane in the order of 2 db compared with an isotropic radiator.

The field strength in the direction of maximum radiation is  $0.582 \times n \times E_0$  where  $E_0$  is the field produced by a single element with the same current. The total radiated power is  $0.582 n \cdot P_0$ , where  $P_0$  is the power radiated by one element. But this total power is radiated into a smaller space angle which yields a gain of 2 db as mentioned above. The total power gain is therefore

$$g_T = 10 \log (0.582 \times n) + 2 \text{ db}$$

$$= 10 \log n - 2.4 + 1.9 = 10 \log n - 0.5 \text{ db}$$

The reason that the total radiated power is  $0.582 \times n P_0$  instead of  $n \times P_0$  is that not all elements contribute equally to the field in a particular direction. The elements which are perpendicular to that direction do not contribute at all in this direction. As an example design data for a circular array for a frequency of 10 Mc are given. The same number of elements ( $n = 27$ ) is chosen as was used for the grid array before, so that the designs can easily be compared. For a frequency of 10 Mc the element length is 4.55 m. The diameter of the circle is chosen as  $2r = 2.13\lambda_0/\pi = 2.13 \times 30/\pi = 20.5$  m for a frequency of 10 Mc (wavelength 30 m). In order to provide sufficient spacing for the 27 elements a Z-type arrangement of the elements is chosen as shown in Figure 6-4. Three elements are connected in series, and the middle element is fed by a feed cable. Thus 9 Z-groups are obtained which are placed on the periphery of a circle of 20.5 m diameter, allowing a spacing of  $2\pi/9 = 20.5 \times \pi/9 = 7.15$  m between groups. The gain is calculated as

$$g = -21.8 + 10 \log 27 - 0.5 = -7.5 - 0.5 = -8 \text{ db}$$

compared to a vertical monopole or -3.25 db with respect to an isotropic radiator.

The maximum number of elements that can be used on the circle is determined by the minimum allowable spacing between elements, this being about  $1.5 \delta$  ( $\delta$  = skin depth).

Thus  $n = 2\pi r / 1.5 \delta \sim 2D/\delta$ . With  $D = 0.675 \lambda_0$  we have

$$n = \frac{\pi}{1.5 \delta} \times 0.675 \lambda_0 = \frac{1.4 \lambda_0}{\delta} = 4.85 \sqrt{\lambda_0}$$

for  $\sigma = 0.01 \text{ mho/m}$  since  $\delta = \lambda_0 / 2\pi \sqrt{1/30 \sigma \lambda_0}$ .

At high frequencies  $n$  is not very large. If  $f = 30 \text{ Mc}$ ,  $\lambda_0 = 10\text{m}$ ,  $\delta = 0.92 \text{ m}$  and  $n = 15$ . More elements can be used by increasing the diameter of the array or by placing the elements on two circles. In this manner one can also change the shape of the vertical radiation pattern. The radius of the second circle can be chosen according to the second maximum of  $J_1$  which occurs at  $kr = 5.33$ ;  $2r = 5.33 \lambda_0 / \pi = 1.7 \lambda_0$ . If the elements on the second ring are phased in opposition to those of the first ring, a radiation pattern is obtained which suppresses radiation elevation angles above  $60^\circ$ . The pattern of this type is shown in Figure 6-7 (left side).

In conclusion, the circular array is an efficient means to obtain omnidirectional radiation. It is more efficient than a grid type array with the same number of elements with the two sections fed in quadrature. It also has the advantage of suppressing vertical radiation. The vertical radiation pattern can be shaped to meet specific requirements, as for instance the enhancement of low angle radiation or on the other hand, suppression of ground radiation.

#### 6.3.6 Feed Arrangements of Buried Dipole Arrays

In arrays a large number of dipoles have to be fed with currents of equal phase. One can feed these dipoles all in parallel, or one

can arrange a number of dipoles in series and feed the remaining groups in parallel.

In the first case each dipole is center-fed with a symmetrical cable of equal length to the transmitter. One can also use a coax cable as feed cable and feed unsymmetrically. Since the input resistance of the half-wave dipole is about 20-40 ohms one has a mismatch condition if conventional feed cables of 50 to 100 ohms are used. The mismatch can be reduced by using a number of dipoles in series thereby increasing the input resistance. A folded arrangement of 3 dipoles has been suggested for this purpose, as shown in Figure 6-5a. The total wire length in this configuration is about  $3 \lambda_c/2$ . By folding the wire in this manner the currents in the three legs of the antenna are in phase and therefore act like three separate dipoles. The input resistance is about three times higher than the input resistance of a single dipole, bringing it up to about 60 to 120 ohms, if the spacing is sufficiently large.

Using a twinax cable with  $2 \times 50 = 100$  ohms impedance accomplishes a good match between antenna and cable and eliminates the necessity for a matching network. In addition, the number of feed cables is reduced to 1/3. The use of this folded Z-type dipole as antenna element instead of the single  $\lambda_c/2$  dipole is therefore preferable.

#### 6.2.7 Summary, Buried Dipole Antennas

The buried horizontal insulated wire antenna of the standing wave type is a structure of simple design which can be made very hard by burying it in the ground at a depth of several feet. The basic antenna element consists of an insulated wire fed by a twin-coaxial cable or a coaxial cable without any matching circuit between antenna wire and feed cable. Thus the basic structure is simple. The main cause of failure through weapons effects appears to be rupture of the cable or antenna wire when severe earth movements occur.

The launch efficiency or gain of the buried dipole antenna is, however, very low, not exceeding -15 to -20 db for one element in the frequency range of 8-30 Mc and even lower in the 2-4 Mc range.

The reason for this is, that the antenna wire is buried in lossy ground. The gain of the antenna can be increased by arraying a number of elements, since the array gain is proportional to the number of elements in the array. The number of elements required to obtain reasonable gains is substantial and may range from 10 to 50 (in round numbers), and areas ranging from  $(\lambda_0/4)^2$  to  $(\lambda_0/2)^2$  are required, depending on the desired gain.

There are trade-off possibilities between hardness and gain. As the burial depth is decreased, hardness is reduced, but the gain increases. In the extreme cases the antenna wires would be either deep underground, or at the surface of the ground. In the latter case the gain could be 2 to 10 db higher, depending on frequency and soil conditions.

Arrays can be formed in many ways. Similar techniques as are employed in air can be used to combine the buried dipoles. Elements can be arrayed parallel to each other and thus yield increased gain in the direction of the dipole axes. Groups of parallel elements can be spaced by  $\lambda_0/4$  and fed in quadrature, thus yielding a cardioidal radiation pattern, with directivity in one direction. Groups of parallel elements can be positioned at right angles and fed in quadrature, thus yielding an omnidirectional array. Single elements can be arranged on a circle to give either an omnidirectional pattern or directional pattern depending on the phasing of the antenna currents. These are only a few examples of arrays, and other combinations exist and give the possibility of shaping the radiation pattern.



### 6.3 BURIED TRAVELING - WAVE ANTENNA

This section deals with the fields of buried horizontal-wire antennas of various configurations using a traveling-wave current distribution. Attention is given to space-wave as well as ground-wave radiation, since in the HF range the ground waves are heavily attenuated and one is particularly interested in radiation directed to the ionosphere at higher elevation angles.

The radiation pattern and efficiency of four basic types of traveling-wave antennas buried a few feet in the ground have been investigated. They are the single horizontal wire, and the zig-zag antenna (both directional); the square, and the circle antenna (both omnidirectional in the ground plane).

### 6.3.1 Characteristics of Basic Current Element

Hasserjian and Guy<sup>17</sup> have shown that in the far field above the ground, the field is identical for dipoles below the ground and at the interface between the conducting ground and the lossless half-space above it, except for the exponential term  $e^{-h/\delta}$  multiplying the field of the buried dipole ( $h$  is the depth and  $\delta$  is the skin depth). (Figure 6-8.) Thus Norton's results for the dipole at the interface can be applied. The far field pattern of the horizontal dipole at the interface is similar to that of a vertical loop at the interface, with the horizontal dipole lying in the plane of the loop. The far field has two components,  $E_\phi$  (horizontal) and  $E_\epsilon$  (vertical). These are given as

$$E_\phi \sim \sin \epsilon \sin \phi I (l) \quad (I)$$

$$E_\epsilon \sim \cos \phi I (l)$$

This is the familiar pattern of a magnetic dipole or small loop. The azimuthal pattern on the ground plane is given as the  $\cos \phi$  function; i.e., it is figure-eight shaped with the maximum in the direction of the dipole axis. The polarization on the ground is vertical, there is only an  $E_\epsilon$  component,  $E_\phi$  being zero. Above the ground  $E_\phi$  is no longer negligible and the field therefore has a horizontal and a vertical component. The maximum of the horizontal component  $E_\phi$  is in the direction perpendicular to the dipole axis.

The field intensity in the far field zone of the horizontal dipole located at the interface can be obtained from the field of an ideal vertical monopole above the interface by multiplying the field components of the vertical monopole by the pattern factor  $G_\epsilon$  and applying the refraction term  $\sqrt{n^2 - 1/n^2}$  to the vertical component. The effect of the burial depth is taken into account by the depth factor  $e^{-h/\delta}$ .

3-1-0595

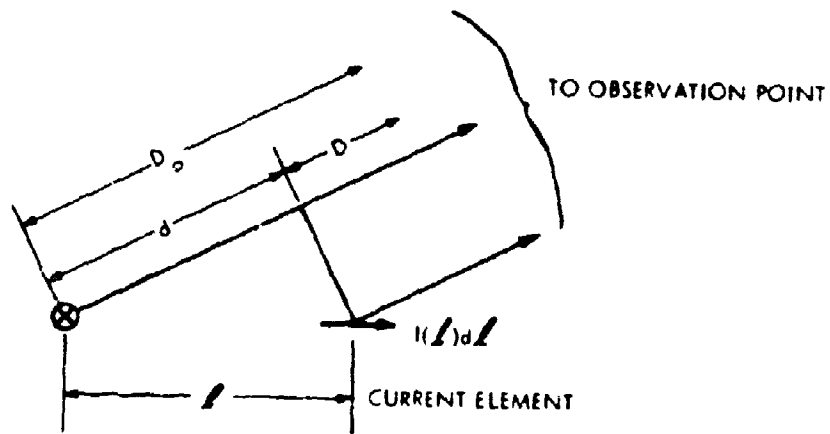
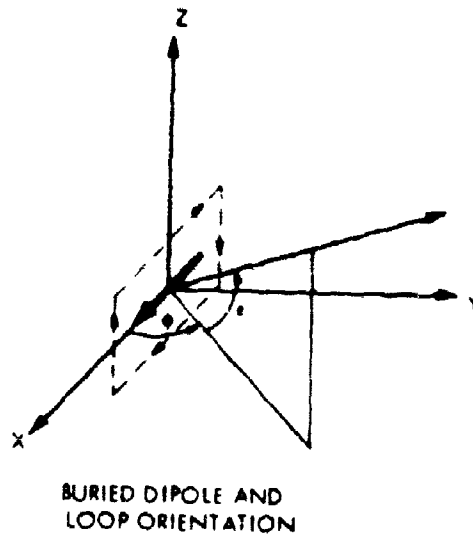


Figure 6-8. Orientation of Basic Current Element.

The refractive index  $n$  is the ratio of the propagation constants of ground and air:

$$n^2 = \frac{\gamma_1^2}{\gamma_0^2} = \epsilon_g - j\sigma/\omega\epsilon_0 = \epsilon_g (1 - j\operatorname{tg}\delta) \quad (2)$$

with

$$\operatorname{tg}\delta = \frac{\sigma}{\omega\epsilon_0\epsilon_g} = \frac{60\sigma\lambda_0}{\epsilon_g}$$

and the skin depth

$$\delta = \frac{\lambda_0}{2\pi} \frac{1}{\sqrt{30\sigma\lambda_0}} = \frac{\lambda}{2\pi} \sqrt{\frac{2}{\operatorname{tg}\delta}}$$

$\sigma$  = conductivity of ground [mho/m]

$\epsilon_g$  = rel., dielectric constant of ground

For low frequencies and high conductivities  $(\sigma/\omega\epsilon_0) \gg \epsilon_g$  the refraction term reduces to

$$\frac{|\sqrt{n^2 - 1}|}{|n^2|} \approx \frac{1}{|n|} = \sqrt{\frac{\omega\epsilon_0}{\sigma}}$$

This is the form used by Hasserjian and Guy in their analysis of LF Subsurface Antennas. Thus the far field intensities for the buried horizontal dipole current element, assuming perfect reflection on the ground in the far field zone, are as follows

$$D \, dE_\epsilon = 60 \frac{|\sqrt{n^2 - 1}|}{|n^2|} (k \cos \phi) I(\ell) d\ell e^{-jkD} e^{-h/\delta} \quad (3)$$

$$De^{jkD} dE_\epsilon = 60 C_\epsilon I(\ell) d\ell e^{+jkD} K$$

and

$$dE_\phi = 60 \frac{|\sqrt{n^2 - 1}|}{|n^2|} (k \sin \epsilon \sin \phi) I(\ell) d\ell e^{-jkD} e^{-h/\delta}$$

$$De^{jkD_o} dE_\phi = 60 C_\phi I(l) dl e^{+jkd} K$$

The equations for the two field components can be combined in one:

$$De^{jkD_o} dE = 60 C I(l) dl e^{+jkd} K \quad (4)$$

where

$$k = \frac{2\pi}{\lambda_o}, \lambda_o = \text{wavelength in free space}$$

$$D = D_o - d, d = l \cos \epsilon \cos \phi = l \cos \gamma$$

$D$  = distance from current element to observation point,

$D_o$  = distance from a reference point to observation point, and

$C$  is the pattern function of the infinitesimal buried current element

It is either  $C_\epsilon = k \cos \phi$  or  $C_\phi = k \sin \epsilon \sin \phi$  depending on the field component one wishes to consider. The factor  $K$  comprises the refraction term and the exponential depth term. It is the same for any horizontal element at the same depth. Since the fields of the antennas investigated will be compared with the field from a single horizontal element at the same depth, we shall disregard  $K$  in the following calculations.

### 6.3.2 Half-Wave Dipole, Center Fed, with Standing Wave Current Distribution

The fields of the various antenna configurations will be compared with the field of a buried half-wave dipole as shown in Figure 6-9. The current distribution on the open-ended dipole is assumed sinusoidal. The attenuation constant  $\alpha$  for an insulated, buried dipole is generally very small so that the error made by setting  $\alpha = 0$  is very small. Thus

$$I(x) = I_0 \cos \beta x \quad \text{with } \beta = \frac{2\pi}{\lambda_c}$$

$\lambda_c$  = wavelength on the insulated antenna wire. The dipole is fed in the center, which is also the reference point, 0.

Using Equation (4), we get (with  $d = x \cos \epsilon \cos \phi = x \cos \gamma$ )

$$\begin{aligned} D e^{jkD} \int_0^D dE &= 60 C I(x) dx e^{+jkd} \\ &= 60 C I_0 \cos \beta x dx e^{jkx \cos \gamma} \end{aligned} \quad (5)$$

disregarding the factor  $K$  as mentioned above. The field on the ground ( $\epsilon = 0$ ), which we shall use for comparison purposes, has only an  $\epsilon$  component. Thus, with  $C_\epsilon = k \cos \phi$

$$D e^{jkD} \int_0^D dE_\epsilon(0) = 60 (k \cos \phi) I_0 \cos \beta x dx e^{jkx \cos \phi} \quad (6)$$

and

$$D e^{jkD} \int_0^D dE_\epsilon(0) = 60 I_0 f_d(\phi, 0)$$

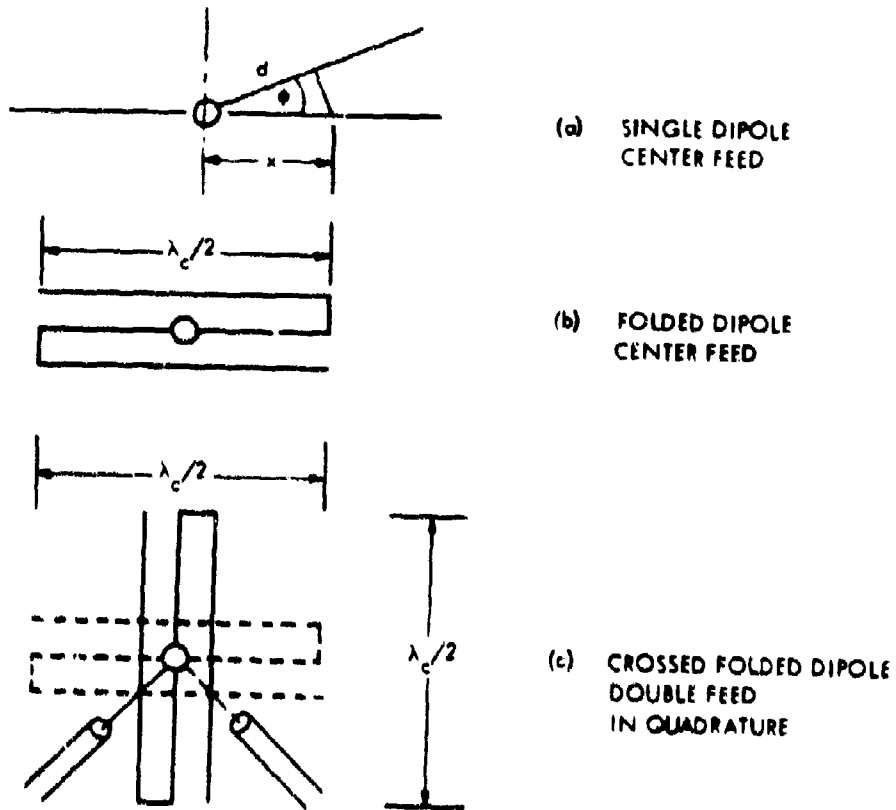


Figure 6-9. Single and Folded Dipole.

with

$$f_d(\phi, 0) = \frac{k \cos \phi}{I_0} \int_{-\lambda_c/4}^{+\lambda_c/4} I_0 \cos \beta x dx e^{jkx \cos \phi} \quad (7)$$

$$= \frac{2p}{1-p^2} \cos \phi \cos \left( \frac{\pi}{2} p \right)$$

where

$$p = \frac{k}{\beta} = \frac{\lambda_c}{\lambda_0} = \frac{\text{wavelength on antenna}}{\text{wavelength in free space}}$$

$$\beta = \frac{2\pi}{\lambda_c}$$

$f_d(\phi, 0)$  as given by (7) is the pattern function of the half-wave buried dipole. The factor  $K$  has been omitted since it occurs in all of the field patterns of horizontal buried wire antennas. In the following we shall determine the relative efficiency  $\eta$  of the horizontal buried traveling wave antennas with reference to the half-wave, standing-wave dipole. For this purpose the ground-wave field intensities in the direction of maximum radiation will be compared. The efficiency ratio of the traveling wave antenna and the horizontal half-wave dipole is defined as

$$\eta = \frac{|DE_t|^2}{|DE_d|^2} = \frac{(80K I_{ot})^2 |f_T(\phi, 0)|^2}{(80K I_{od})^2 |f_d(\phi, 0)|^2} \quad (8)$$

where

$f_T(\phi, 0)$  is the pattern function of the traveling wave antenna in the ground plane.

$f_d(\phi, 0)$  is the pattern function of the half standing wave dipole, as given by (7)

$I_{ot}$  is the reference current of the traveling wave antenna

$I_{od}$  is the reference current of the half-wave dipole.



These currents must be determined for equal power input in each of the antennas: Thus

$$|I_{oT}|^2 Z_o = |I_{od}|^2 R_{in} = \text{Input power} \quad (9)$$

$$\frac{|I_{oT}|^2}{|I_{od}|^2} = \frac{R_{in}}{Z_o} \quad (10)$$

where  $R_{in}$  is the input resistance of the half-wave dipole, and  $Z_o$  is the characteristic impedance of the traveling wave antenna. These quantities have been calculated by Hasserjian and Guy<sup>17</sup> (p. 234, eq.(12)-(15).

For small  $\alpha$ ,

$$R_{in} = \text{gp } 15\pi \frac{\pi}{2} = \text{gp } 7.5 \pi^2$$

For  $l = \frac{\lambda_c}{2}$

$$Z_o = \frac{60\beta}{\epsilon_r k} \ln \frac{b}{a} = \frac{60}{\epsilon_r p} \ln \frac{b}{a} \quad (11)$$

Neglecting  $\alpha$

$$g = \frac{8\alpha\beta}{\pi \epsilon_r k^2} \ln \frac{b}{a} = \frac{8\alpha}{\pi \epsilon_r k p} \ln \frac{b}{a}$$

Thus

$$\frac{R_{in}}{Z_o} = \frac{\alpha}{\beta} \pi = \frac{\alpha_d}{\beta} \pi \quad (12)$$

The attenuation constant  $\alpha$  practically does not affect  $Z_o$ , if it is small, but it does affect  $R_{in}$ . The  $\alpha$  in (12) is the  $\alpha$  that obtains for the dipole. The  $\alpha$  for the traveling wave antenna and for the dipole may be different, because of mutual coupling, which is different in the two cases.  $\alpha_d > \alpha_T$  if several  $\frac{\lambda_c}{2}$  dipoles are used.

$\alpha_T$  is the attenuation constant used for calculation of  $F_T(\phi, 0)$ . With (7) and (8) and  $\phi = 0$  the efficiency ratio is

$$\eta_0 = \frac{\alpha_d \pi}{\beta} \frac{|f_T(\phi_m, 0)|^2 (1-p^2)^2}{4p^2 \cos^2(\frac{\pi}{2} p)} \quad (13)$$

$\phi_m$  is the azimuth angle indicating the direction of maximum ground-wave field intensity of the traveling wave antenna.

In practice the folded dipole is often used. This is a configuration with three parallel half-wave elements separated by one or more skin depths of the soil in which they are imbedded. (Figure 6-9b). The pattern function  $f_d(\phi, 0)$  and the input resistance are both multiplied by a factor of 3 in this case, and the attenuation constant is increased through mutual coupling by a factor which can be as high as 2 to 3 if the spacing between wires is less than one skin depth. In this case the efficiency value is

$$\eta_1 = \frac{3\eta_0}{9} = \frac{\eta_0}{3}, \text{ using the appropriate } \alpha_d.$$

The omnidirectional antennas will be compared to an omnidirectional dipole arrangement consisting of a pair of folded buried dipoles that are fed in quadrature with two cables.

In this case the RF power is split into two equal parts so that the resulting efficiency ratio,

$$\eta_2 = 2 \eta_1 = \frac{2\eta_0}{3} = \frac{\eta_0}{1.5}$$

This is the efficiency ratio of an omnidirectional antenna compared to an omnidirectional dipole antenna consisting of two crossed Z-type elements fed in quadrature.

### 6.3.3 The Single Horizontal Insulated Buried Straight Wire, Center Fed, with Traveling Wave Current Distribution

We consider a straight wire of length  $2b$ , terminated at both ends with its characteristic impedance, and fed in the center (Figure 6-10). The current distribution along the wire is that of a traveling wave

$$I(x) = I_0 e^{-\Gamma|x|} = I_0 e^{-(\alpha + j\beta)|x|}$$

with the propagation constant on the buried wire  $\Gamma = \alpha + j\beta$ .  $\alpha$  and  $\beta$  have been calculated by Hasserjian and Guy<sup>17</sup> for the buried insulated wire. The far field pattern of the buried horizontal current element taking the reference point in the center at the feed point, is given (Equation 4) as

$$\begin{aligned} De^{jkD}_0 dE &= 60 C I(x) dx e^{jkD} \\ &= 60 C I_0 e^{-\Gamma|x|} e^{jkx \cos \gamma} dx \end{aligned} \quad (14)$$

with

$$d = x \cos \epsilon \cos \phi = x \cos \gamma ; \text{ omitting } K$$

The far field of the whole wire is

$$\begin{aligned} De^{jkD}_0 E &= 60 C I_0 \int_{-b}^{+b} e^{-(\alpha + j\beta)|x|} e^{jkx \cos \gamma} dx \\ &= 60 I_0 f_T(\phi, \epsilon) , \end{aligned}$$

where

$$f_T(\phi, \epsilon) = C \epsilon \int_{-b}^{+b} e^{-(\alpha + j\beta)|x|} e^{jkx \cos \gamma} dx$$

3-1-0597

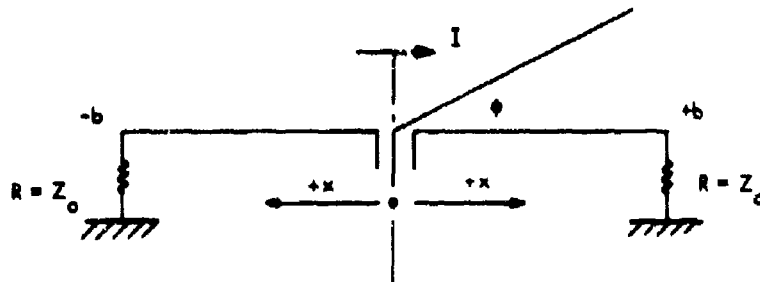


Figure 6-10. Straight Wire - Center Feed.

is the pattern function. The pattern of the  $\epsilon$ -component or  $\phi$ -component is obtained by using  $C_\epsilon$  or  $C_\phi$ , respectively. Evaluating the integral yields:

$$\begin{aligned}
 F_{OH} &= \int_0^b e^{-[\frac{\alpha}{\beta} + j(1-p \cos \gamma)] \beta x} dx \\
 &+ \int_0^b e^{-[\frac{\alpha}{\beta} + j(1+p \cos \gamma)] \beta x} dx \\
 &= \int_0^b e^{[A+jB]x} dx + \int_0^b e^{[A+jB']x} dx \quad (15)
 \end{aligned}$$

$$\begin{aligned}
 &= 2 \frac{e^{[A+jB]b/2}}{A+jB} \sinh (A+jB)b/2 \\
 &+ 2 \frac{e^{[A+jB']b/2}}{A+jB'} \sinh (A+jB')b/2
 \end{aligned}$$

$$\text{Thus } \frac{F_{OH}}{2} = \frac{e^{Ab/2} e^{jBb/2}}{A+jB} \left[ \sinh \frac{Ab}{2} \cos \frac{Bb}{2} + j \cosh \frac{Ab}{2} \sin \frac{Bb}{2} \right]$$

$$+ \frac{e^{Ab/2} e^{jB'b/2}}{A+jB'} \left[ \sinh \frac{Ab}{2} \cos \frac{B'b}{2} + j \cosh \frac{Ab}{2} \sin \frac{B'b}{2} \right] \quad (15a)$$

with

$$A + jB = - \left[ \frac{\alpha}{\beta} + j(1-p \cos \gamma) \right] \beta \quad (15b)$$

$$A + jB' = - \left[ \frac{\alpha}{\beta} + j(1+p \cos \gamma) \right] \beta$$

$$\cos \gamma = \cos \epsilon \cos \phi \quad A = - \alpha$$

The field pattern for various lengths of the antenna has been computed, using the following data:

$$\begin{aligned} f &= 10 \text{ mc} & \sigma &= 0.01 \text{ mho/m} & \lambda_o &= 30 \text{ m} \\ \alpha &= 0.051 & \beta &= 0.691 & \frac{\alpha}{\beta} &= 0.075 \end{aligned}$$

$$\lambda_c = 9.09 \text{ m} \quad p = \frac{\lambda_c}{\lambda_o} = 0.303$$

The  $|E_{\epsilon}|$ - patterns are plotted in Figure 4 and 5 for total lengths  $2b$  of the antenna of 1, 3, 5, 7, and 9 half-antenna-wavelengths:

$$2b = 2m \lambda_c \quad m = \frac{1}{4}; \frac{3}{4}; \frac{5}{4}; \frac{7}{4}; \frac{9}{4}$$

$b$  is the length of one side of the antenna,

$\lambda_c$  is the wavelength on the antenna wire.

The azimuthal patterns are  $\omega$ -shaped and symmetrical to the  $\psi = 90^\circ$  line. The maximum field intensities and efficiency ratios are tabulated below:

$m$	$ E_{\epsilon} $	$\eta_o$
	60 $\kappa$	
1/4	0.781	0.205
3/4	0.806	0.220
5/4	0.649	0.141
7/4	0.708	0.168
9/4	0.735	0.180
4	0.643	0.139

The input resistance of the traveling wave antenna is  $2 Z_o$  in this case, since a balanced feed at the center is used. The efficiency ratio is therefore  $1/2 \eta_o$  using (13). It is evident that the efficiency cannot be increased by increasing the length of the antenna beyond  $3/2 \lambda_c$ . Actually the efficiency

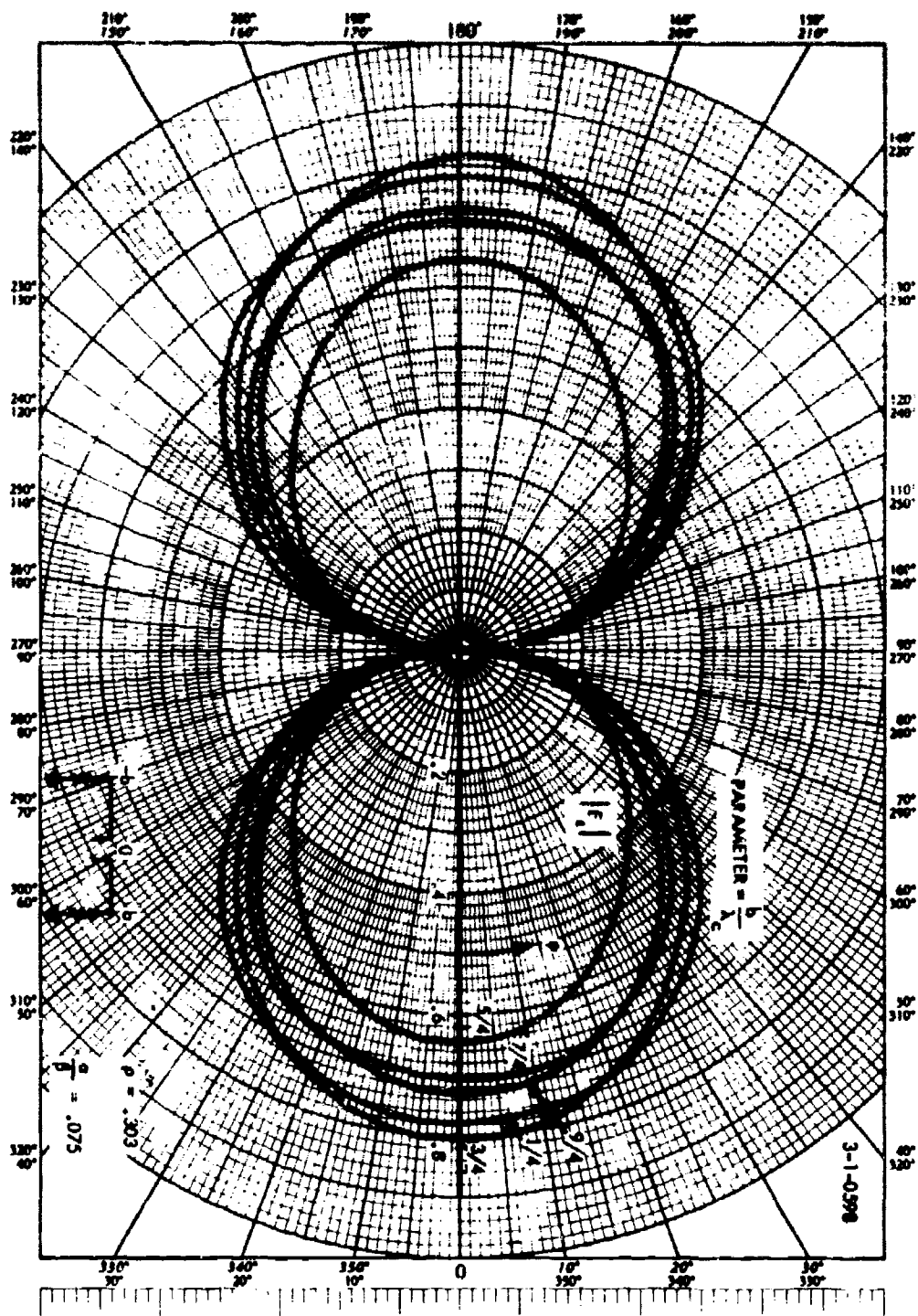
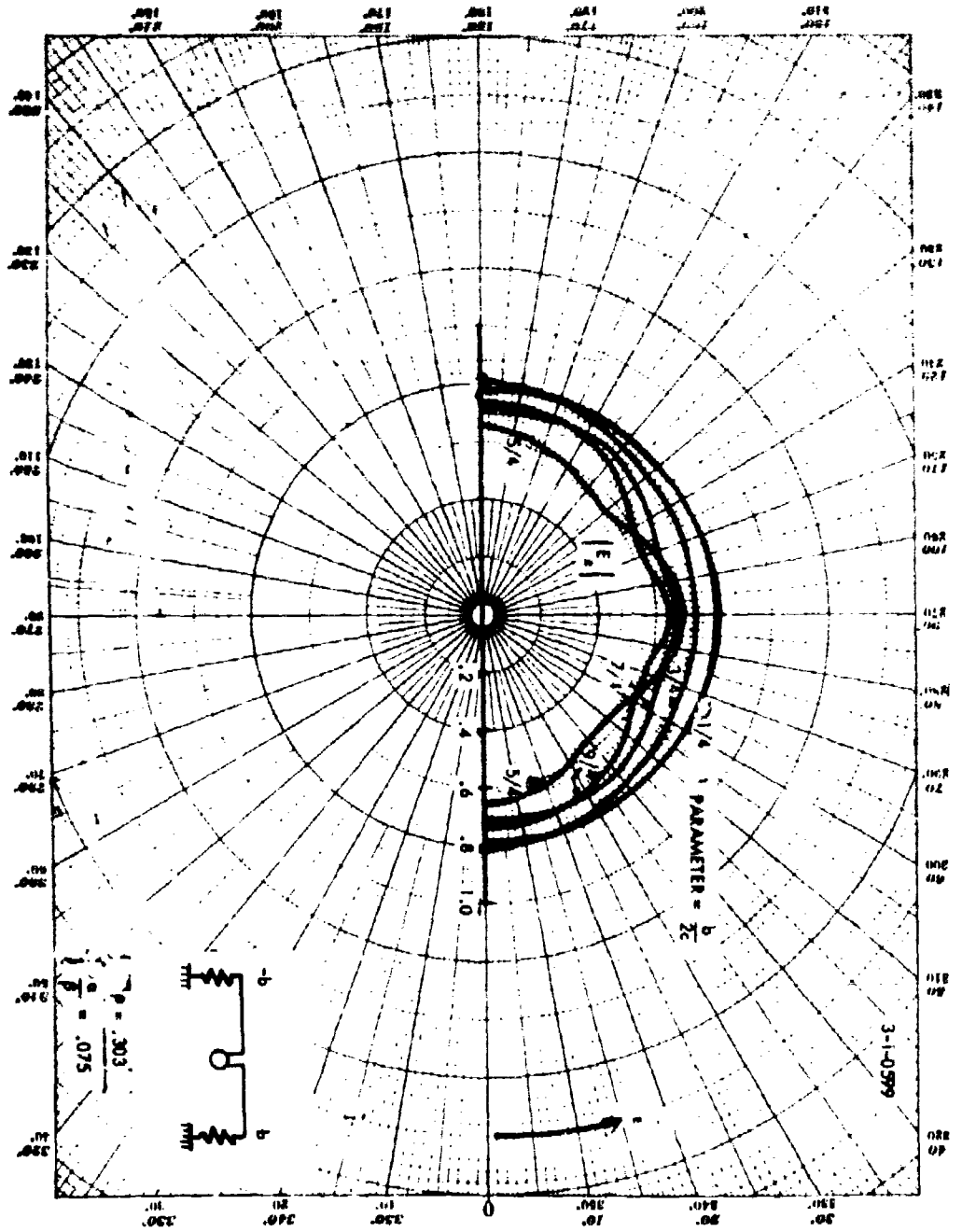


Figure 6-12. Straight Wire - Elevation Pattern  $|E_{\theta}|$ 



at a length of  $1/2$  wavelength is almost as large as that of the  $3/2$  wavelength antenna. The longer antennas have even smaller efficiency than the half-wave antenna. A configuration which yields higher efficiency with increasing length is the zig-zag antenna, which is described in the following section.

The elevation patterns are shown in Figure 6-12. The short antennas have a semicircular pattern; the longer antennas show some lobing.

The pattern of a long straight wire antenna ( $b = 4\lambda_c$ ) is shown in Figures 6-13 and 6-14 for two cases: feed point on one side, and center fed. The center-fed arrangement makes the pattern symmetrical to the  $\psi = 90^\circ$  axis, whereas the feed on one side gives more field intensity in the forward direction than in the backward direction. Considerable lobing occurs with these long wire antennas.

### Conclusion

Straight wire antennas with traveling waves have low efficiency compared to the half-wave standing wave dipole. Long wire antennas have lower efficiency than the shorter antennas and also have a lobing pattern. The input impedance is practically independent of the frequency, as it is for all traveling wave type antennas. The straight wire antenna is therefore, disadvantageous compared to other traveling wave antennas.

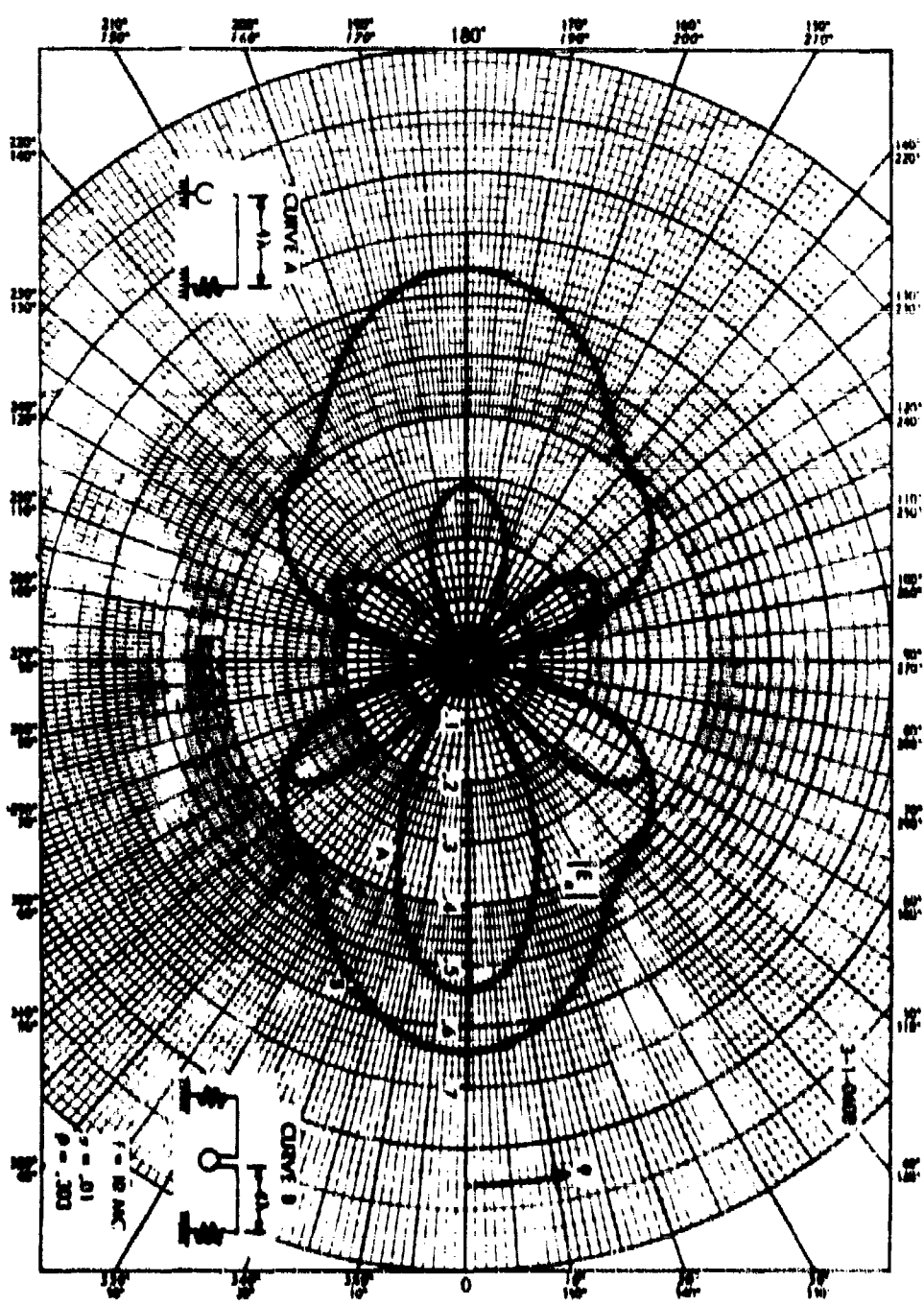
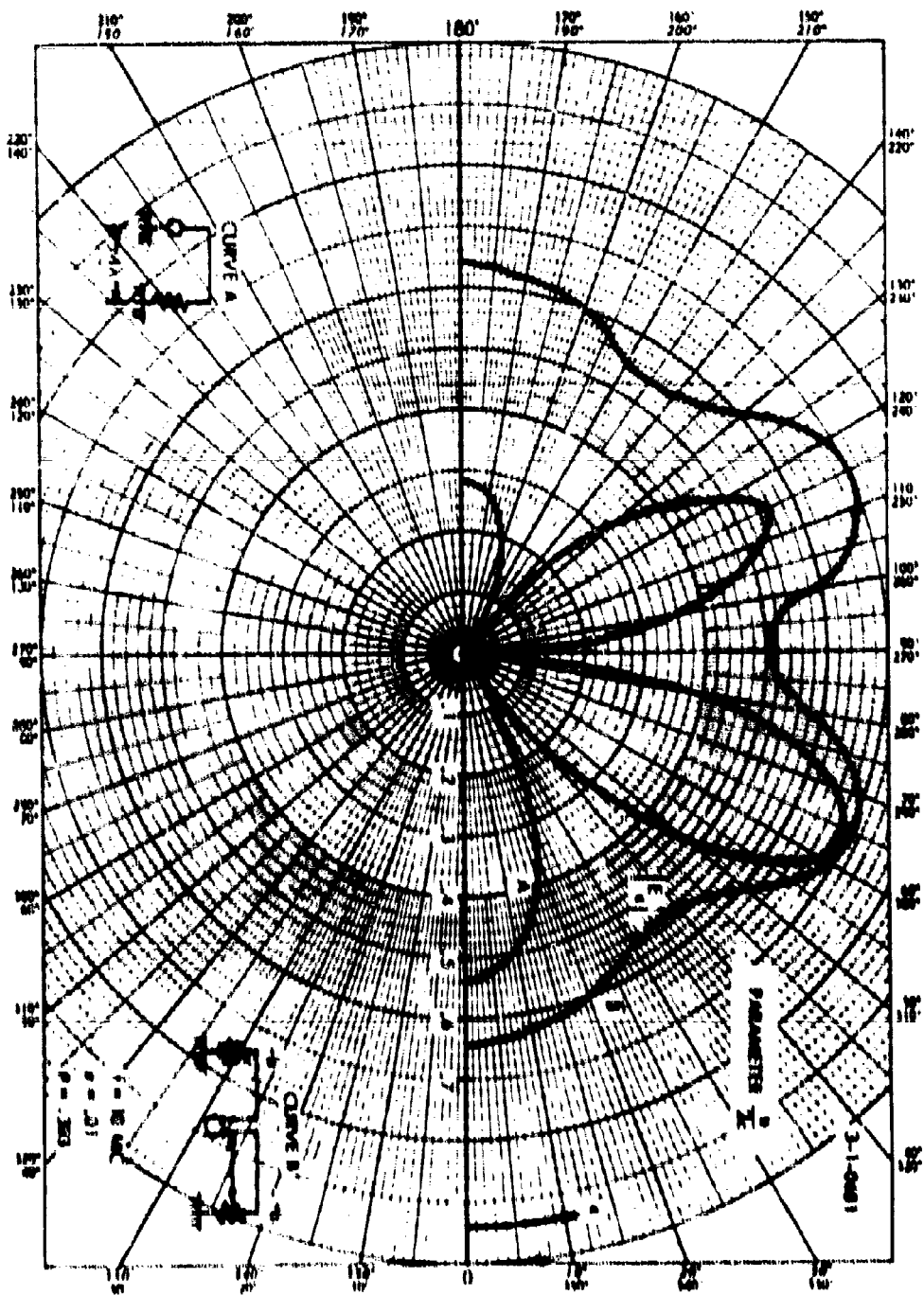


Figure 6-13. Straight Wire: Center Feed - End Feed Azimuthal Pattern  $|E_z|$



#### 6.3.4 Zig-Zag Antenna

##### The Basic Antenna Configuration and Feed Arrangement

In order to get a figure-eight directional pattern, a number of half-wave elements are arranged in ladder fashion yielding a zig-zag array (Figure 6-15). All elements have the length  $2b = \frac{\lambda_c}{2}$  and are buried in a horizontal position a few feet in the ground. There are two groups of elements which are designated as H and V and are perpendicular to each other. To obtain symmetry an even number of V-elements and an odd number of H-elements is always used. The feed point of the array is in the middle of the center H-element. The end elements, either H or V as the case may be, are terminated with a resistor equal to the characteristic impedance of the antenna wire. The resistor is grounded at the other end. In this manner a traveling wave current distribution is obtained on the antenna and the input impedance at the feed point is equal to the characteristic impedance of the antenna wire.

##### The Current Distribution

The current on both sides from the feed point decays according to  $e^{-\Gamma l}$  ( $l$  = distance from feedpoint) since it is assumed that there is no reflection at the end points of the antenna and therefore a traveling current wave exists. At equal distances on both sides from the feed point the currents are identical in magnitude, phase and direction. The positive direction of current flow is indicated on Figure 6-15.

The currents in the center of the H-elements are

$$I_{nH} = I_{0H} e^{-\Gamma n 4b} = I_{0H} e^{-\Gamma n \lambda_c} = I_{0H} e^{-n \alpha \lambda_c} \quad (16)$$

$$n = 1, 2, 3$$

LENGTH OF EACH ELEMENT IS  $2b$

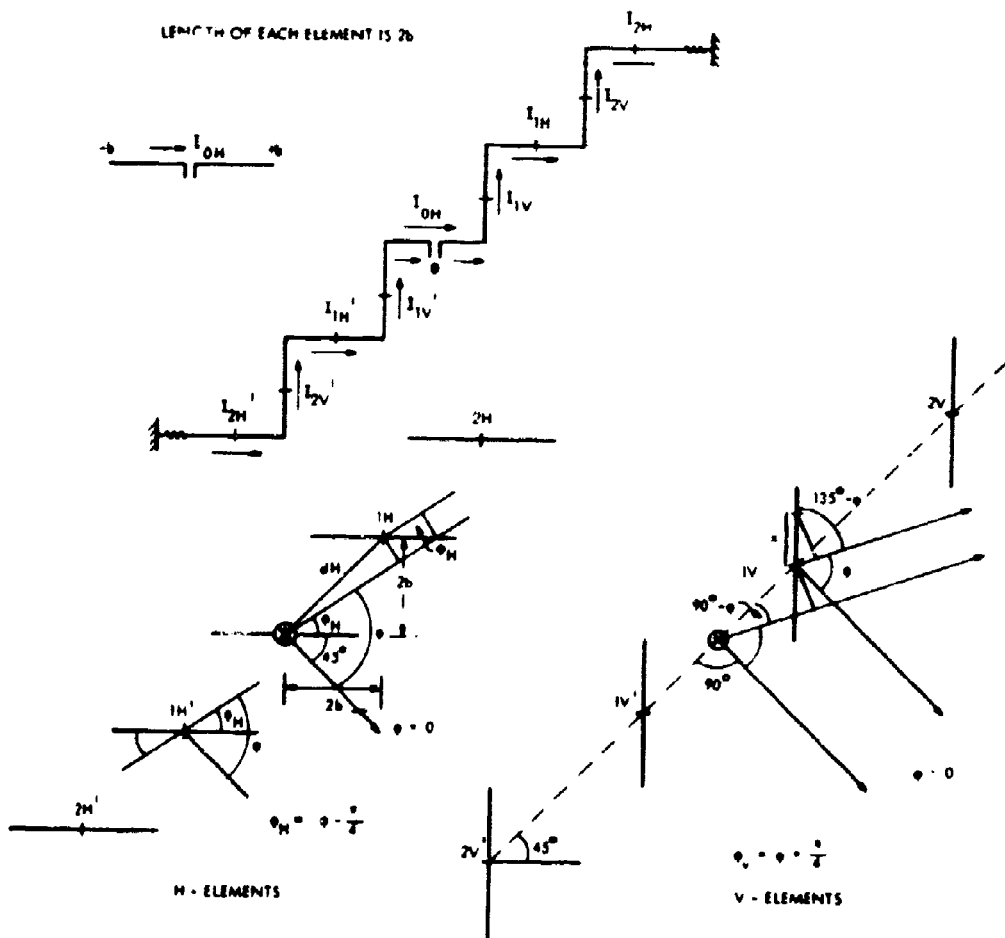


Figure 6-15. Zig-Zag Antenna - Orientation.

where the propagation constant  $\Gamma = \alpha + j\beta$ ;  $\beta = \frac{2\pi}{\lambda_c}$

$I_{oH}$  is the current at the feed point in the central H-element, which is chosen as the reference current. The currents at the centers of the V-elements are:

$$I_{nv} = I_{oH} e^{-\Gamma(2n-1)2b} = I_{oH} e^{-\Gamma(2n-1)\lambda_c/2} = I_{oH} e^{-(2n-1)\alpha\lambda_c/2}$$

$$n = 1, 2, 3$$

(17)

### The Field Pattern

The patterns generated by the H- and V-elements are calculated separately and then combined to give the pattern of the array. The axis of the azimuth angle  $\Psi$  is chosen such that it is perpendicular to the line connecting the centers of the elements, as indicated in Figure 6-15. The pattern function of the center element is the same as that of the straight wire, as calculated in Section 3, Equations (14) and (15);

$$E_{oH} = C_H I_{oH} F_{oH}$$

The coordinate system in the present case is rotated by  $45^\circ$ , and the following relation exists:

$$\Psi = \phi_H + 45^\circ$$

where  $\phi_H$  is the azimuth angle with respect to the H-elements.

$$\text{Thus } F_{oH} = \int_{-b}^{+b} e^{-\Gamma|x|} e^{jkx \cos \gamma_H} dx \quad (18)$$

with  $\cos \gamma_H = \cos \phi_H \cos \epsilon = \cos (\Psi - 45^\circ) \cos \epsilon$

and  $b = \frac{\lambda_c}{4}$ , since the length of each element is  $2b = \frac{\lambda_c}{2}$

The integral  $F_{oH}$  is given by (15), using

$$B = B_H = (1 - p \cos \gamma_H) \beta \quad (19)$$

$$B' = B'_H = (1 + p \cos \gamma_H) \beta$$

In the same manner  $C_H$  is given as

$$C_{H\epsilon} = k \cos \phi_H = k \cos (\Psi - 45^\circ) \quad (20)$$

$$C_{H\Psi} = k \sin \epsilon \sin \phi_H = k \sin \epsilon \sin (\Psi - 45^\circ)$$

The field pattern of one of the H-elements is

$$E_{nH} = C_H I_{nH} \int_{-b}^b e^{-\Gamma x} e^{\pm jkD_H} dx,$$

where the upper sign is for the unprimed elements and the lower for the primed elements.

$$D_H = -nd_H \cos \epsilon \sin \Psi - x \cos \epsilon \cos (\Psi - 45^\circ)$$

$$kD_H = -n\theta_H - kx \cos \gamma_H; \cos \gamma_H = \cos \epsilon \cos (\Psi - 45^\circ)$$

$d_H$  is the distance between two centers of elements.

$$d_H = 2b\sqrt{2} = \frac{\lambda_c}{2}\sqrt{2}$$

$$kd_H \cos \epsilon \sin \Psi = \pi p \sqrt{2} \cos \epsilon \sin \Psi = \theta_H$$

$$\text{with } p = \frac{k}{\beta} = \frac{\lambda_c}{\lambda_o}$$

$$E_{nH} = C_H I_{oH} e^{-n\alpha_c} x \begin{pmatrix} e^{jn\theta_H} F_{nH} \\ e^{-jn\theta_H} F'_{nH} \end{pmatrix} \begin{matrix} \text{for unprimed elements} \\ \text{for primed elements} \end{matrix} \quad (21)$$

with

$$F_{nH} = \int_{-\lambda_c/4}^{\lambda_c/4} e^{-\Gamma x} e^{jkx \cos \gamma_H} dx \quad (22)$$

$$F_{nH} = \int_{-\lambda_c/4}^{\lambda_c/4} e^{-\Gamma x} e^{-jkx \cos \gamma_H} dx$$

The pattern of the array of H-elements is the sum of the individual patterns:

$$E_H = E_{oH} + \sum_{n=1}^{N_H} E_{nH} + \sum_{n=1}^{N_H} E'_{nH} \quad (23)$$

$2N_H$  is the number of the H-elements, not counting the center element.

$$\begin{aligned} E_H &= C_H I_{oH} \left\{ F_{oH} + \sum_{n=1}^{N_H} \left[ e^{-n\alpha \lambda_c} \left( e^{jn\theta_H} F_{nH} + e^{-jn\theta_H} F'_{nH} \right) \right] \right\} \\ &= C_H I_{oH} \left\{ F_{oH} + \sum_{n=1}^{N_H} e^{-n\alpha \lambda_c} G_{nH} \right\} \end{aligned} \quad (24)$$

with

$$G_{nH} = e^{jn\theta_H} F_{nH} + e^{-jn\theta_H} F'_{nH}$$



The field pattern of the V-elements is obtained similarly. The pattern of one of the V-elements is

$$E_{nv} = C_v I_{nv} \int_{-b}^b e^{-\Gamma x} e^{+jkD_v} dx \quad (25)$$

where the upper sign is for the unprimed elements, and the lower sign for the primed elements.

$$D_v = - (2n-1) d_v \cos \epsilon \sin \psi + x \cos \epsilon \cos (\psi + 45^\circ)$$

$$kD_v = - (2n-1) \theta_v + k x \cos \gamma_v$$

$$d_v = \frac{d_H}{2} = b\sqrt{2} = \frac{\lambda_c}{4} \sqrt{2} \quad (26)$$

$$kd_v \cos \epsilon \sin \psi = \pi \sqrt{\frac{2}{2}} \cos \epsilon \sin \psi = \theta_v = \frac{\theta_H}{2}$$

$$\cos \gamma_v = \cos \epsilon \cos (\psi + 45^\circ)$$

$$C_{v\epsilon} = -k \cos (\psi + 45^\circ) \quad C_{v\psi} = k \sin \epsilon \sin (\psi + 45^\circ) \quad (27)$$

$$E_{nv} = -C_v I_{oH} e^{-(2n-1)\alpha \frac{\lambda_c}{2}} \begin{pmatrix} e^{j(2n-1)\theta_v F_v} \\ e^{-j(2n-1)\theta_v F'_v} \end{pmatrix} \begin{matrix} \text{unprimed elements} \\ \text{primed elements} \end{matrix} \quad (28)$$

with

$$F_v = \int_{-\lambda_c/4}^{\lambda_c/4} e^{-\Gamma x} e^{-jkx \cos \gamma_v} dx \quad (29)$$

$$F'_v = \int_{-\lambda_c/4}^{\lambda_c/4} e^{-\Gamma x} e^{+jkx \cos \gamma_v} dx \quad (30)$$

The pattern of the array of V-elements is

$$E_v = \sum_{n=1}^{N_v} E_{nv} + \sum_{n=1}^{N_v} E'_{nv} \quad (31)$$

$2N_v$  is the number of the V-elements

$$\begin{aligned} E_v &= -C_v I_{OH} \sum_{n=1}^{N_v} \left\{ e^{-\alpha(2n-1)\lambda_c/2} \left[ e^{j(2n-1)\theta_v} F_v + e^{-j(2n-1)\theta_v} F'_v \right] \right\} \\ &= -C_v I_{OH} \sum_{n=1}^{N_v} e^{-\alpha(2n-1)\lambda_c/2} G_{nv} \end{aligned} \quad (32)$$

with

$$G_{nv} = e^{j(2n-1)\theta_v} F_v + e^{-j(2n-1)\theta_v} F'_v \quad (33)$$

The field pattern of the zig-zag antenna with  $2N_H$  H-elements and  $2N_v$  V-elements, and one center element in the H-direction (a total of  $2(N_H + N_v) + 1$  elements) is the sum of the individual element patterns, since all patterns have been referred to the same central reference point.

$$z^f(\epsilon, \psi) = C_H \left\{ F_{oH} + \sum_{n=1}^{N_H} e^{-n\alpha c} \cdot G_{nH} \right\} \quad (34)$$

$$- C_V \sum_{n=1}^{N_V} \left[ e^{-\alpha(2n-1)\lambda c/2} \cdot G_{nV} \right]$$

The field intensity at distance D from the center of the array is obtained as

$$E_{\epsilon}^D = 60 \cdot I_{oH} z^f_{\epsilon}(\epsilon, \psi)$$

$$E_{\psi}^D = 60 \cdot I_{oH} z^f_{\psi}(\epsilon, \psi) \quad (35)$$

The current  $I_{oH}$  at the feed point is  $\frac{V}{2Z_0}$  since a balanced feed is used, V is the symmetrical voltage across the feed terminals, and  $Z_0$  the characteristic impedance of each leg of the antenna; i.e., the characteristic impedance of a single buried insulated antenna wire.

The basic integral of the straight wire element is

$$F = \int_{-b}^b e^{-\Gamma x} e^{+jkx \cos \gamma} dx = \int_{-b}^b e^{(A+jB)x} dx \quad (36)$$

$$\text{or} \quad = \int_{-b}^b e^{(A+jB')x} dx$$

$$F^+ = \frac{2}{A+jB} \left\{ \sinh Ab \cos Bb + j \cosh Ab \sin Bb \right\} \quad (37)$$

$F^-$  is the same expression using  $B'$  instead of B.

$$A = -\alpha \quad \left. \begin{matrix} B \\ B' \end{matrix} \right\} = -(1 \mp p \cos \gamma) \beta \quad (38)$$

$$A + jB = - \left[ \frac{\alpha}{\beta} + j(1 - p \cos \gamma) \right] \beta \quad (39)$$

$$A + jB' = - \left[ \frac{\alpha}{\beta} + j(1 + p \cos \gamma) \right] \beta$$

Then

$$F_{nH} = F^+ \text{ using } \gamma_H \quad (40)$$

$$F_{nH'} = F^- \text{ using } \gamma_H$$

$$F_V = F^- \text{ using } \gamma_V$$

$$F_{V'} = F^+ \text{ using } \gamma_V$$

Field patterns  $|E_c|$  have been computed using the same data as used for the straight wire antenna.

$$f = 10 \text{ Mc} \quad \lambda_0 = 30 \text{ m} \quad \sigma = 0.01 \text{ mho/m}$$

$$\alpha = 0.051 \quad \beta = 0.691 \quad \frac{\alpha}{\beta} = 0.075 ; p = 0.303$$

The plots are shown on Figures 9 and 10 for 3 elements and 9 elements, each  $1/2$  wavelength ( $\lambda_c$ ) long. The azimuthal pattern is figure-eight shaped, however there are no sharp nulls. The maximum radiation is at  $\psi = 0$ , perpendicular to the line connecting the centers of the individual elements. The pattern shape does not materially change as more elements are added, but the field intensity increases. The elevation pattern is practically semicircular. There is no lobing in the vertical plane.



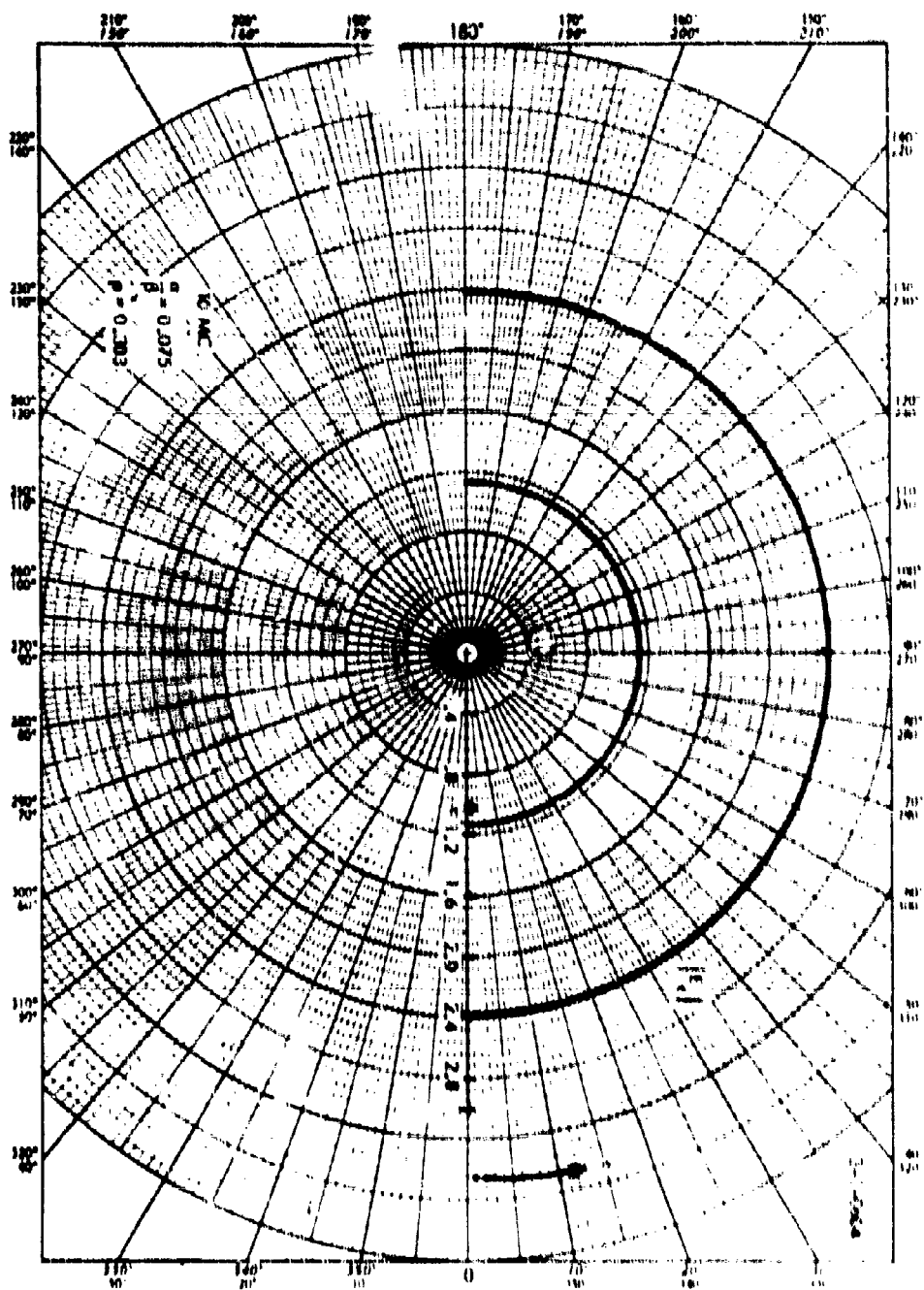


Figure 6-17. Zig-Zag Antenna - Elevation Pattern  $|E|$

The efficiency ratio as a function of the number of elements is tabulated below and plotted in Figure 6-18.

$N_H$	$N_V$	$N_T$ $= 2(N_H + N_V) + 1$	$\eta_0$	$\frac{ E_r }{60x}$
0	1	3	.43	1.13
1	1	5	.60	1.64
1	2	7	1.40	2.06
2	2	9	1.90	2.39
2	3	11	2.4	2.68
3	3	13	2.75	2.86
3	4	15	3.1	3.03
4	4	17	3.35	3.16
4	5	19	3.55	3.26
5	5	21	3.75	3.35

$$\eta_0 = \frac{1}{2} 0.67 |E_r|^2$$

A balanced feed is used, therefore the input impedance is  $2Z_0$  and  $\eta_0$  is multiplied with  $1/2$ . The efficiency ratio increases first linearly with the number of elements but levels off as the number of elements  $N_T > 9$  (see Figure 6-18). The efficiency is always smaller than the efficiency of an array of standing wave  $\lambda_{0,2}$  dipoles with the same number of elements.

### Conclusion

The Zig-Zag antenna has an azimuthal pattern which is figure-eight shaped and symmetrical to the  $\psi = 90^\circ$  axis. The shape is essentially independent of the number of elements. The efficiency increases with the number of elements, but is always lower than the efficiency of a corresponding array of half-wave dipoles (standing wave). The input impedance is constant, not depending on frequency or number of elements. However the pattern changes its shape with frequency. Due to the low efficiency the usefulness of the Zig-Zag antenna is limited to such cases where constant input impedance is of importance.

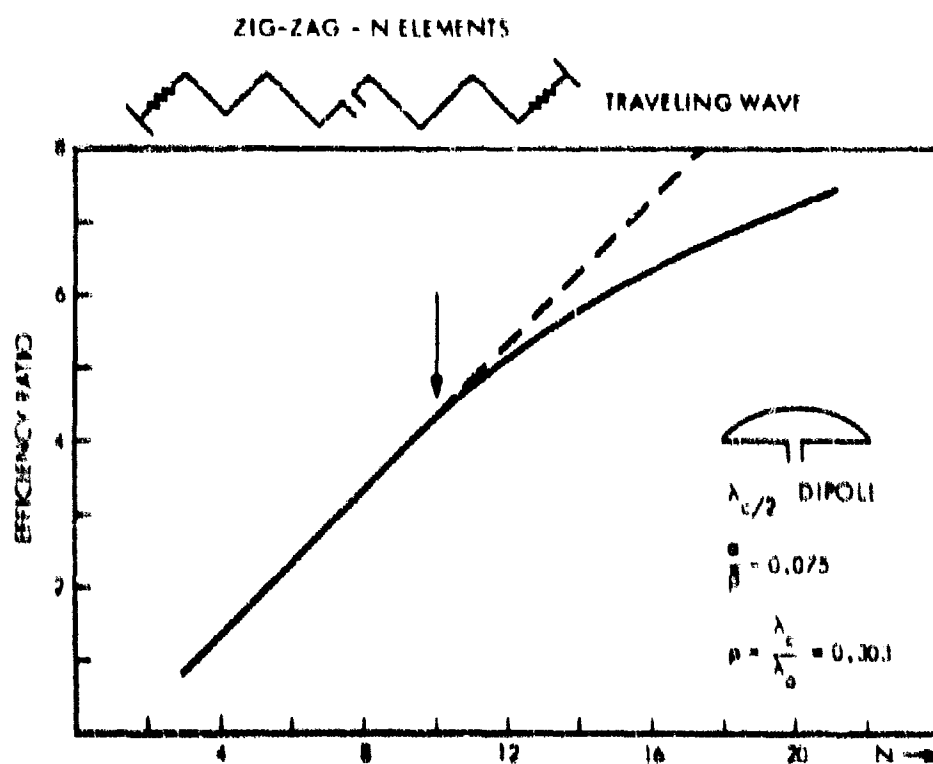


Figure 6-18. Zig-Zag Antenna - Efficiency.



### 6.3.5 Rhombic Antennas

Rhombic antennas in air give a high-gain unidirectional pattern. The pattern changes with frequency, but the input impedance remains practically constant, so that the antenna has a wide bandwidth. Similar results can be obtained with a buried, horizontal rhombic antenna. The theory of the buried rhombic antenna is similar to that of the rhombic in air. The difference between the two cases is that the wavelength on the buried rhombic is considerably reduced, and that the element pattern is changed. Taking these facts into consideration the theory of the rhombic antenna in air can be applied. The length of the legs of the buried rhombic antenna will be shorter, according to the wavelength reduction factor  $p$  which varies approximately from 0.25 to 0.35, and the apex angle will be different from the air case. Thus the overall length of a buried rhombic antenna will be about 1/4 to 1/3 of that in air. Considerable efficiency improvement compared to the half-wave dipole should be possible.

### 6.3.6 Square Antenna

An omnidirectional antenna can be obtained from a circular array of elements which are fed with currents of equal magnitude and a phase which is proportional to the azimuth angle of the element such that a total phase shift of  $360n^\circ$  ( $n=1,2,3$ ) occurs between the first and last element on the circle. This principle is used to develop an omnidirectional buried wire antenna in the following manner.

An insulated cable is bent into a circle and terminated at the end with a resistor equal to the characteristic impedance of the cable. The length of the cable (the perimeter of the circle) is made equal to an integer number of cable-wavelengths. In this manner a traveling wave on the cable is obtained and the phase shift between beginning and end of the cable is a multiple of  $360^\circ$ . This would produce omnidirectional radiation if there would be no attenuation on the antenna cable. Generally there will be some attenuation on the cable; if it is sufficiently small, then the pattern will still be almost omnidirectional. This case will be treated in the next section.

Instead of using a circle one can use a square and obtain a similar effect, however the departure from the ideal omnidirectional pattern will be larger than in the circular case.

#### Feed Arrangement and Current Distribution on Square

The feed arrangement is shown on Figure 6-19. An unbalanced feed from a coax cable is used. The cable has the same characteristic impedance as the insulated, buried antenna wire. The end of the square of wire is adjacent to the feed point and is terminated with a resistor which is also equal to the characteristic impedance of the antenna wire. Thus a traveling wave is produced on the antenna and the input impedance at the feed point is also equal to the characteristic impedance of the antenna. The total length of the antenna wire is equal to an integer multiple of the antenna

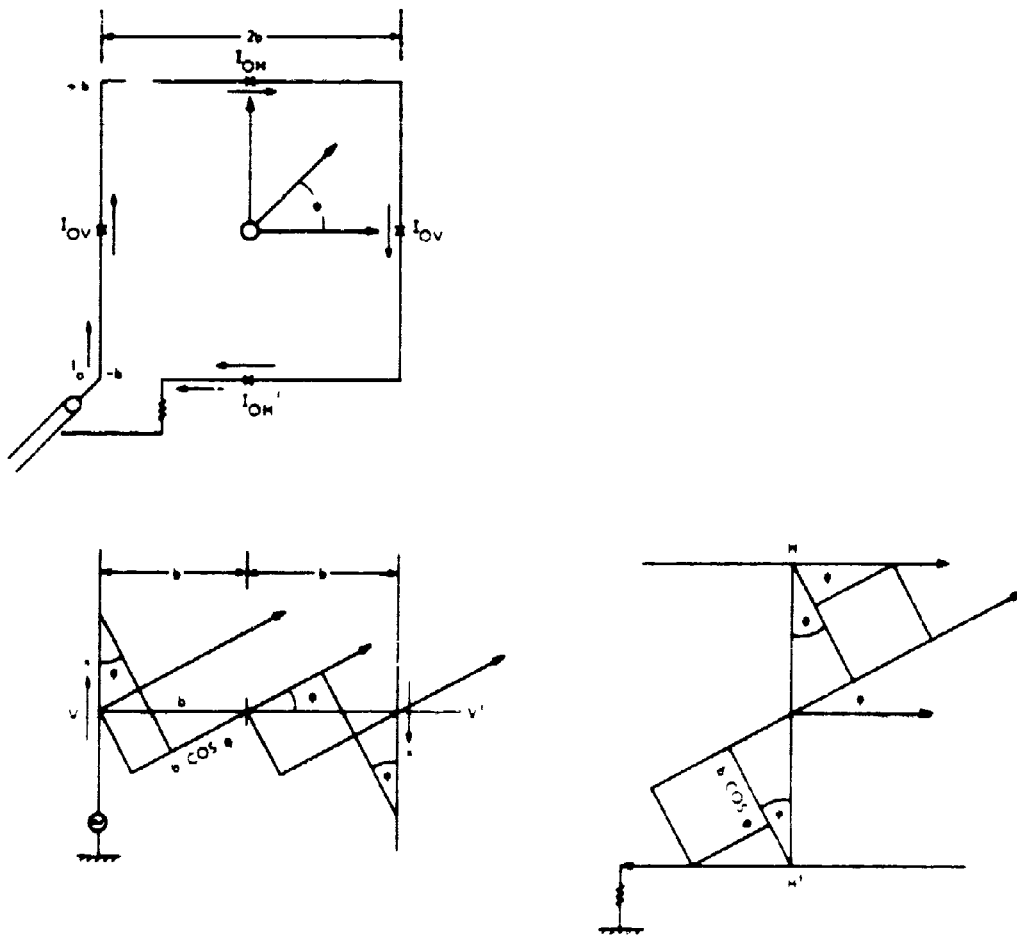


Figure 6-19. Square Antenna - Orientation.

wavelength  $\lambda_c$ . Thus the phase shift along the antenna is a multiple of  $360^\circ$ .

The length of each side of the square is  $2b = 2m\lambda_c$ . The smallest length of one side of the square is  $\frac{\lambda_c}{4} = 2b = 2m\lambda_c$  ( $m = 1/8$ ) to produce a total phase shift of  $360^\circ$ . The four sides of the square are designated as V, V' and H, H'. The currents in the four sides are

$$I_{ov} = I_o e^{-\Gamma b} = I_{oo} \quad (\text{reference current}) \quad (41)$$

$$I_{oH} = I_{oo} e^{-\Gamma 2b} = I_{oo} e^{-2m\alpha\lambda_c} e^{-j4\pi m}$$

$$I_{ov'} = I_{oo} e^{-\Gamma 4b} = I_{oo} e^{-4m\alpha\lambda_c} e^{-j8\pi m}$$

$$I_{oH'} = I_{oo} e^{-\Gamma 6b} = I_{oo} e^{-6m\alpha\lambda_c} e^{-j12\pi m}$$

$2b$  is the length of one side,

$I_o$  = current at feed point.

The positive direction of the currents is indicated by the arrows.

$$\Gamma = \alpha + j\beta = \text{Propagation constant}; \quad b = m\lambda_c; \quad \beta = \frac{2\pi}{\lambda_c}$$

### The Field Pattern

The patterns of the V-element pair and of the H-element pair are calculated separately with reference to the center of the square, and then added to obtain the pattern of the square with traveling wave current distribution.

The field pattern of the two V-elements is

$$\begin{aligned} E_{ov} &= C_v I_{oo} \int_{-b}^b e^{-\Gamma x} e^{-jkD_v} dx \\ &= C_v I_{oo} e^{-jkb} \cos \gamma_H F_{ov} \end{aligned} \quad (42)$$

and

$$E'_{ov} = -C_v I'_{ov} \int_{-b}^b e^{-\Gamma x} e^{+jkD_v} dx \quad (43)$$

$$= -C_v I_{oo} e^{-\Gamma b} e^{+jkb \cos \gamma_H} F'_{ov}$$

with

$$D_v = b \cos \epsilon \cos \psi - x \cos \epsilon \sin \psi$$

$$= b \cos \gamma_H - x \cos \gamma_v$$

and

$$F_{ov} = \int_{-b}^b e^{-\Gamma x} e^{jkx \cos \gamma_v} dx \quad (44)$$

$$F'_{ov} = \int_{-b}^b e^{-\Gamma x} e^{-jkx \cos \gamma_v} dx$$

The field of the V-element group is then

$$E_v = E_{ov} + E'_{ov}$$

$$= C_v I_{oo} \left\{ e^{-jkb \cos \gamma_H} F_{ov} - e^{-\Gamma b} e^{+jkb \cos \gamma_H} F'_{ov} \right\} \quad (45)$$

$$= C_v I_{oo} G_v$$

Similarly the field pattern of the two H-elements is

$$E_{oH} = C_H I_{oo} e^{-\Gamma x} e^{+jkb \cos \gamma_v} F_{oH} \quad (46)$$

and

$$E'_{oH} = C_H I_{oo} e^{-\Gamma b} e^{-jkb \cos \gamma_v} F'_{oH} \quad (47)$$

since

$$\begin{aligned} D_H &= -b \cos \epsilon \sin \psi - x \cos \epsilon \cos \psi \\ &= -b \cos \gamma_v - x \cos \gamma_H \end{aligned}$$

with

$$F_{oH} = \int_{-b}^b e^{-\Gamma x} e^{+j k x \cos \gamma_H} dx \quad (48)$$

$$F_{oH}' = \int_{-b}^b e^{-\Gamma x} e^{-j k x \cos \gamma_H} dx$$

The field of the H-element group is then

$$\begin{aligned} E_H &= E_{oH} + E_{oH}' \quad (49) \\ &= C_H I_{oo} e^{-\Gamma^2 b} \left\{ e^{j k b \cos \gamma_v} F_{oH} - e^{-\Gamma^2 b} e^{-j k b \cos \gamma_v} F_{oH}' \right\} \\ &= C_H I_o e^{-\Gamma^2 b} G_H \end{aligned}$$

The pattern of the square is  $E_v + E_H$  :

$$E^2(\psi, \epsilon) = \sqrt{C\epsilon} G_v + H C\epsilon e^{-\Gamma^2 b} G_H \quad (50)$$

with reference to the current  $I_{oo}$  at the center of the first element.

The integrals  $F_{ov}$ ,  $F_{ov}'$ ,  $F_{oH}$ ,  $F_{oH}'$  are the basic integrals of the straight wire as derived in the previous section

$$F = \int_{-b}^b e^{(A+jB)x} dx ; \text{ or } \int_{-b}^b e^{(A+jB')x} dx$$

with  $A = -\alpha$  ; and  $\frac{B}{B'} = -(1 \mp p \cos \gamma)\beta$

$$F_{ov} = \int_{-b}^b e^{-\Gamma x} e^{jkx \cos \gamma_v} dx = F^+ \text{ using } \gamma_v \quad (51)$$

$$F_{ov}' = \int_{-b}^b e^{-\Gamma x} e^{-jkx \cos \gamma_v} dx = F^- \text{ using } \gamma_v$$

$$F_{oH} = \int_{-b}^b e^{-\Gamma x} e^{jkx \cos \gamma_H} dx = F^+ \text{ using } \gamma_H$$

$$F_{oH}' = \int_{-b}^b e^{-\Gamma x} e^{-jkx \cos \gamma_H} dx = F^- \text{ using } \gamma_H$$

$$G_v = e^{-jkb \cos \gamma_H} F_{ov} - e^{-\Gamma 4b} e^{jkb \cos \gamma_H} F_{ov}' \quad (52)$$

$$G_H = e^{+jkb \cos \gamma_v} F_{oH} - e^{-\Gamma 4b} e^{-jkb \cos \gamma_v} F_{oH}'$$

The basic element pattern in this case are

$$C_{v\epsilon} = k \sin \psi \quad C_{v\psi} = -k \sin \epsilon \cos \psi \quad (53)$$

$$C_{H\epsilon} = k \cos \psi \quad C_{H\psi} = -k \sin \epsilon \sin \psi$$

The angles  $\gamma_v$  and  $\gamma_H$  are defined as

$$\cos \gamma_v = \cos \epsilon \sin \psi \quad (54)$$

$$\cos \gamma_H = \cos \epsilon \sin \psi$$

The field intensity at distance D from the center of the square is obtained as

$$E_e D = 60 I_{oo} f_e(\epsilon, \psi) = 60 I_o e^{-\Gamma b} f_e(\epsilon, \psi) \quad (55)$$

$$E_\psi D = 60 I_{oo} f_\psi(\epsilon, \psi) = 60 I_o e^{-\Gamma b} f_\psi(\epsilon, \psi)$$

The current  $I_o$  is the input current at the feed point. The current  $I_{oo}$  at the center of the first element is  $I_{oo} = I_o e^{-\Gamma b}$ . The feed current  $I_o = \frac{V}{Z_o}$  since an unbalanced feed is used.  $V$  is the unbalanced voltage at the feed point against ground, and  $Z_o$  the characteristic impedance of the buried insulated antenna wire.

Field patterns of  $f_e(\epsilon, \psi)$  for  $E_e$  have been calculated using the same data as for the straight wire and Zig-Zag antenna. The length of one side of the square is  $\frac{\lambda}{4}$  and  $\frac{\lambda}{2}$ , so that the total phase shift around the antenna is  $360^\circ$  and  $720^\circ$ , respectively. The azimuthal patterns are in Figure 6-20, the elevation patterns in Figure 6-21. The azimuthal pattern for the first case ( $\frac{\lambda}{4}$  side length) is almost circular, the maximum and minimum values of  $f_e(0, \psi)$  being

$f_e(0, \psi)_{\max}$	= 0.769	at $\psi = 80^\circ$	
	= 0.757	at $\psi = 280^\circ$	
			Average
$f_e(0, \psi)_{\min}$	= 0.672	at $\psi = 190^\circ$	$f_e(0, \psi) = 0.72$
	= 0.683	at $\psi = 350^\circ$	

The fluctuation is  $0.72 \pm 0.048$  or  $\pm 6.7$  percent.

Inspecting the second case ( $\frac{\lambda}{2}$  side length) shows that the azimuthal pattern is no longer omnidirectional, but very irregular, and the field intensities are lower in every direction than in the  $\frac{\lambda}{4}$  case. This pattern is therefore of no interest. The square with a total length of one wavelength  $\lambda_c$ , producing  $360^\circ$  total phase shift is optimum. A similar result is obtained for the circle, as will be shown in the following section.



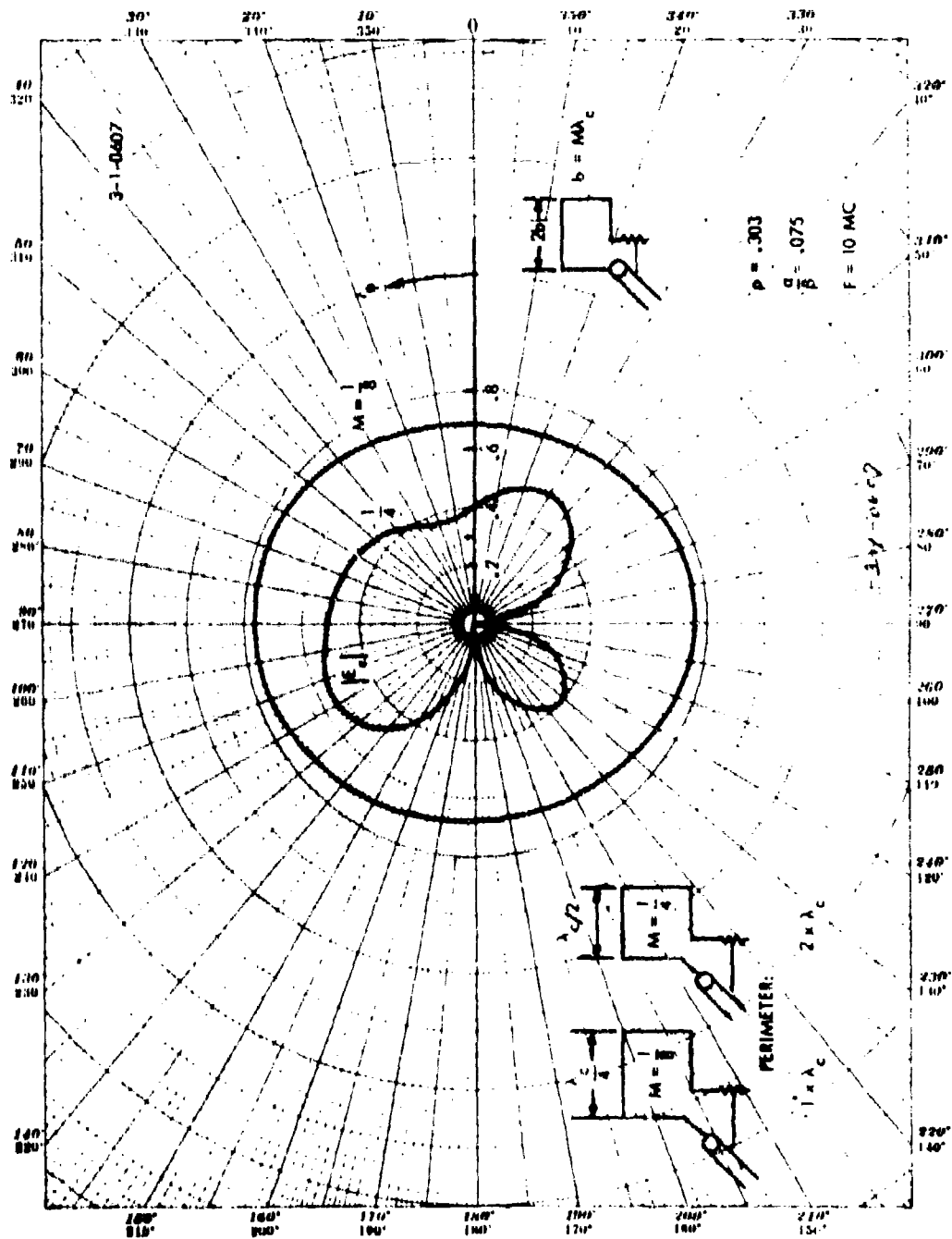


Figure 6-20. Square Antenna - Azimuthal Patterns  $|E_c|$

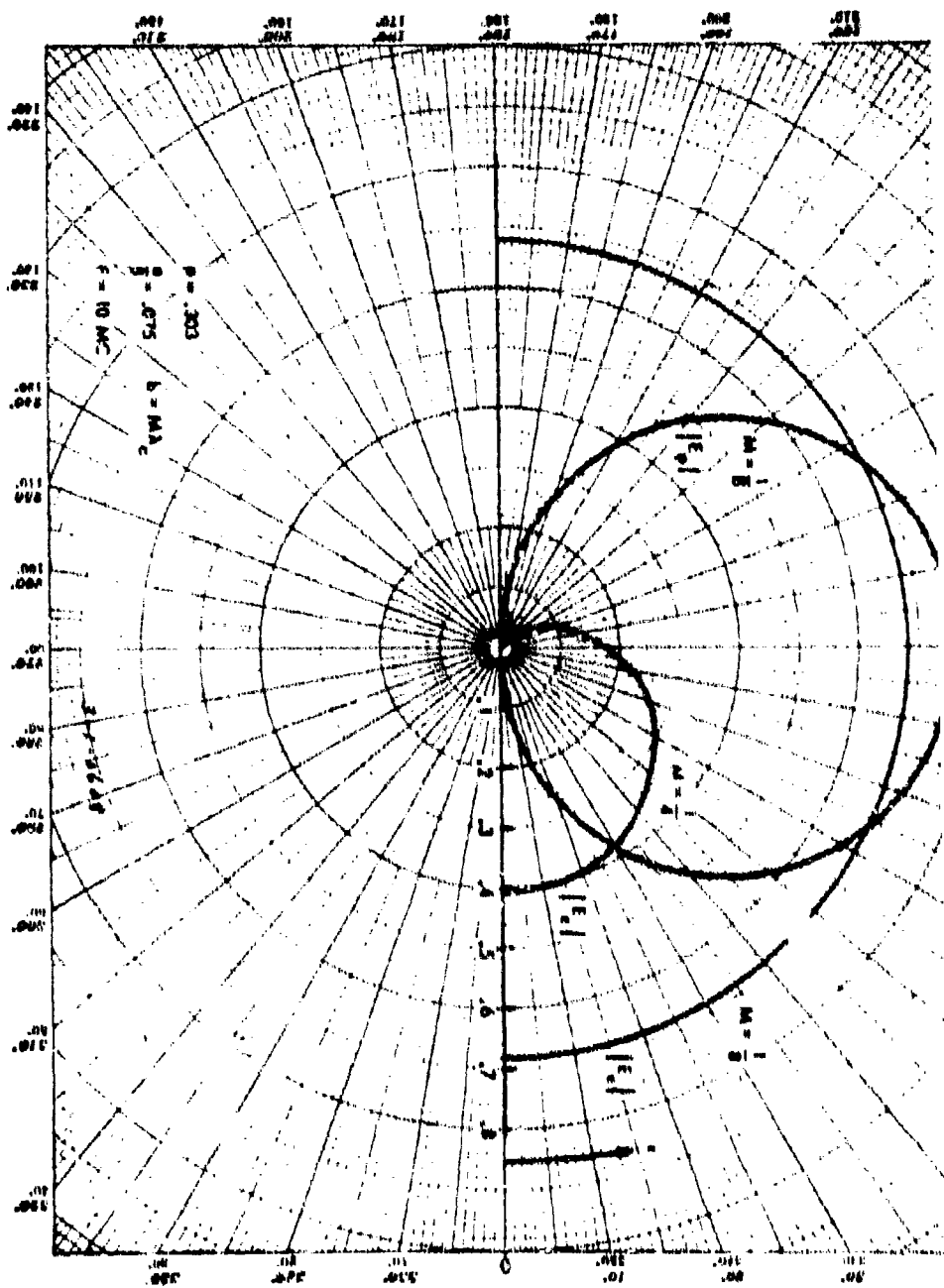


Figure C-21. Square Antenna - Elevation Patterns,  $|E_\phi|$ ,  $|E_\theta|$

The efficiency of the one-way length square will be compared to that of a crossed folded monopole pair. The attenuation of the square is  $\frac{\alpha}{\beta} = 0.075$ ; whereas the attenuation of the folded dipole is taken twice as large: for the dipole  $\frac{\alpha}{\beta} = 0.15$  due to mutual coupling effects which do not exist in the square where all four sides are  $\lambda_c/4$  apart. The percent power loss in the terminating resistor is

$$e^{-2\alpha\lambda_c} = e^{-\frac{\alpha}{\beta} 2\beta\lambda_c} = e^{-\frac{\alpha}{\beta} 2.3\pi} = e^{-0.3\pi} = 0.391 \text{ or } 39 \text{ percent.}$$

This energy can be regained by using a terminating network which does not use a resistor, and connecting the terminal with the feedpoint. In this manner only the losses along the antenna wire need be supplied by the source. The efficiency for the two cases is as follows:

$$\begin{aligned} \text{With terminating resistor} \quad \eta_2 &= \frac{\eta_0}{1.5} = \frac{\eta_0 \eta}{1.5} \frac{|r_a|^2}{|r_d|^2} \\ &= \frac{0.15\pi}{1.5} \quad 0.72^2 \times 2.04 = 0.46 \text{ or } 46 \text{ percent} \end{aligned}$$

$$\text{Without terminal loss} \quad \eta_2 = \frac{\eta_0}{1.5} \frac{1}{1-0.39} = 0.75 \text{ or } 75 \text{ percent.}$$

Thus the efficiency is increased by about 66 percent if the terminal loss is eliminated. Other ways of increasing the efficiency are discussed in the section on the circle antenna.

### Conclusion

The square gives a good omnidirectional azimuthal pattern if the perimeter is equal to one antenna wavelength. The fluctuation of field intensity on the ground plane is about  $\pm 7$  percent. The efficiency of this antenna varies from 45 to 75 percent of that of a crossed folded dipole point. The higher value is obtained when the terminal loss through a terminating resistor is avoided.

### 6.3.7 Circle Antenna

The feed arrangement is the same as that of the square (Figure 6-22). An unbalanced feed from a coax cable is used. The end of the circle of wire is adjacent to the feed point and is terminated with a resistor to produce a traveling wave. The total length of the antenna wire is equal to an integer multiple of the antenna wavelength  $\lambda_0$ , so that the phase shift along the antenna is a multiple of  $360^\circ$ .

The coordinate system is indicated on Figure 6-22. The azimuthal angle is  $\psi$ , the elevation angle is  $\epsilon$ . The loop is in a horizontal plane, buried a few feet below the ground. The feed point is at  $\psi = 0$ , the current flows counterclockwise around the circle. The current at any point on the circle is

$$I = I_0 e^{-j\gamma\theta} \quad | \quad \Gamma = \alpha + j\beta$$

The angle  $\theta$  determines the position of point P on the circle. The far field from the current element has two components; a vertical component  $E_\epsilon$  and a horizontal component  $E_\psi$ .

$$dE_\epsilon D = 60 k I(l) dl e^{-jkD} \cos \Delta \quad (56)$$

$$dE_\psi D = -60 k I(l) dl e^{-jkD} \sin \Delta \sin \epsilon$$

$D$  is the distance from point P on the circle to the far field point,  
 $D_0$  is the distance from the center of the circle,

$$D = D_0 + r \sin(\theta - \phi) \cos \epsilon.$$

The wire element  $dl = r d\theta$

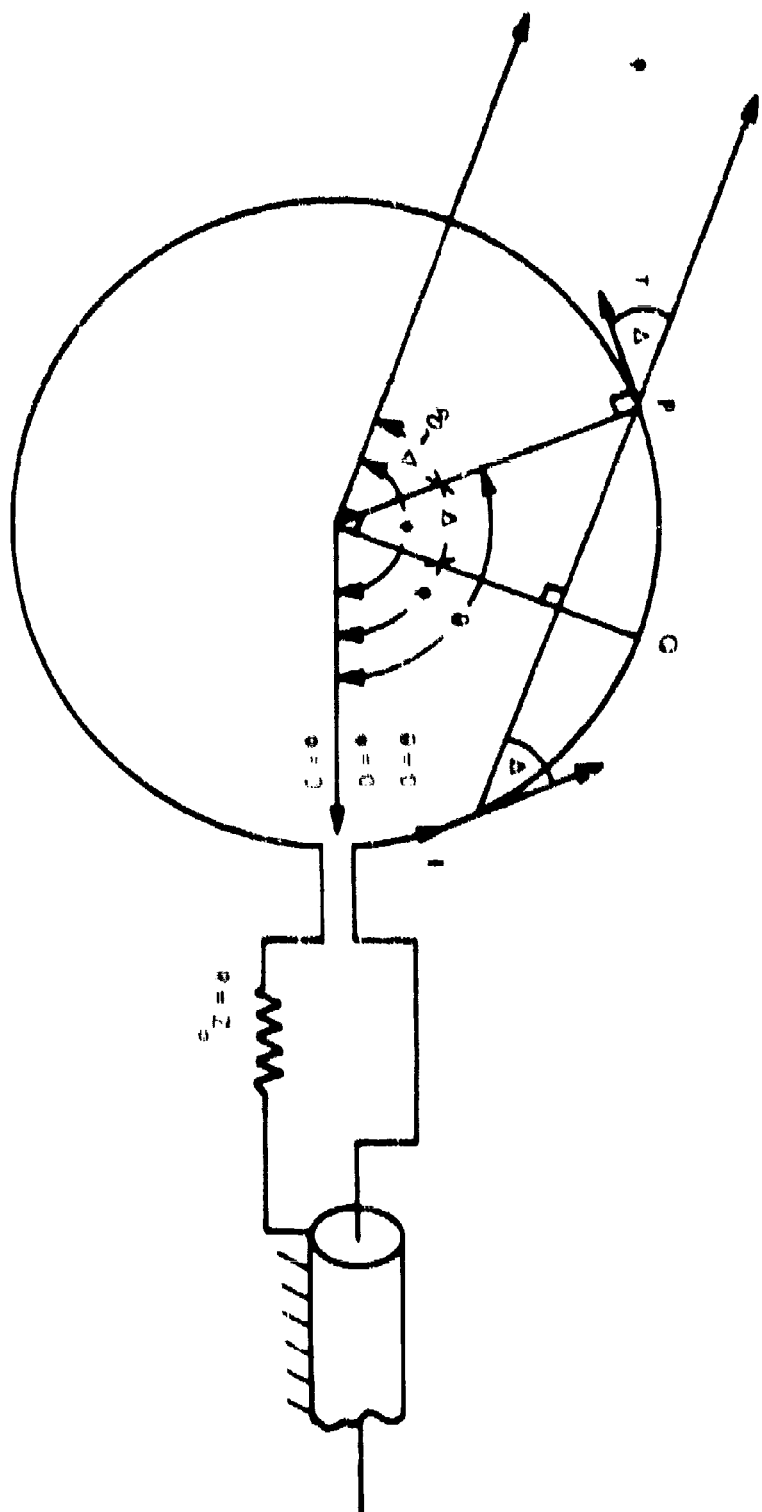


Figure 6-22. Circle Around - Center of an

3-1-5609

The relation between the angles  $\Delta$ ,  $\psi$ , and  $\theta$  is:

$$\phi = \psi - \frac{\pi}{2}; \Delta = \theta - \phi = \theta - \psi + \frac{\pi}{2}$$

$$\text{Thus } E_z D = (60k I_0) \int_0^{2\pi} \cos(\theta - \phi) e^{-\Gamma r \theta} e^{jkr \sin(\theta - \phi) \cos \epsilon} r d\theta \quad (57)$$

$$-E_\psi D = (60k I_0 \sin \epsilon) \int_0^{2\pi} \sin(\theta - \phi) e^{-\Gamma r \theta} e^{jkr \sin(\theta - \phi) \cos \epsilon} r d\theta$$

The following symbols are used:  $2\pi r = n \lambda_c$   $r = \frac{n}{\beta}$   $\beta = \frac{2\pi}{\lambda_c}$

$$A_1 = 60 k I_0 \quad (58)$$

$$A_2 = 60 k I_0 \sin \epsilon$$

$n = 1, 2, 3$  i.e., the perimeter of the circle is an integral number of wavelengths  $\lambda_c$ .

$$\Gamma r = (\alpha + j\beta) \frac{n}{\beta} = \left(\frac{\alpha}{\beta} + j\right) n = \alpha n + jn = a + jn \quad (59)$$

$$\alpha n = \frac{\alpha}{\beta} n = a$$

$$kr = \frac{2\pi r}{\lambda_0} = \beta r p = n p$$

$$p = \frac{\lambda_c}{\lambda_0} = \frac{k}{\beta}$$

$$kr \cos \epsilon = n p \cos \epsilon = nq; q = p \cos \epsilon$$

$$\Gamma r = (\alpha + j\beta) r = \left(\frac{\alpha}{\beta} + j\right) \beta r = \left(\frac{\alpha}{\beta} + j\right) n p$$

Using these symbols the integrals are

$$E_{\epsilon} D = \frac{A_1 n}{\beta} \int_0^{2\pi} \cos(\theta - \phi) e^{-a\theta} e^{-j[n\theta - z \sin(\theta - \phi)]} d\theta \quad (60)$$

$$-E_{\psi} D = A_2 \frac{n}{\beta} \int_0^{2\pi} \sin(\theta - \phi) e^{-a\theta} e^{-j[n\theta - z \sin(\theta - \phi)]} d\theta$$

The two integrals are similar, with the exception of the  $\cos(\theta - \phi)$  and  $\sin(\theta - \phi)$  terms. The  $E_{\epsilon}$  component will be evaluated. With a new variable  $\psi = (\pi + \phi) - \theta$  we get

$$E_{\epsilon} = \frac{A_1 n}{\beta} e^{-a(\pi + \phi)} e^{-jn(\pi + \phi)} \int_{\phi + \pi}^{\phi - \pi} \cos \psi e^{+a\psi} e^{j[n\psi + z \sin \psi]} d\psi \quad (61)$$

The integral can be written as

$$\begin{aligned} & \int_{\phi + \pi}^{\phi - \pi} e^{a\psi} \cos \psi [\cos n\psi + j \sin n\psi] e^{jz \sin \psi} d\psi \\ &= \frac{1}{2} \int_{\phi + \pi}^{\phi - \pi} e^{a\psi} [e^{j(n+1)\psi} + e^{j(n-1)\psi}] e^{jz \sin \psi} d\psi \end{aligned} \quad (62)$$

For the case  $a = 0$ , the factor  $e^{a\psi} = 1$  and the remaining integral is the sum of two Bessel functions, since

$$J_n(z) = \frac{e^{-jn\pi}}{2\pi} \int_{-\pi/2}^{3\pi/2} e^{jz \sin \beta} e^{jn\beta} d\beta$$

Thus for  $\phi = \frac{\pi}{2}$  and  $e^{a\psi} = 1$  we obtain

$$\begin{aligned} E_{\epsilon} &= \frac{A_1 n}{\beta} e^{-(a+jn)\pi} \frac{3\pi}{2} e^{-j\pi n} \left\{ J_{n+1}(z) + J_{n-1}(z) \right\} \\ &= \frac{A_1 n}{\beta} \pi e^{-j\pi n} \frac{5}{2} \frac{2n}{z} J_n(z) \end{aligned} \quad (63)$$

The magnitude of  $E_e$  is

$$|E_e| \approx 60 I_0 \pi p n \frac{2n}{z} J_n(z) \quad (64)$$

Since  $z = np \cos \epsilon$  is independent of  $\psi$ , the pattern is omnidirectional in azimuth.

The case of finite attenuation is treated in the Appendix A. The result is:

$$E_e = \frac{A_1 n}{\beta} B \quad (65)$$

$$= \frac{A_1 n}{\beta} (-1)^n e^{-jn(\pi+\phi)} {}_0F_0(R_n + j S_n)$$

$$\text{with } {}_0F_0 = \frac{1 - e^{-2a\pi}}{2a\pi} \approx 1 - \frac{2a\pi}{2} + \frac{(2a\pi)^2}{6} - + \dots \quad (66)$$

$$\text{and } B_{rn} = R_n + j S_n \quad (67)$$

The pattern function is

$$f(\psi, \epsilon) = \frac{k n}{\beta} B = np\pi e^{-jn(\pi+\phi)} {}_0F_0(R_n + j S_n) \quad (68)$$

For the case  $n = 1$ , with the perimeter of the circle equal to one wavelength  $\lambda_c$ ,  $R_1$  and  $S_1$  are given as



$$\begin{aligned}
 R_1 = & J_0(z) \left[ 1 + a \frac{a \cos 2\phi + 2 \sin 2\phi}{a^2 + 4} \right] \\
 & + J_2(z) \left[ 1 + 2a \frac{a \cos 2\phi + 2 \sin 2\phi}{a^2 + 4} + a \frac{a \cos 4\phi + 4 \sin 4\phi}{a^2 + 16} \right] \\
 & + a \sum_{m=1}^{\infty} J_{2m-1}(z) \left[ \frac{a \cos (2m-3)\phi + (2m-3) \sin (2m-3)\phi}{a^2 + (2m-3)^2} \right. \\
 & \quad \left. + \frac{a \cos (2m+1)\phi + (2m+1) \sin (2m+1)\phi}{a^2 + (2m+1)^2} \right]
 \end{aligned} \tag{69}$$

$$\begin{aligned}
 & + a \sum_{m=2}^{\infty} J_{2m}(z) \left[ 2 \left( \frac{a \cos 2m\phi + 2m \sin 2m\phi}{a^2 + 4m^2} \right) \right. \\
 & \quad + \frac{a \cos 2(m-1)\phi + 2(m-1) \sin 2(m-1)\phi}{a^2 + 4(m-1)^2} \\
 & \quad \left. + \frac{a \cos 2(m+1)\phi + 2(m+1) \sin 2(m+1)\phi}{a^2 + 4(m+1)^2} \right]
 \end{aligned}$$

$$\begin{aligned}
 S_1 = & aJ_0(z) \left[ \frac{a \sin 2\phi - 2 \cos 2\phi}{a^2 + 4} \right] \\
 & + aJ_2(z) \left[ \frac{a \sin 4\phi - 4 \cos 4\phi}{a^2 + 16} \right]
 \end{aligned} \tag{70}$$

$$\begin{aligned}
 & - a \sum_{m=1}^{\infty} J_{2m-1}(z) \left[ 2 \left( \frac{a \sin (2m-1)\phi - (2m-1) \cos (2m-1)\phi}{a^2 + (2m-1)^2} \right) \right. \\
 & \quad + \left( \frac{a \sin (2m+1)\phi - (2m+1) \cos (2m+1)\phi}{a^2 + (2m+1)^2} \right) \\
 & \quad \left. + \frac{a \sin (2m-3)\phi - (2m-3) \cos (2m-3)\phi}{a^2 + (2m-3)^2} \right]
 \end{aligned}$$

$$+ a \sum_{m=2}^{\infty} J_{2m}(z) \left[ \frac{a \sin 2(m+1)\phi - 2(m+1) \cos 2(m+1)\phi}{a^2 + 4(m+1)^2} \right.$$

$$\left. + \frac{a \sin 2(m-1)\phi - 2(m-1) \cos 2(m-1)\phi}{a^2 + 4(m-1)^2} \right]$$

Formulas (69) and (70) have been numerically computed, using the following parameters

$$\begin{array}{llll} n = 1 & \sigma = 0.01 & f = 10 \text{ mc} & \lambda_0 = 30 \text{ m} \\ \alpha = 0.081 & \beta = 0.69 & & \lambda_c = 9.09 \text{ m} \\ \frac{E}{E_0} = 0.075 & \rho = \frac{\lambda_c}{\lambda_0} = \frac{k}{\beta} = 0.303 & & \end{array}$$

The  $E_z$  patterns are plotted on Figures 6-23 and 6-24. The azimuthal pattern of  $|E_z|$  is almost circular, with maximum fluctuation of  $2.48 \pm 0.105$  or  $\pm 4.25$  percent. The average field intensity on the ground ( $z = 0$ ) is

$$|E_z|_0 = I_0 60 \text{ p } 2.48 = 60 I_0 \times 0.751$$

There are two maxima and two minima of field intensity, which are not equal:

$\psi$	E max	E min
40°		2.37
140°	2.58	
230°		2.40
310°	2.56	

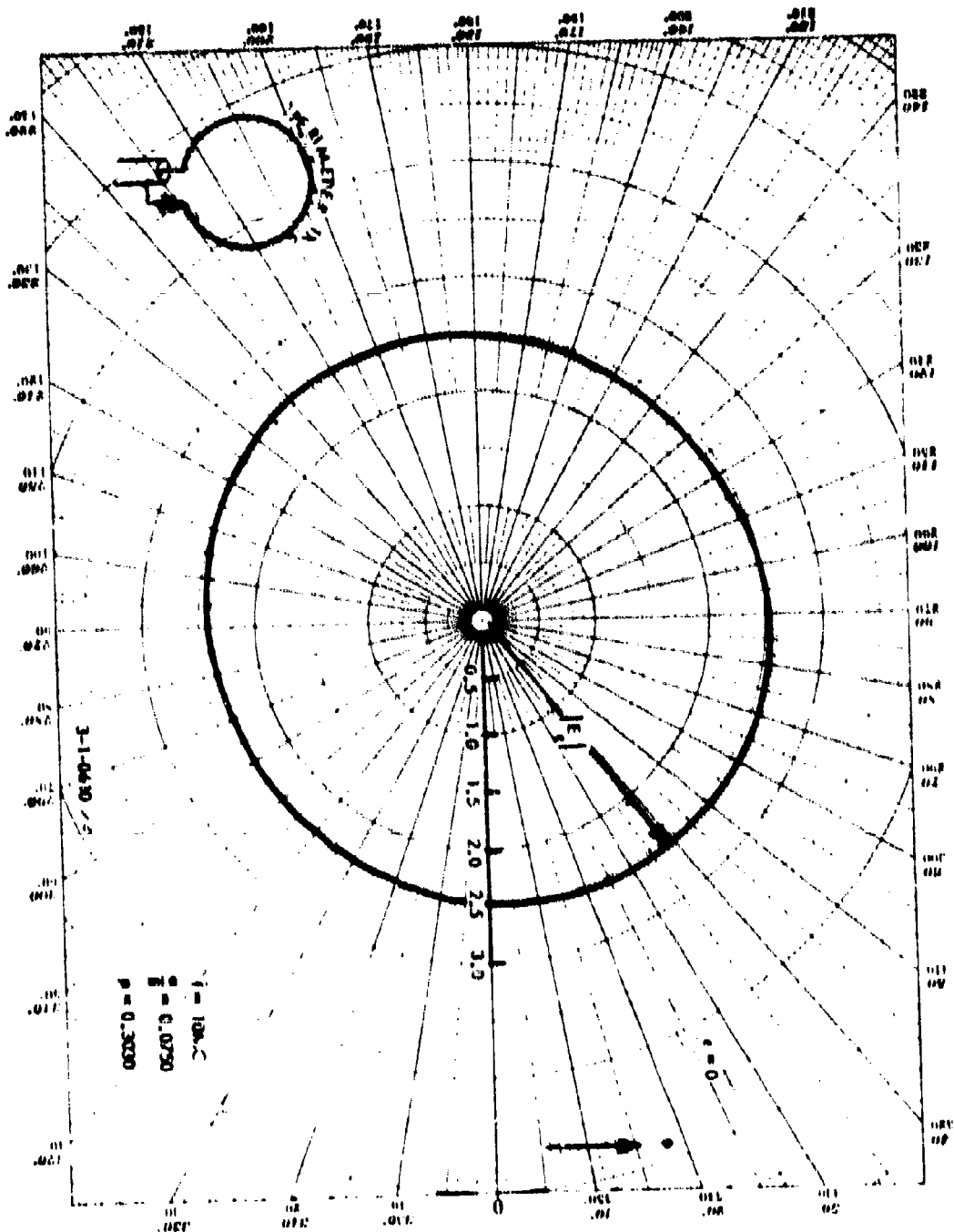
The elevation pattern of  $|E_z|$  in the  $\psi = 0$  plane is practically semicircular, the maximum fluctuation is  $2.495 \pm 0.015$  or  $\pm 0.6$  percent.

The imaginary part  $S_1$  is always small, since all terms are multiplied by  $a$ , which is generally a small quantity ( $a \ll 1$ ). The main contribution to the real part  $R_1$  is from the terms with  $J_0(z)$  and  $J_2(z)$ , since these are the only terms which have a part which is not multiplied by  $a$ .

For  $a = 0$  we have

$$(-1)^{n+1} R_n = J_{n-1}(z) + J_{n+1}(z) = \frac{2n}{z} J_n(z) \quad (71)$$

Figure 6-23. Circle Antenna Azimuthal Pattern  $|E_z|$



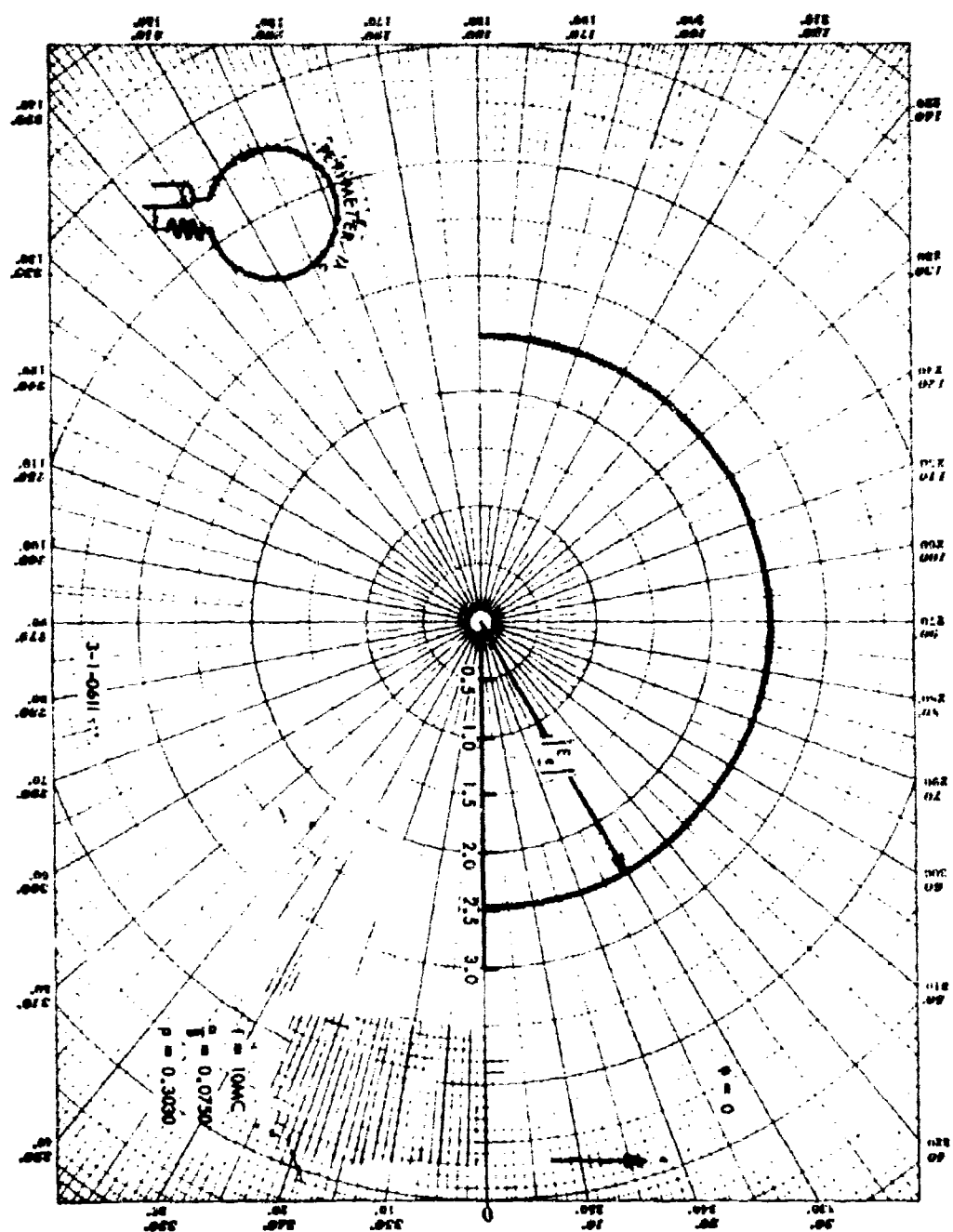


Figure 6-24. Circle Antenna - Elevation Pattern  $E$



Thus for small attenuation the field pattern for the vertical component  $E_\epsilon$  is mainly determined by  $J_n(z)$ . The pattern is nearly omnidirectional in azimuth, independent of  $n$ , as long  $n = \frac{2\pi}{\lambda_c}$  is an integer, since  $z$  is independent on  $\psi$ .

The elevation pattern depends on  $n$  since  $z = k r \cos \epsilon = np \cos \epsilon$  is a function of  $\epsilon$ .

Using the approximation for  $R_n$  which obtains for  $a \ll 1$  the field intensity on the ground is obtained as

$$\begin{aligned} E_\epsilon D &= \frac{A_1 n}{\beta} B \\ &= (-1)^n \frac{A_1 n}{\beta} \pi F_0 (R_n + j S_n) \end{aligned} \quad (72)$$

disregarding the phase factor  $e^{-jn(\pi+\phi)}$

With

$$S_n = 0 \quad R_n = \frac{2n}{z} J_n(z)$$

we get

$$\begin{aligned} E_\epsilon D &= (-1)^n \frac{A_1 n}{\beta} \pi \frac{2n}{z} F_0 J_n(z) \\ &= (-1)^n 60 I_0 2\pi n F_0 J_n(np) \end{aligned} \quad (73)$$

For  $\cos \epsilon = 1$

$$F_0 = \frac{1 - e^{-2n\pi s}}{2n\pi s} \quad (74)$$

This is the same result as was obtained for  $a = 0$  except that the factor  $F_0$  is now added.

The pattern function is therefore

$$f_c(\Psi, \epsilon) = 2 \pi n F_0 \frac{J_n(np \cos \epsilon)}{\cos \epsilon} \quad (75)$$

Equation (73) gives the maximum value of field intensity  $E_c$ , since the effect of attenuation on the antenna wire on  $B_{rn} = R_n + jS_n$  was neglected. But the formula is useful to determine the effect of the diameter of the circle; i.e., the effect of  $n$  and the general effect of attenuation  $a = \frac{\alpha}{\beta}$  on.

The field intensity  $E_c$  decreases as  $n$  is increased.  $E_c$  has its greatest value for  $n = 1$ . The perimeter of the antenna is then equal to one wavelength  $\lambda_c$  and the radius  $r = \frac{\lambda_c}{2\pi}$ .

The effect of attenuation is mainly determined by  $F_0 = \frac{1 - e^{-2a\pi}}{2\pi a}$ .

This factor describes the decline of field intensity with increasing attenuation  $a$ . This is due to the fact that the current along the antenna decreases when attenuation is present. For no attenuation ( $a = 0$ ) the current remains constant and  $F_0$  has its maximum value  $F_0 = 1$ . As  $a$  increases the average current on the antenna gets smaller and  $F_0$  decreases.

There is another effect caused by attenuation. The energy which is dissipated in the terminating resistor at the end of the antenna depends on the attenuation:

$$P_r = I_r^2 Z_0 = \left[ I_0 e^{-\alpha \lambda_c} \right]^2 = I_0^2 e^{-4\pi a}$$

This energy is lost in the resistor. The higher the attenuation the lower the lost power, because the current in the terminating resistor is lower if the attenuation is high. Only the difference between input and output power is used for radiation. This difference is

$$\begin{aligned} P_\Delta &= P_{in} - P_r = I_0^2 Z_0 - I_0^2 e^{-4\pi a} Z_0 \\ &= I_0^2 Z_0 (1 - e^{-4\pi a}) \end{aligned}$$

The current corresponding to  $P_{\Delta}$  is then

$$i_o = \sqrt{\frac{P_{\Delta}}{Z_o}} \sqrt{\frac{1}{1-e^{-4\pi a}}} \quad (76)$$

and the field intensity for this case is

$$E_{\epsilon D} \approx 60 \quad 2\pi \sqrt{\frac{P_{\Delta}}{Z_o}} \frac{1-e^{-2\pi a}}{2\pi a \sqrt{1-e^{-4\pi a}}} \quad (77)$$

This is a case where no power is lost at the output of the antenna, so that only the power lost through attenuation along the antenna is supplied to the antenna. In this manner the field intensity can be increased by the factor  $K = \frac{1}{\sqrt{1-e^{-4\pi a}}}$ , and the efficiency is increased by  $K^2$ . Following is a tabulation of  $F_o^2$  and  $K^2$  for various values of  $a$ :

$a$	$e^{-4\pi a}$	$1-e^{-4\pi a}$	$K^2$	$F_o^2$	$F_o^2 K^2$
0.05	0.532	0.468	2.14	0.74	1.58
0.075	0.389	0.611	1.64	0.64	1.05
0.10	0.285	0.715	1.40	0.55	0.77
0.15	0.152	0.848	1.18	0.42	0.492
0.20	0.081	0.919	1.09	0.325	0.354
0.25	0.043	0.957	1.04	0.254	0.265

The column  $e^{-4\pi a}$  gives the current at the end of the antenna relative to the current at the input.  $K^2$  indicates the possible increase in efficiency for the no-resistor case, and  $(F_o K)^2$  the total field intensity factor. Practical cases for  $a = \frac{\alpha}{\beta}$  range from about 0.05 to 0.15. Thus efficiency increases from 20 percent to over 100 percent are possible. It is also evident that the increase in efficiency becomes very small when  $a > 0.15$ , so that the no-resistor method is not longer worthwhile.

Another method to increase the efficiency is to use multiple turn loops. In order to keep all the turns in the same horizontal plane a spiral



can be employed. Using  $N$  turns of approximately equal diameter ( $d = \frac{\lambda_c}{\pi}$ ) the field intensity is

$$E D \cong 60 \quad 2\pi \quad I_o J_1(p) \quad F_o \quad \left[ 1 + e^{-2a\pi} + e^{-4a\pi} + e^{-6a\pi} + \dots + e^{-2a\pi(N-1)} \right]$$

$$= 120 \pi \quad I_o J_1(p) \quad F_o \quad \frac{1 - e^{-2\pi a N}}{1 - e^{-2\pi a}} = 120 \pi \quad I_o J_1(p) F_o X \quad (78)$$

For example, with  $a = 0.075$  and  $N = 4$  the field improvement factor

$$X = \frac{1 - e^{-0.6\pi}}{1 - e^{-0.15\pi}} = \frac{.85}{.375} = 2.26 \quad (79)$$

and in the limiting case  $N \rightarrow \infty$

$$X = \frac{1}{1 - e^{-0.15\pi}} = \frac{1}{.375} = 2.68$$

However if the turns are close together the attenuation will increase through mutual coupling between the turns. If the separation between the turns is one skin depth then the attenuation is approximately doubled. The following table lists the efficiency improvement, which is proportional to  $(F_o X)^2$ , for  $N = 1, 2, 4$ , for  $a = 0.075$  and  $a = 0.15$

$a$	$F_o$	$X$	$(F_o X)^2$	$X$	$(F_o X)^2$	$X$	$(F_o X)^2$
0.075	0.8	1	0.64	1.62	1.66	2.26	3.27
0.15	0.648	1	0.42	1.39	0.81	1.6	1.08
$N = 1$				$N = 2$		$N = 4$	

This shows that the relative efficiency improvement when using 2 or 4 turns with  $a = 0.15$  compared to the efficiency of one turn and half the attenuation ( $a = .075$ ) is  $\frac{0.81}{0.64} = 1.26$  and  $\frac{1.08}{0.84} = 1.69$  respectively. The efficiency ratio in this case is, according to (13) and (8),

$$\eta_2 = \frac{\eta_o}{1.5} = \frac{2}{3} \pi \frac{\alpha_d}{\beta} \frac{|f_T(\phi_m, o)|^2}{|f_d(\phi, o)|^2} \quad (80)$$

$$\text{where } f_d(\phi, 0) = \frac{2p}{1-p^2} \cos\left(\frac{\pi}{2} p\right)$$

Using the typical data (same data as before)  $p = \frac{\lambda_c}{\lambda_0} = 0.303$  we obtain

$$f_d(0, 0) = 0.593$$

A typical value of  $\frac{\alpha}{\beta}$  for a single wire is 0.075. For the folded dipole with a separation between wires of one skin depth the attenuation is doubled:  $\frac{\alpha_d}{\beta} = 2 \times 0.075 = 0.15$ . Thus the efficiency ratio is

$$\eta_2 = \frac{2}{3} \pi \frac{0.15}{0.593^2} \left| f_T(\phi_m, 0) \right|^2 = 0.893 \left| f_T(\phi_m, 0) \right|^2$$

The average value of ground field intensity of the circle antenna for  $a = \frac{\alpha}{\beta} = 0.075$  and  $p = 0.303$  is

$$\left| E_{\epsilon} \right|_0 = 60 I_0 \times 0.751$$

Thus  $\left| f(\Psi_{av}, 0) \right| = 0.751$  and

$$\eta_0 = 0.893 \times 0.751^2 = 0.5$$

If the antenna is fed from both ends, so that the resistor loss is avoided, the efficiency is improved by 1.64 (see table page 58,  $K^2 = 1.64$  for  $a = 0.075$ ) the efficiency ratio is then

$$\eta_{20} = 0.5 \times 1.64 = 0.82$$

### Conclusion

The circle of one wavelength perimeter is superior to the square antenna of the same perimeter. The azimuthal pattern of the field intensity on the ground has a fluctuation of  $\pm 4.25$  percent. The efficiency of the circle antenna varies from 50 percent to 82 percent of that of a crossed

folded dipole pair, the higher value corresponds to the case of no loss in the terminal resistor. By using more than one turn the efficiency ratio can be further increased to an amount about equal of that of a folded dipole pair.

### 6.3.8 Field Pattern of Circular Antenna with Finite Attenuation

The integral (62) in Section 6.3.7 for the case of finite attenuation is split into four parts.

The  $E_\epsilon$  field component is given as

$$E_\epsilon D = \frac{A_1 n}{\beta} e^{-a(\pi + \phi)} e^{-jn(\pi + \phi)} B_r = \frac{A_1 n}{\beta} B \quad (A-1)$$

$$B_r = \frac{1}{2} \left\{ \int_{\phi+\pi}^{\phi-\pi} e^{a\psi} \cos(n-1)\psi e^{jz \sin \psi} d\psi \right.$$

$$+ \int_{\phi+\pi}^{\phi-\pi} e^{a\psi} \cos(n+1)\psi e^{jz \sin \psi} d\psi \quad (A-2)$$

$$+ \int_{\phi+\pi}^{\phi-\pi} e^{a\psi} \sin(n+1)\psi e^{jz \sin \psi} d\psi$$

$$\left. + \int_{\phi+\pi}^{\phi-\pi} e^{a\psi} \sin(n-1)\psi e^{jz \sin \psi} d\psi \right\}$$

These integrals are expanded with the use of the Jacobi-Anger formula:

$$e^{jz \sin \psi} = J_0(z) + 2 \sum_{m=1}^{\infty} J_{2m}(z) \cos 2m \psi$$

$$+ j 2 \sum_{m=1}^{\infty} J_{2m-1}(z) \sin(2m-1) \psi \quad (A-3)$$

Evaluation of these integrals give the following result:

$$\begin{aligned}
B &= e^{-a(\pi+\phi)} e^{-jn(\pi+\phi)} B_r \\
B_r &= e^{a\phi} \frac{e^{-a\pi} - e^{-a\pi}}{2a} B_{ro} \\
B &= -e^{-jn(\pi+\phi)} \pi \frac{1-e^{-2a\pi}}{2a\pi} B_{rn} \\
&= (-1)^n e^{-jn(\pi+\phi)} \pi F_o (R_n + j S_n)
\end{aligned} \tag{84}$$

with

$$F_o = \frac{1-e^{-2a\pi}}{2a\pi} \cong 1 - \frac{2a\pi}{2} + \frac{(2a\pi)^2}{6} - + \dots \tag{85}$$

and

$$B_{rn} = R_n + j S_n \tag{86}$$

$R_n$  and  $S_n$  are as follows:

$$\text{The real part of } \left( \frac{B_{rn}}{a} \right) \text{ is} \tag{87}$$

$$\begin{aligned}
(-1)^{n+1} \frac{R_n}{a} &= + J_o(z) \left[ \frac{a \cos (n-1)\phi + (n-1) \sin (n-1)\phi}{a^2 + (n-1)^2} \right. \\
&\quad \left. + \frac{a \cos (n+1)\phi + (n+1) \sin (n+1)\phi}{a^2 + (n+1)^2} \right] \\
&\quad - \sum_{m=1}^{\infty} J_{2m-1}(z) \left[ - \left( \frac{a \cos (2m-n)\phi + (2m-n) \sin (2m-n)\phi}{a^2 + (2m-n)^2} \right) \right. \\
&\quad \left. + \left( \frac{a \cos (2m+n-2)\phi + (2m+n-2) \sin (2m+n-2)\phi}{a^2 + (2m+n-2)^2} \right) \right] .
\end{aligned}$$

$$\begin{aligned}
& - \left( \frac{a \cos (2m-n-2)\phi + (2m-n-2) \sin (2m-n-2)\phi}{a^2 + (2m-n-2)^2} \right) \\
& + \left( \frac{a \cos (2m+n)\phi + (2m+n) \sin (2m+n)\phi}{a^2 + (2m+n)^2} \right) \Big] \\
& + \sum_{m=1}^{\infty} J_{2m}(z) \frac{a \cos (2m-n+1)\phi + (2m-n+1) \sin (2m-n+1)\phi}{a^2 + (2m-n+1)^2} \\
& + \frac{a \cos (2m+n-1)\phi + (2m+n-1) \sin (2m+n-1)\phi}{a^2 + (2m+n-1)^2} \\
& + \frac{a \cos (2m-n-1)\phi + (2m-n-1) \sin (2m-n-1)\phi}{a^2 + (2m-n-1)^2} \\
& + \frac{a \cos (2m+n+1)\phi + (2m+n+1) \sin (2m+n+1)\phi}{a^2 + (2m+n+1)^2}
\end{aligned}$$

The imaginary part of  $\left(\frac{B_{rn}}{a}\right)$  is

$$(-1)^{n+1} \frac{S_n}{a} = + J_0(z) \frac{a \sin (n-1)\phi - (n-1) \cos (n-1)\phi}{a^2 + (n-1)^2} \quad (88)$$

$$+ \frac{a \sin (n+1)\phi - (n+1) \cos (n+1)\phi}{a^2 + (n+1)^2}$$

$$\begin{aligned}
& - \sum_{m=1}^{\infty} J_{2m-1}(z) \frac{a \sin (2m+n-2)\phi - (2m+n-2) \cos (2m+n-2)\phi}{a^2 + (2m+n-2)^2} \\
& + \frac{a \sin (2m-n)\phi - (2m-n) \cos (2m-n)\phi}{a^2 + (2m-n)^2} \\
& + \frac{a \sin (2m+n)\phi - (2m+n) \cos (2m+n)\phi}{a^2 + (2m+n)^2} +
\end{aligned}$$

$$\begin{aligned}
& + \frac{a \sin (2m-n-2)\phi - (2m-n-2) \cos (2m-n-2)\phi}{a^2 + (2m-n-2)^2} \\
& + \sum_{m=1}^{\infty} J_{2m}(z) \frac{a \sin (2m+n-1)\phi - (2m+n-1) \cos (2m+n-1)\phi}{a^2 + (2m+n-1)^2} \\
& - \frac{a \sin (2m-n+1)\phi - (2m-n+1) \cos (2m-n+1)\phi}{a^2 + (2m-n+1)^2} \\
& + \frac{a \sin (2m+n+1)\phi - (2m+n+1) \cos (2m+n+1)\phi}{a^2 + (2m+n+1)^2} \\
& - \frac{a \sin (2m-n-1)\phi - (2m-n-1) \cos (2m-n-1)\phi}{a^2 + (2m-n-1)^2}
\end{aligned}$$

## SECTION 7

### SUMMARY OF ADDITIONAL HF ANTENNA CHARACTERISTICS

#### 7.1 LETTER-RACK FLUSH SLOT ARRAY

Two configurations were studied for the letter-rack flush slot array<sup>18</sup>-- one consisting of an open pit structure which would serve as a debris pit and the second technique involved the embedding of the complete array in asphaltic concrete.

A summary of the antenna characteristics together with antenna configuration and design parameters follows.

- a) Configuration - See Figures 7-1 and 7-2 for 10-20 Mc array.
- b) Bandwidth - No tuning  $\sim 15$  percent.
- c) Useful Frequency Range -  $\sim 2:1$  for a 5-slot array.
- d) Efficiency  $\eta$  - At any particular midband frequency, anticipated efficiency will be that of the linear slot antenna (midband frequency is point at which single slot in array is optimized).
- e) Radiation Pattern - Directional, same as linear slot.
- f) Directivity,  $D$   $\geq 1.76$  db compared to an isotropic antenna above perfect ground at midband frequency.
- g) Gain =  $nD$ ,  $\geq 1.35$  or 1.3 db.
- h) Hardness -
  - (1) When embedded in asphaltic concrete, antenna carries a hardness rating of class D.
  - (2) For open pit structure serving as a debris pit, hardness rating is class A.
- i) Cost\*
  - (1) When embedded in asphaltic concrete, a slot array in 9-16 Mc (or  $\sim 10$ -20 Mc) region would cost approximately \$43,000; in the 16-23 Mc

\*Cost figures in this section are "best estimates" at this time



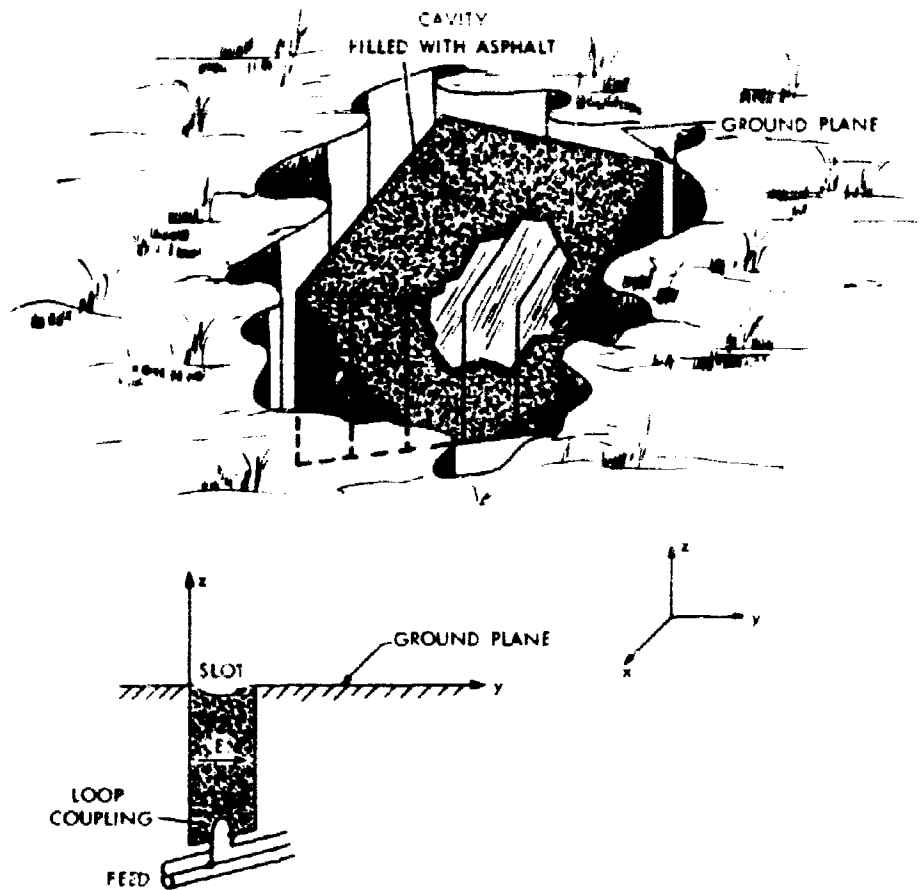


Figure 7-1. Configuration for Letter Rock Flush Slot Array.

4-1-0605

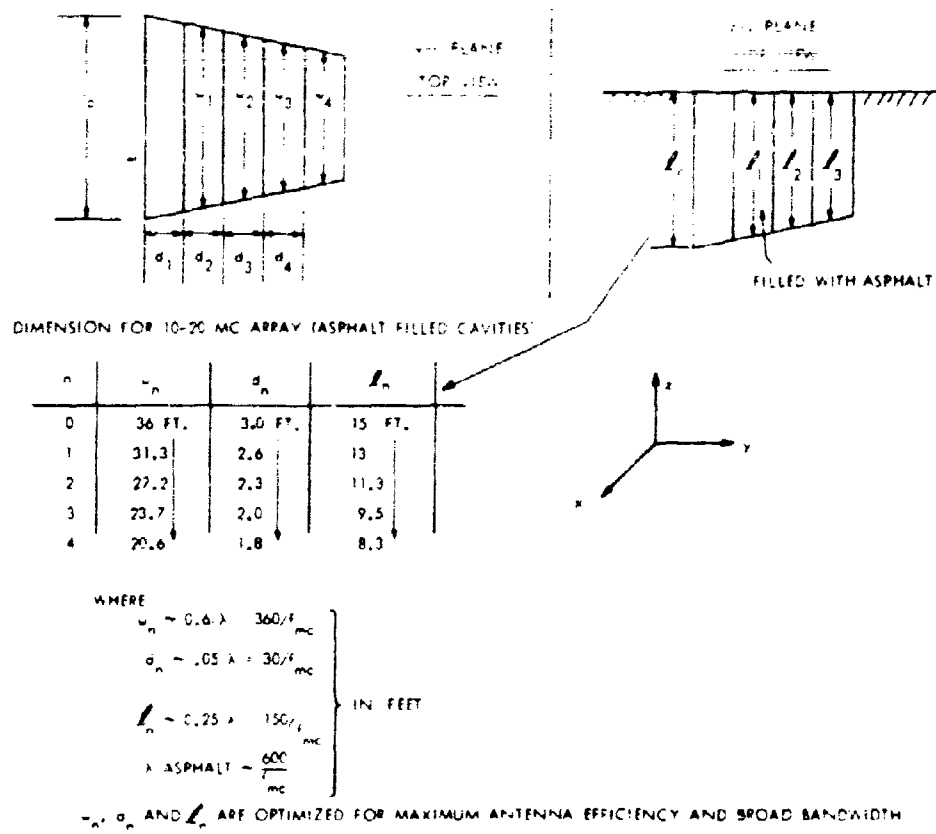


Figure 7-2. Design Data for Letter Rack Flush Slot Array.

region cost estimates are \$28,000; and from 23-30 Mc, the 5-slot array cost estimates are \$17,000.

- (2) For open pit structure, a 5-slot array in the 9-16 Mc (or ~10-20 Mc) region would cost \$155,000 due to the elaborate foundation and construction costs; in the 16-23 Mc region cost estimate is \$95,000; in the 23-30 Mc region cost estimate is \$54,000.

j) Effects of Debris - Same as the linear slot antenna.

k) Polarization - Vertical on the ground.

l) Advantages - Same as those of the linear slot.

m) Disadvantages -

- (1) For the structure embedded in asphaltic concrete. Debris will not allow operation at the computed high efficiency.
- (2) Open pit structure represents a costly antenna of very low hardness rating and does not appear to be a promising configuration in the HF band.

n) Areas Requiring Further Investigation -

- (1) Optimum techniques for feeding the individual slots in the array.
- (2) Optimization of array parameters for maximum bandwidth, and their effects on antenna efficiency and directivity.

o) Further Comments on the Open Pit Structure - There appear to be two practical ways of constructing this antenna. Technique No. 1 involves a rather large foundation and the stretching of a series of cables to make up the cavities for the radiating elements. Under high thermal loading from a nuclear blast, these cables will yield and stretch. An initial tension must be applied to the cables of such magnitude that after thermal loading there will still be enough residual tension to keep the cables from sagging excessively. The ability of providing reasonable assurance that the cables will have adequate residual tension will severely limit the over-pressure rating of this antenna to

class A. Foundation costs (exclusive of cables, pretensioning devices, etc.) would probably be in the order of \$100,000 in 10-20 Mc range.

The additional costs of the cables and thermal protection for the cables is estimated to be \$55,000 bringing the total cost of a 5-slot letter-rack antenna (in the 10-20 Mc range) to approximately \$155,000.

Technique No. 2 utilizes a series of concrete walls with steel surfaces (together with a peripheral foundation) to make up the cavities of the letter-rack arrangement. This type of structure carries a hardness rating of class A and is limited by the failure of the concrete walls separating the slots in the array due to cantiliver action. Foundation costs alone for a 5-slot array in the 10-20 Mc region would probably be in the order of \$167,000. Based upon our preliminary investigation of the open-pit letter-rack antenna, it is our opinion that such a configuration is not practical in the HF band. The letter-rack antenna, when embedded in asphaltic concrete, represents a hardened antenna in class D. Its electrical performance in asphaltic concrete can be predicted from the performance of a single linear slot (since a letter-rack antenna consists of an array of linear slots) which was discussed in an earlier section.

## 7.2 LOG PERIODIC STRUCTURES

The log periodic monopole (LPM) array was found to be applicable as a hardened antenna (class B) from 12-30 Mc. The basic limitation of this particular structure is the height of the longest monopole in the array, which at 12 Mc would be approximately 20 feet high. Increased hardness ratings (class C) can be achieved for arrays designed in the 25-30 Mc band. Typical configurations are shown in Figure 7-3 and 7-4. A dielectric sleeve 3 feet high is shown at the base of each monopole to minimize the effect of debris loading on the performance of the LPM array.

Appendix D contains a detailed discussion of the Log Periodic Monopole array together with the necessary curve used to design a particular array. A summary of the significant characteristics is given below.

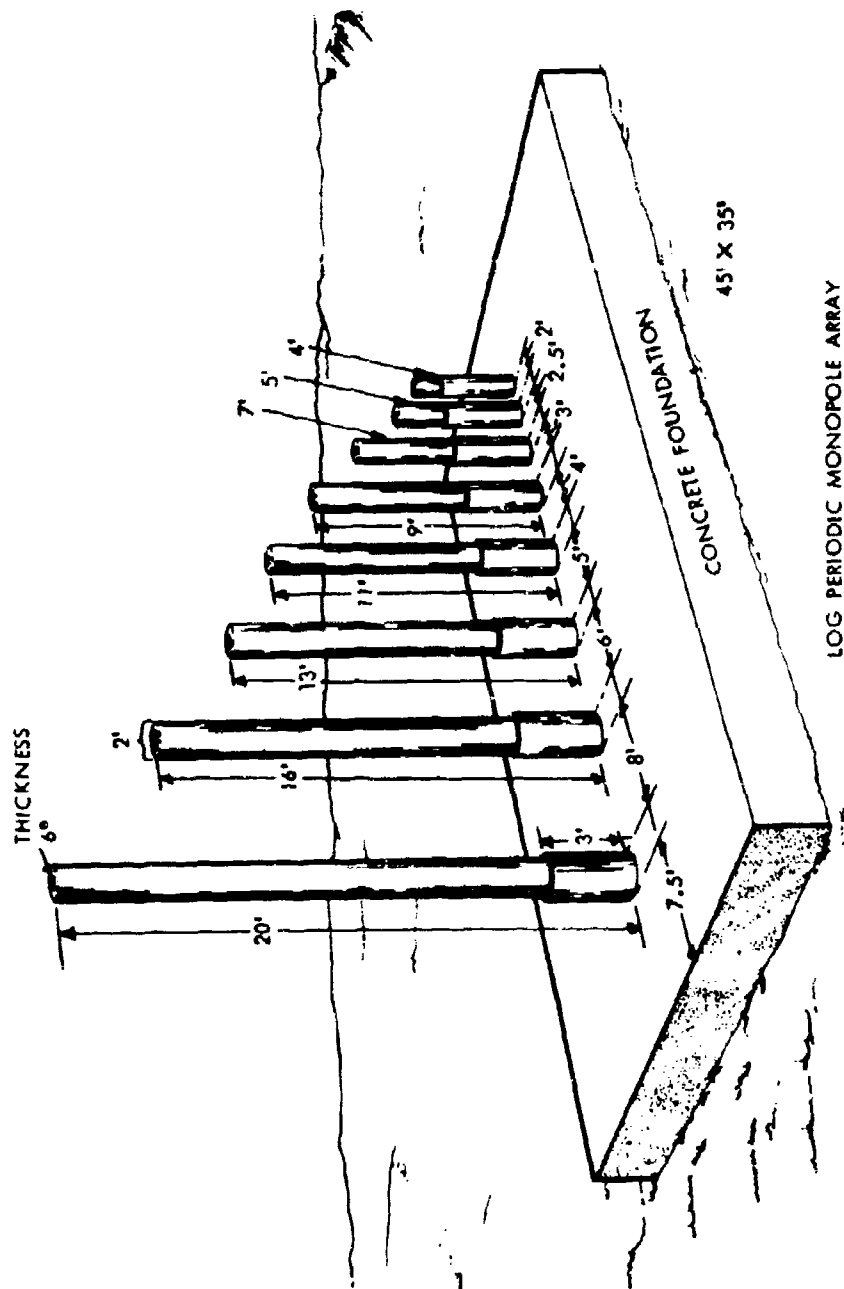


Figure 7-3. Log Periodic Monopole Array (12-30 mc).

4-1-0581

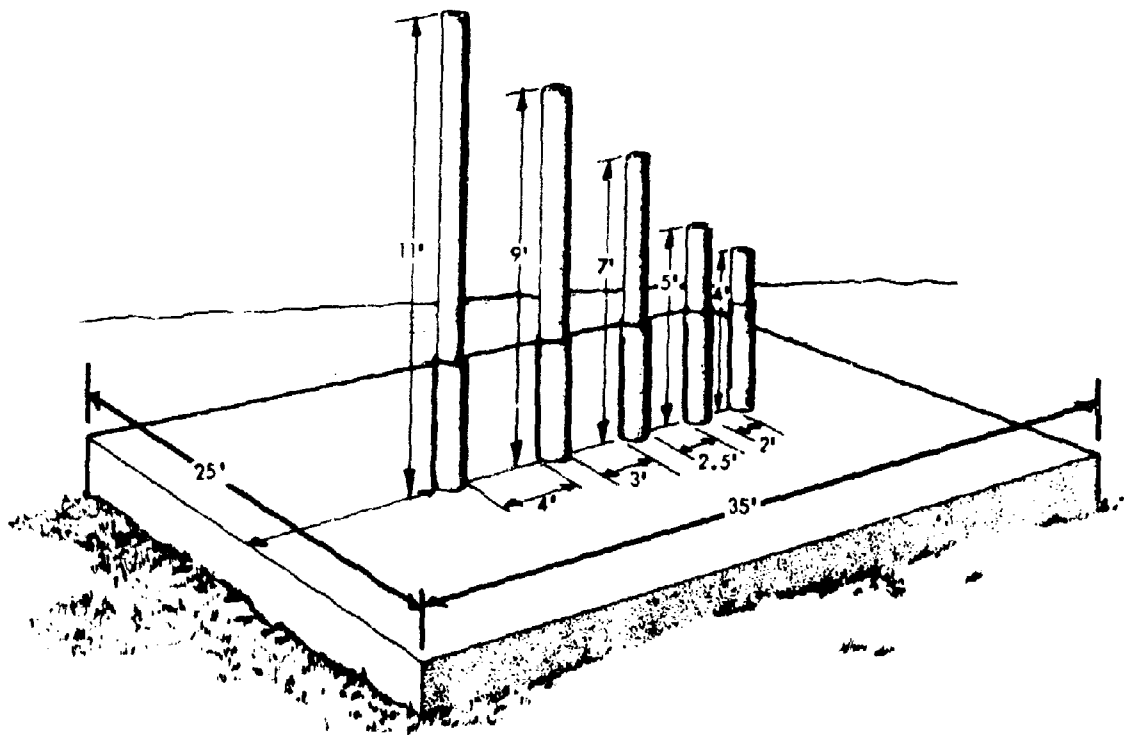


Figure 7-4. Log Periodic Monopole Array ( 25-30 mc ).

For Vertical Monopoles in Air -

- (a) Configuration - see Figures 7-3 and 7-4.
- (b) Bandwidth - From hardness consideration, the limit on this type of antenna is 12-30 Mc for a hardness rating of B and from 25-30 Mc, hardness rating C is possible.
- (c) Efficiency - ~75-80 percent for individual elements.
- (d) Radiation Pattern - Main lobe of beam, E-plane  $30^\circ$ , H-plane  $60^\circ$ .
- (e) Gain - ~8 db.
- (f) Hardness - 12-30 Mc design - class B  
25-30 Mc design - class C
- (g) Cost - 12-30 Mc (8 element) - \$130,400  
25-30 Mc (5 element) - \$57,900
- (h) Polarization - Vertical on the ground.
- (i) Effects of Debris - Small at the low end of band, and high in vicinity of 30 Mc where the short 4' monopoles would be covered with debris.
- (j) Advantages of LP Structure in Air -
  - (1) High efficiency and broad band operation.
  - (2) Debris effects appear to be low at 12 Mc and more severe at 30 Mc.
- (k) Disadvantages of LP Structure in Air -
  - (1) Represents an antenna of low hardness rating, class B, C.
  - (2) Cost of structure is very high compared to hardness rating.

### 7.3 OTHER CONFIGURATIONS

The characteristics of five additional antenna techniques -- the Surface Wave types, Hula Hoop, Spherical, Prolate Spherical, and Helical antennas which appeared to have less desirable properties as hardened HF antennas such as size, low hardness rating, and poor cost to performance ratios are discussed in Appendix E.

Unclassified  
Security Classification

DOCUMENT CONTROL DATA - R&D			
(Security classification of title, body of abstract and indexing annotation must be entered when the overall report is classified)			
1. ORIGINATING ACTIVITY (Corporate author) Sylvania Electron Systems East Sylvania Electric Products, Inc. Waltham, Massachusetts		2a. REPORT SECURITY CLASSIFICATION <b>SECRET RD</b>	
		2b. GROUP <b>1</b>	
3. REPORT TITLE  (U) Hardened Antenna Studies			
4. DESCRIPTIVE NOTES (Type of report and inclusive dates) Final 15 Mar 63 - 15 Mar 64			
5. AUTHOR(S) (Last name, first name, initial) Stephaniac, E. Underhill, W. O'Neil, S. Tahan, E. Snitkoff, J. Ng, T. Sabin, E. Windt, R. Zeltzer, H. MacDonald, G. Wilkinson, E. Meyers, D.E.			
6. REPORT DATE April 1964		7a. TOTAL NO OF PAGES	7b. NO OF REFS 88
8a. CONTRACT OR GRANT NO. AF30(602)-2932 b. PROJECT NO. 4519 c. Task - 451906 d.		9a. ORIGINATOR'S REPORT NUMBER(S) P607-1 9b. OTHER REPORT NO(S) (Any other numbers that may be assigned this report) RADC-TDR-64-184	
10. AVAILABILITY/LIMITATION NOTICES Qualified Requesters may obtain copies of this report from DDC.			
11. SUPPLEMENTARY NOTES Vol Ia - Uncl. Vol III - SECRET RD Vol Ib - SECRET Vol IV - SECRET Vol II - SECRET		12. SPONSORING MILITARY ACTIVITY RADC GRIFFISS AFB NY	
13. ABSTRACT <p>This report discusses the results of a twelve month engineering investigation of Hardened HF and UHF Antennas sponsored by the Communications Division of Rome Air Development Center, Air Force System Command. This engineering study has resulted in the generation of efficient antenna techniques consistent with the capabilities to withstand the effects of nuclear weapons. The HF antenna techniques considered in this study are useful throughout the 2-30 mc frequency band; the UHF antennas operate in the 225-400 mc region.</p> <p>The program was divided into two phases. Phase I was a theoretical study of antenna techniques which were investigated with regard to feasibility, configuration required, bandwidth possibilities, efficiency, radiation patterns, hardness ratings, debris effects and economic analysis. Phase II involved the fabrication and test of electrical models of the most promising designs. This phase resulted in design data, cost and hardness estimates for antennas for the HF and UHF bands.</p>			

DD FORM 1473  
1 JAN 64

Unclassified  
Security Classification



14 KEY WORDS	LINK A		LINK B		LINK C	
	ROLE	WT	ROLE	WT	ROLE	WT
<b>Antennas</b> <b>Antenna Configurations</b> <b>Communications Systems</b>						

#### INSTRUCTIONS

1. **ORIGINATING ACTIVITY:** Enter the name and address of the contractor, subcontractor, grantee, Department of Defense activity or other organization (corporate author) issuing the report.
- 2a. **REPORT SECURITY CLASSIFICATION:** Enter the overall security classification of the report. Indicate whether "Restricted Data" is included. Marking is to be in accordance with appropriate security regulations.
- 2b. **GROUP:** Automatic downgrading is specified in DoD Directive 5200.10 and Armed Forces Industrial Manual. Enter the group number. Also, when applicable, show that optional markings have been used for Group 3 and Group 4 as authorized.
3. **REPORT TITLE:** Enter the complete report title in all capital letters. Titles in all cases should be unclassified. If a meaningful title cannot be selected without classification, show title classification in all capitals in parentheses immediately following the title.
4. **DESCRIPTIVE NOTES:** If appropriate, enter the type of report, e.g., interim, progress, summary, annual, or final. Give the inclusive dates when a specific reporting period is covered.
5. **AUTHOR(S):** Enter the name(s) of author(s) as shown on or in the report. Enter last name, first name, middle initial. If military, show rank and branch of service. The name of the principal author is an absolute minimum requirement.
6. **REPORT DATE:** Enter the date of the report as day, month, year; or month, year. If more than one date appears on the report, use date of publication.
- 7a. **TOTAL NUMBER OF PAGES:** The total page count should follow normal pagination procedures, i.e., enter the number of pages containing information.
- 7b. **NUMBER OF REFERENCES:** Enter the total number of references cited in the report.
- 8a. **CONTRACT OR GRANT NUMBER:** If appropriate, enter the applicable number of the contract or grant under which the report was written.
- 8b, 8c, & 8d. **PROJECT NUMBER:** Enter the appropriate military department identification, such as project number, subproject number, system numbers, task number, etc.
- 9a. **ORIGINATOR'S REPORT NUMBER(S):** Enter the official report number by which the document will be identified and controlled by the originating activity. This number must be unique to this report.
- 9b. **OTHER REPORT NUMBER(S):** If the report has been assigned any other report numbers (either by the originator or by the sponsor), also enter this number(s).
10. **AVAILABILITY/LIMITATION NOTICES:** Enter any limitations on further dissemination of the report, other than those

imposed by security classification, using standard statements such as:

- (1) "Qualified requesters may obtain copies of this report from DDC."
- (2) "Foreign announcement and dissemination of this report by DDC is not authorized."
- (3) "U. S. Government agencies may obtain copies of this report directly from DDC. Other qualified DDC users shall request through \_\_\_\_\_."
- (4) "U. S. military agencies may obtain copies of this report directly from DDC. Other qualified users shall request through \_\_\_\_\_."
- (5) "All distribution of this report is controlled. Qualified DDC users shall request through \_\_\_\_\_."

If the report has been furnished to the Office of Technical Services, Department of Commerce, for sale to the public, indicate this fact and enter the price, if known.

11. **SUPPLEMENTARY NOTES:** Use for additional explanatory notes.

12. **SPONSORING MILITARY ACTIVITY:** Enter the name of the departmental project office or laboratory sponsoring (paying for) the research and development. Include address.

13. **ABSTRACT:** Enter an abstract giving a brief and factual summary of the document indicative of the report, even though it may also appear elsewhere in the body of the technical report. If additional space is required, a continuation sheet shall be attached.

It is highly desirable that the abstract of classified reports be unclassified. Each paragraph of the abstract shall end with an indication of the military security classification of the information in the paragraph, represented as (TS), (S), (C), or (U).

There is no limitation on the length of the abstract. However, the suggested length is from 150 to 225 words.

14. **KEY WORDS:** Key words are technically meaningful terms or short phrases that characterize a report and may be used as index entries for cataloging the report. Key words must be selected so that no security classification is required. Identifiers, such as equipment model designation, trade name, military project code name, geographic location, may be used as key words but will be followed by an indication of technical context. The assignment of links, rules, and weights is optional.